Design and Synthesis of Complex and Fluorescent Labeled Cellulose-Based Derivatives for Orally Administered Drug Delivery Systems

Diana Cecilia Novo

Dissertation submitted to the faculty of the Virginia Polytechnic Institute and State University in partial fulfillment of the requirements for the degree of

Doctor of Philosophy
In
Chemistry

Kevin J. Edgar, Chair
John B. Matson, Co-Chair
Lynne S. Taylor
Judy Riffle

July 27, 2023
Blacksburg, VA

Keywords: cellulose ethers, oral drug delivery, polysaccharides, reductive-amination, amorphous solid dispersions

Design and Synthesis of Complex and Fluorescent Labeled Cellulose-Based Derivatives for Orally Administered Drug Delivery Systems

Diana Cecilia Novo

ABSTRACT

Cellulose ethers are valuable matrices for drug-delivery systems (DDS), namely amorphous solid dispersions (ASD). ASD are efficient vehicles that can solubilize and stabilize poorly soluble drugs by increasing the time that it takes for drugs to crystallize, thereby allowing higher drug concentrations and providing increased bioavailability. However, most commercially available cellulose derivatives were not specifically designed for this application, leading to gaps in understanding the key mechanisms by which ASD operate. This creates the need for polysaccharide derivatives specifically conceptualized for ASD and for elucidating structure-property relationships. In this dissertation, I successfully demonstrated regioselective and chemoselective techniques to functionalize cellulose to prepare new ASD as well as smart tracking devices. I efficiently and successfully create complex structures via appending bile salt substituents using olefin cross-metathesis. I ascertained that high performance crystallization inhibitors can be achieved with enhanced hydrophilicity by the marriage of two classes crystallization inhibitors (cellulose and bile salts), as illustrated with the commercial, fast crystallizing prostate cancer drug, enzalutamide.

I obtained ketone-functionalized cellulose derivatives using oxidation chemistry to produce fluorescent poly- and oligosaccharides (hydroxypropyl cellulose, hydroxypropyl methylcellulose, and hydroxypropyl beta cyclodextrin). Schiff-base chemistry was then explored to append a commercially available fluorescent label, Nile Blue. Due to the dynamic nature and hydrolytic lability of Schiff-bases, I applied

reductive-amination chemistry with either one pot, or two-step techniques and evaluated the efficiency of these approaches. I characterized the new fluorescent polymers, and with the objective of elucidating ASD mechanisms, I investigated their response in solvents of different polarities to probe environment-sensitivity.

Flavonoids are interesting drug candidates; they have been explored for many biomedical applications, including as inducers of apoptosis and functioning as antioxidants by radical scavenging. I prepared high-performance ASD polymer candidates, then prepared and characterized ASDs with different loadings of the flavonoids, genistein and quercetin. I explored the performance of polymers with different functionalities, hydrophilicity/hydrophobicity, and carboxylic acid content (cellulose acetate glutarate, 5-carboxypentyl hydroxypropyl cellulose, and hydroxypropyl methyl cellulose acetate succinate as positive control) by using *in vitro* dissolution studies. In this screening process, I determined that cellulose acetate glutarate provides the most advantageous enhancement, possessing the appropriate amphiphilicity to increase drug concentration in this study, supported by the similarity of the polymer and drug solubility parameters. I was further able to confirm via polarized light microscopy that advantageous nanodroplet formation occurs during the drug-release process.

Design and Synthesis of Complex and Fluorescent Labeled Cellulose-Based Derivatives for Orally Administered Drug Delivery Systems

Diana Cecilia Novo

GENERAL AUDIENCE ABSTRACT

As sources for future ecofriendly materials, derivatives from nature offer fertile ground. One group of natural materials that attracts increasing attention to fulfill both performance and sustainability are polysaccharides, long chains of carbohydrates, that can be found in plant cell walls, exoskeletons of bugs or oceanic bottom feeders, algae, and indeed in all living things. Cellulose derivatives provide biologically safe materials that are biomedically relevant, including in the field of oral drug delivery. While most orally administered drugs are not 100% effective or absorbable, a class of drug delivery systems named amorphous solid dispersions can improve drug absorption with the aid of polysaccharide derivatives. Although amorphous solid dispersions are highly effective, there is still much room for improvement, and important opportunities to learn about the precise mechanisms that make such systems work. With fluorescent markers, I can also explore the surrounding environment of the drug delivery systems in preliminary studies. By understanding the environment of such polysaccharides, I determined important insight into how they improve oral drug availability and performance. Herein, I explored new amorphous solid dispersion polysaccharide derivatives, and how I have attached fluorescent labels to track them to learn how they work.

Dedication

This dissertation is dedicated to my loving parents,
Rita Chinchilla-Novo and Jose I. Novo,
and my dearly departed love of my life,
Andrew Bolhassani.
No words can express how much I love you.

Acknowledgements

Family is number one: I would first like to acknowledge my immediate family, The 5 Novos. Thank you to my mother and father Rita and Jose Novo, for your unconditional love, for always striving to be the best version of oneself, and showing me to never be lazy! Thank you to my big brothers, Giancarlo and Richard for all the inspiration, support, nagging, ridiculousness, and love. Thank you for giving me amazing nephews and nieces! My trailblazing grandparents (Miriam and Nazario Chinchilla; Ignacio and Olimpia Novo) each of them so brave to make all of the opportunities that I have had possible.

I am forever grateful for my adviser, Dr. Kevin Edgar, for his wisdom, guidance, compassion, and patience! I would never have been able to complete my degree without him as my guide, as well as his insurmountable support. Thank you for always believing in me. Thank you for your high standards, and for giving us the autonomy needed to be independent and critical scientists. There is good reason why we nominated you, and why you have won the Best Graduate Student Mentor award.

Thank you to my committee members -- Dr. John Matson, Dr. Lynne Taylor, and Dr. Judy Riffle for your support and advise throughout my tenure at Virginia Tech. You have all provided invaluable knowledge. Thank you to my collaborators, Laura I. Mosquera-Giraldo, Chengzhe Gao, Qingqing Qi, Emily Benson, Glenn Spiering, and Dr. Robert Moore. Thank you to Dr. Ed Smith and my IMSD family, for I would not be here if it weren't for you!

Dr. Yifan Dong, thank you for being inspiring lab mentor, colleague, and a great friend. Thank you to the Edgar Group, my very good friend Brittany L.B. Nichols, Junyi Chen, Chengzhe Gao, Shu Liu, Yang Zhou, Zhenghao Zhai, Jeffrey Thompson, Fiorella Manzzini, Brenna Knight, and Stella Petrova for being collaborative and kind lab colleagues. "The Kelly

Hall girls": Yifan again, Ami Jo, Shreya Roy Choudhury, and Brittany L.B. Nichols; you are all inspiring and amazing women I am proud of, and we will be lifelong friends to enjoy and share our multicultural dining! Our coffee breaks were also essential! My brilliant friend and lab neighbor, Austin Fergusson, our lab rants, your insight, and our time spent outside lab has helped me stay sane. My soul sister, Stella Petrova, we have gone through so many highs and lows, including the pandemic together! Thank you for your bluntness, constructive feedback, and valuing friendship like I do! My Kuchkas -- Rachel Bianculli, and Ophelia Wadsworth, thank you for dealing with me. I have thoroughly enjoyed your company, relentless spirits and intellectual discourse! Ashley Peralta, Brady & Katy Hall, Chanelle Brown, and Raging Myrtle group (Ashley Toland, Mike Badzmierowski, Marion Nieto, Jesse Radolinski, Abby Baxter) – our times together in and out of Blacksburg have given me life. Gemma Rosello (my person), Mel Moreno, and Jackie Otero -- my lovely girls from home. I am grateful for The Bolhassanis, you are my family and I love you. Mohsen and Maria, I hope to keep you in my life and get picked on by Maria forever! My sister, Patty, thank you for being so loving and sweet.

Thank you, Andrew, for being such a gem of a human. You have given me the best years of my life, and have been my rock during my PhD. Only you can be so successful at being the chameleon you are, and become a doctor, cook the best meals, be a wordsmith, one of the best comedians, supportive and most fun partners to have existed. Even in your absence, you push me to be a better person and to have 'elephant skin'.

Table of Contents

Preface/Attribution

Prof. Kevin J. Edgar was the principal investigator, advisor, and primary contributor for all of the research projects, manuscripts, and chapters described herein.

Prof. John B. Matson has provided insight questions and meaningful perspectives in this dissertation.

Prof. Lynne S. Taylor has provided extremely valuable expertise in experimental design to evaluate polymer selection and performance in pharmaceutical applications. She is also co-author for Chapters 3-5.

Dr. Yifan Dong has been an excellent mentor, providing copious insight on cross-metathesis and experimental design.

Dr. Laura I. Mosquera-Giraldo, who was a graduate student from Dr. Taylor's group, has conducted induction experiments in Chapter 3, and solubility parameter calculations for Chapters 4-5. She is co-author in Chapters 3-5.

Qingqing Qi and Chengzhe Gao, were post-docorates of Dr. Taylor. They have performed induction time studies and fluorometry experiments in Chapters 5 and 6, respectively. They are also co-authors for Chapters 5-6.

Emily Benson, a graduate student from Dr. Taylor's group, has conducted the in vitro dissolution studies, polarized light microscopy and nanotracking analyses in chapter 5.

Stella P. Petrova has provided insight in amorphous solid dispersion studies and preparation of polymers for drug testing, she is also co-author to Chapter 5.

Jeffrey Thompson helped perform drug release analyses in Chapter 5. He is also co-author for Chapter 5.

Glenn A, Spiering, a student from Dr. Moore's group performed and provided thermal analyses, he is also a co-author to Chapter 3.

Dr. Brady Hall, a post-doctorate from GlycoMIP, has performed and provided SEC analyses in Ch. 3-5.

Jonathan Mase, a student of Dr. Schulz group, has performed and provided SEC analyses in Ch. 4-5.

Rachel Bianculli from Dr. Schulz lab and Dr. Ashley Peralta of Dr. Santos lab has provided aid in purification in Chapter 3.

Chapter 1: Dissertation Overview

In a modern world that requires a sustainable future, ubiquitous polysaccharides are necessary, attractive feedstocks and alternatives to synthetic materials. The applications for polysaccharides are endless; these materials find use in, to cite a few examples, home and personal care, packaging, medical appliances or pharmaceuticals, coatings, thickening agents (food and cosmetics), compatibilizing agents, or as an option for hybrid materials such as composites. The abundance and benign nature of cellulose evokes wide use of its derivatives in biomedical applications such as wound dressings, hydrogels, controlled and targeted drug-delivery.

Oral delivery is plagued by poor aqueous solubility of many drugs and, consequently, poor absorption and bioavailability in the bloodstream. Amorphous solid dispersions (ASD) are able to eliminate the energy barrier constituted by the heat of fusion of the drug while it is molecularly dispersed in a polymer matrix, thereby promoting drug dissolution and stability against crystallization. While some commercial synthetic polymers and polysaccharides were serendipitously found to succeed in this application, they were not specifically designed for this purpose, leading to gaps in understanding how ASD systems work. Recent findings have shown desirable ASD criteria include amphiphilicity, hydrophobic character necessary to be miscible with the drug, and hydrophilicity to promote drug dissolution in physiologically relevant conditions. The goal of this dissertation is to synthesize purpose-designed cellulose derivatives for use in ASD, as matrices and environment-sensitive tracking devices. An outline for this dissertation is as follows: advances in environment-sensitive polysaccharides are discussed in Chapter 2. We explore fluorescent labeling strategies, their selection based on application, and how the smart, stimuli-responsive polysaccharide materials have recently been used.

While several modification techniques have been employed to broaden the utility of cellulose by tailoring derivatives, esterification and etherification methods dominate. Click chemistry has changed the landscape and speed at which it is possible to efficiently reach a variety of new materials. Herein, we employ olefin cross-metathesis (CM), which has many of the features of click reactions, as a means to modularly impart new and complex functionalities to cellulose ethers. In Chapter 3, we explore the potential to enhance the hydrophilicity of two classes of crystallization inhibitors found in nature, bile salts and cellulose ethers using chemoselective and regioselective strategies, as well as CM chemistry. We probe structure-property relationships using this new variety of conjugates, and explore whether the ASD candidates can work synergistically to reduce crystallization with enzalutamide. In Chapter 4, fluorescently labeled polysaccharides and oligosaccharides are synthesized. Oxidation chemistry is employed to introduce amine-containing fluorophores to ASD candidates via reductive amination. The novel fluorescently labeled polysaccharides and oligosaccharides are then characterized, and we close by probing their environmental sensitivity using fluorometric studies. In Chapter 5, high performing ASD polymer candidates which are cellulose derivatives designed and synthesized by the Edgar lab for ASD are employed to enhance the poor solubility of an interesting class of drug candidates, flavonoids. ASD were formulated, characterized, and explored via in vitro dissolution studies using two different flavonoids, genistein and quercetin. In Chapter 6, we conclude the work investigated in this dissertation, and close with new questions to investigate as future opportunities that could further unveil structure-property relationships.

Chapter 2. Smart Fluorescent Polysaccharides: Recent Developments and Applications

Adapted from "Novo, D.C. [a, b]; Edgar, K.J. [a, c, d] Carbohydrate Polymers, 2023 Submitted."

Diana C. Novo [a, b] and Kevin J. Edgar* [a, c, d]

[a]*Department of Sustainable Biomaterials, Virginia Tech, Blacksburg, VA 24061, United States*

[b]*Department of Chemistry, Virginia Tech, Blacksburg, VA 24061, United States*

[c]*Macromolecules Innovation Institute, Virginia Tech, Blacksburg, VA 24061, United States*

[d]*GlycoMIP, National Science Foundation Materials Innovation Platform*

Abstract

Polysaccharides are ubiquitous, generally benign in nature, and compatible with many tissues in biomedical situations, making them appealing candidates for new materials such as therapeutic agents and sensors. Fluorescent labeling can create the ability to sensitively monitor distribution and transport of polysaccharide-based materials, which can for example further illuminate drug-delivery mechanisms and therefore improve design of delivery systems. Herein, we review fluorophore selection and ways of appending polysaccharides, utility of the product fluorescent polysaccharides as new smart materials, and their stimulus-responsive nature, with focus on their biomedical applications as environment-sensitive biosensors, imaging, and as molecular rulers. Further, we discuss the advantages and disadvantages of these methods, and future prospects for creation and use of these self-reporting materials.

1. Introduction

Low oral bioavailability is a crucial challenge to drug designers and formulators. Highly crystalline drugs are particularly problematic in this sense, as their lattice energy must be overcome for molecules of the solute to dissolve in the body (Teja, Patil, Shete, Patel, & Bansal, 2016). In addition to solubility issues, the drug must face several obstacles in the gastrointestinal (GI) tract (including chemical degradation in the acidic stomach) before absorption (primarily)

through the epithelium of the small intestine. The amount of absorbed drug may be further reduced by other processes, such as metabolism by the liver and/or efflux transport (Collnot et al., 2010, 2007; Martinez & Amidon, 2002; Wempe et al., 2009). Drug-delivery systems (DDS) designed to dodge these obstacles are therefore in high demand.

Integration of functionally modified polysaccharides (PS) into DDS using amorphous solid dispersions (ASD) (Dong & Edgar, 2015; Ilevbare, Liu, Edgar, & Taylor, 2013; Xiangtao Meng, Matson, & Edgar, 2014a; Mosquera-Giraldo et al., 2018; Novo et al., 2022; V. Wilson et al., 2018; V. R. Wilson et al., 2020), nanoparticles (Cheng et al., 2020; G. Ricarte et al., 2019; González et al., 2022), or nanogels (Adav et al., 2010; Debele, Mekuria, & Tsai, 2016; Sun et al., 2018; Wang et al., 2020) has been reported to enhance drug solubility (Dong & Edgar, 2015; H. Liu, Taylor, & Edgar, 2015; Xiangtao Meng, Matson, & Edgar, 2014b; Teja et al., 2016). These DDS show promise for improving bioavailability (Chhatbar, Meena, Prasad, Chejara, & Siddhanta, 2011; Ilevbare et al., 2013) and controlled release of drugs and genetic material, including plasmid DNA, oligonucleotide, and signaling RNA (siRNA) (dos Santos & Grenha, 2015; Efiana, Kali, Fürst, Dizdarević, & Bernkop-Schnürch, 2023; Fayazpour et al., 2006; Karimi Jabali et al., 2022; Messai et al., 2005; Samal et al., 2012; Weecharangsan et al., 2008). Being able to monitor these DDS using fluorescent probes can not only improve material design, but also can contribute to understanding how these drug-delivery systems work. Most polysaccharide derivatives used in DDS do not have strong chromophores. Natural PS typically do not possess UV absorbers, while the most typical alkanoate or alkyl substituents also do not absorb strongly in the UV (phthalate substituents being the only (somewhat) common exception). This absence of chromophores in PS makes them a challenge to detect spectroscopically, particularly in a diverse matrix of naturally occurring substances (including

metabolites). Current methods for tracking PS include colorimetric (Englyst & Hudson, 1987; Janda & Work, 1971; Kohn & Wilchek, 1978; Lai et al., 2021), immunoassay (Mansur, Mansur, Soriano-Araujo, & Lobato, 2014; S. Natarajan, Jayaraj, & Prazeres, 2021; Nualnoi et al., 2016; Salgado, Mansur, Mansur, & Monteiro, 2021; J. Zhou et al., 2022), radioisotopic (Kaneo, Tanaka, Nakano, & Yamaguchi, 2001; Z.-M. Zheng et al., 2022) and fluorescent labeling strategies (Mary, Koshy, Arunima, Thomas, & Pothen, 2022; Nawaz, Zhang, Chen, You, & Xu, 2021; Z. Zheng et al., 2020), with the latter two being the most sensitive. While radiolabeling most minimally changes structure and properties of the molecule that one wants to track, fluorescent labeling is more convenient as it does not require the special licensing or training necessary to run a radioactive facility, which is costly to create and maintain. This review will focus on recent developments in environment-sensitive and stimuli-responsive fluorescent PS used for metal ion detection (in nature, including in the human body) (Li et al., 2022), or in delivering and monitoring therapeutic cargo as observed via changes in polarity or pH. Herein, we provide a brief background on labeling technique and selection, properties, advantages, and caveats for these applications.

1.1. Fluorescent Labeling Technique

Fluorescent labeling is one of the most sensitive and selective spectroscopic techniques, able to detect even single molecules. Drug and drug delivery polymer concentrations in the human body can often be in the nanomolar range, so fluorescence sensitivity is of crucial importance for monitoring such dilute systems. Prior to de-excitation, fluorescent molecules stay in the excited singlet state (10^{-9}- 10^{-8} s) for a time greater than the time required for molecules to absorb light (10^{-15} s). In contrast to the absorbing species, this timescale gives the fluorescing species greater sensitivity to its environment. Thus, several important types of events can be

detected, including proton transfer, solvent cage relaxation, conformational change, and translational or rotational change (Cantor & Schimmel, 1980). This method is highly useful, describing the local environment of the probe via solvatochromic red/blue shift effects, intermolecular interactions between two FRET pair molecules that are sensitive to the distance separating them (Behanna, Rajangam, & Stupp, 2007), and the location of the probe via spatial monitoring of fluorescent signals.

Solvatochromic labels are often the only method available to study membranes and lipid layers at a molecular level (Reichardt, 1994). Several fluorophores characteristically quench in polar/aqueous environments (i.e., bathochromic dyes), whereas quenching is suppressed in nonpolar/hydrophobic and/or rigid environments (Cantor & Schimmel, 1980). Hypsochromic dyes are those which quench in nonpolar solvents and increase emission intensity in polar environments.

FRET is an excited state, nonradiative energy transfer between a donor and acceptor pair via dipole-dipole coupling, which occurs when there is spectral overlap between the emission of a fluorophore (donor) and the absorption of another molecule (acceptor) (Förster, 1948). The energy transfer between the FRET pair (**Fig. 2.1)** results in fluorescence intensity increase for the acceptor and reduction for the donor (as well as reduced donor fluorescence lifetime).

FRET is a powerful tool that can measure small changes in distance between two fluorescent donor and acceptor molecules since energy transfer efficiency, E, is inversely related to the donor- acceptor distance (r) to the sixth power **(Eq.1)** (Lakowicz, 2006b).

$$E = \frac{{R_0}^6}{{R_0}^6 + r^6} \qquad \textbf{(Eq.1)}$$

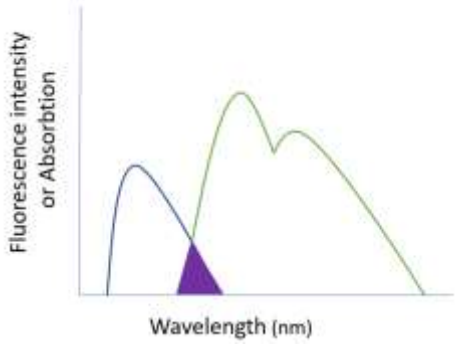

Figure 2.1: FRET Spectral Overlap (Figure adapted from Lakowicz, (2006a)). The excitation spectrum of the acceptor species (blue) in the absence of donor, and emission spectrum of the donor (green) in the absence of acceptor are depicted. The shaded region depicts the overlap integral between the two spectra.

A fluorescent polymer that forms a FRET pair with the drug permits measurement of the drug-polymer intermolecular distance for DDS (Ilevbare et al., 2013; Lakowicz, 2006a) since the R_0 term is in the range of biomacromolecule size (30-60 Å). FRET is highly useful as close proximity facilitates detection of drug-polymer interactions — believed to be a key element influencing drug crystallization and nucleation kinetics (Ilevbare et al., 2013). Thus, inhibition of drug crystallization can be confirmed with real-time fluorescent labeling techniques that reinforce to comparative nucleation induction time data (Ilevbare et al., 2013). Furthermore, photobleaching experiments can establish whether changes in fluorescence are due to FRET phenomena. This is visualized by confocal microscopy by comparing pre- and post-photobleaching, indicating FRET with bleaching from the acceptor and recovery of emission via the donor chromophore (Behanna et al., 2007).

Fluorescence spectroscopy has become the gold standard for analysis of tagged biomolecules as fluorescence detection is highly sensitive, offering the ability to detect polymers containing low fluorophore loadings (degree of substitution (DS) = 0.05-0.001) with minimal

depolymerization (de Belder & Wik, 1975). Multiple labels can be applied simultaneously if they do not spectrally overlap with FRET pairs, allowing high-throughput and automated instrumentation. Currently, radiolabeling methods only allow simultaneous analysis for up to two isotopes and require special instrumentation for analysis (e.g., dual channel detectors or imaging screens for isotopes (Belovolova & Glushkov, 2021), e.g., ^{3}H and ^{33}P). There are some potential disadvantages to fluorescent labeling compared to radiolabeling, such as toxicity, more significant structure modification, and spectral overlap with autofluorescent samples.

Several PS have been successfully fluorescently labeled and analyzed using UV-VIS, near-infrared (NIR) and fluorescence spectroscopic methods (J. M. Pereira, 2013; Wu et al., 2015), confocal laser scanning microscopy, fluorescent *in situ* hybridization, and flow cytometry (Adav et al., 2010; Behanna et al., 2007; Pramod, Takamura, Chaphekar, Balasubramanian, & Jayakannan, 2012). These methods can qualitatively identify tagged species and quantitatively map their biodistributions, biological mechanisms, intermolecular interactions, and thus, their roles in biologically significant events. This information lets one monitor the controlled release of drugs from delivery systems. This review aims to showcase the development of labeling techniques for PS derivatives, their selection, tagging methodologies, as well as their applications.

1.2 Fluorophore Selection

A fluorophore is a molecular entity that is excited by absorption of electromagnetic radiation of a certain wavelength, followed by re-emission of a lower energy photon that corresponds to a longer wavelength. Fluorophores can be classified as either intrinsic or extrinsic, both of which possess conjugated π systems (polyaromatic hydrocarbons and / or heterocycles). Some common fluorophores are depicted in **Fig. 2.2**. Intrinsic fluorophores fluoresce in their native form, while

extrinsic fluorophores fluoresce because an external fluorophore has been appended to them.

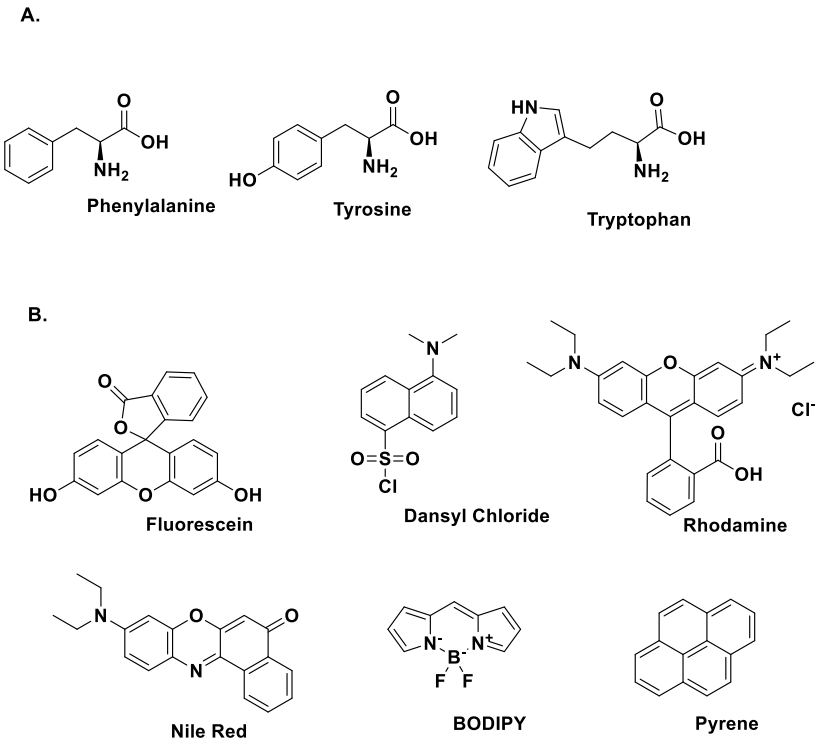

Figure 2.2: Common fluorophores **A.** Intrinsic and **B.** Extrinsic

Intrinsic fluorophores found in nature include aromatic amino acid residues (**Fig. 2.2A**), flavins, and chlorophyll. Extrinsic fluorophores give fluorescence to compounds that lack the ability to fluoresce, or modify the sample's spectral properties if intrinsic fluorescence is inadequate or undesirable for the experimental design (Lakowicz, 2006a). The remainder of this review will focus on extrinsic fluorophores.

Ideal characteristics for a polysaccharide-linked fluorophore include a stable chemical linkage, high quantum yields and molar absorptivities, and the ability to operate at longer wavelength - a safer range resulting in reduced sample photodecomposition compared to using high energy radiation (Adav et al., 2010). Ideal tags have excitation maxima accessible using simple light sources (laser diodes instead of LED) (Lakowicz, 2006a), chemical/photochemical stability, and readily accessible reactive groups to directly modify the PS of interest (Briggs et

al., 1997). Should the polymer of interest contain an intrinsic fluorophore, the dye selected must possess a fluorescent profile which spectrally overlaps if desired for FRET measurements. Biological interferences caused by the tag's presence must be taken into account in order to consider its utility for the experimental objective. For example, the fluorophore could alter metabolism or transport in undesirable ways (Adav et al., 2010). The environment around the biomolecule of interest (i.e., its polarity or pH) can be probed with environment-sensitive fluorophores, divulging whether the molecule is in a hydrophobic or polar environment (Ilevbare et al., 2013; Lakowicz, 2006a). In order for any of these traits to be measurable, the fluorophore must be delivered and remain at its targeted destination long enough to be analyzed (Adav et al., 2010).

Fluorophores can be attached to biomolecules covalently, or through non-covalent associations via hydrophobic or electrostatic interactions (Lakowicz, 2006a; Webber, 1999). Modified fluorophores containing reactive electrophilic groups can undergo coupling to amines or undergo addition by nucleophiles to target macromolecules (**Fig. 2.3A)** (Adav et al., 2010; Waggoner, 1995), while those in **Fig. 2.3B** can react with thiols (Lakowicz, 2006a). Fluorescent alkyl halides can esterify carboxylic acid derivatives and react with thiols (Wiederschain, 2011). BODIPY 493/503 MeBr and 5-bromomethylfluorescein have the strongest fluorescence and absorptivities of any carboxyl derivative described to date (Wiederschain, 2011).

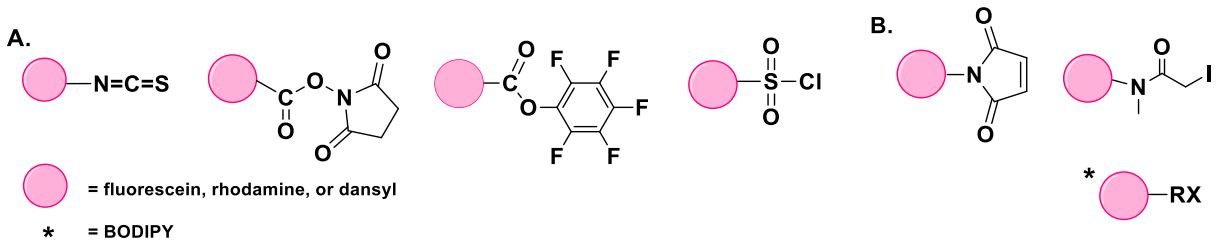

Figure 2.3. Common Reactive Fluorophores. A. Isothiocyanates (ITC), succinimidyl (NHS) and pentafluorophenyl esters, and sulfonyl chlorides, **B.** Maleimide, Iodoacetamide, bromoacetamide, and alkyl halides (RX).

Dansyl groups offer sensitivity to polar solvents, long emission maxima (520 nm), and long fluorescence lifetimes, but have short wavelength absorption maxima (350 nm). Non-solvatochromic dyes that tend to self-quench include fluorescein, Rh, and BODIPY. Fluorescein and Rh are attractive labels as they are sensitive (indicated by their high molar extinction coefficients, 80,000 $\frac{M}{cm}$), high quantum yields, and operate in long excitation (480 nm and 600 nm) and emission wavelength regions (510 and 615 nm), respectively (Lakowicz, 2006a). However, these dyes are being replaced with BODIPYs due to reduced self-quenching, higher quantum yields, and narrower emission spectra which permit greater resolution from other dyes (Lakowicz, 2006a). Unfortunately, BODIPYs have small Stokes shifts that can cause self-quenching from dye-dye energy transfers at sufficiently close Förster distances.

Although several environmental probes are available, the most well-studied is pyrene. Pyrene can probe structural changes, such as the concentration at which polymers begin to assemble or disassemble. The various microdomains of a nonlinear polymer chain, such as hydrophilic vs. hydrophobic, can begin to self-associate as a response to changes in the local environment. For example, changes in polarity or pH can lead to a shift in the concentration of hydrophobic domains, causing a shift in the emission spectrum of pyrene, specifically if there is an increase in

the concentration of a hydrophobic domains which begin to solubilize the probe. This point is defined as the critical aggregation concentration (CAC), critical micelle concentration (CMC), or critical vesicle concentration (CVC). Pyrene's characteristic emission spectrum provides values for the ratio of fluorescence intensities at 375 nm and 386 nm ($I_I/I_{III} = I_{375}/I_{386}$) for varying concentrations of sample. These ratios were plotted vs. log [polymer], and indicate the CVC at the instantaneous initial increase of of I_I/I_{III} (Belovolova, Glushkov, Vinogradov, Babintsev, & Golovanov, 2009; Pramod et al., 2012; Webber, 1999).

2. Applications

2.1 Toxic and heavy metal ion sensors

Decontaminating the environment is a critical global dilemma. Serious health concerns can emerge from organic and inorganic impurities that remain even after passage through a wastewater treatment plant, thereby reaching bodies of water and even downstream (to direct water consumers, to crops, and to other food sources). Chief sources of pollution from effluents include heavy metal ions and dyes from textile industries. Current decontamination methods such as hybrid ion exchange materials, activated carbon, or electrocoagulation are simply not always fully effective, or cost effective. Environmentally friendly, economical, and benign materials are thus highly attractive sources as antifoulants to remove heavy-metal toxins or dyes that are otherwise not degradable.

Chitosan is a randomly alternating linear polymer with β-(1→4) -linked D-glucosamine and *N*-acetyl-D-glucosamine units, derived from natural chitin found in crustacean exoskeletons by alkaline deacetylation. It is also found as a natural polymer in fungal cell walls (Abo Elsoud & El Kady, 2019). Chitosans have gained attention as abundant, renewable, and relatively nontoxic sources for an array of applications including in pesticides (Elsherbiny, Galal,

Ghoneem, & Salahuddin, 2022), paint coatings, biomedical products (wound dressings and antibacterial (Huang, Dan, Dan, & Zhao, 2019; Xin Meng et al., 2010)), hydrogels, and as excellent metal ion (Gabris et al., 2022; Wan Ngah, Teong, & Hanafiah, 2011) and dye adsorbents (F. A. R. Pereira et al., 2017; Shahadat et al., 2022).

Chitosan has served as an eco-friendly clarifying agent with excellent chelating ability and high affinity for heavy metal ions including mercury (A Bejan, Doroftei, Cheng, & Marin, 2020; L. Li et al., 2018b), arsenic(V) (Gabris et al., 2022), chromium (Wani, Khan, Manea, Salem, & Shahadat, 2021), copper (Li, F. et al., 2020), and iron (Virmani, Deshpande, Pathan, & Jayakannan, 2021). Chitosan's multifunctionality also permits binding to effluent dyes.

Recently, Bejan et al., 2018 synthesized a novel UV absorbing gel (xerogel) via Schiff-base chemistry linking the nontoxic formyl-phenothiazine and chitosan. The xerogel removes 15 environmentally threatening metals (Na^{+}, K^{+}, Ca^{2+}, Sr^{2+}, Ba^{2+}, Cr^{3+}, Mn^{2+}, Co^{2+}, Ni^{2+}, Cu^{2+}, Zn^{2+}, Cd^{2+}, Pb^{2+}, Eu^{3+}, Hg^{2+}) with high affinity and sensitivity to mercury (0.001 ppm) (Bejan et al., 2020). This porous xerogel displayed bathochromism, with a red shift when bound to mercury (yellow-green to green-yellow) along with changes in morphology to a rubber-like material. Swelling behavior was influenced by metal chelation, with an observed reduction for mass equilibrium swelling (20.8 when bound to just H, vs 11.8 for H-Ba).

Li et al., 2018 prepared magnetic fluorescent nanoparticles with chitosan as a selective mercury (II) adsorbent with low detection limits of 12.43 nM. This recyclable system has chitosan as the shell, Fe_3O_4 nanoparticles as the core, and carbon dots (CDs) as the fluorescent probe, with only slight losses in adsorption (13%) and photoluminescence (5%) after recycling 5 times. This system has a well-defined structure with adsorption capacity of 110.52 mg/g, and quenches when Hg couples to the antifoulants as supported by the photoluminescence spectra.

Nanoaggregate polyelectrolytes of hyaluronic acid and/or chitosan complexes with luminescent lanthanide were recently designed to capture Eu^{3+} (Guo et al., 2018). The lanthanide-induced polysaccharide aggregates have employed either a single complex with one polyelectrolyte (polyanionic hyaluronic acid), or two oppositely charged polyelectrolytes (chitosan and hyaluronic acid). Fluorescence was significantly enhanced when using thenoyltrifluoroacetone (TTA) and 1,10-phenanthroline monohydrate (Phen) as ligands for Eu^{3+}.

A new fluorescent cotton fabric smart material with alginate-silver nanoparticles (AgNP) simultaneously detects bacteria (*Escherichia coli* and *Staphylococcus aureus*) while also removing transition metals (Na^{+}, K^{+}, Ca^{2+}, Cu^{2+}, and Zn^{2+}) that are toxic at elevated concentrations (Li et al., 2022). Silver nanoparticles are known to have antimicrobial properties, but are also toxic to humans and other organisms at higher concentrations. In contrast to an uncoated rare-earth complex, sodium alginate provided a supportive matrix for the stable, layer-by-layer formation of uniform sized nanoparticles (Nowak et al., 2021) with reduced toxicity confirmed by the cytochemical toxicity assay (MCC). Sodium alginate-AgNP and cotton were bonded via etherification with pentaerythritol. (Horrocks, Kandola, Davies, Zhang, & Padbury, 2005), and 3-chloro-2-hydroxypropyl trimethylammonium chloride enhanced binding between cotton and dye (Arivithamani & Giri Dev, 2017). Meanwhile, Eu^{3+}/TTA/Phen ligands induced nanoparticle assembly and enhanced fluorescence. This wearable fabric with relatively enhanced compatible technology allows straightforward evaluation by non-experts by exhibiting a strong red fluorescence that quenches when detecting increasing concentrations of toxin or metal. While unable to completely prevent the growth of bacteria, the smart fabric displayed antimicrobial activity by producing a 5 mm inhibition zone for *E. coli*, and 8 mm for *S. aureus*.

Water-soluble nitrogen-doped fluorescent CDs offer a straightforward and economical synthetic route to fluorescent materials with high performance, via one-pot carbonization of natural peach gum PS and ethylenediamine. This product offers enhanced quantum yields (23 % increase) vs. their undoped forms, low cytotoxicity, and fluorescence stability at various pH and ionic strength values, with rapid, selective, sensitive sensing of Au^{3+} ions. Au^{3+} sensing occurs via quenching effects, offering one of the lowest detection limits (6.4×10^{-8} M) in biological environments and river water. These traits make nitrogen-doped CDs promising, enhanced, and label-free alternatives for bioimaging and sensors (Liao, Cheng, & Zhou, 2016).

2.2 Enzyme /Conjugate Screening Assays: Localization and Biological Role Determination

An important advantage of fluorescent labeling is the ability to distinguish modified PS in the presence of endogenous PS (e.g. mannan, dextran, heparin, chondroitin sulfate, fucoidan). This approach permits localizing and quantifying cell surface proteins that bind to carbohydrates (lectins) (Adav et al., 2010; Glabe, Harty, & Rosen, 1983). Dextrans have been tagged with FITC and its *N*-fluoresceinyl thiocarbamate and fluoresceinyl triazine derivatives (**Scheme 2.1A-2.1B**) to monitor cellular location of endosomes in kidneys (Lencer, Weyer, Verkman, Ausiello, & Brown, 1990), blood-brain barrier permeability (R. Natarajan, Northrop, & Yamamoto, 2017), gut barrier integrity (Gerkins, Hajjar, Oliero, & Santos, 2022), and controlled release (e.g. nasal (Ohtake, Natsume, Ueda, & Morimoto, 2002) and dermal (Panda et al., 2022)). However, this FITC coupling strategy (**Scheme 2.1**) is not suitable for sulfated PS since conditions require solvolysis which promotes desulfation (Glabe et al., 1983). Stable linkages have been achieved with FITC-derivatized hyaluronic acids via isocyanate condensation, which can be extended to other carboxyl-containing PS (de Belder & Wik, 1975). Early fluorescein-PS derivatives

(mannan, dextran, heparin, chondroitin sulfate and fucoidan) prepared by Glabe et al., (1983) with minimally altered structure and therefore retaining of structure-properties. This approach required pre-activation of the PS using cyanogen bromide (CNBr), followed by coupling with fluorescein amine (**Scheme 2.1B**). Effects of pH, incubation time, and equivalents of CNBr were found to impact the DS (Glabe et al., 1983).

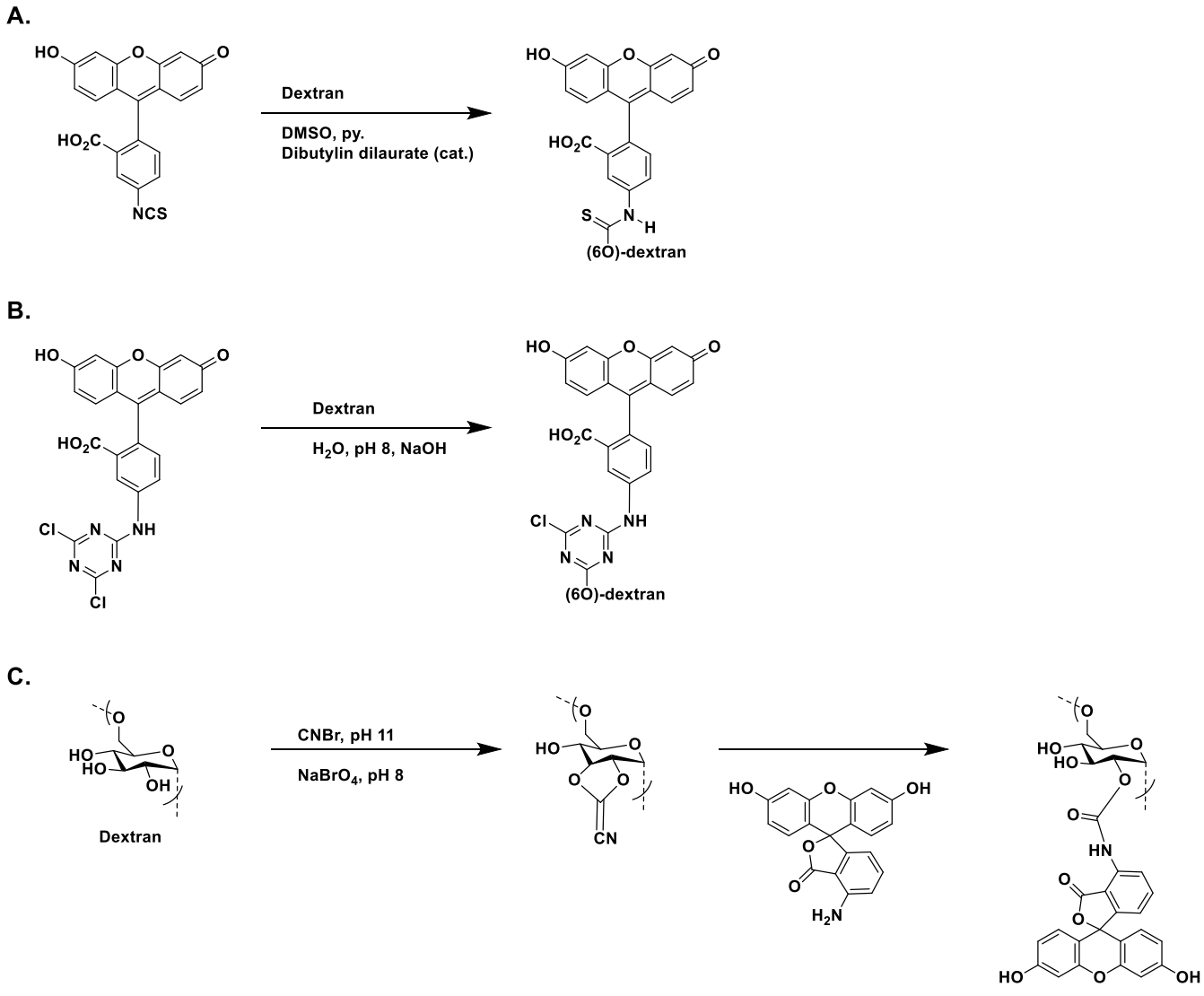

Scheme 2.1: Fluorescein-dextran tagging method: A) with FITC, B) with triazine derivative (de Belder & Wik, 1975), and C) activation of dextran with CNBr and coupled to fluoresceinamine (Glabe et al., 1983)

The inhibiting activity of the resulting fluorescent PS was unaffected relative to underivatized PS (fucoidan, mannan, and heparin). Successes using this method include conservation of PS inhibiting activity for lectin-mediated hemagglutination and improved stability profiles (Glabe et al., 1983). The latter was determined by the absence of detectable free fluorescein post-incubation 3 months at -10°C, 4°C for 1 week, and for 2 days at 22°C under alkaline conditions (up to pH 8) which are known to promote uncoupling. Product stability is postulated to result partially from lower p*K* values of fluoresceinamine's aromatic amine groups relative to those of previously studied saturated alkylamine groups. Retention of inhibitory activity from the lectin conjugates and site binding onto the cellular monolayer suggests their potential utility as cytochemical probes to study cell surface and PS interactions (Glabe et al., 1983).

Tags have been introduced to polymeric substances and exo-enzymes in bioaggregates to identify and quantify their significance in biological processes by generating aggregate distribution profiles (Adav et al., 2010). Localization and distribution of extracellular polymeric components were visualized by combining multiple color staining using fluorophores with confocal laser scanning microscopy, fluorescent *in situ* hybridization, and flow cytometry. Glycoconjugates of glycoproteins in bioaggregates have been stained using a FITC–labeled lectin, Concanavalin-A (Cerca, Oliveira, & Azeredo, 2007; De Beer, O'Flaharty, Thaveesri, Lens, & Verstraete, 1996; Lawrence, Neu, & Swerhone, 1998; Michael & Smith, 1995; Neu, 2000; Wang Yu Liu Joo-Hwa Tay, 2005). On/off quenching abilities of FITC-Concanavalin-A were discovered, as the FITC-Con-A-glycogen conjugate formation induces quenching (off), while dequenching (on) when disassembly is provoked by adding to the conjugate solution (Sato

& Anzai, 2006). α-Mannopyranosyl and α-glucopyranosyl residues in bioaggregates have been stained with Con A-rhodamine conjugates (Adav et al., 2010; M Y Chen, Lee, & Tay, 2007; Ming Yuan Chen, Lee, Tay, & Show, 2007). Calcofluor White (CW), a fluorescence brightener, has been applied to β-linked PS for their identification and quantification in bioaggregates. CW staining techniques have characterized the distribution of three different PS in biofilms (M Y Chen et al., 2007). However, despite the high affinity of CW for cellulose and chitin, it may also interact with other PS (i.e., sialic acids, terminal glycan residues and lectins), creating the possibility of off-target results.

Smart polysaccharides, molecular rulers:

Aggregation of co-assembled peptide amphiphile (PA) nanofibers (as donors) has been probed with commercial fluorescein-tagged heparin (the acceptor) (Behanna et al., 2007). This oppositely charged co-assembly consists of a bioactive heparin-selective binding epitope, and a non-bioactive stilbene tagged PA. The latter species can be viewed as an intrinsic fluorophore, as it contains branched stilbene. When the co-assembly contains a dilute chromophore component and is mixed with commercially tagged heparin, FRET indicates binding by increased fluorescein emission and quenched chromophoric PA emission. Specific vs. non-specific binding was confirmed, with ratio of acceptor to donor emission intensity plots for the PA pair containing an epitope and an epitope lacking PA pair control. Greater emissions were observed for the epitope-containing pair, indicating FRET events (as opposed to aggregate entanglement inducing spectral changes). Furthermore, FRET-induced fluorescent changes were confirmed by donor fluorescence recovery in photobleaching experiments. Thus, these epitope-containing probes can be used to sense and study PS interactions with other molecules (Behanna et al., 2007).

2.3 DDS, controlled release, and sensors

There are several routes available for drug administration including intravenous, inhalation, and transdermal, but the most patient-accepted route is oral administration. Development of high-performance DDS is motivated by the low bioavailability of many orally ingested drugs. Promising designs with enhanced fluorescence profiles for monitoring DDS, sensing, and controlled release have been observed in crosslinked non-nanoencapsulated systems and nanotherapeutics, including the naturally photoluminescent quantum dots.

2.3.1 Non-encapsulated DDS

A straightforward water-based method for amine grafting onto PS has been performed on the backbone of seaweed PS (including alginate, kappa-carrageenan, and agarose, **Fig. 2.4**) permitting observation of the influence of the amines on fluorogenic properties (Chhatbar et al., 2011; Oza, Meena, Prasad, Paul, & Siddhanta, 2010; Oza, Meena, & Siddhanta, 2012; Oza, Prasad, & Siddhanta, 2012; Siddhanta, Sanandiya, Chejara, & Kondaveeti, 2015). Since amides typically possess strong quenching abilities (Lukomska, Rzeska, Malicka, & Wiczk, 2001; Mrozek, Banecki, Karolczak, & Wiczk, 2005), it was surprising that fluorescent alginate-amide derivatives were afforded upon crosslinking (Chhatbar et al., 2011). This emerging fluorescence is thought to result from π-π^* transitions from the newly introduced extended conjugated system when crosslinked with genipin (Chhatbar et al., 2011). This rapid and environmentally friendly method can be used even under neat conditions (Perreux, Loupy, & Volatron, 2002).

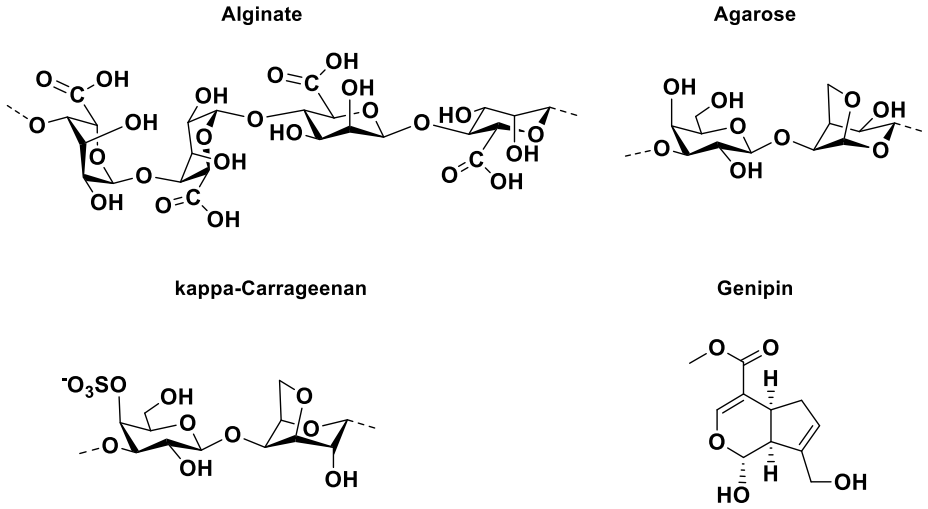

Figure 2.4: PS used in microwave amidations employing the natural crosslinker genipin

Apart from the amide of alginate and ethylenediamine, other alginate – amide derivatives (hydrazine, ethylenediamine, hexanediamine and 1,4-cyclohexanediamine) exhibit fluorescence only after crosslinking with genipin (**Scheme 2.2B**). Increased fluorescence emissions were observed when the appended diamines had shorter oligo(methylene) spacers (**Fig. 2.5A**). Thus, alginate hydrazide was the most intensely fluorescent of this series when crosslinked with genipin, while the alginate amide with ethylenediamine fluoresced most intensely when not crosslinked (Chhatbar et al., 2011).

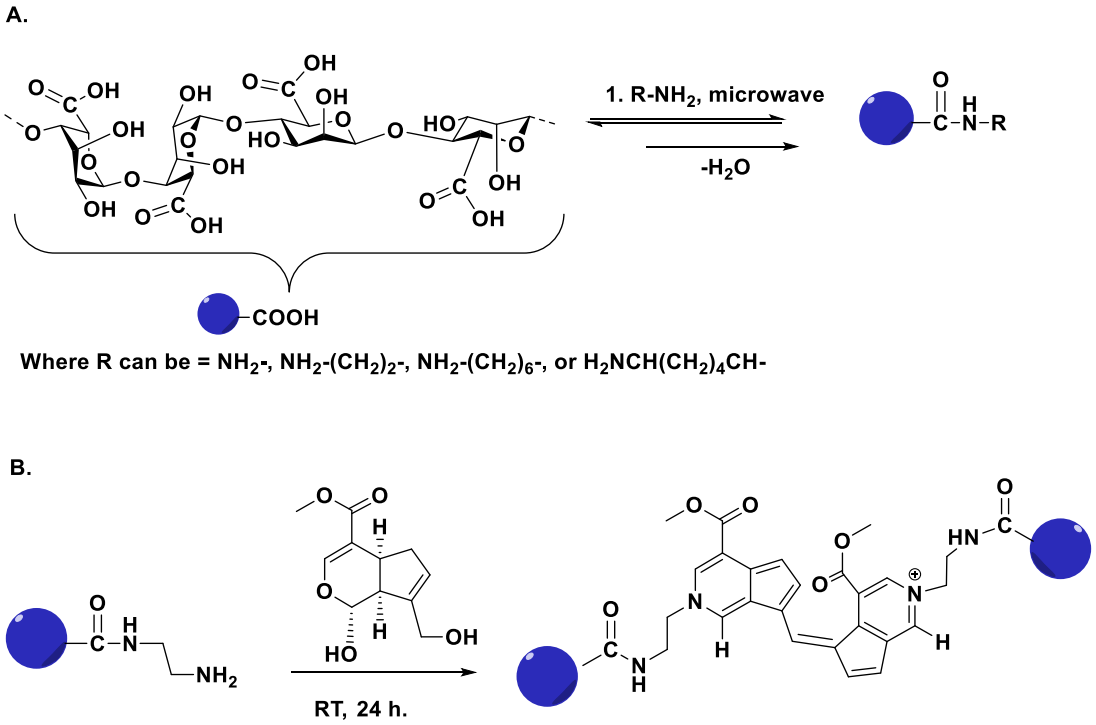

Scheme 2.2: A. Synthetic route for alginate amide derivatives **B.** Sample genipin crosslinking step for alginate-ethylenediamine derivative (Chhatbar et al., 2011).

A)

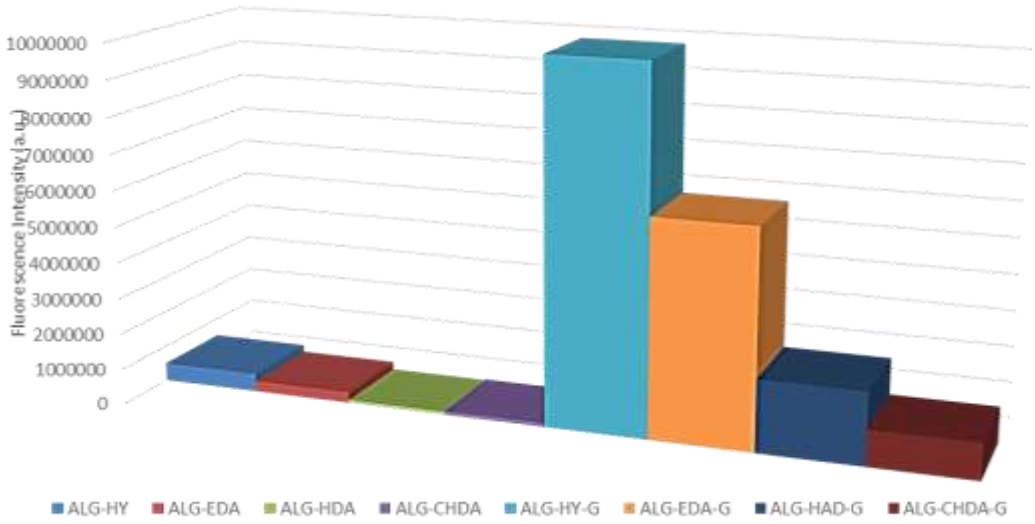

B)

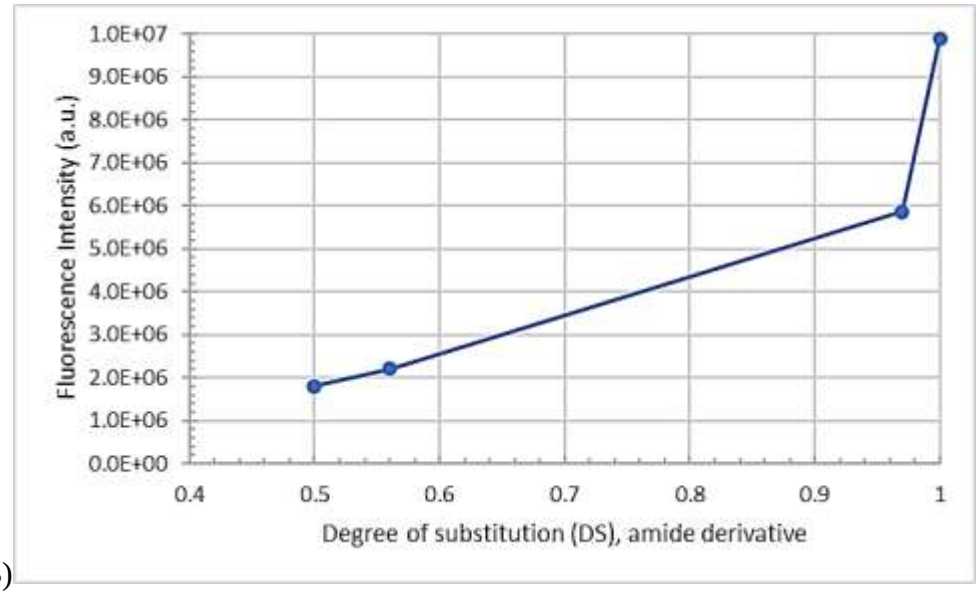

Figure 2.5: (A) Fluorescence intensity of alginate (ALG) amide derivatives (hydrazine (HY), ethylenediamine (EDA), hexamethylenediamine (HDA), 1, 4-cyclohexanediamine (CHDA), and ALG amide-genipin crosslinked analogs (G)). **(B)** Fluorescence Intensity vs. DS of amide derivatives. Figures adapted from Chhatbar et al., (2011) and Siddhanta et al., 2015)(2015).

Crosslinked alginate derivatives containing the shortest difunctional amines studied, hydrazine and ethylenediamine, and higher DS (amide) produced the greatest emission intensities, producing an inverse correlation between the length of oligo(methylene) units and

fluorescence emission (**Fig. 2.5B**) (Chhatbar et al., 2011). The observed weakened fluorescence for this crosslinked series as -CH_2- units increase is in agreement with diminished electron acceptor ability resulting from steric and inductive effects, caused by shortened spacer units (Braun, Rettig, Delmond, Létard, & Lapouyade, 1997). The dual fluorescence observed from alginate-ethylenediamine and the other crosslinked products (except alginate hydrazide) aligns with quenching induced via the torsion of the dimethylamino group with transfer of an electron (i.e., twisted intramolecular charge transfer (TICT) mechanism model), and nonradiative deactivation of the amide's n-π^*transition energy states. Thus, amide acceptor ability can be tuned via alkyl group selection (Braun et al., 1997).

Labeled seaweed PS resulting from the grafting of nucleobases offer the ability to sense environments in biomedical applications (**Scheme 2.3)**. Published examples include nucleobase modified agarose and kappa-carrageenan (Oza et al., 2010; Oza, Meena, et al., 2012; Oza, Prasad, et al., 2012).

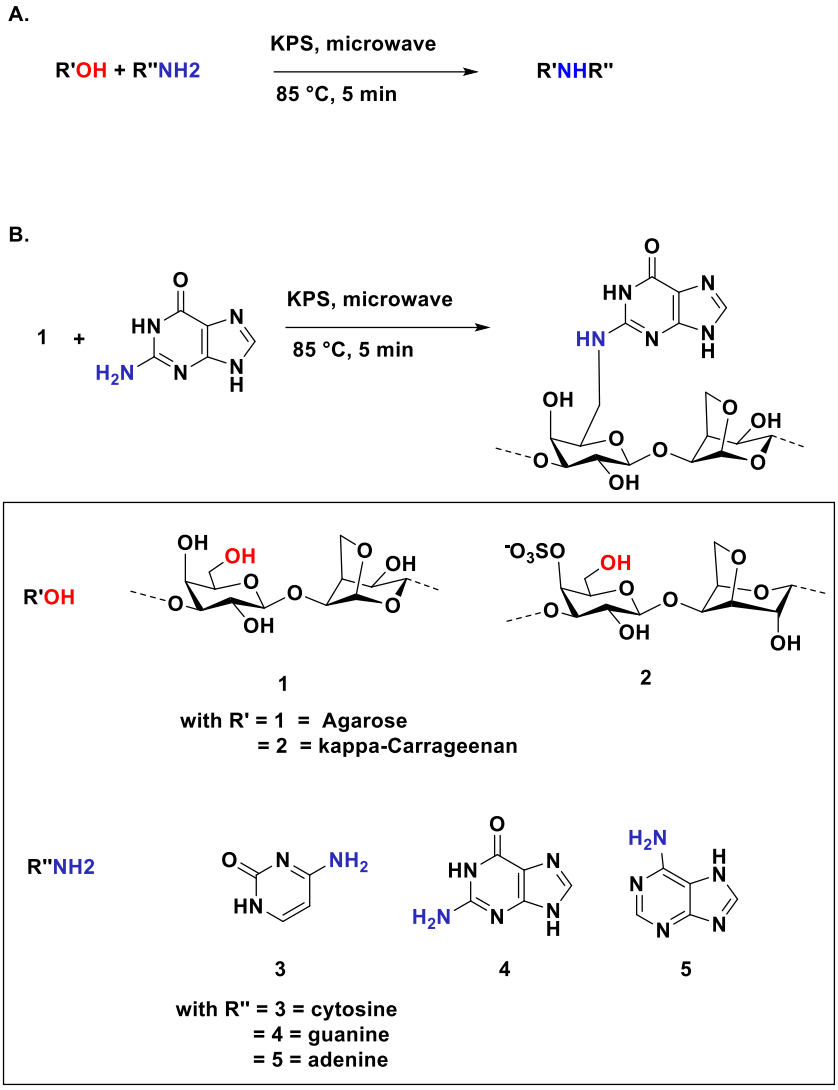

Scheme 2.3: General reaction scheme for **A.** nucleobase grafting onto agarose or kappa-carrageenan initiated by potassium persulfate (KPS), and **B.** a sample reaction.

These nucleobase-grafted PS were prepared using potassium persulfate as an initiator. When dye content is held at equal concentrations, the grafted products offered increased fluorescence intensities relative to the already fluorescent, free nucleobases (control). At the emission maximum, agarose grafted with guanine, cytosine, or adenine showed increased fluorescence intensity by 85%, 143%, and 30% vs. agarose, respectively, while intensities of K-carrageenan grafted with adenine or cytosine increased by 40% and 81% vs. K-carrageenan itself,

respectively. In contrast to guanine and cytosine, the intensity enhancement from the grafted adenine analogs were similar when comparing to either controls at equal or higher dye content. Both cases produced greater emission intensities for agarose vs. κ-carrageenan.

The fluorescence enhancement in solutions containing free dye at higher concentration relative to the grafted analogs can be attributed to diminished inter-nucleobase interactions (Oza et al., 2010; Oza, Meena, et al., 2012; Oza, Prasad, et al., 2012). This is because quenching likely occurs from stronger intermolecular interactions induced by greater concentrations (Callis, 1979), as was observed for higher concentrations of free nucleobase solutions. Reduced emission from adenine was attributed to the absence of a carbonyl group in contrast to guanine and cytosine, and π-π* transitions arising from adenine's increased nitrogen content. The former was unexpected since carbonyl-containing compounds typically quench in the presence of acidic proton sources and π-electron systems (Oza et al., 2010). Thus, greater emission from cytosine and guanine may be due to the carbonyl's rigid position which prevents internal proton transfers that would otherwise result in quenching (Oza, Meena, et al., 2012). This effect is in agreement with reported emissions of grafted guanine and cytosine compared to the free dye at comparable concentrations, partly from participation of fluorescence emissions from water and dilute aqueous media in PS-water matrices (Belovolova & Glushkov, 2021; Kondaveeti, Mehta, & Siddhanta, 2014).

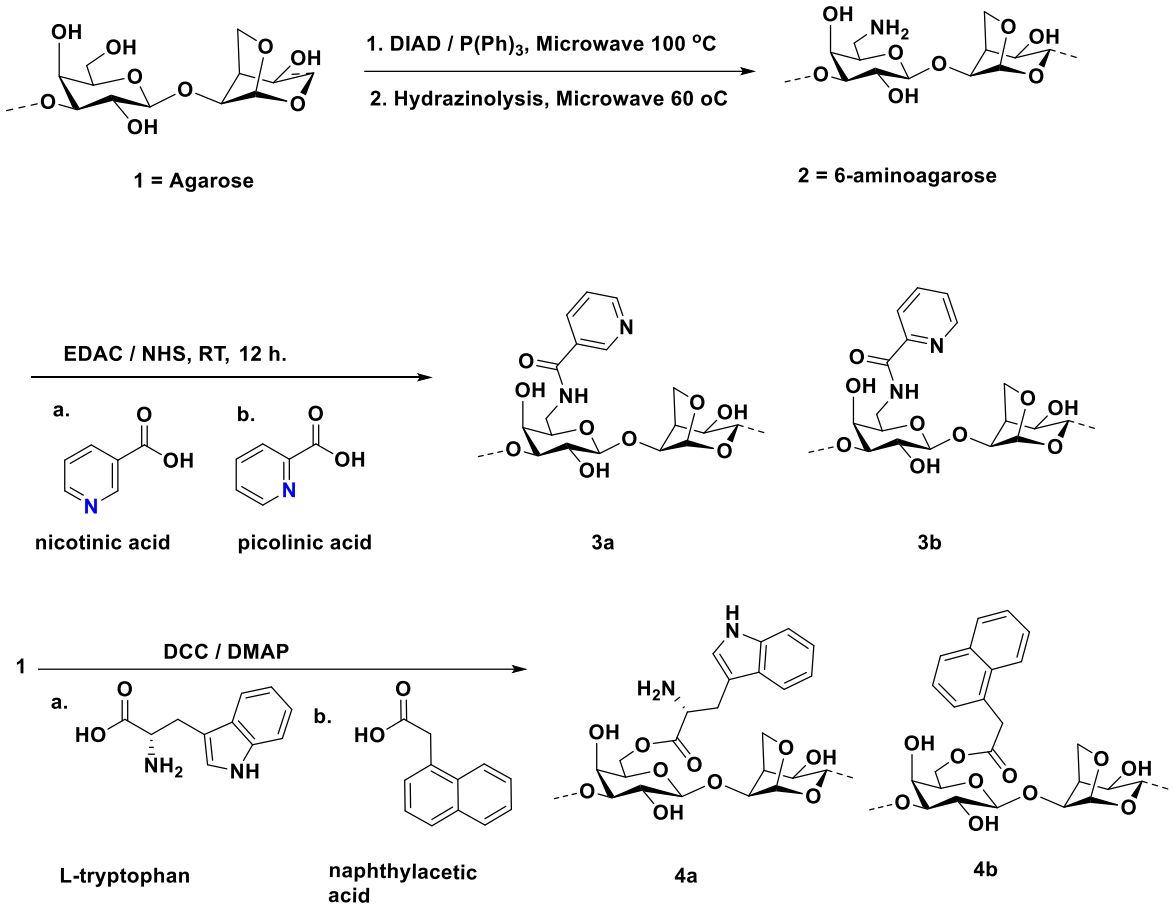

Scheme 2.4: Synthesis of 6-amino agarose (2), agarose amides: picolinic acid (3a), and nicotinic acid (3b), or agarose esters: L-tryptophan (4a), and 1-naphthylacetic acid (4b).

Other fluorescent labeling reactions of agarose are summarized in **Scheme 2.4**. Agarose has been linked with phthalimide to produce 6-deoxy-6-phthalimidoagarose, with subsequent removal of the phthaloyl protecting group by condensation with hydrazine hydrate. This method of introducing an accessible and protonated amine is promising for use in gene and drug delivery systems, creating the potential to derivatize 6-amino-6-deoxyagarose and other PS into polycationic polymers (Samal et al., 2012; Siddhanta et al., 2015). Fluorescence intensities of genipin-crosslinked 6-amino-6-deoxyagarose (produced similarly as shown in **Scheme 2.2, B**)

with picolinic and nicotinic acid were increased vs. free picolinic and nicotinic acids (Kondaveeti et al., 2014).

Fluorescent labels have been introduced by esterification of agarose catalyzed by carbodiimides. Fluorescent agarose-L-tryptophan ester hydrogels synthesized using DCC/DMAP catalyst produced increased fluorescence emissions vs. free tryptophan. The corresponding crosslinked genipin hydrogels were stable under ambient conditions and over a wide pH range (Kondaveeti, Chejara, & Siddhanta, 2013). Agarose has been esterified to append fluorescent 6-*O*-naphthylacetyl moieties using DCC/DMAP. This method shows promise as a sensor that controls release of the plant growth regulator, naphthyl acetic acid, in hydrolytic conditions (Kondaveeti et al., 2013).

2.3.2 Nanotherapeutic Systems

Quercetin is a highly crystalline natural flavonoid which has been explored as a drug candidate. Both research studies and any clinical applications are impeded by its low bioavailability, caused in part by its poor water solubility (Gilley et al., 2017; Li et al., 2013). Zhou et al., 2022 employed a novel encapsulation structure with a low molecular weight chitosan nanoparticle composite as a DDS with the motivation to invoke antimicrobial properties, impart solubility, and thus enhance bioavailability. Chitosan formed uniform nanoparticles under acidic conditions; the nanoparticles were subsequently loaded with quercetin using sodium tripolyphosphate as crosslinker. The chitosan amine groups were then functionalized with FITC via EDC amide coupling to enable monitoring of antimicrobial properties towards *E. coli* using the Oxford cup method. The latter method is a standard test used to determine bacteriostatic properties, measured by how well the nanomaterial inhibits the spread of *E. coli* as determined by measuring colony diameter on a Petri dish. The further photoluminescence is observed from

the sample spot, the less bacteriostatic is the material. Chitosan-quercetin drug-loaded nanoparticle spot diameter was equal to the inhibition zone, indicating highly successful antimicrobial performance. Chitosan-FITC nanoparticles have promise for tracking drug release and illuminating release mechanism.

Renewable polymersomes, which can load water-soluble or lipophilic drugs, were designed for cancer treatment using dextran, 3-pentadecylphenol, and tetraphenylethylene (TPE) (Virmani et al., 2021). This unique assembly manipulates FRET as a turn-off probe with the energy transfer between the aggregation induced emission polymersome host, TPE (donor), and encapsulated DOX (red luminescent acceptor) to detect breast cancer cells (MCF 7 cancer line). This phenomenon allows tracking DOX release kinetics, and for the first time, tracking the DDS within cells. Real-time enzymatic cleavage (esterase with higher cleavage efficiency vs. papain, trypsin, α-chymotrypsin, and glutathione) of the polymersome was observed with live-cell confocal microscopy by monitoring the restoration of the blue-luminescent signal as they 'turn-on', with DOX (in nucleus) and TPE (in lysosome) during endocytosis. Polymeric encapsulation was found to induce apopotosis to an extent equivalent to free DOX (80%). Separately, cisplatin was conjugated to the polymersome and maintained blue luminescence while turning off during endocytosis. A cisplatin-loaded scaffold presented enhanced efficiency vs. free cisplatin, inducing apoptosis at 95%.

Near infrared (NIR)-797 isothiocyanate (**Fig. 2.6**) has been used to label a bioreducible, disulfide-crosslinked heparin nanogel loaded with doxorubicin by conjugating ITC to heparin hydroxyl groups. Labeled heparin acts as a biomarker that can track the site and incidence of drug release monitored by *in vivo* real-time NIR fluorescent imaging and confocal microscopy. Tracking the fluorescent nanogel enables recording of time-dependent biodistributions as

average % of injected dose/gram wet tissue. This indicated long circulation times of the doxorubicin-loaded nanogel concentration in blood and effective targeting, since the nanogel concentration increased at the tumor site by two-fold within 24 hours of injection (Wu et al., 2015).

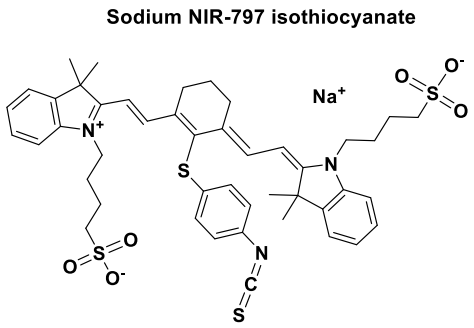

Figure 2.6: NIR-797-isothiocyanate

NIR-797-heparin nanogels were incubated in fetal bovine serum (FBS) at 37 °C in order to evaluate NIR-797 physiological stability by UV-Vis spectroscopy. Stability was confirmed by the absence of released NIR-797 in FBS, thus NIR-797-heparin was deemed a viable tag for heparin nanogels. The disulfide bond is reduced in the intracellular environment, effectively eliminating crosslinks in the heparin nanogel and selectively releasing the encapsulated drug into the cytosol (Wu et al., 2015).

Hollow nanocapsules with aqueous cores prepared by cross-metathesis (CM) were created for targeting the water-oil interface using dextran acrylate and biodegradable unsaturated poly(phosphoester)s (PPEs). The therapeutic target is conveniently unaffected since the reaction occurs at the interface, producing stable microemulsions which form defined and discrete nanocapsules. Dextran acrylate was prepared in-house to control hydrophobicity, targeting DS (acrylate) of 0.13-0.55. **Scheme 2.5** shows how one can target dye-tagging at either site of the nanocapsule: **2a)** externally coupling onto the capsule's surface, or **2b)** within the nanocapsule shell on the crosslinker's (PPE) pendent phosphoester. The latter uses a BODIPY derivative that

simultaneously acts as a chain terminating agent during polycondensation as, unlike **2b**, it lacks a terminal olefin (Malzahn et al., 2014).

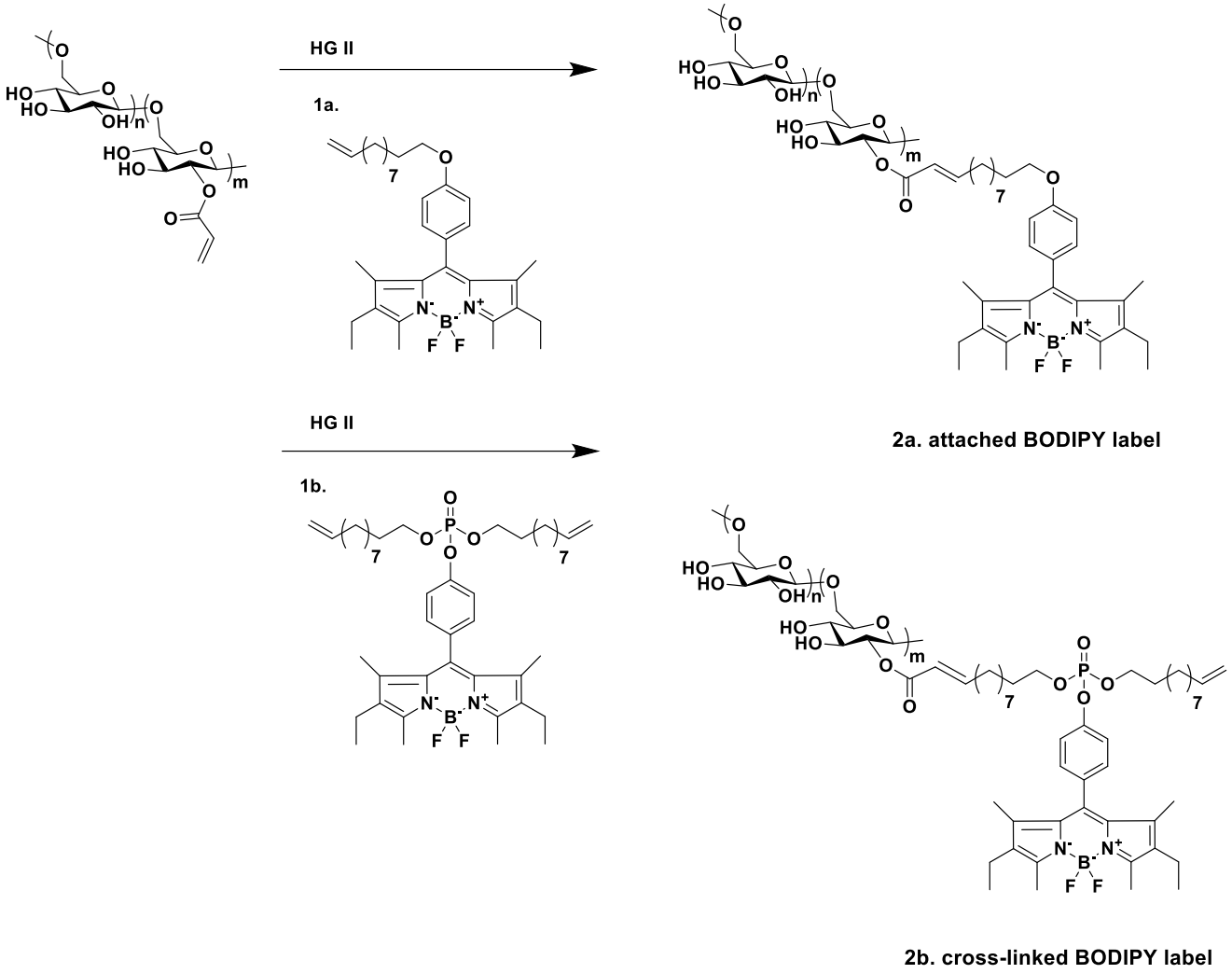

Scheme 2.5. CM of dextran acrylate using Hoveyda-Grubbs 2nd generation catalyst (HG II) to tag BODIPY onto **2a** capsule's surface, or with **2b** crosslinked phosphoester (Malzahn et al., 2014).

Bonding between the nanocapsules and dye was confirmed using UV/VIS and fluorescence, and fluorescence correlation spectroscopy confirmed covalent bonding. The crosslinked product was initially inferred by its insolubility in all common solvents—possibly an

undesirable trait for some drug-delivery applications. The versatility of this method is afforded through altering the olefin partners for CM either by using a different type of macromolecule for the type II olefin, or by varying the small molecule type I olefin. However, high conversion for CM has been reported for PS containing type I olefins tethered to type II olefin small molecules (Dong & Edgar, 2015; Dong, Mosquera-Giraldo, Taylor, & Edgar, 2016, 2017; Dong, Novo, Mosquera-Giraldo, Taylor, & Edgar, 2019; Xiangtao Meng & Edgar, 2015; Xiangtao Meng et al., 2014b; Novo et al., 2022). Promising applications of these biomolecule-loaded nanocapsules include targeted drug delivery and controlled release (Malzahn et al., 2014).

Amphiphilic dextran nanoscaffolds can selectively encapsulate hydrophilic and hydrophobic molecules for cellular drug delivery. This allows a PS-based vesicle to encapsulate either hydrophobic drugs in the shell, or water-soluble molecules in the core (**Fig. 2.7)** (Pramod et al., 2012).

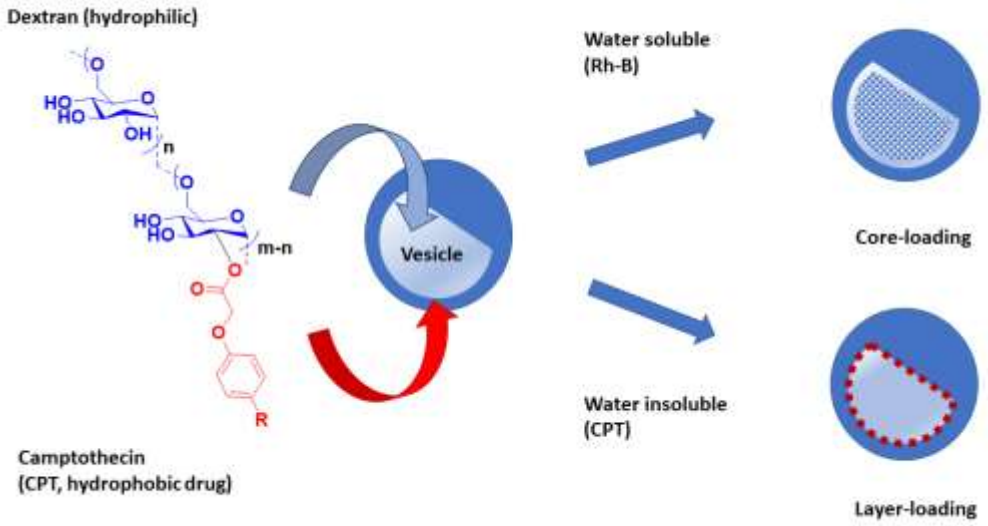

Figure 2.7. Dextran vesicular delivery of hydrophobic or hydrophilic molecules. Figure adapted from Pramod *et. al* . (2012).

This amphiphilic dextran derivative comprises a hydrophilic polymer backbone decorated with a hydrophobic tail (3-pentadecyl phenol (PDP), cardanol (CAR) or stearic acid (SA)), linked by an aliphatic ester. The amphiphilic character allows the polymer to assemble into vesicles in water or phosphate buffered saline via hydrophilic and hydrophobic interactions. The hydrophobic layer permits hydrophobic drug encapsulation, as its hydrophilic core can be loaded with hydrophilic drug. In physiological conditions, cytoplasmic esterase cleaves the ester linkage, resulting in rapid release of the encapsulated molecules. Molecules used in these loading experiments included the hydrophilic / water soluble Rhodamine-B and the hydrophobic polyaromatic anticancer drug, camptothecin (Pramod et al., 2012).

Rhodamine-B- and camptothecin-loaded vesicle uptake by mouse embryonic fibroblast cells was confirmed using confocal microscopy to produce fluorescence micrographs, demonstrating localization by comparing fluorescence intensity vs. cell location (Pramod et al., 2012). Dextran-PDP was able to deliver hydrophilic dye, Rh-B, as confirmed by its cellular uptake. The dye's strong emission profile also permitted direct visualization inside cells (Pramod et al., 2012). This methodology provides understanding of the endocytic cellular uptake mechanism and localization in healthy vs. cancer cells. The new and hydrolytically stable amphiphilic DDS design also allows simultaneous dual loading and delivery by encapsulation of both hydrophilic and hydrophobic drug molecules in a single nanoscaffold (Pramod et al., 2012). Stability against hydrolysis was enhanced by 10-fold for camptothecin-loaded polymer vs. free camptothecin which was confirmed by monitoring a red-shifted fluorescent absorbance relative to its non-encapsulated form in phosphate buffered saline.

2.3.3 Carbon dots (CDs)

Quantum dots are 1-10 nm, hydrophilic/polar materials, with adjustable particle size and high quantum yield, typically comprising C, Si, Se, or Cd (J. W. Zhou, Zou, Song, & Chen, 2018). CDs offer application opportunities across several fields, particularly in biolabeling and biosensing, as inherently luminescent materials. However, due to their high carbon content, several PS-CD tend to present low quantum yields and hydrophobicity in aqueous environments, thus making it desirable to enhance CD hydrophilicity (Ganguly et al., 2020; Richter et al., 2015).

Carboxymethyl chitosan quantum dots have been invented for lysozyme detection with high sensitivity (1.1-1.2 ng/mL). Zinc was found to reduce fluorescence detection limit to 0.031 ng/mL. This on-off sensor quenches as carboxymethyl chitosan is hydrolyzed upon the presence of lysozyme, triggering Zn^{2+} release while the quantum dots complex to lysozyme (Song et al., 2014). Quenching was observed with increasing temperature, reaction time, lower Zn^{2+} concentrations, and when decreasing in acidity in the range of pH 4-6.

Alginate nitrogen-doped CDs (urea) were thermally (microwave-induced) coupled via carbonization (Ganguly et al., 2020). EDAC-NHS was used to couple DOX onto alginate and explore *in vitro* release kinetics for controlled drug delivery. Enhanced solubility was observed as indicated by the transparent solution, imparted by the hydrophilicity of poly(anionic) alginate. Multiple labels can be employed with this material as it displays excitation dependence with a red shift in λ_{em} from 458 to 508 nm when increasing the λ_{ex} from 340 to 440 nm. The alginate urea carbon dot (AUCD) has blue fluorescence and 48% quantum yield that is rather appreciable compared to other CDs (Table 2.1). The AUCD is stable in a range of conditions, displaying minimal change in fluorescence intensity after 3 months at room temperature, at 4-25ºC in the

dark (9 months), and at different ionic strengths (0.25-2.5M NaCl). The lifetime of these AUCD (2.90 ns) permits use in biological and electronic applications.

Table 2.1. Studies of different carbon dots comparing quantum yields with respect to AUCD, adapted from Ganguly et al., (2020).

Precursor	**Quantum yield (%)**	**Reference**
Dopamine / cysteine	5.1	(Jana et al., 2016)
Polyethylene glycol (microwave)	16.0	(Jaiswal, Sankar Ghosh, & Chattopadhyay, 2011)
Polyethylene glycol (reflux)	45.1	(Kong et al., 2014)
Thioglycolic acid / CdCl	47.0	(Arivarasan, Sasikala, & Jayavel, 2014)
Mannose/ammonium citrate	9.80	(Weng et al., 2015)
Anthracite/water	20.0	(Hu, Wei, Chang, Trinchi, & Yang, 2016)
Glucosamine/water	16.8	(S. Liu, Zhao, Cheng, & Liu, 2015)
L-glutamic acid	17.8	(Yu, Xu, Tian, Lin, & Shi, 2016)
Alginate-urea	48.7	(Ganguly et al., 2020)

3. Conclusion

PS are important sustainable feedstocks as they are abundant, ecofriendly, often compatible with particular biological systems and circumstances, and are typically of low toxicity. The self-reporting abilities of smart fluorescent materials enable ease of detection with high specificity, selectivity, and sensitivity. Herein we highlight recent progress in stimulus-responsive labeled PS and how these promising biomaterials may be used to investigate and address emerging global challenges. PS-based carbon quantum dots are photoluminescent, high quantum yielding,

economical materials for optical, environmental protection, bioimaging and biosensing applications. Chitosan, alginate, cellulose, heparin, and hyaluronic acid have served as important and efficient clarifying agents for the environment by removing toxic dyes and heavy metal toxic ions (in some cases, efficiently removing 15 metal ions at a time). PS-based labels have been employed to localize and determine the biological roles of enzymes or lectins, as well as in bioimaging, sensing, and theranostic applications to illuminate potential mechanisms including drug release kinetics in drug delivery systems and in animal trials. We discussed effective approaches to append dyes onto PS with high conversion and fluorescence emissions with examples including cross-metathesis to probe drug loading, and facile coupling reactions with amides, esters, or protonated amines to decorate seaweed PS (alginate, kappa-carrageenan, and agarose) that have afforded highly fluorescent nucleobase or ester tagged materials that can be used in drug delivery or sensors. Use of newly developed turn-on/off probes such as polysaccharide-based smart fabrics or luminescent xerogels could be useful as straightforward, universal indicators to visually detect a broad array of hazards including pathogens such as bacteria (*E. coli*, *Staphylococcus aureus*) or viruses, or heavy metal ions. The economical, ecofriendly, smart materials discussed hold promise for large scale reduction of toxic waste, containment of pathogens, as well as common day-to-day use across disciplines (food packaging and anti-counterfeiting security). We hope this review will stimulate further interest in and synthesis of efficient, novel, fluorescently-labelled PS with the ability to report environments of interest while remaining stable, and providing high Stokes shifts, large quantum yields, while effecting minimal destruction of the polymer structure and targeted properties.

References

Abo Elsoud, M. M., & El Kady, E. M. (2019). Current trends in fungal biosynthesis of chitin and chitosan. *Bulletin of the National Research Centre 2019 43:1*, *43*(1), 1–12. https://doi.org/10.1186/S42269-019-0105-Y

Adav, S. S., Lin, J. C. Te, Yang, Z., Whiteley, C. G., Lee, D. J., Peng, X. F., & Zhang, Z. P. (2010, March 1). Stereological assessment of extracellular polymeric substances, exo-enzymes, and specific bacterial strains in bioaggregates using fluorescence experiments. *Biotechnology Advances*. Elsevier. https://doi.org/10.1016/j.biotechadv.2009.08.006

Arivarasan, A., Sasikala, G., & Jayavel, R. (2014). In situ synthesis of CdTe:CdS quantum dot nanocomposites for photovoltaic applications. *Materials Science in Semiconductor Processing*, *25*, 238–243. https://doi.org/10.1016/J.MSSP.2013.12.018

Arivithamani, N., & Giri Dev, V. R. (2017). Sustainable bulk scale cationization of cotton hosiery fabrics for salt-free reactive dyeing process. *Journal of Cleaner Production*, *149*, 1188–1199. https://doi.org/10.1016/J.JCLEPRO.2017.02.162

Behanna, H. A., Rajangam, K., & Stupp, S. I. (2007). Modulation of fluorescence through coassembly of molecules in organic nanostructures. *Journal of the American Chemical Society*, *129*(2), 321–327. https://doi.org/10.1021/JA062415B/SUPPL_FILE/JA062415BSI20060801_123301.PDF

Bejan, A, Doroftei, F., Cheng, X. J., & Marin, L. (2020). Phenothiazine-chitosan based eco-adsorbents: A special design for mercury removal and fast naked eye detection. *INTERNATIONAL JOURNAL OF BIOLOGICAL MACROMOLECULES*, *162*, 1839–1848. https://doi.org/10.1016/j.ijbiomac.2020.07.232

Bejan, Andrei, Ailincai, D., Simionescu, B. C., & Marin, L. (2018). Chitosan hydrogelation with

a phenothiazine based aldehyde: a synthetic approach toward highly luminescent biomaterials †. *Polymer Chemistry*, *9*, 2359. https://doi.org/10.1039/c7py01678f

Belovolova, L. V., & Glushkov, M. V. (2021). Porous Matrices and Specific Features of Water in Nanostructures. *Physics of Wave Phenomena 2021 29:3*, *29*(3), 249–277. https://doi.org/10.3103/S1541308X21030031

Belovolova, L. V, Glushkov, M. V, Vinogradov, E. A., Babintsev, V. A., & Golovanov, V. I. (2009). Ultraviolet Fluorescence of Water and Highly Diluted Aqueous Media. *Physics of Wave Phenomena*, *17*(1), 21–31. https://doi.org/10.3103/S1541308X0901004X

Braun, D., Rettig, W., Delmond, S., Létard, J. F., & Lapouyade, R. (1997). Amide derivatives of DMABN: A new class of dual fluorescent compounds. *Journal of Physical Chemistry A*, *101*(37), 6836–6841. https://doi.org/10.1021/jp970168f

Briggs, M. S. J., Bruce, I., Miller, J. N., Moody, C. J., Simmonds, A. C., & Swann, E. (1997). Synthesis of functionalised fluorescent dyes and their coupling to amines and amino acids. *J. Chem. Soc., Perkin Trans. 1*.

Callis, P. R. (1979). Polarized fluorescence and estimated lifetimes of the DNA bases at room temperature. *Chemical Physics Letters*, *61*(3), 568–570. https://doi.org/10.1016/0009-2614(79)87174-2

Cantor, C. R., & Schimmel, P. R. (1980). *Biophysical chemistry: Part II: Techniques for the study of biological structure and function*. Macmillan.

Cerca, N., Oliveira, R., & Azeredo, J. (2007). Susceptibility of Staphylococcus epidermidis planktonic cells and biofilms to the lytic action of staphylococcus bacteriophage K. *Letters in Applied Microbiology*, *45*(3), 313–317. https://doi.org/10.1111/J.1472-765X.2007.02190.X

Chen, M Y, Lee, D. J., & Tay, J. H. (2007). Distribution of extracellular polymeric substances in aerobic granules. *Applied Microbiology and Biotechnology*, *73*(6), 1463–1469. https://doi.org/10.1007/s00253-006-0617-x

Chen, Ming Yuan, Lee, D. J., Tay, J. H., & Show, K. Y. (2007). Staining of extracellular polymeric substances and cells in bioaggregates. *Applied Microbiology and Biotechnology*, *75*(2), 467–474. https://doi.org/10.1007/s00253-006-0816-5

Cheng, Q., Qin, W., Yu, Y., Li, G., Wu, J., & Zhuo, L. (2020). Preparation and Characterization of PEG-PLA Genistein Micelles Using a Modified Emulsion-Evaporation Method. *Journal of Nanomaterials*, *2020*, 1–15. https://doi.org/10.1155/2020/3278098

Chhatbar, M. U., Meena, R., Prasad, K., Chejara, D. R., & Siddhanta, A. K. (2011). Microwave-induced facile synthesis of water-soluble fluorogenic alginic acid derivatives. *Carbohydrate Research*, *346*(5), 527–533. https://doi.org/10.1016/j.carres.2011.01.002

Collnot, E.-M., Baldes, C., Schaefer, U. F., Edgar, K. J., Wempe, M. F., & Lehr, C.-M. (2010). Vitamin E TPGS P-Glycoprotein Inhibition Mechanism: Influence on Conformational Flexibility, Intracellular ATP Levels, and Role of Time and Site of Access. *Molecular Pharmaceutics*, *7*(3), 642–651. https://doi.org/10.1021/mp900191s

Collnot, E.-M., Baldes, C., Wempe, M. F., Kappl, R., Hüttermann, J., Hyatt, J. A., … Lehr, C.-M. (2007). Mechanism of Inhibition of P-Glycoprotein Mediated Efflux by Vitamin E TPGS: Influence on ATPase Activity and Membrane Fluidity. *Molecular Pharmaceutics*, *4*(3), 465–474. https://doi.org/10.1021/mp060121r

De Beer, D., O'Flaharty, V., Thaveesri, J., Lens, P., & Verstraete, W. (1996). Distribution of extracellular polysaccharides and flotation of anaerobic sludge. *Applied Microbiology and Biotechnology*, *46*(2), 197–201. https://doi.org/10.1007/s002530050805

de Belder, A. N., & Wik, K. O. (1975). Preparation and properties of fluorescein-labelled hyaluronate. *Carbohydrate Research*, *44*(2), 251–257. https://doi.org/10.1016/S0008-6215(00)84168-3

Debele, T. A., Mekuria, S. L., & Tsai, H. C. (2016, November 1). Polysaccharide based nanogels in the drug delivery system: Application as the carrier of pharmaceutical agents. *Materials Science and Engineering C*. Elsevier Ltd. https://doi.org/10.1016/j.msec.2016.05.121

Dong, Y., & Edgar, K. J. (2015). Imparting functional variety to cellulose ethers via olefin cross-metathesis. *Polymer Chemistry*, *6*(20), 3816–3827. https://doi.org/10.1039/C5PY00369E

Dong, Y., Mosquera-Giraldo, L. I., Taylor, L. S., & Edgar, K. J. (2016). Amphiphilic Cellulose Ethers Designed for Amorphous Solid Dispersion via Olefin Cross-Metathesis. *Biomacromolecules*, *17*(2), 454–465. https://doi.org/10.1021/acs.biomac.5b01336

Dong, Y., Mosquera-Giraldo, L. I., Taylor, L. S., & Edgar, K. J. (2017). Tandem modification of amphiphilic cellulose ethers for amorphous solid dispersion via olefin cross-metathesis and thiol-Michael addition. *Polymer Chemistry*, *8*(20), 3129–3139. https://doi.org/10.1039/C7PY00228A

Dong, Y., Novo, D. C., Mosquera-Giraldo, L. I., Taylor, L. S., & Edgar, K. J. (2019). Conjugation of bile esters to cellulose by olefin cross-metathesis: A strategy for accessing complex polysaccharide structures. *Carbohydrate Polymers*, *221*, 37–47. https://doi.org/10.1016/j.carbpol.2019.05.061

dos Santos, M. A., & Grenha, A. (2015). Polysaccharide Nanoparticles for Protein and Peptide Delivery: Exploring Less-Known Materials. In *Advances in Protein Chemistry and Structural Biology* (Vol. 98, pp. 223–261). Academic Press. https://doi.org/10.1016/bs.apcsb.2014.11.003

Efiana, N. A., Kali, G., Fürst, A., Dizdarević, A., & Bernkop-Schnürch, A. (2023). Betaine-modified hydroxyethyl cellulose (HEC): A biodegradable mucoadhesive polysaccharide exhibiting quaternary ammonium substructures. *European Journal of Pharmaceutical Sciences*, *180*. https://doi.org/10.1016/j.ejps.2022.106313

Elsherbiny, A. S., Galal, A., Ghoneem, K. M., & Salahuddin, N. A. (2022). Novel chitosan-based nanocomposites as ecofriendly pesticide carriers: Synthesis, root rot inhibition and growth management of tomato plants. *Carbohydrate Polymers*, *282*. https://doi.org/10.1016/J.CARBPOL.2022.119111

Englyst, H. N., & Hudson, G. J. (1987). Colorimetric method for routine measurement of dietary fibre as non-starch polysaccharides. A comparison with gas-liquid chromatography. *Food Chemistry*, *24*(1), 63–76. https://doi.org/10.1016/0308-8146(87)90084-7

Fayazpour, F., Lucas, B., Alvarez-Lorenzo, C., Sanders, N. N., Demeester, J., & De Smedt, S. C. (2006). Physicochemical and transfection properties of cationic hydroxyethylcellulose/DNA nanoparticles. *Biomacromolecules*, *7*(10), 2856–2862. https://doi.org/10.1021/bm060474b

Förster, T. (1948). Zwischenmolekulare energiewanderung und fluoreszenz. *Annalen Der Physik*, *437*(1–2), 55–75.

G. Ricarte, R., J. Van Zee, N., Li, Z., M. Johnson, L., P. Lodge, T., & A. Hillmyer, M. (2019). Recent Advances in Understanding the Micro- and Nanoscale Phenomena of Amorphous Solid Dispersions. *Molecular Pharmaceutics*, *16*(10), 4089–4103. https://doi.org/10.1021/acs.molpharmaceut.9b00601

Gabris, M. A., Rezania, S., Rafieizonooz, M., Khankhaje, E., Devanesan, S., AlSalhi, M. S., … Shadravan, A. (2022). Chitosan magnetic graphene grafted polyaniline doped with cobalt oxide for removal of Arsenic(V) from water. *Environmental Research*, *207*, 112209.

https://doi.org/10.1016/J.ENVRES.2021.112209

Ganguly, S., Das, P., Itzhaki, E., Hadad, E., Gedanken, A., & Margel, S. (2020). Microwave-Synthesized Polysaccharide-Derived Carbon Dots as Therapeutic Cargoes and Toughening Agents for Elastomeric Gels. *ACS Applied Materials and Interfaces*, *12*(46), 51940–51951. https://doi.org/10.1021/acsami.0c14527

Gerkins, C., Hajjar, R., Oliero, M., & Santos, M. M. (2022). Assessment of Gut Barrier Integrity in Mice Using Fluorescein-Isothiocyanate-Labeled Dextran. *JoVE (Journal of Visualized Experiments)*, *2022*(189), e64710. https://doi.org/10.3791/64710

Gilley, A. D., Arca, H. C., Nichols, B. L. B., Mosquera-Giraldo, L. I., Taylor, L. S., Edgar, K. J., & Neilson, A. P. (2017). Novel cellulose-based amorphous solid dispersions enhance quercetin solution concentrations in vitro. *Carbohydrate Polymers*, *157*, 86–93. https://doi.org/10.1016/j.carbpol.2016.09.067

Glabe, C. G., Harty, P. K., & Rosen, S. D. (1983). Preparation and properties of fluorescent polysaccharides. *Analytical Biochemistry*, *130*(2), 287–294. https://doi.org/10.1016/0003-2697(83)90590-0

González, N. N., Cerri, G., Molpeceres, J., Cossu, M., Rassu, G., Giunchedi, P., & Gavini, E. (2022). Surfactant-Free Chitosan/Cellulose Acetate Phthalate Nanoparticles: An Attempt to Solve the Needs of Captopril Administration in Paediatrics. *Pharmaceuticals*, *15*(6). https://doi.org/10.3390/ph15060662

Guo, J., Tang, J., Wang, J., Mao, S., Li, H., Wang, Y., … Belfiore, L. A. (2018). Europium(III)-induced water-soluble nano-aggregates of hyaluronic acid and chitosan: structure and fluorescence. *MRS Communications*, *8*(3), 1224–1229. https://doi.org/10.1557/mrc.2018.107

Horrocks, A. R., Kandola, B. K., Davies, P. J., Zhang, S., & Padbury, S. A. (2005). Developments in flame retardant textiles – a review. *Polymer Degradation and Stability*, *88*(1), 3–12. https://doi.org/10.1016/J.POLYMDEGRADSTAB.2003.10.024

Hu, S., Wei, Z., Chang, Q., Trinchi, A., & Yang, J. (2016). A facile and green method towards coal-based fluorescent carbon dots with photocatalytic activity. *Applied Surface Science*, *378*, 402–407. https://doi.org/10.1016/J.APSUSC.2016.04.038

Huang, Y., Dan, N., Dan, W., & Zhao, W. (2019). Reinforcement of Polycaprolactone/Chitosan with Nanoclay and Controlled Release of Curcumin for Wound Dressing. https://doi.org/10.1021/acsomega.9b02217

Ilevbare, G. A., Liu, H., Edgar, K. J., & Taylor, L. S. (2013). Impact of polymers on crystal growth rate of structurally diverse compounds from aqueous solution. *Molecular Pharmaceutics*, *10*(6), 2381–2393. https://doi.org/10.1021/mp400029v

Jaiswal, A., Sankar Ghosh, S., & Chattopadhyay, A. (2011). One step synthesis of C-dots by microwave mediated caramelization of poly(ethylene glycol). *Chemical Communications*, *48*(3), 407–409. https://doi.org/10.1039/C1CC15988G

Jana, J., Ganguly, M., Das, B., Dhara, S., Negishi, Y., & Pal, T. (2016). One pot synthesis of intriguing fluorescent carbon dots for sensing and live cell imaging. *Talanta*, *150*, 253–264. https://doi.org/10.1016/J.TALANTA.2015.12.047

Janda, J., & Work, E. (1971). A colorimetric estimation of lipopolysaccharides, *16*.

Kaneo, Y., Tanaka, T., Nakano, T., & Yamaguchi, Y. (2001). Evidence for receptor-mediated hepatic uptake of pullulan in rats. *Journal of Controlled Release*, *70*(3), 365–373. https://doi.org/10.1016/S0168-3659(00)00368-0

Karimi Jabali, M., Allafchian, A. R., Jalali, S. A. H., Shakeripour, H., Mohammadinezhad, R., &

Rahmani, F. (2022). Design of a pDNA nanocarrier with ascorbic acid modified chitosan coated on superparamagnetic iron oxide nanoparticles for gene delivery. *Colloids and Surfaces A: Physicochemical and Engineering Aspects*, *632*, 127743. https://doi.org/10.1016/j.colsurfa.2021.127743

Kohn, J., & Wilchek, M. (1978). A colorimetric method for monitoring activation of sepharose by cyanogen bromide. *Biochemical and Biophysical Research Communications*, *84*(1), 7–14. https://doi.org/10.1016/0006-291X(78)90255-3

Kondaveeti, S., Chejara, D. R., & Siddhanta, A. K. (2013). A facile one-pot synthesis of a fluorescent agarose-O-naphthylacetyl adduct with slow release properties. *Carbohydrate Polymers*, *98*(1), 589–595. https://doi.org/10.1016/j.carbpol.2013.06.046

Kondaveeti, S., Mehta, G. K., & Siddhanta, A. K. (2014). Modification of agarose: 6-Aminoagarose mediated syntheses of fluorogenic pyridine carboxylic acid amides. *Carbohydrate Polymers*, *106*(1), 365–373. https://doi.org/10.1016/j.carbpol.2014.02.051

Kong, W., Liu, R., Li, H., Liu, J., Huang, H., Liu, Y., & Kang, Z. (2014). High-bright fluorescent carbon dots and their application in selective nucleoli staining. *Journal of Materials Chemistry B*, *2*(31), 5077–5082. https://doi.org/10.1039/C4TB00579A

Lai, X., Han, Y., Zhang, J., Zhang, J., Lin, W., Liu, Z., & Wang, L. (2021). Peroxidase-like platinum clusters synthesized by ganoderma lucidum polysaccharide for sensitively colorimetric detection of dopamine. *Molecules*, *26*(9). https://doi.org/10.3390/molecules26092738

Lakowicz, J. R. (2006a). *Principles of fluorescence spectroscopy, 3rd Principles of fluorescence spectroscopy, Springer, New York, USA, 3rd edn, 2006. Principles of fluorescence spectroscopy, Springer, New York, USA, 3rd edn, 2006.* https://doi.org/10.1007/978-0-387-

46312-4

Lakowicz, J. R. (2006b). *Principles of fluorescence spectroscopy*. *Principles of Fluorescence Spectroscopy*. https://doi.org/10.1007/978-0-387-46312-4

Lawrence, J. R., Neu, T. R., & Swerhone, G. D. W. (1998). Application of multiple parameter imaging for the quantification of algal, bacterial and exopolymer components of microbial biofilms. *Journal of Microbiological Methods*, *32*(3), 253–261. https://doi.org/10.1016/S0167-7012(98)00027-X

Lencer, W. I., Weyer, P., Verkman, A. S., Ausiello, D. A., & Brown, D. (1990). FITC-Dextran as a probe for endosome function and localization in kidney. *American Journal of Physiology - Cell Physiology*, *258*(2 27-2). https://doi.org/10.1152/ajpcell.1990.258.2.c309

Li, B., Konecke, S., Harich, K., Wegiel, L., Taylor, L. S., & Edgar, K. J. (2013). Solid dispersion of quercetin in cellulose derivative matrices influences both solubility and stability. *Carbohydrate Polymers*, *92*(2), 2033–2040. https://doi.org/10.1016/j.carbpol.2012.11.073

Li, C., Tang, Q., Wei, H., Liu, J., Wang, Q., Wang, Y., … Tang, J. (2022). Smart Wearable Fluorescence Sensing of Bacterial Pathogens and Toxic Contaminants by Eu3+-Induced Sodium Alginate/Ag Nanoparticle Aggregates. *ACS Applied Nano Materials*, *5*(6), 8393–8403. https://doi.org/10.1021/acsanm.2c01525

Li, F., Liu, Y. T., Li, Z. M., Li, Q., Liu, X. Y., & Cui, H. (2020). Cu(II)-Regulated On-Site Assembly of Highly Chemiluminescent Multifunctionalized Carbon Nanotubes for Inorganic Pyrophosphatase Activity Determination. *ACS APPLIED MATERIALS & INTERFACES*, *12*(2), 2903–2909. https://doi.org/10.1021/acsami.9b20259

Li, L., Jia, C., Wang, F., Fan, H., Jiao, W., & Shao, Z. (2018a). Facile synthesis of magnetic fluorescent nanoparticles: Adsorption and selective detection of Hg(II) in water. *Journal of*

Materials Chemistry C, *6*(9), 2360–2369. https://doi.org/10.1039/c7tc05564a

Li, L., Jia, C., Wang, F., Fan, H., Jiao, W., & Shao, Z. (2018b). Facile synthesis of magnetic fluorescent nanoparticles: adsorption and selective detection of Hg(II) in water †. *2360 | J. Mater. Chem. C*, *6*, 2360. https://doi.org/10.1039/c7tc05564a

Liao, J., Cheng, Z., & Zhou, L. (2016). Nitrogen-Doping Enhanced Fluorescent Carbon Dots: Green Synthesis and Their Applications for Bioimaging and Label-Free Detection of Au 3+ Ions. *ACS Sustainable Chem. Eng*, *4*, 3061. https://doi.org/10.1021/acssuschemeng.6b00018

Liu, H., Taylor, L. S., & Edgar, K. J. (2015). The role of polymers in oral bioavailability enhancement; a review. *Polymer*, *77*, 399–415. https://doi.org/10.1016/J.POLYMER.2015.09.026

Liu, S., Zhao, N., Cheng, Z., & Liu, H. (2015). Amino-functionalized green fluorescent carbon dots as surface energy transfer biosensors for hyaluronidase †, *7*, 6836. https://doi.org/10.1039/c5nr00070j

Lukomska, J., Rzeska, A., Malicka, J., & Wiczk, W. X. (2001). Influence of a substituent on amide nitrogen atom on fluorescence efficiency quenching of Tyr(Me) by amide group. *Journal of Photochemistry and Photobiology A: Chemistry*, *143*(2–3), 135–139. https://doi.org/10.1016/S1010-6030(01)00521-4

Malzahn, K., Marsico, F., Koynov, K., Landfester, K., Weiss, C. K., & Wurm, F. R. (2014). Selective interfacial olefin cross metathesis for the preparation of hollow nanocapsules. *ACS Macro Letters*, *3*(1), 40–43. https://doi.org/10.1021/MZ400578E/SUPPL_FILE/MZ400578E_SI_001.PDF

Mansur, A. A. P., Mansur, H. S., Soriano-Araujo, A., & Lobato, Z. I. P. (2014). Fluorescent Nanohybrids Based on Quantum Dot-Chitosan-Antibody as Potential Cancer Biomarkers.

ACS APPLIED MATERIALS & INTERFACES, *6*(14), 11403–11412. https://doi.org/10.1021/am5019989

Martinez, M. N., & Amidon, G. L. (2002). A mechanistic approach to understanding the factors affecting drug absorption: A review of fundamentals. *Journal of Clinical Pharmacology*, *42*(6), 620–643. https://doi.org/10.1177/00970002042006005

Mary, S. K., Koshy, R. R., Arunima, R., Thomas, S., & Pothen, L. A. (2022). A review of recent advances in starch-based materials: Bionanocomposites, pH sensitive films, aerogels and carbon dots. *Carbohydrate Polymer Technologies and Applications*, *3*. https://doi.org/10.1016/J.CARPTA.2022.100190

Meng, Xiangtao, & Edgar, K. J. (2015). Synthesis of amide-functionalized cellulose esters by olefin cross-metathesis. *Carbohydrate Polymers*, *132*, 565–573. https://doi.org/https://doi.org/10.1016/j.carbpol.2015.06.052

Meng, Xiangtao, Matson, J. B., & Edgar, K. J. (2014a). Olefin cross-metathesis, a mild, modular approach to functionalized cellulose esters. *Polymer Chemistry*, *5*(24), 7021–7033. https://doi.org/10.1039/C4PY01102C

Meng, Xiangtao, Matson, J. B., & Edgar, K. J. (2014b). Olefin Cross-Metathesis as a Source of Polysaccharide Derivatives: Cellulose ω-Carboxyalkanoates. *Biomacromolecules*, *15*(1), 177–187. https://doi.org/10.1021/bm401447v

Meng, Xin, Tian, F., Yang, J., He, C. N., Xing, N., & Li, F. (2010). Chitosan and alginate polyelectrolyte complex membranes and their properties for wound dressing application. *Journal of Materials Science: Materials in Medicine*, *21*(5), 1751–1759. https://doi.org/10.1007/s10856-010-3996-6

Messai, I., Lamalle, D., Munier, S., Verrier, B., Ataman-Önal, Y., & Delair, T. (2005).

Poly(D,L-lactic acid) and chitosan complexes: Interactions with plasmid DNA. *Colloids and Surfaces A: Physicochemical and Engineering Aspects*, *255*(1–3), 65–72. https://doi.org/10.1016/j.colsurfa.2004.12.023

Michael, T., & Smith, C. M. (1995). Lectins probe molecular films in biofouling: characterization of early films on non-living and living surfaces. *Marine Ecology Progress Series*, *119*(1–3), 229–236. https://doi.org/10.3354/MEPS119229

Mosquera-Giraldo, L. I., H. Borca, C., S. Parker, A., Dong, Y., J. Edgar, K., P. Beaudoin, S., … S. Taylor, L. (2018). Crystallization Inhibition Properties of Cellulose Esters and Ethers for a Group of Chemically Diverse Drugs: Experimental and Computational Insight. *Biomacromolecules*, *19*(12), 4593–4606. https://doi.org/10.1021/acs.biomac.8b01280

Mrozek, J., Banecki, B., Karolczak, J., & Wiczk, W. (2005). Influence of the separation of the charged groups and aromatic ring on interaction of tyrosine and phenylalanine analogues and derivatives with β-cyclodextrin. *Biophysical Chemistry*, *116*(3), 237–250. https://doi.org/10.1016/J.BPC.2005.04.011

Natarajan, R., Northrop, N., & Yamamoto, B. (2017). Fluorescein Isothiocyanate (FITC)-Dextran Extravasation as a Measure of Blood-Brain Barrier Permeability. *Current Protocols in Neuroscience*, *79*(1), 9.58.1-9.58.15. https://doi.org/10.1002/CPNS.25

Natarajan, S., Jayaraj, J., & Prazeres, D. M. F. (2021). A Cellulose Paper-Based Fluorescent Lateral Flow Immunoassay for the Quantitative Detection of Cardiac Troponin I. *Biosensors*, *11*(2), 49. https://doi.org/10.3390/BIOS11020049

Nawaz, H., Zhang, X., Chen, S., You, T., & Xu, F. (2021). Recent studies on cellulose-based fluorescent smart materials and their applications: A comprehensive review. *Carbohydrate Polymers*, *267*. https://doi.org/10.1016/J.CARBPOL.2021.118135

Neu, T. R. (2000). In situ cell and glycoconjugate distribution in river snow studied by confocal laser scanning microscopy. *Aquatic Microbial Ecology*, *21*(1), 85–95. https://doi.org/10.3354/ame021085

Novo, D. C., Gao, C., Qi, Q., Mosquera-Giraldo, L. I., Spiering, G. A., Moore, R. B., … Edgar, K. J. (2022). Designing synergistic crystallization inhibitors: Bile salt derivatives of cellulose with enhanced hydrophilicity. *Carbohydrate Polymers*, *292*, 119680. https://doi.org/10.1016/j.carbpol.2022.119680

Nowak, N., Grzebieniarz, W., Gohar, K., Khachatryan, K., Konieczna-Molenda, A., Krzan, M., … Pl, A. K. (2021). Synthesis of Silver and Gold Nanoparticles in Sodium Alginate Matrix Enriched with Graphene Oxide and Investigation of Properties of the Obtained Thin Films. https://doi.org/10.3390/app11093857

Nualnoi, T., Kirosingh, A., Pandit, S. G., Thorkildson, P., Brett, P. J., Burtnick, M. N., & AuCoin, D. P. (2016). In vivo Distribution and Clearance of Purified Capsular Polysaccharide from Burkholderia pseudomallei in a Murine Model. *PLoS Neglected Tropical Diseases*, *10*(12), e0005217. https://doi.org/10.1371/journal.pntd.0005217

Ohtake, K., Natsume, H., Ueda, H., & Morimoto, Y. (2002). Analysis of transient and reversible effects of poly-L-arginine on the in vivo nasal absorption of FITC-dextran in rats. *Journal of Controlled Release*, *82*(2–3), 263–275. https://doi.org/10.1016/S0168-3659(02)00128-1

Oza, M. D., Meena, R., Prasad, K., Paul, P., & Siddhanta, A. K. (2010). Functional modification of agarose: A facile synthesis of a fluorescent agarose–guanine derivative. *Carbohydrate Polymers*, *81*(4), 878–884. https://doi.org/10.1016/J.CARBPOL.2010.03.062

Oza, M. D., Meena, R., & Siddhanta, A. K. (2012). Facile synthesis of fluorescent polysaccharides: Cytosine grafted agarose and κ-carrageenan. *Carbohydrate Polymers*,

87(3), 1971–1979. https://doi.org/10.1016/j.carbpol.2011.10.004

Oza, M. D., Prasad, K., & Siddhanta, A. K. (2012). One-pot synthesis of fluorescent polysaccharides: Adenine grafted agarose and carrageenan. *Carbohydrate Research*, *357*, 23–31. https://doi.org/10.1016/j.carres.2012.05.016

Panda, A., Sharma, P. K., McCann, T., Bloomekatz, J., Repka, M. A., & Murthy, S. N. (2022). Fabrication and development of controlled release PLGA microneedles for macromolecular delivery using FITC-Dextran as model molecule. *Journal of Drug Delivery Science and Technology*, *68*, 102712. https://doi.org/10.1016/j.jddst.2021.102712

Pereira, F. A. R., Sousa, K. S., Cavalcanti, G. R. S., França, D. B., Queiroga, L. N. F., Santos, I. M. G., … Jaber, M. (2017). Green biosorbents based on chitosan-montmorillonite beads for anionic dye removal. *Journal of Environmental Chemical Engineering*, *5*(4), 3309–3318. https://doi.org/10.1016/j.jece.2017.06.032

Pereira, J. M. (2013). *Synthesis of New Pullulan Derivatives for Drug Delivery Synthesis of New Pullulan Derivatives for Drug Delivery*. Retrieved from http://hdl.handle.net/10919/23884

Perreux, L., Loupy, A., & Volatron, F. (2002). Solvent-free preparation of amides from acids and primary amines under microwave irradiation. *Tetrahedron*, *58*(11), 2155–2162. https://doi.org/10.1016/S0040-4020(02)00085-6

Pramod, P. S., Takamura, K., Chaphekar, S., Balasubramanian, N., & Jayakannan, M. (2012). Dextran Vesicular Carriers for Dual Encapsulation of Hydrophilic and Hydrophobic Molecules and Delivery into Cells, *13*, 47. https://doi.org/10.1021/bm301583s

Reichardt, C. (1994). Solvatochromic dyes as solvent polarity indicators. *Chemical Reviews*, *94*(8), 2319–2358. https://doi.org/10.1021/cr00032a005

Richter, A. P., Brown, J. S., Bharti, B., Wang, A., Gangwal, S., Houck, K., … Velev, O. D.

(2015). An environmentally benign antimicrobial nanoparticle based on a silver-infused lignin core. *Nature Nanotechnology*, *10*(9), 817–823. https://doi.org/10.1038/nnano.2015.141

Salgado, C. L., Mansur, A. A. P., Mansur, H. S., & Monteiro, F. J. M. (2021). Bioengineered Fluorescent Nanoprobe Conjugates for Tracking Human Bone Cells: In Vitro Biocompatibility Analysis. *MATERIALS*, *14*(16). https://doi.org/10.3390/ma14164422

Samal, S. K., Dash, M., Vlierberghe, S. Van, Kaplan, D. L., Chiellini, E., Blitterswijk, C. van, … Dubruel, P. (2012). Cationic polymers and their therapeutic potential. *Chemical Society Reviews*, *41*(21), 7147–7194. https://doi.org/10.1039/c2cs35094g

Sato, K., & Anzai, J. I. (2006). Fluorometric determination of sugars using fluorescein-labeled concanavalin A-glycogen conjugates. *Analytical and Bioanalytical Chemistry*, *384*(6), 1297–1301. https://doi.org/10.1007/s00216-005-0279-z

Shahadat, M., Jha, A., Shahid-ul-Islam, Adnan, R., Ali, S. W., Ismail, I. M. I., … Ahammad, S. Z. (2022). Recent advances in chitosan-polyaniline based nanocomposites for environmental applications: A review. *Polymer*, *254*. https://doi.org/10.1016/J.POLYMER.2022.124975

Shen, P., Gao, J., Cong, J., Liu, Z., Li, C., & Yao, J. (2016). Synthesis of Cellulose-Based Carbon Dots for Bioimaging. *ChemistrySelect*, *1*(7), 1314–1317. https://doi.org/10.1002/SLCT.201600216

Siddhanta, A. K., Sanandiya, N. D., Chejara, D. R., & Kondaveeti, S. (2015). Functional modification mediated value addition of seaweed polysaccharides – a perspective. *RSC Advances*, *5*(73), 59226–59239. https://doi.org/10.1039/c5ra09027j

Song, Y., Li, Y., Liu, Z., Liu, L., Wang, X., Su, X., & Ma, Q. (2014). A novel ultrasensitive

carboxymethyl chitosan-quantum dot-based fluorescence “turn on-off” nanosensor for lysozyme detection. *Biosensors and Bioelectronics*, *61*, 9–13. https://doi.org/10.1016/J.BIOS.2014.04.036

Sun, M., Wang, X., Cheng, X., He, L., Yan, G., & Tang, R. (2018). TPGS-functionalized and ortho ester-crosslinked dextran nanogels for enhanced cytotoxicity on multidrug resistant tumor cells. *Carbohydrate Polymers*, *198*, 142–154. https://doi.org/10.1016/J.CARBPOL.2018.06.079

Teja, S. B., Patil, S. P., Shete, G., Patel, S., & Bansal, A. K. (2016). Drug-excipient behavior in polymeric amorphous solid dispersions. *Journal of Excipients and Food Chemicals*, *4*(3).

Virmani, M., Deshpande, N. U., Pathan, S., & Jayakannan, M. (2021). Self-Reporting Polysaccharide Polymersome for Doxorubicin and Cisplatin Delivery to Live Cancer Cells, *2*, 181–193. https://doi.org/10.1021/acspolymersau.1c00042

Waggoner, A. (1995). [15] Covalent labeling of proteins and nucleic acids with fluorophores. *Methods in Enzymology*, *246*(C), 362–373. https://doi.org/10.1016/0076-6879(95)46017-9

Wan Ngah, W. S., Teong, L. C., & Hanafiah, M. A. K. M. (2011, February 1). Adsorption of dyes and heavy metal ions by chitosan composites: A review. *Carbohydrate Polymers*. https://doi.org/10.1016/j.carbpol.2010.11.004

Wang, C., Wang, F., Zhang, J., Liu, L., Xu, G., & Dou, H. (2020). Fluorescent Polysaccharide Nanogels for the Detection of Tumor Heterogeneity in Drug-Surviving Cancer Cells. *Advanced Biosystems*, *4*(2), 1–10. https://doi.org/10.1002/adbi.201900213

Wang Yu Liu Joo-Hwa Tay, Z.-W. (2005). APPLIED MICROBIAL AND CELL PHYSIOLOGY Distribution of EPS and cell surface hydrophobicity in aerobic granules. *Appl Microbiol Biotechnol*, *69*, 469–473. https://doi.org/10.1007/s00253-005-1991-5

Wani, A. A., Khan, A. M., Manea, Y. K., Salem, M. A. S., & Shahadat, M. (2021). Selective adsorption and ultrafast fluorescent detection of Cr(VI) in wastewater using neodymium doped polyaniline supported layered double hydroxide nanocomposite. *Journal of Hazardous Materials*, *416*. https://doi.org/10.1016/J.JHAZMAT.2021.125754

Webber, S. E. (1999). Fluorescence of polymers: A probe of polymer assemblies. *Macromolecular Symposia*, *143*, 359–370. https://doi.org/10.1002/masy.19991430126

Weecharangsan, W., Opanasopit, P., Ngawhirunpat, T., Apirakaramwong, A., Rojanarata, T., Ruktanonchai, U., & Lee, R. J. (2008). Evaluation of chitosan salts as non-viral gene vectors in CHO-K1 cells. *International Journal of Pharmaceutics*, *348*(1–2), 161–168. https://doi.org/10.1016/j.ijpharm.2007.07.011

Wempe, M. F., Wright, C., Little, J. L., Lightner, J. W., Large, S. E., Caflisch, G. B., … Edgar, K. J. (2009). Inhibiting efflux with novel non-ionic surfactants: Rational design based on vitamin E TPGS. *International Journal of Pharmaceutics*, *370*(1–2), 93–102. https://doi.org/10.1016/j.ijpharm.2008.11.021

Weng, C. I., Chang, H. T., Lin, C. H., Shen, Y. W., Unnikrishnan, B., Li, Y. J., & Huang, C. C. (2015). One-step synthesis of biofunctional carbon quantum dots for bacterial labeling. *Biosensors and Bioelectronics*, *68*, 1–6. https://doi.org/10.1016/J.BIOS.2014.12.028

Wiederschain, G. Y. (2011). The Molecular Probes handbook. A guide to fluorescent probes and labeling technologies. *Biochemistry (Moscow)*, *76*(11), 1276–1276. https://doi.org/10.1134/s0006297911110101

Wilson, V., Lou, X., Osterling, D. J., Stolarik, D. F., Jenkins, G., Gao, W., … Taylor, L. S. (2018). Relationship between amorphous solid dispersion in vivo absorption and in vitro dissolution: phase behavior during dissolution, speciation, and membrane mass transport.

Journal of Controlled Release : Official Journal of the Controlled Release Society, *292*, 172–182. https://doi.org/10.1016/j.jconrel.2018.11.003

Wilson, V. R., Lou, X., Osterling, D. J., Stolarik, D. F., Jenkins, G. J., Nichols, B. L. B., … Taylor, L. S. (2020). Amorphous solid dispersions of enzalutamide and novel polysaccharide derivatives: investigation of relationships between polymer structure and performance. *Scientific Reports*, *10*(1), 18535. https://doi.org/10.1038/s41598-020-75077-7

Wu, W., Yao, W., Wang, X., Xie, C., Zhang, J., & Jiang, X. (2015). Bioreducible heparin-based nanogel drug delivery system. *Biomaterials*, *39*, 260–268. https://doi.org/10.1016/J.BIOMATERIALS.2014.11.005

Yu, J., Xu, C., Tian, Z., Lin, Y., & Shi, Z. (2016). Facilely synthesized N-doped carbon quantum dots with high fluorescent yield for sensing Fe 3+. *New J. Chem*, *40*, 2083. https://doi.org/10.1039/c5nj03252k

Zheng, Z.-M., Zhang, Y., Zhang, Q.-L., Luo, L., Pan, X.-L., & Wang, K.-P. (2022). Polysaccharide Radioisotopic Labeling and Its Application in Pharmacokinetics Study In Vivo. *Chinese Pharmaceutical Journal*, *57*(8), 599–604. https://doi.org/10.11669/cpj.2022.08.003

Zheng, Z., Pan, X., Xu, J., Wu, Z., Zhang, Y., & Wang, K. (2020). Advances in tracking of polysaccharides in vivo: Labeling strategies, potential factors and applications based on pharmacokinetic characteristics. *International Journal of Biological Macromolecules*, *163*, 1403–1420. https://doi.org/https://doi.org/10.1016/j.ijbiomac.2020.07.210

Zhou, J., Li, N., Liu, P., Liu, Z., Gao, L., & Jiao, T. (2022). Preparation of Fluorescently Labeled Chitosan-Quercetin Drug-Loaded Nanoparticles with Excellent Antibacterial Properties. *Journal of Functional Biomaterials*. https://doi.org/10.3390/jfb13030141

Zhou, J. W., Zou, X. M., Song, S. H., & Chen, G. H. (2018, February 14). Quantum Dots Applied to Methodology on Detection of Pesticide and Veterinary Drug Residues. *Journal of Agricultural and Food Chemistry*. American Chemical Society. https://doi.org/10.1021/acs.jafc.7b05119

Chapter 3. Designing synergistic crystallization inhibitors: bile salt derivatives of cellulose with enhanced hydrophilicity

(Published Carbohydrate Polymers, 2022, DOI: 10.1016/j.carbpol.2022.119680)

Diana C. Novo[a, b], Chengzhe Gao[d], Qingqing Qi[d], Laura I. Mosquera-Giraldo[d,e], Glenn A. Spiering[c], Robert B. Moore[b,c], Lynne S. Taylor[d], and Kevin J. Edgar*[a, c]

[a]*Department of Sustainable Biomaterials, Virginia Tech, Blacksburg, VA 24061, United States*

[b]*Department of Chemistry, Virginia Tech, Blacksburg, VA 24061, United States*

[c]*Macromolecules Innovation Institute, Virginia Tech, Blacksburg, VA 24061, United States*

[d]*Department of Industrial and Physical Pharmacy, College of Pharmacy, West Lafayette, Indiana 47907, United States*

[e]**Current address:** *Pharmaceutical Candidate Optimization, Bristol Myers Squibb, Route 206 and Province Line Road, Princeton, NJ 08540, USA*

Abstract

Crystallization inhibitors in amorphous solid dispersions (ASD) enable metastable supersaturated drug solutions that persist for a physiologically relevant time. Olefin cross-metathesis (CM) has successfully provided multifunctional cellulose-based derivatives as candidate ASD matrix polymers. In proof of concept studies, we prepared hydrophobic bile salt/cellulose adducts by CM with naturally occurring bile salts. We hypothesized that increased hydrophilicity would enhance the ability of these conjugates to maximize bioactive supersaturation. Their selective preparation presents a significant synthetic challenge, given polysaccharide reactivity and polysaccharide and bile salt complexity. We prepared such derivatives using a more hydrophilic hydroxypropyl cellulose (HPC) backbone, employing a pent-4-enyl tether (Pen) for appending bile acids. We probed structure-property relationships by varying the nature and degree of substitution of the bile acid substituent (lithocholic or deoxycholic acid).

These conjugates are indeed synergistic inhibitors, as demonstrated with the fast-crystallizing prostate cancer drug, enzalutamide. The lithocholic acid methyl ester derivative, AcrMLC-PenHHPCPen (0.64), increased induction time 68 fold vs. drug alone.

Keywords: olefin cross-metathesis, bile-salts, cellulose, amorphous solid dispersion, enzalutamide, chemoselectivity

1. Introduction

Bile acids are complex, interfacially active, amphiphilic compounds comprising of a planar steroid nucleus with hydroxyl groups, and flanked by a flexible carboxylic acid chain at the C24 position. They promote the emulsification of fats and solubilize poorly aqueous-soluble drugs through micelle formation (Mukhopadhyay & Maitra, 2004). These properties inspire use of bile acids and derivatives in biomedical applications, including to solubilize hydrophobic drugs and aid permeation (Pavlović et al., 2018). Bile acids can enhance supersaturated systems by promoting liquid-liquid or glass-liquid phase separation (LLPS or GLPS), stabilizing the sub-micron diameter droplets of highly concentrated drug (Jackson et al., 2016; Trasi & Taylor, 2015). Recently, bile salts have been shown to inhibit crystallization of structurally diverse drugs (Chen, Mosquera-Giraldo, Ormes, Higgins, & Taylor, 2015; Li et al., 2016; Lu, Ormes, Lowinger, Mann, Xu, Litster, et al., 2017; Lu, Ormes, Lowinger, Mann, Xu, Patel, et al., 2017). Molecular dynamic simulations indicate that van der Waals and hydrogen bonding interactions strongly influence crystallization inhibition (Li et al., 2016), while the degree of aggregation was found to influence effectiveness in delaying crystallization, as monomeric bile salts presented superior inhibition properties (comparable to HPMCAS-MF) for telaprevir (Lu, Ormes, Lowinger, Mann, Xu, Litster, et al., 2017). Poorly water soluble drugs currently pose challenges for oral therapy. ASDs are molecular dispersions of drug in polymeric matrices, from which the drug rapidly dissolves in the

gastrointestinal (GI) tract to form a supersaturated solution. ASD polymers play multiple roles, including providing adequately high formulation glass transition temperature (T_g) even when challenged by high humidity or drugs which are plasticizers, to prevent drug aggregation and crystallization. The polymer also must dissolve in the aqueous GI milieu at a rate similar to that of the drug (Craig, 2002; Taylor & Zhang, 2016). Sufficient dissolved polymer thereby can associate with the drug and prevent it from nucleating from the supersaturated solution, or if crystal seeds are present, from undergoing crystal growth via polymer adsorption to kinks or steps, therefore blocking molecular incorporation (Hasegawa et al., 1988). Some critical ASD challenges are still unmet by current polymers, including formulations that must contain a high bioactive concentration, and/or where the drug is a fast crystallizer (Baird et al., 2010; Van Eerdenbrugh et al., 2010, 2014). Thus synthesis of high-performance ASD polymers is crucial, informed by elucidation of the complex and interwoven structure-property relationships that are key to meeting all performance criteria (Arca et al., 2018; Frank & J. Matzger, 2018; Ricarte et al., 2019; Liu et al., 2014, 2015; Mosquera-Giraldo et al., 2016; Mosquera-Giraldo, H. Borca, et al., 2018; Pereira et al., 2013; Wilson et al., 2020).

Recently we reported synthesis of the first model bile salts and steroids substituted with Grubbs type II olefins (Chatterjee et al., 2003; Dong, Matson, et al., 2017) as substrates for conjugation with cellulose ether derivatives, e.g. ethyl 5-pent-1-enyl cellulose (EC2.30C5) (Dong et al., 2019). The objective was to form a construct between these two known classes of crystallization inhibitors that would exhibit synergistic performance. While the CM approach was successful, these bile ester derivatives of polysaccharides did not exhibit the expected synergy. In fact they *reduced* the time to crystallization of the poorly soluble drug, telaprevir, vs. drug alone. We hypothesize that the hydrophobicity of both the ethyl cellulose backbone, (DS(Et) = 2.3,

DS(Pen) = 0.7), and the bile acids caused the observed poor ASD performance, creating a mismatch between polymer and drug dissolution rates. We now hypothesize that bile salt/cellulosic polymer conjugates based on benign, water-soluble cellulose derivatives will have improved dissolution rates, therefore showing crystallization inhibition synergy.

We report attempts to design and prepare a series of conjugates with enhanced hydrophilicity, based on water-soluble HPC. Building on our previous work (Dong et al., 2019), we sought to etherify HPC with a Type I olefin-terminated side chain for olefin CM (PenHPC) (Dong et al. 2016). We broadened the series of bile acid derivatives by probing two attachment sites (A-ring –OH vs. D-ring COOH) to determine which bile salt most influences crystal growth inhibition. Bile salt carboxyl groups were previously protected as methyl esters (Dong et al., 2019), while in this study we examine both ester and carboxylate-terminated conjugates. Carboxyl substituents are frequently elements of effective ASD polymers (Liu et al., 2014; Mosquera-Giraldo et al., 2016; Mosquera-Giraldo, H. Borca, et al., 2018). We investigate the influence of these polymers upon nucleation induction times of enzalutamide, an important, fast-crystallizing, hydrophobic drug for prostate cancer.

2. Experimental

2.1. Materials and methods

Hydroxypropyl cellulose (HPC, M_w = 100 kg mol^{-1}, DP = 100, DS(HP) 2.2, MS(HP) 4.4) (Dong, Mosquera-Giraldo, Troutman, et al., 2016)), sodium hydride (95%), anhydrous tetrahydrofuran (THF), 5-bromo-pent-1-ene, Hoveyda-Grubbs' 2nd generation catalyst, 3,5-di-*tert*-butylhydroxytoluene (BHT), triethylamine (TEA), lithocholic acid, deoxycholic acid, ethylene glycol, *para*-toluenesulfonyl hydrazide (*p*TSH), and potassium bromide (KBr) were from Sigma-Aldrich (Saint Louis, MO, USA). *N*, *N*-Dimethylacetamide (DMAc), *N*, *N*-dimethylformamide

(DMF), lithium chloride (LiCl), dichloromethane (DCM), methanol, ethanol, and dialysis tubing (MWCO 3.5k Da) were from Fisher Scientific (Fair Lawn, NJ, USA). Enzalutamide was obtained from ChemShuttle (Hayward, California).

^{1}H and ^{13}C NMR spectra were acquired on a Bruker Avance II spectrometer operating at 500 MHz except as indicated. Polymer (ca. 10 mg for ^{1}H NMR, 50 mg for ^{13}C NMR) was dissolved in ca. 1 mL $CDCl_3$ or dimethylsulfoxide (DMSO-d_6); CF_3CO_2H (three drops) was added to shift the water peak downfield. Fourier transform-infrared (FT-IR) spectra were recorded in transmission mode with a Thermo Nicolet 8700 instrument (Madison, WI, USA); samples prepared as KBr pellets (1 mg polymer / 99 mg KBr mixed by mortar and pestle). Glass transition temperatures (T_g) were measured by a TA Instruments Q2000 using modulated differential scanning calorimetry (MDSC), with N_2 as purge gas. Each polymer sample (~0.3-6 mg in a Tzero aluminum pan) was first equilibrated at −50 °C and then heated as high as 270°C at ramp rate 3°C/min, with modulation amplitude of 1 °C and oscillation period of 60s (results from first heating cycle). Molecular weights (M_w) were measured by size exclusion chromatography (SEC) applying a Wyatt Technologies TRIOS II light scattering and Optilab T-REX refractive index (RI) detectors, using two Agilent Technologies PLgel 10 μm mixed-bed columns, DMAc/LiCl solvent, and a Shimadzu LC-20AD at 50 °C at a flowrate of 1 mL min^{-1}.

2.2. Synthetic methods

2.2.1. Synthesis of hydroxypropyl 1-pent-4-enyl cellulose (PenHPC DS 0.60 and 1.00)

PenHPC (DS = 0. 6, 1) was prepared according to Dong et al., (2016) (NMR (**Fig. 3.2a, 3.3a**), FTIR (**Fig. S3.1a-d,** top) and DS calculations **(Fig. S3.7**) in ESI (**S3.2.2.1**).

2.2.2. Syntheses of lithocholic acid (LCA) and deoxycholic acid (DCA) methyl esters

Syntheses carried out as adapted from Dong, et al., 2019; characterization information in ESI (**S3.2.2.2.**).

2.2.3. Acrylation of A-ring bile acids and their methyl esters (exemplary procedure for LCA provided)

LCA (0.500 g, 1.32 mmol) was dissolved in anhydrous THF (5 mL, 0 ^{o}C), and triethylamine (0.134 g, 1 eq), then acrylic anhydride (Acr_2O, 0.201 g, 1.2 eq) was added gradually. The solution was stirred at RT for 20 h, then concentrated under rotary evaporation. The crude lithocholate 3-*O*-acrylate (AcrLC) product thus obtained was recrystallized from water. The product was isolated by filtration, then dried under vacuum at 80 ^{o}C. Methyl lithocholate acrylate (AcrMLC) and methyl deoxycholate acrylate (MDCAc) were prepared according to Dong et al., (2019) (NMR data in ESI).

Lithocholate acrylate (AcrLC). Yield: 0.37 g, 64.5 %. ^{1}H NMR (selected signals, $CDCl_3$): 0.63 (s, CH_3), 0.91 (s, CH_3), 0.93 (s, CH_3), 4.80 (m, 1H, C3 CH_2=CHCOOC<u>H</u>), 5.78 (dd, COOCH=C<u>H</u>$_2$, *trans*), 6.06 (dd, COOC<u>H</u>=CH_2), 6.36 (dd, COOCH=C<u>H</u>$_2$, *cis*). ^{13}C NMR δ 12.1, 18.2, 20.8, 23.3, 24.2, 26.3, 26.6, 27.0, 28.2, 30.75, 31.0, 32.2, 34.6, 35.0, 35.3, 35.8, 40.1, 40.4, 41.9, 42.7, 55.9, 56.5, 74.6 (C3 CH_2=CHCOO<u>C</u>H), 129.1 (COOCH=<u>C</u>H_2), 130.2 (COO<u>C</u>H=CH_2), 165.8 (CH_2=CH<u>C</u>OO), 180.3 (<u>C</u>=OOH).

Deoxycholate acrylate (AcrDC) was prepared similarly by dissolving DCA (3.714 g, 9.57 mmol) in 20 mL anhydrous DCM containing 1 eq trimethylamine and 1 eq Acr_2O for 12 h. The solution was then concentrated under rotary evaporation, then the material was recrystallized from acetone, and collected as a pellet via centrifugation (0.782 g, 18 % DCA). The liquid filtrate was collected, concentrated, and dried under vacuum at 80 ^{o}C. The resulting crude oil was then redissolved in DCM, and purified by column chromatography (silica gel, 15% EtOAc in DCM) to

isolate the A-ring 3-*O*-acrylate, AcrDC (15% EtOAc/DCM, TLC Rf = 0.35), DCA (15% EtOAc/DCM, TLC Rf = 0), and D-ring 12-*O*-acrylate (15% EtOAc/DCM, TLC Rf = 0.65).

Deoxycholate acrylate (***C3-O-AcrDC).*** Yield: 1.17 g, 27%. ^{1}H NMR (selected signals, $CDCl_3$): δ 0.69, 0.93, 4.00 (t, 1H, C12 HOC<u>H</u>), 4.80 (m, 1H, C3 CH_2=CHCOOC<u>H</u>), 5.78, 6.05, 6.35. ^{13}C NMR (DMSO) δ 12.87, 17.41, 23.25, 23.72, 26.13, 26.61, 27.07, 27.56, 28.80, 30.78, 31.13, 32.26, 33.78, 34.27, 34.98, 35.18, 36.09, 41.97, 46.60, 47.43, 48.39, 73.36 (C3 CH_2=CHCOO<u>C</u>H), 74.58 (C12 HO-<u>C</u>H), 129.19 (COOCH=<u>C</u>H_2), 130.42 (COO<u>C</u>H=CH_2), 165.98 (<u>C</u>OOCH=CH_2), 179.98 (24C <u>C</u>=OOH).

Deoxycholate diacrylate **(C3 & C12-O-*AcrDC).*** Yield: 2 g, 46.1%. ^{1}H NMR ($CDCl_3$) δ 0.86, 0.90, 0.92, 1.25, 1.48, 1.51, 1.62, 1.63, 1.69, 1.71, 1.80, 1.85, 2.24, 2.27, 2.33, 2.35, 2.37, 4.77, 5.17, 5.77, 5.80, 5.85, 5.88, 6.06, 6.08, 6.12, 6.16, 6.18, 6.20, 6.23, 6.34, 6.39, 6.42, 6.46**.** ^{13}C NMR δ 12.45, 14.14, 17.40, 22.70, 23.09, 23.45, 24.69, 25.69, 25.91, 26.50, 26.88, 27.34, 29.07, 29.25, 29.37, 29.44, 29.60, 29.65, 29.67, 29.71, 30.56, 30.85, 31.93, 32.24, 33.97, 34.48, 34.66, 34.72, 35.69, 41.81, 45.23, 47.59, 49.64, 74.37, 76.00, 128.91, 129.03, 130.28, 130.61, 165.62, 179.60, 179.88.

2.2.4. General procedure for olefin CM of PenHPC (DS (Pen) =1.00)

Preparation of AcrLC-PenHPC(1.00) exemplifies the process: PenHPC(1.00) (190 mg, 0.22 mmol C=C), AcrLC (500 mg, 1.2 mmol, 2.9 equiv), and BHT (25 mg) were dissolved in ethyl acetate (EtOAc,12 mL) under N_2. HG II catalyst (39 mg, 12 mol%) was dissolved in anhydrous EtOAc (1 mL) and gradually added to the solution, which was stirred at 50 ^{o}C for 3 h before adding three drops of ethyl vinyl ether to terminate the reaction. The solution was concentrated under vacuum and added to hexanes to precipitate the product, which was redissolved in THF and

reprecipitated into water, then dried overnight under vacuum at 40 ^{o}C. Additional NMR data in ESI, **S2.2.4**.

AcrLC-PenHPC(1.00). Yield: 350 mg, 87.5%. ^{1}H NMR ($CDCl_3$): δ = 0.64 (s, C<u>H</u>$_3$), 0.91 (s, C<u>H</u>$_3$), 0.92 (s, C<u>H</u>$_3$), 1.00-2.57 (m, steroid ring protons, OCH$_2$C<u>H</u>$_2$C<u>H</u>$_2$CH=CHCOO-LCAc), 2.90-4.68 (m, cellulose backbone, OC<u>H</u>$_2$CH$_2$CH$_2$CH=CHCOO-LCAc, 4.77 (m, LCAc C3 C<u>H</u>), 5.77 (OCH$_2$CH$_2$CH$_2$CH=C<u>H</u>COO-LCAc), 6.94 (OCH$_2$CH$_2$CH$_2$C<u>H</u>=CHCOO-LCAc). ^{13}C NMR (126 MHz, DMSO) δ 12.32, 17.78, 18.59, 20.71, 23.50, 24.28, 24.90, 25.71, 26.44, 26.76, 28.19, 28.89, 29.52, 29.81, 31.16, 32.38, 34.62, 35.27, 35.76, 41.64, 42.72, 56.05, 56.40, 65.73, 67.97, 68.52, 72.98 - 79.16 (cellulose C2, C3, C5 and bile acid C3 CH$_2$=CHCOO<u>C</u>H), 83.10 (cellulose C4), 101.72 (cellulose C1), 121.78 (OCH$_2$CH$_2$CH$_2$CH=<u>C</u>HCOO-LCAc), 149.38 (OCH$_2$CH$_2$CH$_2$<u>C</u>H=CHCOO-LCAc), 172.65 (<u>C</u>=OOAcrLC), 175.25 (24C <u>C</u>=OOH).

2.2.5. General procedure for hydrogenation of PenHPC-Bile ester conjugates

Preparation of AcrDC-PenHHPC(1.00) was adapted from Dong et al., 2019; all details found in ESI (**S3.2.2.5**), with remaining hydrogenated product characterizations on (**Fig. S3.4 and S3.6**).

AcrDC-PenHHPC(1.00). Yield: 160 mg, 71%. ^{1}H NMR (selected, DMSO) δ 0.58 (s, C<u>H</u>$_3$) 0.86 (s, C<u>H</u>$_3$), 1.01-2.21 (m, steroid ring protons, OCH$_2$C<u>H</u>$_2$C<u>H</u>$_2$C<u>H</u>$_2$C<u>H</u>$_2$COO-DCAcAn), 2.76-4.54 (m, cellulose backbone, OC<u>H</u>$_2$CH$_2$CH$_2$CH$_2$CH$_2$COO-DCAcAn, C12 HO-C<u>H</u>), 4.60 (DCAcAn C3 -OC<u>H</u>). ^{13}C NMR δ 12.44, 16.94, 17.34, 19.12, 20.29, 22.83, 23.49, 24.45, 25.25, 25.92, 26.14, 26.67, 27.18, 28.53, 29.37, 30.77, 30.88, 31.89, 32.83, 33.79, 34.55, 34.97, 35.55, 41.18, 46.03, 46.24, 47.42, 64.98, 65.29, 68.14, 71.06 -79.28 (cellulose C2, C3, C5, and bile ester C3

$CH_2CH_2COO\underline{C}H$ and C12 HO-$\underline{C}$H), 82.52 (cellulose C4), 101.37 (cellulose C1), 172.28 ($\underline{C}$=OODCAc), 174.97 ($\underline{C}$=OODCAc).

2.2.6. Selective hydrolysis of D-ring methyl ester, AcrMLC-PenHHPC

AcrMLC-PenHHPC(1.00) (250 mg, 0.29 mmol -OMe) dissolved in 5 mL THF was heated to reflux (~ 59°C) with stirring, followed by dropwise addition of 2M NaOH (5 mL). The solution was stirred 1h, then cooled to RT, followed by partitioning between EtOAc/water; water extraction was repeated 3X. Aqueous layer was dialyzed against methanol (1 day) and water (2 days), then lyophilized.

Yield: 18 %, ^{1}H and ^{13}C NMR signals agreed with those of AcrLC-PenHHPC obtained via direct acrylation and CM of the bile acid (section 2.2.5).

2.3. Measurement of nucleation induction times

Polymer was dissolved in DMSO (20 mg/mL) by sonication (60 min, 40 °C). Next, small aliquots (125 µL) of this solution were added, using constant agitation, to 50 mL of pH 6.8 100 mM buffer at 37 °C to obtain 50 µg/mL polymer solutions (<1% DMSO). Supersaturated enzalutamide solutions (35 µg/mL) were prepared by adding 175 µL of the enzalutamide methanolic stock solution (10 mg/mL) to 50 mL phosphate buffer (0.100M) with polymer concentration 50 µg/mL, maintained at 37 °C and magnetically stirred (300 rpm). Crystallization induction time from unseeded samples was measured using an SI Photonics UV/vis spectrometer (Tucson, AZ) coupled to a fiber optic probe (path length 5 mm). Wavelength scans (200-450 nm) were performed at 60s time intervals. Crystal formation onset time was determined from the drop in drug concentration (absorbance at 237 nm) in the absence and presence of pre-dissolved polymer at 37 °C, designated as the nucleation induction time; measurement repeated 3X.

2.4. Solubility parameter (SP) calculation

Cellulose derivatives and enzalutamide SP were determined using Fedor's method (Fedors, 1974). Procedural details in ESI of Dong, Mosquera-Giraldo, Taylor, et al., 2016.

3. Results and discussion

Our strategy exploited the 4-pent-1-enyl ether of HPC (PenHPC, Scheme 3.1) as the Grubbs Type I olefin in CM (Dong, Mosquera-Giraldo, Troutman, et al., 2016; Grubbs, 2004) with an acrylated bile salt derivative (Type II olefin). We faced chemoselectivity challenges, including selectivity between the neutral A-ring hydroxyl and the anionic D-ring carboxylate nucleophiles of LCA.

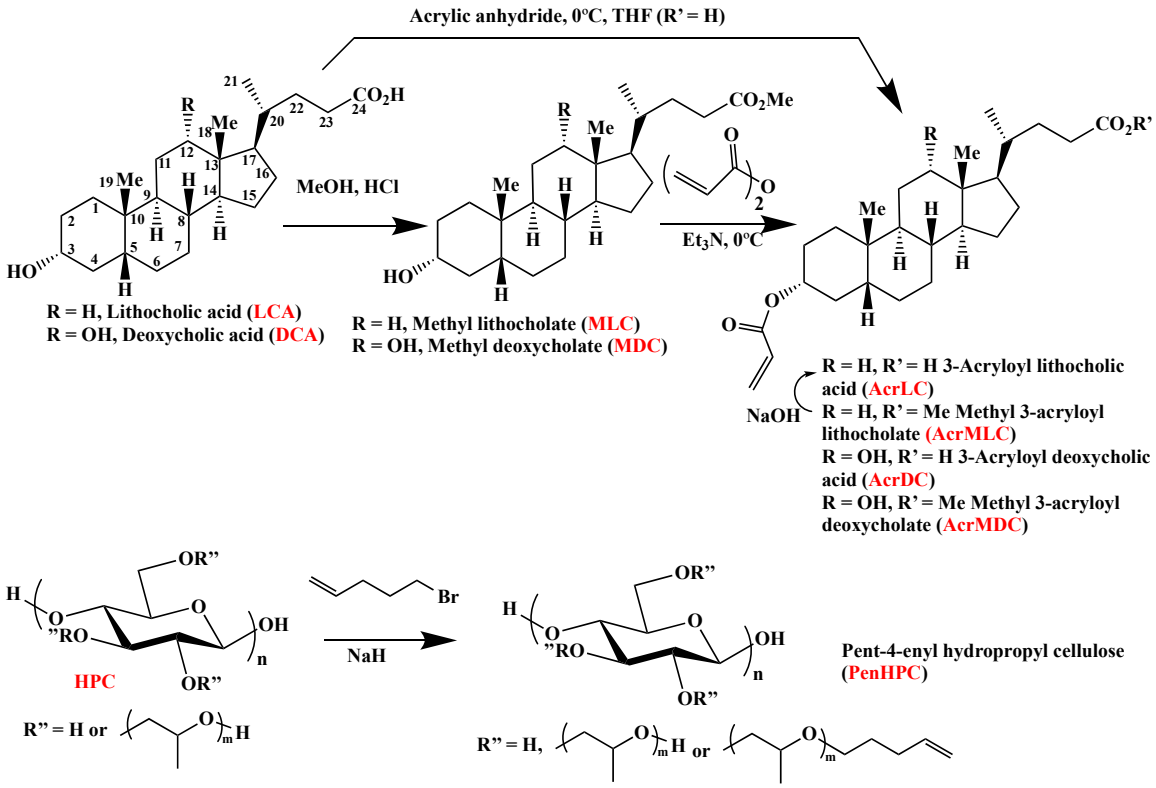

Scheme 3.1. CM partner syntheses. Structures do not imply regioselectivity; particular positions of substitution in all schemes only for convenience of depiction and clarity.

The DCA A-ring OH-nucleophile competes with both the D-ring carboxylate and the C-ring hydroxyl. Cellulose derivatives are relatively unreactive since they diffuse slowly, have relatively high Mw, and hydroxyls have relatively narrow approach angles; all non-conducive to regioselectivity (Fox et al., 2011). Fortunately, PenHPC has a flexible oligo(HP) tether and broader approach angles.

The key issue was selective bile salt acrylation. We began by making bile acid methyl esters to eliminate carboxylate/hydroxyl competition (Scheme 3.1). LCA (methyl lithocholate, MLC) and deoxycholic acid (methyl deoxycholate, MDC) esters were prepared by Fischer esterification (Fischer & Speier, 1895) as reported previously (Dong et al., 2019). Acrylation of bile salt methyl esters was by Dong's procedures, catalyzed by triethylamine at 0°C using Acr_2O, with excellent yield from MLC, and moderate, somewhat selective acrylation yield from difunctional MDC. ^{1}H NMR spectra for bile acid and acrylates are shown on **Fig. 3.1**; ^{13}C NMR spectra are in **Fig. S3.2**. As exemplified for LCA reactions, successful methyl esterification was confirmed by the new ^{1}H NMR singlet at 3.66 ppm and the methyl ester ^{13}C NMR resonance (C25) at 51.39 ppm. Subsequent A-ring hydroxyl acrylation was confirmed by downfield shift of the C3-OCH methine multiplet (3.62 to 4.66 ppm) due to presence of 3-*O*-acrylate (**Fig. 3.1b**). Product acrylate olefin protons were observed as doublets (5.79, 6.10, 6.39 ppm) (**Fig. 3.1b**), with corresponding ^{13}C NMR quaternary resonances (129.15, 130.2 ppm) (**Fig. S32b**).

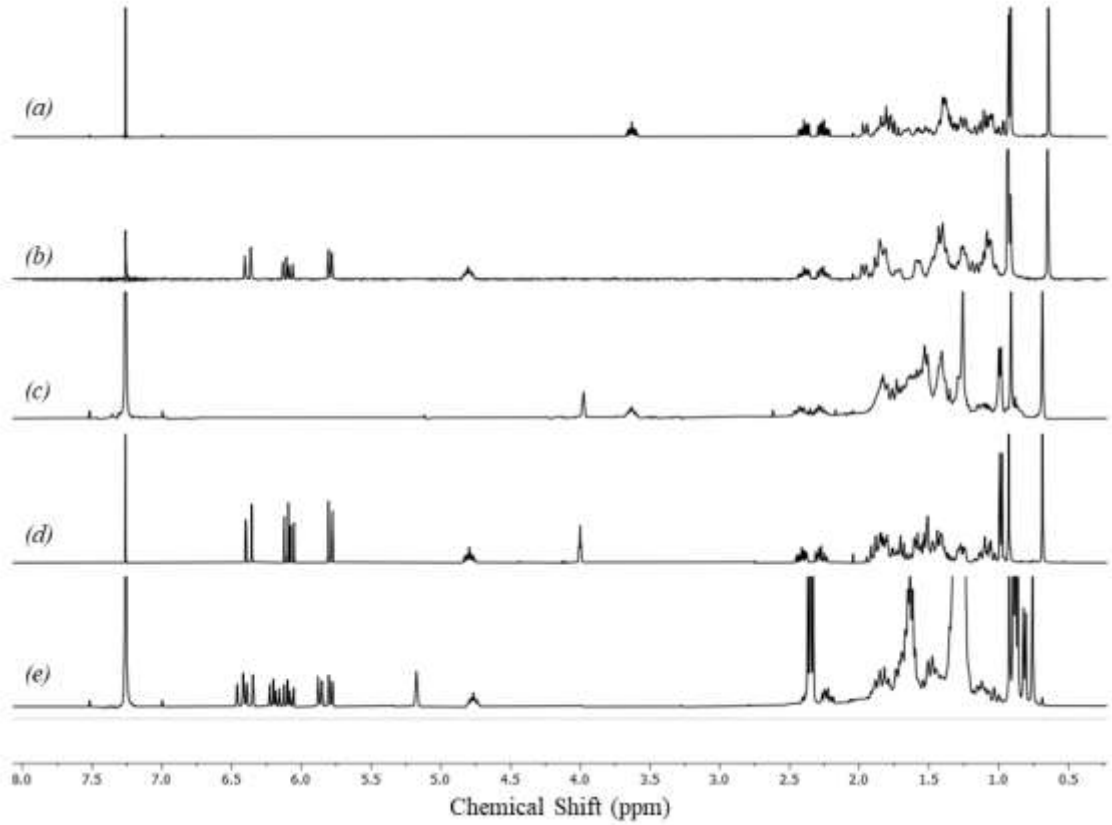

Figure 3.1: Proton NMR spectra of a) LCA, b) acrylated LCA (AcrLC), c) DCA, d) monoacrylated C3-OAc DCA (AcrDC), and e) diacrylated DCA (AcrDC).

Direct bile salt acrylation would afford a carboxyl-functionalized adduct, which we hypothesized would be an effective crystallization inhibitor based on earlier structure-property studies (Mosquera-Giraldo et al., 2016; Mosquera-Giraldo, Li, et al., 2018). We chose Acr_2O to effect selective acrylation of the less hindered LCA A-ring hydroxyl (Dong et al., 2019; Hu et al., 2005; Li & Ray Dias, 1997; Zhu & Nichifor, 2002); Table 1. C3-OH selectivity was maximized by limiting the Acr_2O /OH ratio. One equivalent each of Acr_2O and triethylamine worked best; after 20h, we were gratified to observe complete C3-OH chemoselectivity. Purity and identity of the 3-*O*-acrylated AcrLC product were confirmed by FTIR and NMR spectroscopy. Downfield shift of the 3-C<u>H</u>-OH proton (3.63 to 4.66 ppm) upon acrylation was diagnostic; (**Figs. 3.2a, 3.2b**), supported by the downfield ^{13}C NMR shift of <u>C</u>3-OAcr (71.39 to 74.6 ppm). Additional strong

evidence was provided by the acrylate proton resonances (5.79, 6.05, 6.36 ppm), acrylate carbons (129.1, 130.2), and the new ester carbonyl (165.8 ppm) (**Fig. 3.2b, Fig. S3.3c**). FT-IR spectroscopy was also supportive, with new olefinic stretches at 1621 cm^{-1} (**Fig. S3.1**).

With its additional C-ring hydroxyl (C12-OH), regioselective DCA acrylation is more challenging (Hu et al., 2005). We sought selectivity by brief esterification with Acr_2O at 0 ºC. Selectivity was modest, affording 57% 3-*O*-Ac, 20% 12-*O*-Ac, and 42% unreacted DCA by ^1H NMR (emergence of three acrylate olefin protons, and characteristic downfield shifts protons alpha to acrylation sites). Disappearance of the methine (alpha to methoxyl) resonance at 3.62 ppm was accompanied by emergence of the 3-*O*-Ac C3-OC<u>H</u> monoacrylate at 4.44 ppm, as well as new olefinic protons (5.78, 6.05, 6.35 ppm) (**Fig. 3.1d**); analogously, the C12-OC<u>H</u> methine proton (4.0 ppm) disappeared, replaced by the deshielded monoacrylate 12-*O*-Ac-OC<u>H</u> (5.17 ppm), whereas new olefinic acrylate protons emerged (5.84, 6.16, 6.40 ppm) in the diacrylate mixture (**Fig. 3.1e**). Longer reaction times, more acrylate, and use of more reactive acryloyl chloride all harmed regioselectivity (Table 3.1). Despite modest selectivity, we were able to isolate pure deoxycholic acid 3-acrylate by flash column chromatography.

Table 3.1. Selectivity vs. conditions for esterification of A-ring hydroxyl (C3-OH)

Substrate	**Acrylate/TEA molar ratio**	**Time (h)**	**Starting material (%)**	**3-*O*-Acrylate (%)**	**12-*O*-Acrylate (%)**
LCA	1.2 : 1	12 16 16	0	100	n/a
	1.2 : 3	12	56.7	43.2	n/a
	1.2 : 5	12	31	69	n/a
DCA	1.2 : 1	12 16 16	42 63 40*	57 36 50*	20 29 30*

	1.2 : 3	16	60*	41*	32*

* = 16 h using acryloyl chloride

Our previous successful CM with ethyl pent-4-enyl cellulose (EC2.30C5; Dong et al., 2019) inspired the methodology herein, reacting PenHPC (Grubbs type I olefin) with acrylated bile acids and esters (Grubbs Type II olefins) (Chatterjee et al., 2003; Dong, Matson, et al., 2017). Exemplary reaction of 3-*O*-acryloyl-lithocholic acid (AcrLCA) with pent-4-enyl HPC is shown (Scheme 3.2).

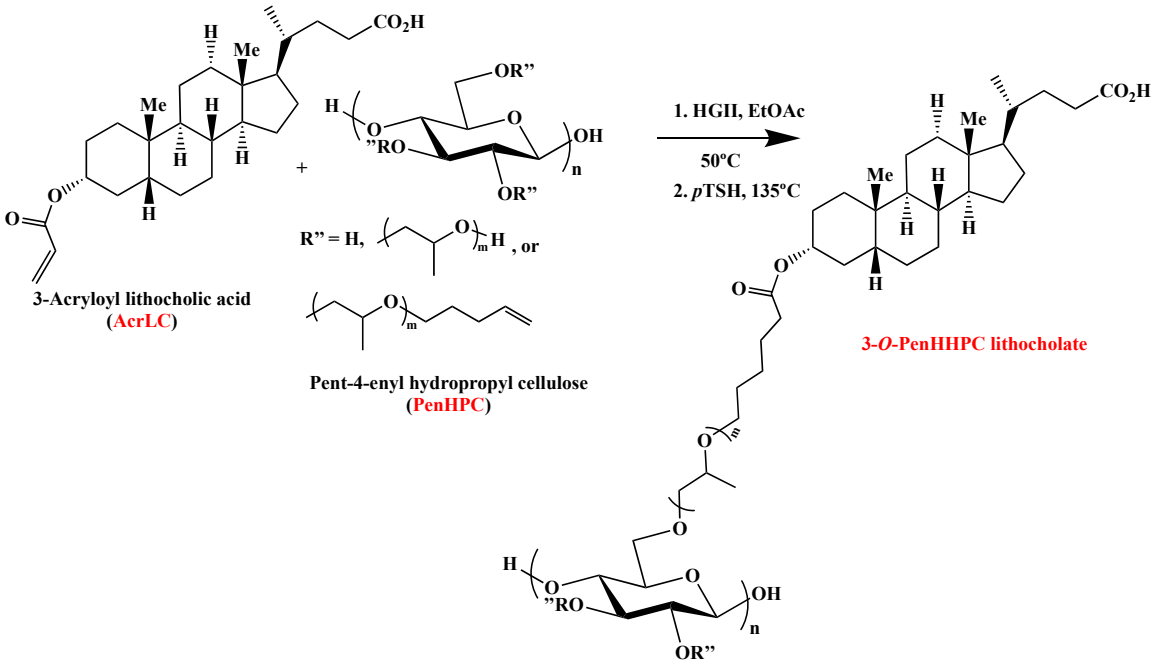

Scheme 3.2. Bile salt CM chemistry.

We explored effects of solvent (EtOAc, THF, DCM) and temperature (37, 50°C) on CM reaction time and conversion (Table 3.2). Earlier bile ester CM conjugation with ethyl cellulose derivatives reached completion within 24 h (37 °C) (Dong et al., 2019), but here we made the useful observation that EtOAc accelerates CM, affording higher efficiency (< equiv (2.9) of precious acrylate required, vs. 5 equiv in THF or CH_2Cl_2 (Dong et al., 2019)) in reaching 100% conjugation. Even with this smaller excess, kinetics in EtOAc were significantly faster; 100%

conversion within 5h at 37 °C. At 50 °C, achievable because of the higher EtOAc boiling point, 100% completion was reached within 3h even at only 2.9:1 type II:type I olefin.

Table 3.2. Reaction times, conversion achieved (DS $_{\text{bile acid conjugate}}$) vs. acrylated bile acid, solvent, and reaction temperature*.

PenHPC DS(pent-4-enyl)	**Solvent, (Temp. (ºC))**	**Conversion (reaction time, h)**			
		AcrMLC	AcrLC	AcrMDC	AcrDC
1.00	THF (37ºC)	100 (36)	--	--	--
	DCM (37ºC)	100 (14.5)	50 (12)	--	--
	EtOAc (50ºC)	100 (3)	100 (3)	100 (3)	100 (3)
0.60	THF (37ºC)	50 (39.5)	50 (39.5)	--	--
	DCM (37ºC)	80 (24)	100 (54)	--	--
		100 (36)	--	--	--
	EtOAc (50ºC)	100 (3)	100 (3)	100 (3)	100 (3)

Catalyst HGII, 10 mol%.

Conjugate formation was monitored by disappearance of terminal olefin proton resonances (4.96, 5.82 ppm) from PenHPC and 5.78-6.36 ppm from the acrylates (e.g. **Figs. 3.2a-b**) along with emergence of new, distinct conjugated olefin proton resonances (5.82, 6.89 ppm). Products also showed expected steroid nucleus proton resonances, between 2.4-0.6 ppm (**Fig. 3.2c**). Adduct structures were further supported by new olefinic carbon resonances (**Figs. 3.3b, S3.3**), which shifted as expected upon conjugation (PenHPC from 114.5, 138.4; acrylate from 129.1, 130.2 ppm) to 121 and 149.4 ppm, respectively (**Fig. 3.3a,b**). After CM completion, we demonstrated the possibility of recovering valuable, unreacted bile salt acrylate, by concentrating the hexanes fitrate

after precipitation, and redissolving the resulting crude solid in minimal solvent for subsequent injection into a silica plug for further isolation from residual catalyst or polymer. The more polar PenHPC or PenHPC-bile ester conjugate residue was retained by the silica, while the less polar acrylate and potentially some HG II catalyst coeluted with the mobile hexanes, from which it was readily recovered by evaporation.

We have previously shown that α, β-unsaturated CM products are prone to radical-initiated γ-H-atom abstraction (Meng & Edgar, 2015), followed by undesired radical reactions. We eliminated this risk in our CM adducts by final transfer hydrogenation of the conjugated olefins (Dong et al., 2017; Dong & Edgar, 2015; Meng et al., 2014; Meng & Edgar, 2015), refluxing the conjugate at 135°C in the presence of *p*-toluene sulfonyl hydrazide (*p*TSH). Complete hydrogenation was clearly indicated by the absence of vinyl proton or carbon resonances in product ^{1}H and ^{13}C NMR spectra (**Fig. S3.4**). Further, expected FT-IR shifts and absorbance reductions were observed for conjugates and their corresponding hydrogenated products (**Fig. S3.1a-d, bottom**). We refer to the hydrogenated conjugate of PenHPC and AcrLC as 3-*O*-PenHHPC lithocholate (Scheme 3.2; where the "H" that precedes "HPC" refers to "hydrogenated"); in this case DS(pent-4-enyl) was 1.0 (exemplary ^{1}H NMR spectra **Fig. 3.2, 3.3**).

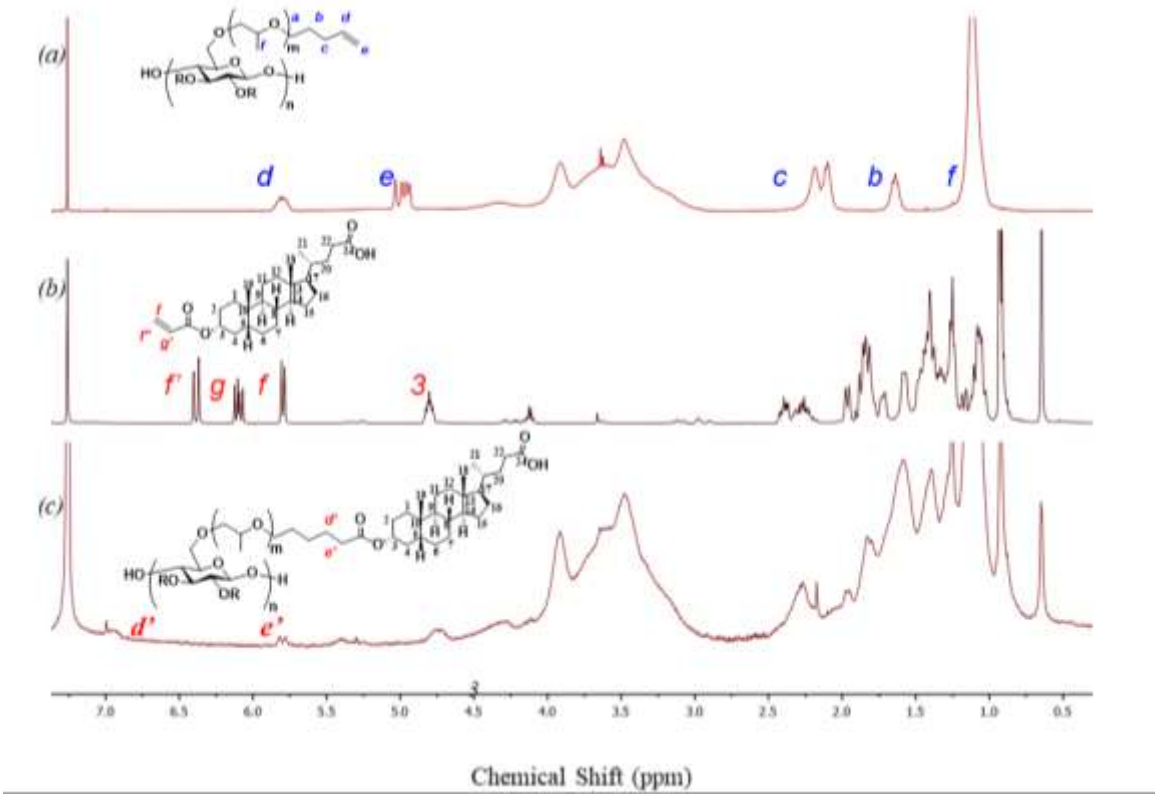

Figure 3.2. Proton NMR spectra of a) PenHPC b) AcrLC , c) CM conjugate, 3-*O*-PenHHPC lithocholate (1.00).

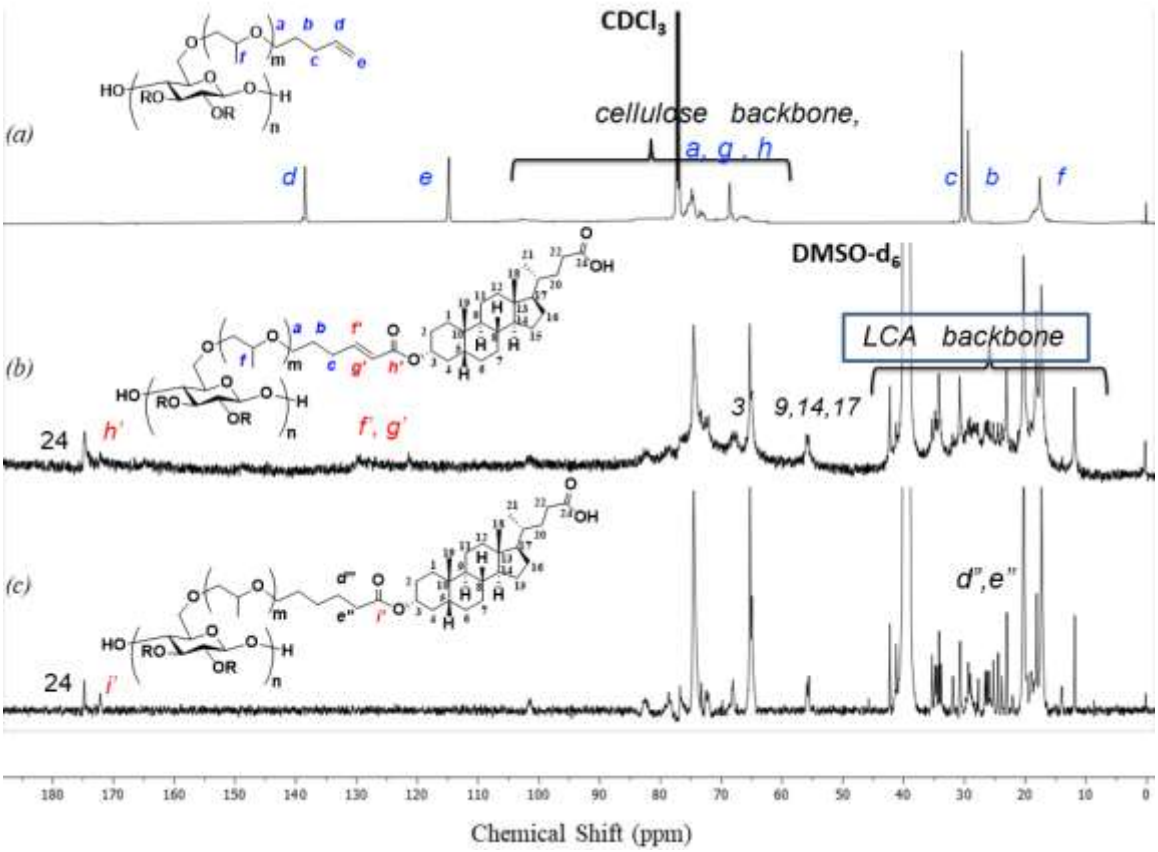

Figure 3.3. ^{13}C NMR spectra of a) PenHPC b) AcrLC , c) CM conjugate, 3-*O*-PenHHPC lithocholate (1.00).

We demonstrated selective hydrolysis of 3-*O*-PenHHPC lithocholate D-ring methyl ester. Hydrolysis was performed after hydrogenation, via brief reflux (2M NaOH, 1h). This afforded a ready, straightforward approach to obtain two of our target compounds (methyl ester- or carboxylic acid-bearing), avoiding potential cleavage of acrylate ester. In spite of this success, purification afforded a modest yield (~18%). It is possible that, despite the brief heating, sufficient depolymerization may have occurred to cause polymer loss during dialysis (MWCO 3.5kDa).

Polymers with sufficiently high T_g (40-50°C above ambient temperature) are desired to combat effects of humidity and possible drug plasticization upon the formulation. Many cellulose derivatives have high T_g values (Dong et al., 2019), but it was important to investigate possible internal plasticization by bile acid substituents. PenHPC (DS (Pen) = 1.00) T_g is 91 °C, (Dong,

Mosquera-Giraldo, Taylor, et al., 2016). Each hydrogenated conjugate displayed T_g well above ambient temperature, from 80.71 - 145 °C, though some were quite weak. The higher *Tg* derivatives have significant potential for sustaining ASD formulations in the glassy state (**Fig. S3.9-3.16**, Table S3.1).

We tested performance of these complex bile acid- and bile ester-tethered polysaccharides *in vitro* as drug crystallization inhibitors. The time at which drug crystallization became detectable due to drop in drug solution content (inflection point in $A_{237\ nm}$) was designated as the nucleation induction time, measured in the absence and presence of each polymer. Enzalutamide is a hydrophobic, fast crystallizing, poorly water-soluble (crystalline solubility = 2.9 μg/mL) prostate cancer therapeutic (Wilson et al., 2018).

We had hypothesized that more hydrophilic polymers would result in effective crystallization inhibition. In the absence of polymer (**Fig. 3.4**), the drug crystallized quickly, within 7 min.

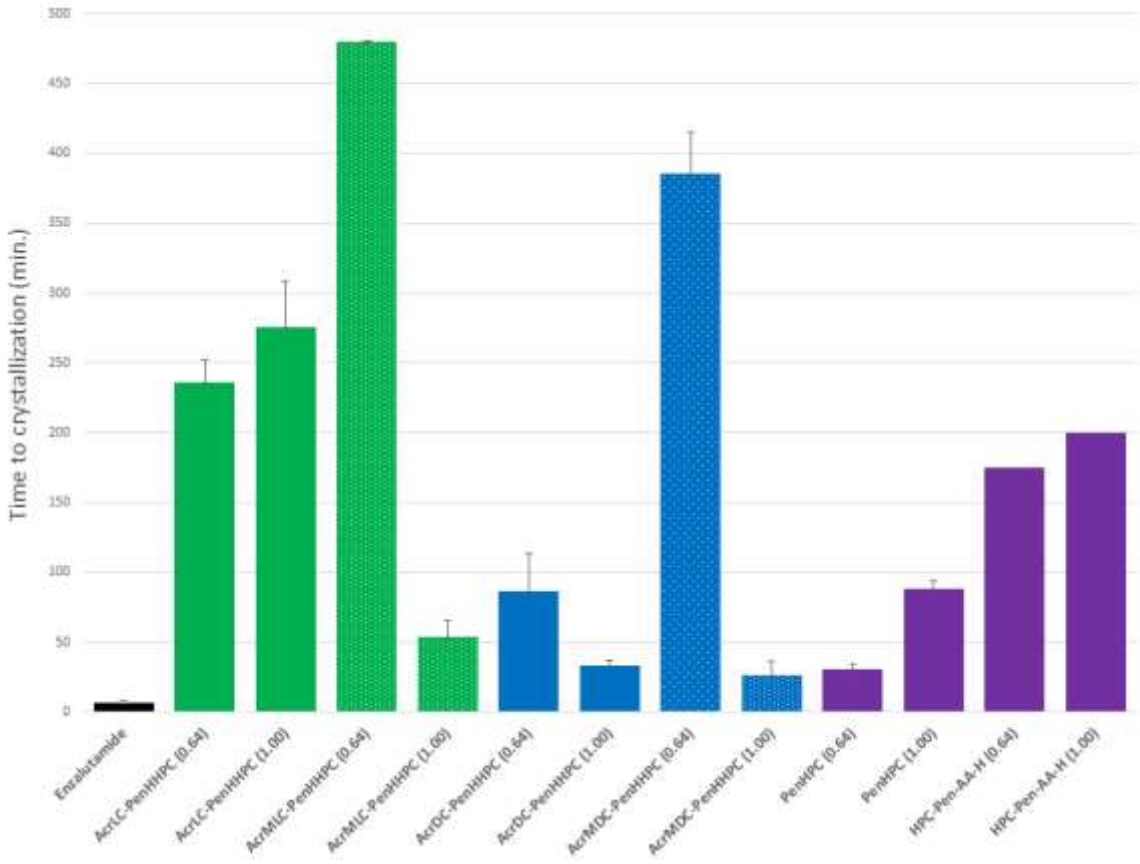

Figure 3.4: Enzalutamide nucleation induction times in absence and presence of pre-dissolved polymers (n = 3; polymer abbreviations and structures see Table S3.2).

Previous studies showed the importance of carboxylic acids in effective crystallization inhibitors (Mosquera-Giraldo et al., 2016), but also showed that higher DS(CO_2H) at some point does not enhance polymer effectiveness (Mosquera-Giraldo, Borca, et al., 2018). Using computer simulations, we have shown that drug molecules tended to interact with the hydrophobic portion of the polymer rather than forming specific interactions with the carboxylic acids. This suggested that carboxylic acids may provide amphiphilicity, but do not necessarily form specific interactions with drug molecules. Herein, we found that the best performing ASD polymers with regard to inhibition of enzalutamide crystallization were methyl esterified, in particular those with lower DS(bile salt ester). 3-*O*-PenHHPC methyl lithocholate (DS(bile ester) 0.64) can effectively

maintain supersaturation for ca. 8h (when experiment was terminated). Meanwhile, 3-*O*-PenHHPC methyl deoxycholate (DS bile ester 0.64) afforded induction time until crystallization of ca. 385 min. It appears that for enzalutamide, hydrophobic interactions between bile salt ester and drug were more important than amphiphilicity provided by the carboxylic acid substituents, which seemed to be of importance for many polysaccharide derivatives (Arca et al., 2018; Dong, Mosquera-Giraldo, et al., 2017; Dong, Mosquera-Giraldo, Troutman, et al., 2016; Ilevbare et al., 2013b; Liu et al., 2014; Tanno et al., 2004). Alternatively, the combination of bile ester and hydrophilic cellulose ether backbone generates a degree of ampiphilicity that enables the appropriate balance between polymer-water interactions and polymer-drug interactions, as suggested in previous studies (Mosquera-Giraldo, Borca, et al., 2018). All of our bile acid/ester conjugates with HPC pentyl ether prolonged enzalutamide crystallization time. We were pleased to observe that LCA derivatives (simpler to make) consistently out-performed DCA derivatives.

We compared performance of these novel ASD polymer candidates to their cellulose ether precursors (pent-4-enyl HPC, DS(pent-4-enyl) 0.64, 1.0), which were not conjugated to bile salts and thus could serve as negative controls. As positive controls, we used CM adducts of pentenyl HPC with acrylic acid (after hydrogenation), HPC-Pen-AA-H (0.64) and HPC-Pen-AA-H (1.00), since we previously shown that they are effective crystallization inhibitors (Wilson et al., 2020). Enzalutamide crystallizes in < 150 min using similar conditions (50 μg/mL polymer, 50 mM phosphate buffer) in the presence of 5-carboxypentyl HPC with DS(carboxypentyl) 1.0 (Wilson et al., 2020), supporting the concept that sufficiently hydrophilic bile salt-appended cellulose ethers are synergistic and effective crystallization inhibitors.

Fedor SPs of our derivatives were calculated (Table S3.3). Effective crystallization inhibitors have been associated with moderate hydrophobicity, ranging from SP 20-23 $MPa^{1/2}$ for

promising cellulose esters (Ilevbare et al., 2013a, 2013b) and ethers (Dong, Mosquera-Giraldo, Taylor, et al., 2016). The pentenyl HPC derivatives are more hydrophilic, with SP values 22.8 and 21.8 $MPa^{1/2}$ for DS (Pen) = 0.64 and 1, respectively; vs. the more hydrophobic pentenyl substituted EC2.30C5 DS(Pen) = 0.69 (SP values 18.0 to 19.9 $MPa^{1/2}$). Thus SP values for HPC-bile salt adducts prepared herein, falling within 21.0-23.2 $MPa^{1/2}$ indicate improved hydrophilicity, which contributes to longer nucleation induction times in most cases.

Conclusions

We confirmed our original hypothesis by demonstrating synergistic, enhanced ASD performance of conjugates of bile acids with HPC derivatives, with their improved hydrophilicity. Grubbs Type II olefin acrylates of bile salts or their methyl esters were prepared chemo- and regioselectively by acrylation of bile salts and esters, followed by efficient, mild CM, in order to probe both A- and D-ring structure-property relationships regarding crystal growth inhibition. Careful selection of acrylating agent, minimizing its excess, and optimizing base stoichiometry allowed us to achieve chemoselective acrylation of the LCA A-ring hydroxyl. By so doing we eliminate the extra methyl esterification step as well as the sensitive saponification of the methyl ester in the presence of the acrylate ester. These methods also provided a degree of regioselectivity in acrylation of the equatorial 3-OH of DCA in the A-ring vs. to the C-ring 12-OH. We significantly improved both CM kinetics and efficiency of preparing these complex structures by optimizing conditions. EtOAc provides much faster CM conversion. Rates of initiation in olefin methathesis are known to increase with solvent polarity (Sanford et al., 2001), and DCM (20.2) has a higher Hildebrand SP than EtOAc (18.2), so the faster rates in EtOAc are an important and pleasant surprise. The higher EtOAc boiling point must certainly be influential on kinetics; for example, AcrMLC CM completion in EtOAc taking 3h at 50 °C vs. 14.5 h in DCM at 37°C (**Table**

3.2). Although their polarities are similar and THF boiling point is slightly higher (Hildebrand SP 18.3, BP 66ºC (Sanford et al., 2001)), CM was faster in EtOAc than in THF, 100% conversion of AcrMLC in the latter solvent for example taking 36h. The better ability of THF to coordinate metals may be a factor, perhaps by competing for Ru coordination sites. Superior CM performance in EtOAc promises greater efficiency than previously reported bile salt CM chemistry (Dong et al., 2019), reducing usage of expensive bile acid starting materials, and allowing recycle of unreacted bile salt acrylate; virtually 100% efficiency with regard to bile salt acrylate may be possible.

These results illuminate structure-property relationships of bile acid vs. bile ester decorated polysaccharides for oral drug delivery, simultaneously highlighting the remarkable potential of mild, flexible, and efficient CM chemistry for synthesis of complex polysaccharide derivatives. It is worth emphasizing that even with large, sterically demanding, slow diffusing molecules like these cellulose derivatives, and even when the CM type II olefin partner is a relatively bulky small molecule like a bile salt derivative, relatively rapid and fully complete, selective CM conversions were achieved, enabling preparation of these challenging structures in a few synthetic steps.

The improved hydrophilicity of each ASD polymer vs. the corresponding ethyl cellulose-bile salt adduct led to substantially increased nucleation-induction times (e.g., slower crystallization) even with the fast-crystallizing prostate cancer drug, enzulatamide. In some cases, bile salt adduct methyl esters performed better than the corresponding acids. This was a surprising result, given our earlier studies showing the value of carboxylic acid substituents in prolonging nucleation times. While carboxyl-containing polysaccharides have often performed well in crystallization inhibition (e.g., hydroxypropyl methyl cellulose acetate succinate is a leading commercial ASD polymer (Curatolo et al., 2009)) and in structure-property studies (Liu et al.,

2014), it is also true that neutral cellulose ethers like HPC and hydroxypropyl methyl cellulose are effective ASD polymers for certain drugs (Arca et al., 2018), and neither contains carboxyl groups. This study highlights the importance of amphiphilic character of the polymer to ASD performance, indicating that, in this family of polymers at least, the absence of a pendent carboxylic acid to act as a pH trigger and provide amphiphilicity can be overcome by interactions between the hydrophobic bile salt methyl ester substituent and the drug. It also illustrates the complex nature of these structure property relationships, illustrated in **Fig. S3.17** by comparing crystallization induction time of these polymers to solubility parameter, bile salt type and DS, and whether the terminus of the bile salt substituent was a carboxylic acid or a methyl ester. It is clear from the relationship that LCA derivatives performed better, as did those with higher DS(bile salt). While the methyl esterified LCA adduct gave the best performance, there was not a clear overall trend to better performance for the methyl esters. Rather than acting as an ASD, we suspect the presence of micelles may arise from either the additional hydroxyl in DCA-containing derivatives or less substituted analogs due to interactions between the flexible bile salt tethers and hydroxyl groups from either the cellulose backbone or hydroxypropyl chains. Prior studies have shown CMC driven aggregation may eliminate inhibitor activity from the bile salts (Lu, Ormes, Lowinger, Mann, Xu, Patel, et al., 2017), which can be investigated with nucleation induction times pre- and post- CMC of the analogs. The best performers had solubility parameters between 21.5-22.5, but there were also several poor performers in that SP range.

In the best case, the methyl ester of LCA and pentenyl HPC adduct, *in vitro* enzalutamide crystallization time was nearly 8 h, considerably exceeding normal small intestine residence time. It was also gratifying and useful that the LCA derivatives performed best, since they are simpler to synthesize and pose less complex regioselectivity problems. It will be of great interest to probe

further the structure property relationships of these cellulose ether–bile salt adducts, further illuminating features needed for truly superior crystallization inhibition even in difficult cases like enzalutamide, and providing further insight into the fundamental nature of and structural requirements for crystallization inhibition.

References

Arca, H. C., Mosquera-Giraldo, L. I., Bi, V., Xu, D., Taylor, L. S., & Edgar, K. J. (2018). Pharmaceutical Applications of Cellulose Ethers and Cellulose Ether Esters. *Biomacromolecules*, *19*(7), 2351–2376. https://doi.org/10.1021/acs.biomac.8b00517

Arca, H. Ç., Mosquera-Giraldo, L. I., Pereira, J. M., Sriranganathan, N., Taylor, L. S., & Edgar, K. J. (2018). Rifampin Stability and Solution Concentration Enhancement Through Amorphous Solid Dispersion in Cellulose ω-Carboxyalkanoate Matrices. *Journal of Pharmaceutical Sciences*, *107*(1), 127–138. https://doi.org/10.1016/J.XPHS.2017.05.036

Baird, J. A., Van Eerdenbrugh, B., & Taylor, L. S. (2010). A Classification System to Assess the Crystallization Tendency of Organic Molecules from Undercooled Melts. *Journal of Pharmaceutical Sciences*, *99*(9), 3787–3806. https://doi.org/10.1002/JPS.22197

Carter Fox, S., Li, B., Xu, D., & J. Edgar, K. (2011). Regioselective Esterification and Etherification of Cellulose: A Review. *Biomacromolecules*, *12*(6), 1956–1972. https://doi.org/10.1021/bm200260d

Chatterjee, A. K., Choi, T.-L., Sanders, D. P., & Grubbs, R. H. (2003). A General Model for Selectivity in Olefin Cross Metathesis. *Journal of the American Chemical Society*, *125*(37), 11360–11370. https://doi.org/10.1021/ja0214882

Chen, J., Mosquera-Giraldo, L. I., Ormes, J. D., Higgins, J. D., & Taylor, L. S. (2015). Bile salts as crystallization inhibitors of supersaturated solutions of poorly water-soluble compounds.

Crystal Growth and Design, *15*(6), 2593–2597. https://doi.org/10.1021/acs.cgd.5b00392

Craig, D. Q. M. (2002). The mechanisms of drug release from solid dispersions in water-soluble polymers. *International Journal of Pharmaceutics*, *231*(2), 131–144. https://doi.org/https://doi.org/10.1016/S0378-5173(01)00891-2

Curatolo, W., Nightingale, J. A., & Herbig, S. M. (2009). Utility of Hydroxypropylmethylcellulose Acetate Succinate (HPMCAS) for Initiation and Maintenance of Drug Supersaturation in the GI Milieu. *Pharmaceutical Research*, *26*(6), 1419–1431. https://doi.org/10.1007/s11095-009-9852-z

Dong, Y., & Edgar, K. J. (2015). Imparting functional variety to cellulose ethers via olefin cross-metathesis. *Polymer Chemistry*, *6*(20), 3816–3827. https://doi.org/10.1039/C5PY00369E

Dong, Y., Matson, J. B., & Edgar, K. J. (2017). Olefin Cross-Metathesis in Polymer and Polysaccharide Chemistry: A Review. *Biomacromolecules*, *18*(6), 1661–1676. https://doi.org/10.1021/acs.biomac.7b00364

Dong, Y., Mosquera-Giraldo, L. I., Taylor, L. S., & Edgar, K. J. (2016). Amphiphilic Cellulose Ethers Designed for Amorphous Solid Dispersion via Olefin Cross-Metathesis. *Biomacromolecules*, *17*(2), 454–465. https://doi.org/10.1021/acs.biomac.5b01336

Dong, Y., Mosquera-Giraldo, L. I., Taylor, L. S., & Edgar, K. J. (2017). Tandem modification of amphiphilic cellulose ethers for amorphous solid dispersion via olefin cross-metathesis and thiol-Michael addition. *Polymer Chemistry*, *8*(20), 3129–3139. https://doi.org/10.1039/C7PY00228A

Dong, Y., Mosquera-Giraldo, L. I., Troutman, J., Skogstad, B., Taylor, L. S., & Edgar, K. J. (2016). Amphiphilic hydroxyalkyl cellulose derivatives for amorphous solid dispersion prepared by olefin cross-metathesis. *Polymer Chemistry*, *7*(30), 4953–4963.

https://doi.org/10.1039/C6PY00960C

Dong, Y., Novo, D. C., Mosquera-Giraldo, L. I., Taylor, L. S., & Edgar, K. J. (2019a). Conjugation of bile esters to cellulose by olefin cross-metathesis: A strategy for accessing complex polysaccharide structures. *Carbohydrate Polymers*, *221*, 37–47. https://doi.org/10.1016/j.carbpol.2019.05.061

Dong, Y., Novo, D. C., Mosquera-Giraldo, L. I., Taylor, L. S., & Edgar, K. J. (2019b). Conjugation of bile esters to cellulose by olefin cross-metathesis: A strategy for accessing complex polysaccharide structures. *Carbohydrate Polymers*, *221*, 37–47. https://doi.org/10.1016/J.CARBPOL.2019.05.061

Edgar, K., Arnold, K., Blount, W., Lawniczak, J., & Lowman, D. (1995). Synthesis and Properties of Cellulose Acetoacetates. *Macromolecules*, *28*(12), 4122–4128. https://doi.org/10.1021/ma00116a011

Fedors, R. F. (1974). A method for estimating both the solubility parameters and molar volumes of liquids. Supplement. *Polymer Engineering & Science*, *14*(6), 472–472. https://doi.org/10.1002/pen.760140611

Fischer, E., & Speier, A. (1895). Darstellung der Ester. *Berichte Der Deutschen Chemischen Gesellschaft*, *28*(3), 3252–3258. https://doi.org/10.1002/CBER.189502803176

Frank, D. S., & J. Matzger, A. (2018). Probing the Interplay between Amorphous Solid Dispersion Stability and Polymer Functionality. *Molecular Pharmaceutics*, *15*(7), 2714–2720. https://doi.org/10.1021/acs.molpharmaceut.8b00219

G. Ricarte, R., J. Van Zee, N., Li, Z., M. Johnson, L., P. Lodge, T., & A. Hillmyer, M. (2019). Recent Advances in Understanding the Micro- and Nanoscale Phenomena of Amorphous Solid Dispersions. *Molecular Pharmaceutics*, *16*(10), 4089–4103.

https://doi.org/10.1021/acs.molpharmaceut.9b00601

Grubbs, R. H. (2004). Olefin metathesis. *Tetrahedron*, *60*(34), 7117–7140. https://doi.org/https://doi.org/10.1016/j.tet.2004.05.124

HASEGAWA, A., TAGUCHI, M., SUZUKI, R. I. E., MIYATA, T., NAKAGAWA, H., & SUGIMOTO, I. (1988). Supersaturation Mechanism of Drugs from Solid Dispersions with Enteric Coating Agents. *CHEMICAL & PHARMACEUTICAL BULLETIN*, *36*(12), 4941–4950. https://doi.org/10.1248/cpb.36.4941

Hu, X., Zhang, Z., Zhang, X., Li, Z., & Zhu, X. X. (2005). Selective acylation of cholic acid derivatives with multiple methacrylate groups. *Steroids*, *70*(8), 531–537. https://doi.org/https://doi.org/10.1016/j.steroids.2004.11.015

Ilevbare, G. A., Liu, H., Edgar, K. J., & Taylor, L. S. (2013a). Maintaining Supersaturation in Aqueous Drug Solutions: Impact of Different Polymers on Induction Times. *Crystal Growth & Design*, *13*(2), 740–751. https://doi.org/10.1021/cg301447d

Ilevbare, G. A., Liu, H., Edgar, K. J., & Taylor, L. S. (2013b). Impact of Polymers on Crystal Growth Rate of Structurally Diverse Compounds from Aqueous Solution. *Molecular Pharmaceutics*, *10*(6), 2381–2393. https://doi.org/10.1021/mp400029v

Jackson, M. J., Kestur, U. S., Hussain, M. A., & Taylor, L. S. (2016). Dissolution of Danazol Amorphous Solid Dispersions: Supersaturation and Phase Behavior as a Function of Drug Loading and Polymer Type. *Molecular Pharmaceutics*, *13*(1), 223–231. https://doi.org/10.1021/ACS.MOLPHARMACEUT.5B00652/ASSET/IMAGES/ACS.MOLPHARMACEUT.5B00652.SOCIAL.JPEG_V03

Li, N., Mosquera-Giraldo, L. I., Borca, C. H., Ormes, J. D., Lowinger, M., Higgins, J. D., Slipchenko, L. V, & Taylor, L. S. (2016). A Comparison of the Crystallization Inhibition

Properties of Bile Salts. *Crystal Growth & Design*, *16*(12), 7286–7300. https://doi.org/10.1021/acs.cgd.6b01470

Li, Y., & Ray Dias, J. (1997). Dimeric and Oligomeric Steroids. *Chemical Reviews*, *97*(1), 283–304. https://doi.org/10.1021/cr9600565

Liu, H., Ilevbare, G. A., Cherniawski, B. P., Ritchie, E. T., Taylor, L. S., & Edgar, K. J. (2014). Synthesis and structure-property evaluation of cellulose ω-carboxyesters for amorphous solid dispersions. *Carbohydrate Polymers*, *100*, 116–125. https://doi.org/10.1016/j.carbpol.2012.11.049

Liu, H., Taylor, L. S., & Edgar, K. J. (2015). The role of polymers in oral bioavailability enhancement; a review. *Polymer*, *77*, 399–415. https://doi.org/10.1016/J.POLYMER.2015.09.026

Lu, J., Ormes, J. D., Lowinger, M., Mann, A. K. P., Xu, W., Litster, J. D., & Taylor, L. S. (2017). Maintaining Supersaturation of Active Pharmaceutical Ingredient Solutions with Biologically Relevant Bile Salts. *Crystal Growth & Design*, *17*(5), 2782–2791. https://doi.org/10.1021/acs.cgd.7b00237

Lu, J., Ormes, J. D., Lowinger, M., Mann, A. K. P., Xu, W., Patel, S., Litster, J. D., & Taylor, L. S. (2017). Impact of Bile Salts on Solution Crystal Growth Rate and Residual Supersaturation of an Active Pharmaceutical Ingredient. *Crystal Growth & Design*, *17*(6), 3528–3537. https://doi.org/10.1021/acs.cgd.7b00464

Meng, X., & Edgar, K. J. (2015). Synthesis of amide-functionalized cellulose esters by olefin cross-metathesis. *Carbohydrate Polymers*, *132*, 565–573. https://doi.org/https://doi.org/10.1016/j.carbpol.2015.06.052

Meng, X., Matson, J. B., & Edgar, K. J. (2014). Olefin cross-metathesis, a mild, modular

approach to functionalized cellulose esters. *Polymer Chemistry*, *5*(24), 7021–7033. https://doi.org/10.1039/C4PY01102C

Mosquera-Giraldo, L. I., Borca, C. H., Meng, X., Edgar, K. J., Slipchenko, L. V, & Taylor, L. S. (2016). Mechanistic Design of Chemically Diverse Polymers with Applications in Oral Drug Delivery. *Biomacromolecules*, *17*(11), 3659–3671. https://doi.org/10.1021/acs.biomac.6b01156

Mosquera-Giraldo, L. I., H. Borca, C., S. Parker, A., Dong, Y., J. Edgar, K., P. Beaudoin, S., V. Slipchenko, L., & S. Taylor, L. (2018). Crystallization Inhibition Properties of Cellulose Esters and Ethers for a Group of Chemically Diverse Drugs: Experimental and Computational Insight. *Biomacromolecules*, *19*(12), 4593–4606. https://doi.org/10.1021/acs.biomac.8b01280

Mosquera-Giraldo, L. I., Li, N., Wilson, V. R., Nichols, B. L. B., Edgar, K. J., & Taylor, L. S. (2018). Influence of Polymer and Drug Loading on the Release Profile and Membrane Transport of Telaprevir. *Molecular Pharmaceutics*, *15*(4), 1700–1713. https://doi.org/10.1021/acs.molpharmaceut.8b00104

Mukhopadhyay, S., & Maitra, U. (2004). Chemistry and biology of bile acids. *Current Science*, *87*(12), 1666–1683. http://www.jstor.org/stable/24109764

Pavlović, N., Goločorbin-Kon, S., Danić, M., Stanimirov, B., Al-Salami, H., Stankov, K., & Mikov, M. (2018). Bile acids and their derivatives as potential modifiers of drug release and pharmacokinetic profiles. *Frontiers in Pharmacology*, *9*(NOV). https://doi.org/10.3389/FPHAR.2018.01283/FPHAR_09_01283_PDF.PDF

Pereira, J. M., Mejia-Ariza, R., Ilevbare, G. A., McGettigan, H. E., Sriranganathan, N., Taylor, L. S., Davis, R. M., & Edgar, K. J. (2013). Interplay of degradation, dissolution and

stabilization of clarithromycin and its amorphous solid dispersions. *Molecular Pharmaceutics*, *10*(12), 4640–4653. https://doi.org/10.1021/MP400441D/SUPPL_FILE/MP400441D_SI_001.PDF

Sanford, M. S., Love, J. A., & Grubbs, R. H. (2001). Mechanism and Activity of Ruthenium Olefin Metathesis Catalysts. *Journal of the American Chemical Society*, *123*(27), 6543–6554. https://doi.org/10.1021/ja010624k

Tanno, F., Nishiyama, Y., Kokubo, H., & Obara, S. (2004). Evaluation of Hypromellose Acetate Succinate (HPMCAS) as a Carrier in Solid Dispersions. *Drug Development and Industrial Pharmacy*, *30*(1), 9–17. https://doi.org/10.1081/DDC-120027506

Taylor, L. S., & Zhang, G. G. Z. (2016). Physical chemistry of supersaturated solutions and implications for oral absorption. *Advanced Drug Delivery Reviews*, *101*, 122–142. https://doi.org/10.1016/J.ADDR.2016.03.006

Trasi, N. S., & Taylor, L. S. (2015). Dissolution performance of binary amorphous drug combinations—Impact of a second drug on the maximum achievable supersaturation. *International Journal of Pharmaceutics*, *496*(2), 282–290. https://doi.org/10.1016/J.IJPHARM.2015.10.026

Van Eerdenbrugh, B., Baird, J. A., & Taylor, L. S. (2010). Crystallization Tendency of Active Pharmaceutical Ingredients Following Rapid Solvent Evaporation—Classification and Comparison with Crystallization Tendency from Under cooled Melts. *Journal of Pharmaceutical Sciences*, *99*(9), 3826–3838. https://doi.org/10.1002/JPS.22214

Van Eerdenbrugh, B., Raina, S., Hsieh, Y. L., Augustijns, P., & Taylor, L. S. (2014). Classification of the crystallization behavior of amorphous active pharmaceutical ingredients in aqueous environments. *Pharmaceutical Research*, *31*(4), 969–982.

https://doi.org/10.1007/S11095-013-1216-Z/TABLES/5

Wilson, V., Lou, X., Osterling, D. J., Stolarik, D. F., Jenkins, G., Gao, W., Zhang, G. G. Z., & Taylor, L. S. (2018). Relationship between amorphous solid dispersion in vivo absorption and in vitro dissolution: phase behavior during dissolution, speciation, and membrane mass transport. *Journal of Controlled Release : Official Journal of the Controlled Release Society*, *292*, 172–182. https://doi.org/10.1016/j.jconrel.2018.11.003

Wilson, V. R., Lou, X., Osterling, D. J., Stolarik, D. F., Jenkins, G. J., Nichols, B. L. B., Dong, Y., Edgar, K. J., Zhang, G. G. Z., & Taylor, L. S. (2020). Amorphous solid dispersions of enzalutamide and novel polysaccharide derivatives: investigation of relationships between polymer structure and performance. *Scientific Reports*, *10*(1), 18535. https://doi.org/10.1038/s41598-020-75077-7

Zhu, X.-X., & Nichifor, M. (2002). Polymeric Materials Containing Bile Acids. *Accounts of Chemical Research*, *35*(7), 539–546. https://doi.org/10.1021/ar0101180

Chapter 4. Tracking polysaccharides: Synthesis of environment-sensitive, polysaccharide-based fluorophores via reductive-amination

Diana C. Novo [a, b], Chengzhe Gao [d], Qingqing Qi [d], Lynne S. Taylor [d], and Kevin J. Edgar* [a, c]

[a]*Department of Sustainable Biomaterials, Virginia Tech, Blacksburg, VA 24061, United States*

[b]*Department of Chemistry, Virginia Tech, Blacksburg, VA 24061, United States*

[c]*Macromolecules Innovation Institute, Virginia Tech, Blacksburg, VA 24061, United States*

[d]*Department of Industrial and Physical Pharmacy, College of Pharmacy, West Lafayette, Indiana 47907, United States*

Abstract

Polysaccharides (PS) and derivatives are extraordinarily valuable materials in drug delivery, tissue engineering, and other biomedical fields due to their (typically) benign, renewable, often biodegradable natures, as well as the ability to modify PS to enhance processing and function by substitution of their hydroxyl and other reactive groups. Therefore, the ability to track the fate of PS, especially *in vivo*, is of special importance. Herein we exploit chemoselective and regioselective oxidation chemistry that enables ready conversion of terminal OH groups of oligo(hydroxypropyl) polysaccharides (or oligosaccharides) to ketones. We have previously shown that these ketones are valuable precursors to pro-drugs and hydrogels; herein we demonstrate that Schiff-base chemistry can transform these terminal ketone groups by reductive amination into pendant fluorophores. Amorphous solid dispersions (ASD) are particularly important applications of PS derivatives to drug delivery, as they address the crucial issue of enhancing the poor aqueous solubility of hydrophobic drugs by creating a supersaturated solution of the drug in a polymer matrix. The precise mechanisms by which ASD polymers solubilize and stabilize amorphous drugs and enable supersaturated drug solutions are still incompletely understood, but may be illuminated by use of fluorescent probes. We demonstrate

herein convenient fluorophore attachment chemistry using ethers of PS and oligosaccharides (e.g. oligo(hydroxypropyl) celluloses and hydroxypropyl β-cyclodextrin) that are important drug delivery polymers. These polymers were first oxidized to targeted degrees of substitution (Ox-HPC DS(ketone) = 0.2, 0.5, 0.8; Ox-HPMC DS(ketone) = 0.06 and 0.17; and Ox-HPβCD DS(ketone) = 0.14, 1.05, and 2.2, respectively), then were subjected to either step-wise or one-pot reductive amination with Nile Blue amine in various solvents (MeOH/THF, dichloroethane (DCE), or *N*, *N*-dimethylformamide (DMF)) in order to append the fluorophore by a stable amine bond. We show fluorescent activity and sensitivity of these fluorophore-substituted PS and oligomers to hydrophobic and hydrophilic environments as exhibited in polar and non-polar solvents; dimethyl sulfoxide (DMSO), *N*, *N*-dimethylformamide (DMF), 10% toluene/DMSO, 10% toluene/DMF, and 10% *t*-BuOH/DMSO.

1. Introduction

It would seem straightforward to dismiss the possibility that PS and derivatives could be orally bioavailable. Lipinski's "rules of 5", which allow for predicting oral bioavailability of drug candidate structures, predict that PS possess too many hydrogen bond donors and acceptors, have excessively high molecular weights, and are too polar to pass through the epithelium from the small intestine to the bloodstream. Yet bioavailability of PS is still an important topic of discussion, and certain PS have been said to be orally bioavailable (e.g. low molecular weight heparin (D. Y. Lee et al., 2008; Y. Lee et al., 2006)). Tracking PS oral bioavailability is thus important; so is tracking the fate of intravenously administered poly- and oligosaccharides. Linear dextran is routinely administered to patients intravenously, for purposes that include enhancing delivery of iron and maintaining osmotic balance (Auerbach et al., 2011; Johnson & Angeles, n.d.; Mamula et al., 2002; Mays & Mays, 1976). Pullulan has been demonstrated to distribute, after intravenous

administration, largely to the liver (Kaneo et al., 2001). Thus, considerable research has been devoted to exploiting this property of pullulan to develop pullulan-based prodrugs to treat liver ailments (Hosseinkhani et al., 2002; Joshi & Devarajan, 2014). Substituted cyclodextrins, with hydroxypropyl β-cyclodextrin (HPβCD) perhaps most prominent among them, are included in approved intravenous drug formulations (Pitha et al., 1988) to enhance solubility of otherwise poorly soluble drugs, and have also been investigated for oral formulations for the same purpose (Evrard et al., 2002; Loftsson & Brewster, 2011). Tracking, e.g., HPβCD *in vivo* is important for the same reasons as for PS and derivatives; in addition, certain less soluble cyclodextrins such as β-CD itself are known to have the potential to cause harm if they reach the kidney microtubules (Frömming & Szejtli, 1994; Perrin et al., 1978).

Tracking PS and oligosaccharides *in vivo*, where they typically are at very low concentrations, is not a simple matter. The two main methods for doing so are radiolabeling and fluorescent labeling. Each has advantages and drawbacks. Radiolabeling is advantaged because it is very sensitive, and because the substitution of a radioisotope of a particular atom (e.g. ^{14}C for ^{12}C) is unlikely to change bulk molecular properties. On the other hand, radiolabeling by definition requires handling of radioactive substances, which requires trained, qualified personnel, as well as proper facilities, and approvals of each.

Fluorescent labeling is also a sensitive method for tracking molecules. It does not involve radioactivity, and does not require special facilities or approvals. On the other hand, fluorescent labeling of a molecule is much more likely to change its physical properties than is radiolabeling. So one can measure the distribution of a fluorescently labeled entity, but does it faithfully reflect the distribution of the unlabeled entity? In the end, for most laboratories fluorescent labeling is the only practical alternative, and care must simply be taken to control the extent of labeling

(substitution) well, so that it is adequate for detection but modifies the structure of the entity being tracked to the minimum extent.

A large proportion of both commercially available and developmental, orally administered drugs are afflicted by poor aqueous solubility (Amidon et al., 2014; Benet, 2013; Fahr & Liu, 2007). Poor water solubility can limit oral bioavailability and thereby negatively impact the patient through increased drug costs, leading to potentially higher side effects, greater within patient and between patient variability, and environmental pollution due to excreted drug. ASD is an increasingly important approach to resolve solubility issues, but to date commercial ASD polymers have been repurposed rather than designed for ASD, and the mechanism by which they enhance bioavailability, and thus design criteria are imperfectly understood. This successful and widely used ASD approach involves generation of a supersaturated solution of drug in the GI tract, released from a molecular drug dispersion in a polymer matrix (Liu et al., 2015). The ASD polymer must stabilize the metastable drug dispersion against drug crystallization in the pill as well as in solution in the small intestine, after release. Release rate of polymer and drug must be matched (Saboo et al., 2020), and this requires deep understanding of polymer-drug interactions. Effective ASDs improve bioavailability (Miller et al., 2012; Pokharkar et al., 2006; Wilson et al., 2020), maintaining stability against crystallization for a physiologically relevant time.

Understanding mechanisms by which ASD/polymer matrices enhance dissolution of even hydrophobic, fast-crystallizing (poorly water-soluble) drugs is challenging. Only a narrow range of commercially available synthetic and cellulosic polymers have been identified as efficient ASD matrices and have been included in formulations approved by the FDA, including poly(vinyl pyrollidone-co-vinyl acetate) (copividone or PVP-VA), hydroxypropylmethyl cellulose (HPMC, also known as hypromellose), and hydroxypropylmethyl cellulose acetate succinate (hypromellose

acetate succinate, HPMCAS). Recently, researchers have designed several cellulose ethers and esters specifically for ASD applications (Arca et al., 2018; Dong, Mosquera-Giraldo, Troutman, et al., 2016; Dong, Mosquera-Giraldo, Taylor, et al., 2016; Dong et al., 2019; Liu et al., 2014, 2015; Ting et al., 2018). Although these new polysaccharide derivative families were devised and studied to provide insight to overarching themes related to polymer function in ASD (Mosquera-Giraldo et al., 2016, 2018), gaps in knowledge regarding drug release and inhibition mechanism still hinder rational design of optimal ASD polymers. This incomplete understanding has significant consequences; problems with current ASD polymers include difficulty with coping with fast crystallizing drugs, and lower potency drugs (that inevitably require higher drug and lower polymer concentration in the formulation).

The Taylor laboratory has identified the importance of drug nanodroplets in effective ASD formulations. When drug release from an ASD exceeds the maximum supersaturation for that drug, phase separation can occur, resulting in formation of nanodroplets that are highly enriched in (typically amorphous) drug. There is a growing recognition of the importance of these nanodroplets and their stabilization by ASD polymers; as soluble drug passes from the intestinal lumen, through the epithelium, into the bloodstream, supersaturation in the small intestine can be rapidly reestablished by drug dissolution from the nanodroplets. Environment-sensitive fluorescence is potentially a highly appropriate tool for examining the mechanism by which a particular polymer structure stabilizes nanodroplets against agglomeration or crystallization, since the drug nanodroplet is virtually always far more hydrophobic than the aqueous milieu of the lumen.

Recently, Nichols et al. have pioneered a green, efficient, economical, chemo-and-regioselective design to introduce ketones onto polysaccharides (Chen et al., 2020; Nichols et al.,

2020). Inspired by Stevens' work on oxidation of small molecule secondary alcohols by household bleach (Stevens et al., 1980), this reaction similarly proceeds with the selective oxidation of the secondary alcohols present at termini of oligo(hydroxypropyl) substituents of, e.g. hydroxypropyl cellulose or hydroxypropyl dextran. We termed the resulting oxidized, ketone-substituted HPC derivative "Ox-HPC". DS(ketone) is easily controlled by bleach stoichiometry. Those ketone-functionalized polymers were shown to condense with small molecule amines (e.g. *p*-aminobenzoic acid or *t*-butyl amine), to form imine linked, prodrug-like molecules. Alternatively, in the presence of a reductant like sodium cyanoborohydride, reductive amination was achieved, appending the substituent more permanently by an amine bond. The ketone-terminated polymers also formed hydrogels by reaction with amine-containing PS, in particular chitosan. The resulting dynamically imine-linked hydrogels were self-healing, injectable, and were devoid of potentially toxic small-molecule crosslinkers (Chen et al., 2020, 2021). We viewed this oxidation/imine formation approach as having potential for extension, by reductive amination, to fluorescent labeling of biologically important poly- and oligosaccharide derivatives. Schellenberg reported the first one-pot, or 'direct' reductive-amination carried out with $NaBH_4$, aldehydes and ketones with amine salts in buffer at 0 °C (Schellenberg, 1963). Although sodium cyanoborohydride ($NaCNBH_3$) offers high selectivity towards imine (rather than ketone) reduction, and was used successfully to reduce Ox-HPC imines in our previous work (Nichols et al., 2020), we chose to explore sodium triacetoxyborohydride ($Na(OAc)_3BH$) as imine reducing reagent as it has less potential to produce toxic byproducts (HCN or NaCN), and has potential for selective one-pot or two-step reductive-amination (Abdel-Magid et al., 1996; Abdel-Magid & Mehrman, 2006).

Traditional biomedical imaging strategies that employ long wavelength dyes encompass either derivatizing the known dyes into further conjugated systems, or performing a two-photon

absorption experiment using a short excitation wavelength and even shorter emitted wavelength. The latter approach is damaging and non-ideal for imaging tissue; a less detrimental alternative such as FRET (Forster Resonance Energy Transfer) utilizes donor/acceptor pairs. FRET occurs when there is a nonradiative energy transfer from an excited donor species (fluorophore) to the acceptor species, such as a biomolecule. The donor possesses a large two-photon cross-section and the acceptor possesses longer wavelength and emission maxima. This results in spectral overlap between the species, increasing the intensity of the acceptor while reducing intensity and lifetime of the donor. This phenomenon can serve as a means to measure the distance between the donor-acceptor species since energy transfer energy is inversely related to the donor-acceptor distance (30-60 Å), and can thus provide insight into drug-polymer interactions that may be key to the success of ASD polymers.

Nile Blue is solvatochromic (that is to say, it is responsive to the solvent polarity environment) and possesses a Stokes shift from ~ 40 – 100 nm (Jose & Burgess, 2006). In polar environments, this shift is reduced to 40 nm. The fluorescence lifetime of Nile Blue is ca. 1.42 ns but depends on temperature, solvent, and occurs at concentrations greater than 10^{-6}-10^{-11} mol/mL (Jose & Burgess, 2006). Lifetime does not depend upon viscosity or concentration. We are not aware of previous reports of Nile Blue or its derivatives having been used as FRET pairs (Martinez & Henary, 2016).

We hypothesize that the new ability to oxidize the terminal, secondary hydroxyl groups of oligo(hydroxypropyl) substituents will provide the opportunity for precisely controlled, relatively simple, facile attachment of amine-containing fluorophores to PS and oligosaccharide (including cyclodextrin) derivatives. With these fluorescent derivatives in hand, we hypothesize that they will be valuable tools for tracking biodistribution and bioavailability of these poly- and oligosaccharide

derivatives, particularly as it pertains to their use in biomedicine. These fluorescently labeled derivatives should, thanks to their environmentally-sensitive fluorescence characteristics, also prove valuable for illuminating interactions with the medium and with other solutes, and in particular the precise mechanisms by which ASD polymers solubilize and stabilize supersaturated concentrations of bioactive molecules. We report the design and synthesis of cellulose- and β-CD-based fluorescent probes starting with the readily available oligo(hydroxypropyl) cellulose derivatives and well-known crystallization inhibitors, hydroxypropylmethyl cellulose (HPMC, also known as hypromellose) and hydroxypropyl cellulose (HPC), as well as HPβCD. Further, we expect that the solvatochromic character of the Nile Blue dye will be retained in the newly tagged cellulose derivatives, providing insight about the environment around the ASD polymer during the generation and maintenance of supersaturation. We report proof of concept for appending amine-containing fluorophores, in this case Nile Blue, to hydroxypropyl-containing poly- and oligosaccharide derivatives via oxidation followed by reductive amination, including characterization and fluorometric studies.

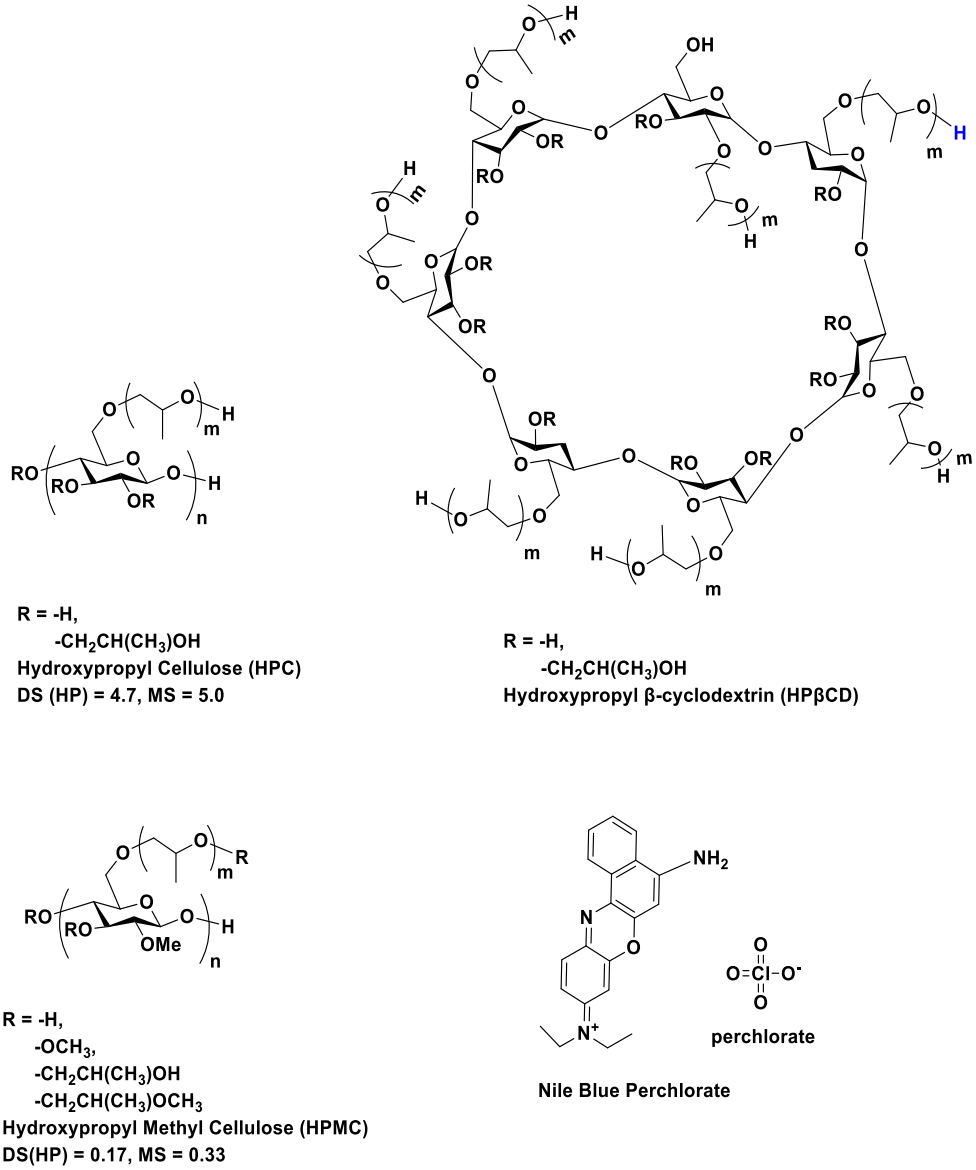

Figure 4.1. Structures of HPC, HPMC, HP*β*CD and Nile Blue perchlorate. Please note that polysaccharide and oligosaccharide structures in this and subsequent figures are not meant to indicate regioselective substitution; structures are depicted in this way for simplicity and clarity.

2. Experimental

2.1. Materials and methods

HPC (M_w = 100 kg mol^{-1}, DP = 100, DS (HP) 2.2, MS (hydroxypropyl, HP) 4.4) (Dong, Mosquera-Giraldo, Troutman, et al., 2016), anhydrous tetrahydrofuran (THF), ethylene glycol, potassium bromide (KBr), sodium tri(acetoxy)borohydride ($NaBH(OAc)_3$), Nile Blue perchlorate ($NBClO_4$), sodium hypochlorite (10-14.5% available chlorine), dichloroethane (DCE), and 3Å and 4Å molecular sieves were from Sigma-Aldrich (Saint Louis, MO, USA). HPβCD (M_w = 1390.64, DP = 7, DS (HP) = 4.5) was graciously provided by Cyclolab. Hydroxypropyl methylcellulose (HPMC 2910 or Pharmacoat grade 603, 36.6% methoxy, 9.45% HP, M_w = 16 kg mol^{-1}, DP = 79, PDI = 2, DS (OMe) 2.39, DS (HP) 0.16, MS (HP) 0.32 (determined by a method adapted from Dong et al., 2016, see ESI **Fig. S4.1-S4.4**). *N*, *N*-Dimethylformamide (DMF), lithium chloride (LiCl), methanol, ethanol, acetic acid, and dialysis tubing (MWCO 3.5k Da) were from Fisher Scientific (Fair Lawn, NJ, USA). All reagents were used as received without further purification.

NMR spectra were acquired on a Bruker Avance II spectrometer operating at 500 MHz (^1H and ^{13}C) and 600 MHz (HSQC). Polymer (ca. 10 mg for ^1H NMR and 50 mg for ^{13}C NMR) was dissolved in ca. 0.7 mL of deuterated water (D_2O), chloroform, or dimethylsulfoxide ($CDCl_3$ or DMSO-d_6, respectively) and three drops of trifluoroacetic acid was added to shift the water peak downfield. Fourier transform-infrared (FT-IR) spectra were recorded in transmission mode with a Thermo Nicolet 8700 instrument (Madison, WI, USA) prepared by using the KBr pellet method (1 mg polymer / 99 mg KBr) mixed by mortar and pestle.

2.2. Synthetic methods

2.2.1. Synthesis of Ox-HPC via selective oxidation

The oxidation procedures described for the polysaccharide ethers were adapted from Nichols et al., 2020. HPC (2.00 g, 14.4 mmol OH) was dissolved in 30 mL DI water at room temperature. Aqueous NaOCl (10-14%, 12 mL, 19.3 mmol, 5.07 equiv. / OH) was gradually added to the

solution, followed by the dropwise addition of acetic acid (1.4 mL, 26.2 mmol, 0.18 equiv. / OH) diluted in 3 mL DI water. The solution was stirred for 2h, and subsequently quenched with isopropanol (20 mL). The solution was then neutralized with 10% $NaHCO_3$ for 15 min, and dialyzed against 1L pH 7.4 sodium phosphate buffer (1 day) and water (3 days). The resulting solution was then lyophilized to isolate the final product as the retentate.

Ox-HPC. Yield: 1.79 g, 94.8%. DS by ^{1}H NMR: DS (ketone) = 0.14.

^{1}H NMR (selected signals, 500 MHz, $CDCl_3$) δ 0.85-1.45 (br, d, -$OCH_2CH(C\underline{\mathbf{H}_3})OH$, 3H), 2.15 (s, C$\underline{\mathbf{H}_3}$-CO- ketone methyl on oxidized HP), 2.99-4.64 (m, cellulosic backbone + -OC$\underline{\mathbf{H}_2}$C$\underline{\mathbf{H}}$(CH_3)OH; br, s, 3.01-3.22, 3.60), 4.80-5.33 ppm (m, anomeric proton).

^{13}C NMR (selected signals, 500 MHz, D_2O):15.82-18.32 ppm $\underline{\mathbf{C}}H_3$ (HP), 25.47 ppm O═C$\underline{\mathbf{C}}H_3$ (CH_3, oxidized 2-hydroxypropyl), 59.82–81.67 ppm ($\underline{\mathbf{C}}_2$–$\underline{\mathbf{C}}_6$ + $\underline{\mathbf{C}}H_2\mathbf{C}H$ HP + CH_2 of terminal oxidized HP group), 101.86 ppm (anomeric carbon ‘C1’), 210.80 ppm $\underline{\mathbf{C}}$═O.

2.2.2. Synthesis of Ox-HPMC via selective oxidation.

HPMC (3.08 g, 7.4 mmol OH) was dissolved in 30 mL DI water at room temperature. Aqueous 10-14% NaOCl (30 mL, 87.6 mmol, 30.9 equiv/OH) was gradually added to the solution, followed by the dropwise addition of acetic acid (1.4 mL, 26.2 mmol, 0.18 equiv/OH) diluted in 3 mL DI water. The solution was stirred for 3h, and subsequently quenched with isopropanol (20 mL). The product was then neutralized with 10% $NaHCO_3$ for 15 min, and dialyzed against 1L pH 7.4 sodium phosphate buffer (1 day) and water (3 days). The resulting solution was then lyophilized to isolate the final product as the retentate.

Ox-HPMC. Yield: 2.76 g, 91%. DS by ^{1}H NMR: DS (ketone) = 0.06.

^{1}H NMR (selected signals, 500 MHz, D_2O) δ 1.07 -1.29 (br, d, -$OCH_2CH(\underline{\mathbf{CH}_3})OH$, 3H), 2.17 (s, C$\underline{\mathbf{H}_3}$-CO- ketone methyl on oxidized HP), 2.96-4.64 (m, cellulosic backbone + -

OC**H**$_2$C**H**(CH_3)OH; br, s, 3.01-3.22, 3.60, and 3.42 -OC**H**$_3$ methoxy), 4.80-5.33 ppm (m, anomeric proton).

^{13}C NMR (selected signals, 500 MHz, D_2O): δ 15.12-18.25 ppm **C**H_3 (HP), 25.34 ppm O═C**C**H_3 (CH_3, oxidized 2-hydroxypropyl), 55.42-60.52 (HPMC -O**C**H_3), 66.17–82.98 ppm (**C**$_2$–**C**$_6$ + **C**H_2**C**H HP + CH_2 of terminal oxidized HP group), 102 ppm (anomeric carbon 'C1'), 209.57-210.37, ppm **C**═O.

2.2.3. Synthesis of Ox-HPβCD via selective oxidation.

HP*β*CD (4.36 g, 46.4 mmol OH) was dissolved in 20 mL DI water at room temperature. Aqueous 10-14% NaOCl (57.2 mL, 167 mmol, 2.5 equiv/OH) was gradually added to the solution, followed by the dropwise addition of acetic acid (2.5 mL, 44 mmol, 0.94 equiv. /OH) diluted in 3 mL DI water. The solution was stirred for 3h, and subsequently quenched with isopropanol (20 mL). The product was then neutralized with 10% $NaHCO_3$ for 15 min, and dialyzed against 1L pH 7.4 sodium phosphate buffer (1 day) and water (3 days). The resulting solution was then lyophilized to isolate the final product as the retentate.

Ox-HPβCD. Yield: 0.90 g, 45.7%. DS by ^{1}H NMR: DS (ketone) = 2.20.

^{1}H NMR (selected signals, 500 MHz, DMSO-d_6) δ 0.96 -1.38 (br, d, -OCH_2CH(**C**H_3)OH, 3H) , 2.14 (s, C**H**$_3$-CO- ketone methyl on oxidized HP), 2.92-6.75 (m, cellulosic backbone + -OC**H**$_2$C**H**(CH_3)OH; br, s, 3.66-3.80, 4.03), 4.23-4.52 ppm (m, anomeric proton).

^{13}C NMR (selected signals, 500 MHz, DMSO-d_6): 15.87-20.82 ppm **C**H_3 (HP), 24.47-26.95 ppm O═C**C**H_3 (CH_3, oxidized 2-hydroxypropyl), 58.25–85.44 ppm (**C**$_2$–**C**$_6$ + **C**H_2**C**H HP + CH_2 of terminal oxidized HP group), 91.83-102 ppm (anomeric carbon, 'C1'), 206.64, ppm **C**═O.

2.2.4. General Procedure for One-pot Reductive-amination of Ox-HPC, Ox-HPMC, and Ox-HPβCD.

Ox-HPC (138 mg, 0.25 mmol ketone, MS (HP) 3.9, DS (ketone = 0.8)) or Ox-HPMC (178 mg, 0.111 mmol ketone, MS (HP) 0.32, DS (ketone) = 0.16) was dissolved in anhydrous DMF under inert atmosphere and left to stir at RT overnight. An excess of Nile Blue perchlorate ($NBClO_4$, 217 mg, 0.52 mmol, 5 mole equivalents (equiv)/ketone for OxHPC; 55.4 mg, 0.132 mmol, 1.2 equiv/ketone for Ox-HPMC, and 371 mg, 0.88 mmol, 1 equiv/ketone for Ox-HPβCD), TEA (35.4 mg, 0.35 mmol, 1 equiv/ ketone; 15.4 mg, 0.146 mmol, 1 equiv./ ketone for Ox-HPMC; and 123 mg, 1.24 mmol, 1 equiv/ ketone for Ox-HPβCD), and acetic acid (15 mg, 0.262 mmol, 1 equiv/ ketone; 15.4 mg, 0.146 mmol, 1 equiv/ketone for Ox-HPMC; and 61 mg, 0.29 mmol, 1.2 equiv/ketone for Ox-HPβCD) were added at 50° C and allowed to stir for 24 h. The solution was cooled to room temperature prior to the slow addition of $Na(OAc)_3BH$ (75.5 mg, 0.35 mmol, 1.4 equiv/ketone; 15.4 mg, 0.146 mmol, 1 equiv/ketone for Ox-HPMC; and 376 mg, 1.77 mmol, 2 equiv/ketone for Ox-HPβCD) and proceeded to stir for 24 h. The reaction mixture was filtered, and the filtrate was dialyzed against anhydrous methanol (3-5 days), followed by DI water (2 days). The corresponding product (denoted Ox-HPC-NB-H, Ox-HPMC-NB-H, or Ox-HPβCD-NB-H) was collected from the retentate of the lyophilized solution.

Ox-HPC-NB-H: Yield: 0.112 g, 70%. DS by ^{1}H NMR: DS (amine) = 0.34, 46.25% conversion from ketone.

^{1}H NMR (500 MHz, selected signals, MeOH-d_4):δ 0.88.01-1.35 (br, d, -$OCH_2CH(CH_3)OH$, 3H), 1.29 (t, Nile Blue terminal methyl, -CH_2CH_3, 6H), 1.34 (α-methyl to reduced amine –HNCHCH_3) 2.14 (ketone α–methyl –CH_3), 2.97 - 4.63 (m, cellulosic backbone; q, Nile Blue ethylene -CH_2CH_3, 4H), Nile Blue aromatic region = 8H total : 6.99 (d) 2H, 7.30 (d) 1H (d), 7.85-7.96 (ddd) 3H, 8.34 (1h), 8.97 (d) = 1H.

^{13}C NMR (500 MHz, $MeOD_4$) δ 12.87 (Nile Blue terminal methyl, -$CH_2C\underline{\mathbf{H}_3}$), 17.55, 19.87, 26.52, 30.77 (β-methyl to amine on reduced Nile Blue moiety HNCH$\underline{\mathbf{C}}H_3$, denoted f"), 46.97 (Nile Blue methylene, -$\underline{\mathbf{C}}H_2\mathbf{C}H_3$), 55.70 (C-N), 57.40-84.47 ($\underline{\mathbf{C}}_2$–$\underline{\mathbf{C}}_6$ + $\underline{\mathbf{C}}H_2\mathbf{C}$H HP + α-methine of reduced Nile Blue amine, denoted e"), 103.66 (anomeric carbon 'C1'), 116.57-155.77 (Nile Blue aromatic region), 209.69.

Ox-HPMC-NB-$\underline{\mathbf{H}}$. Yield: 0.135 g, 60%. DS by ^{1}H NMR: DS (amine) = 0.06, 35.4% conversion from ketone.

^{1}H NMR (500 MHz, selected signals, MeOH-d_4): δ1.01-1.25 (br, d, -$OCH_2CH(C\underline{\mathbf{H}_3})OH$, 3H), 2.14 (ketone α–$C\underline{\mathbf{H}_3}$), 1.29 (t, Nile Blue methyl -$CH_2C\underline{\mathbf{H}_3}$, 6H + α-methyl to reduced amine – $HNCHC\underline{\mathbf{H}_3}$), 2.70 - 4.63 (m, cellulosic backbone; q, Nile Blue ethylene -$C\underline{\mathbf{H}_2}CH_3$, 4H), Nile Blue aromatic region = 8H + -N$\underline{\mathbf{H}}$: 7.22, 7.46, 7.76, 7.99, 8.09, 8.52.

^{13}C NMR (500 MHz, $MeOD_4$) δ 13.77 (Nile Blue terminal methyl, -$CH_2C\underline{\mathbf{H}_3}$), 16.

77, 19.78, 26.28, 30.74 (β-methyl to amine on reduced Nile Blue moiety HNCH$\underline{\mathbf{C}}H_3$, denoted f"), 46.62 (Nile Blue methylene, -$\underline{\mathbf{C}}H_2\mathbf{C}H_3$), 57.03-61.26 (HPMC -O$\underline{\mathbf{C}}H_3$ + α-methine of reduced Nile Blue amine denoted e"), 67.34–87.63 ppm ($\underline{\mathbf{C}}_2$–$\underline{\mathbf{C}}_6$ + $\underline{\mathbf{C}}H_2\mathbf{C}$H HP), 104.30 ppm (anomeric carbon 'C1'), 116.57-155.77 (Nile Blue aromatic region), 208.75.

Ox-HPβCD-NB-$\underline{\mathbf{H}}$. *Not isolated.*

2.2.5. Stepwise Reductive amination of Ox-HPC and Ox-HPMC

$\underline{\text{Schiff-Bases}}$ Ox-HPC-NB and Ox-HPMC-NB.

Preparation of Ox-HPC-NB exemplifies the process: Ox-HPC: (365 mg, 0.67 mol ketone, MS (HP) 4.7, DS (oxopropyl = 0.8) was dissolved in anhydrous MeOH under N_2 and left to stir at 50 °C overnight. An excess of Nile Blue perchlorate ($NBClO_4$, 800 mg, 1.91 mmol, 2.8 equiv/

ketone), TEA (93.8 mg, 0.93 mmol, 1 equiv/ketone), and acetic acid (0.021 mg, 0.367 mmol, 1.2 equiv/ketone) were added at 50 °C and allowed to stir for 24 h. The solution was then cooled to room temperature and 100 mL anhydrous acetone was added, leading to formation of a precipitate. The solid precipitate (excess Nile Blue) was filtered, and the filtrate was dialyzed against anhydrous methanol (3-5 days). The solvent was removed under reduced pressure by rotary evaporation, and the dark blue product was dried under vacuum overnight at 50 °C.

Ox-HPC-NB: Yield: 170 mg, 40%. DS by ^{1}H NMR: DS (imine) = 0.30, 35% conversion from ketone. Elemental analysis: %C 68.37, %H 9.57, %N 1.56, (theoretical (DS, imine = 0.8) ; DS (imine) by elemental analysis = 0.25, 29%.

^{1}H NMR (500 MHz, selected signals, MeOH-d_4): δ 0.88.01-1.35 (br, d, -OCH$_2$CH(C**H$_3$**)OH, 3H), 1.34 (t, Nile Blue terminal methyl, -CH$_2$C**H$_3$**, 6H), 2.14 (ketone α–methyl –C**H$_3$**), 2.97 – 4.63 (m, cellulosic backbone; q, Nile Blue ethylene -C**H$_2$**CH$_3$, 4H), Nile Blue aromatic region = 8H total : 6.89 (d) 2H, 7.30 (d) 1H (d), 7.82-8.01 (ddd) 3H, 8.36 (1h), 8.97 (d) = 1H.

^{13}C NMR (500 MHz, DMF-d$_7$) δ 13.13 (Nile Blue methyl, -CH$_2$**C**H$_3$), 17.84, 26.73, 40.51, 46.60 (Nile Blue methylene, -**C**H$_2$**C**H$_3$), 102.99, 116.04 – 133.80 (Nile Blue aromatic region), 160.10 (**C**=N imine), 208.03.

Ox-HPMC-NB: Yield: 82 mg, 63.1%. Elemental analysis: %C 48.36, %H 7.32, %N 0.41, (theoretical (DS, imine = 0.16) ; DS = (imine) by elemental analysis: 0.07, 42.7% conversion from ketone.

2.2.6. Step-wise Reductive-amination of Ox-HPC and Ox-HPMC:

Reduction

Preparation of Ox-HPC-NB-H exemplifies the process: Ox-HPC-NB (150 mg, 6.02 mmol imine, MS (HP) 4.5, DS (oxopropyl = 0.8), DS (imine) = 0.20) was dissolved in anhydrous DMF under inert atmosphere and left to stir at RT for 24-72 h. A slight excess of $Na(OAc)_3BH$ (200 mg, mmol, 2.7 equiv/ketone) was added at RT and allowed to stir for 3 days. The solution was subsequently precipitated by addition of dry acetone or water, filtered, and the filtrate was collected and dialyzed against methanol (3-5 days), followed by DI water (2 days). The retentate was filtered, and the product was collected by lyophilization of the filtrate.

Ox-HPC-NB-H: Yield: 106.4 mg, 60% yield. ^{1}H and ^{13}C NMR signals agreed with those of Ox-HPC-NB-H obtained via direct, one-pot reductive-amination.

Ox-HPMC-NB-H: Yield: 69.5 mg, 72%. DS by ^{1}H NMR: DS (amine) = 0.07, 42.3% conversion from ketone. ^{1}H and ^{13}C NMR signals agreed with those of Ox-HPMC-NB-H obtained via direct, one-pot reductive-amination.

2.3. Fluorometry measurements

2.3.1 Preparation of polymer solution in organic solvent at 200 μg/mL

To a 40 mL vial was added polymer (20 mg) and target solvent (20 mL DMSO, DMF or toluene if soluble), then the mixture was stirred overnight to afford a clear stock solution at 1 mg/mL. Then 4 mL stock solution was transferred into 25 mL vial and diluted with 16 mL solvent to give polymer solution at 200 μg/mL for fluorescence measurement.

2.3.2 Fluorescence measurements of 200 μg/mL polymer solution

To a quartz cuvette was added above prepared solution, and the wavelength of maximum absorbance (λ_{max}) was measured with UV-visible spectrophotometer (Varian, Bio300). Then

fluorescence spectroscopy was carried by exciting at three different wavelengths near λ_{max} to provide the emission spectra.

3. Results and discussion

I)

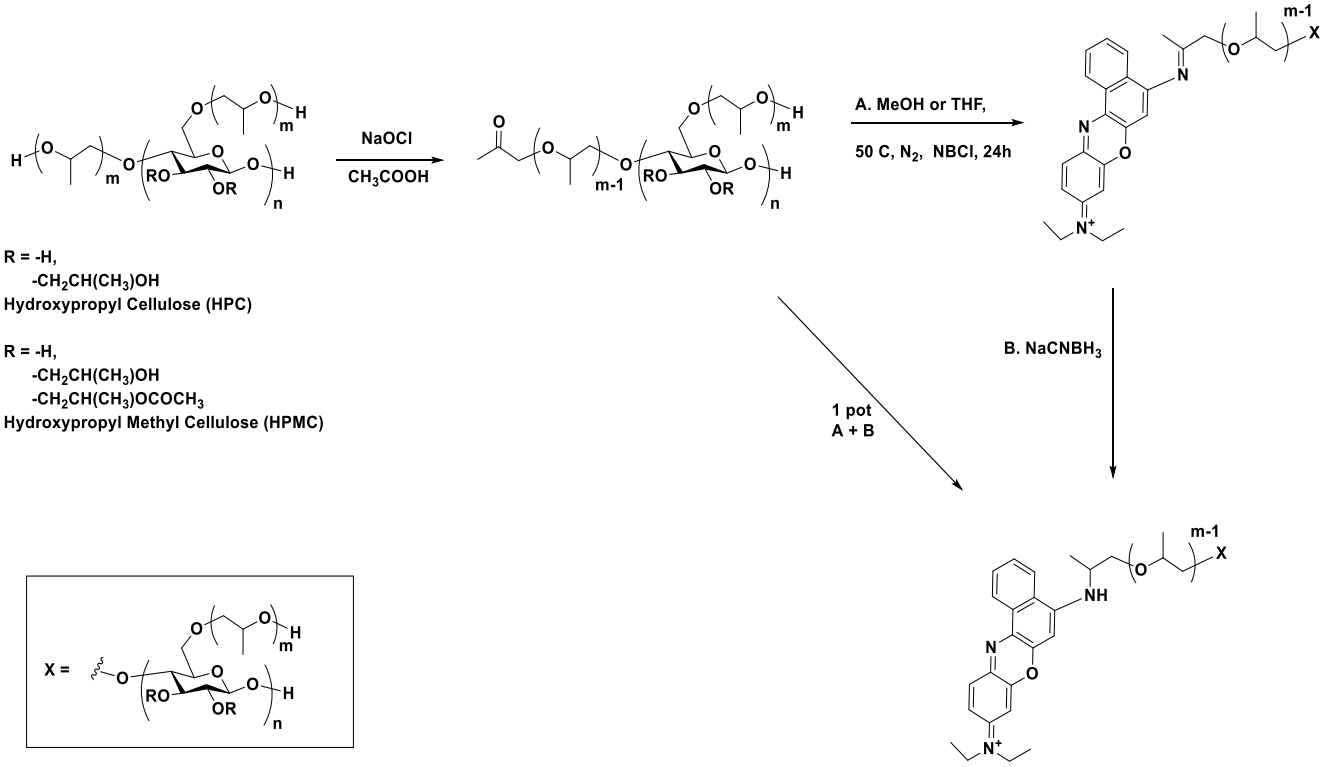

II)

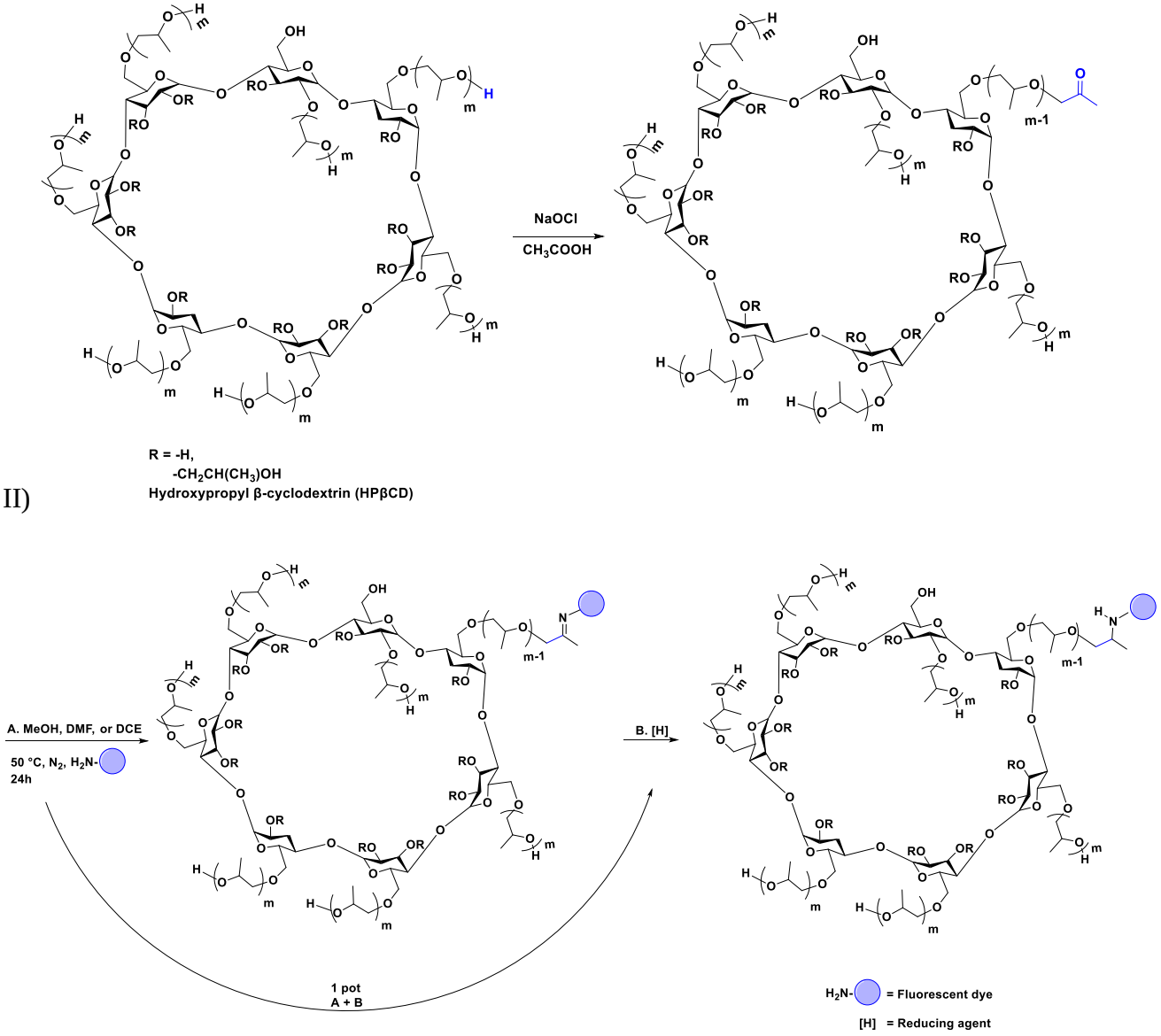

Scheme 4.1. Overall synthetic strategy for I) Ox-HPC, Ox-HPMC, and II) Ox-HPβCD via oxidation and subsequent reductive amination to afford the respective amines, Ox-HPC-NB-H, Ox-HPMC-NB-H, and Ox-HPβCD-NB-H via stepwise or one-pot procedures.

3.1. Preparation and characterization of Ox—HPC, Ox-HPMC, and Ox-HPβCD

In the present study, we successfully access fluorescent polysaccharides using the economical and commercially available Nile Blue perchlorate ($NBClO_4$) and oligo(hydroxypropyl) cellulose and cyclodextrin derivatives, HPC, HPMC, and HPβCD (**Fig. 4.1**). The regio- and chemoselective oxidation of oligo(hydroxypropyl) containing polysaccharides previously reported by our laboratory (Chen et al., 2020, 2021; Nichols et al., 2020) has conveniently provided access to new and chemically benign imine or amine-containing materials for biomedical applications. This chemistry permits regioselective access to the ketones via the oxidation of the secondary alcohols from the hydroxypropyl end-groups using household bleach (NaOCl, 10-15% active chlorine) (**Scheme 4.1**) (Stevens et al., 1980), in DI water containing a small amount of acetic acid in ambient conditions (RT, open to atmosphere), with NaCl as the only side-product. This straightforward strategy efficiently produces polysaccharides containing terminal ketones, which were previously difficult to synthesize, and only in limited circumstances and with harsh reagents (lachrymator in the case of ketenes (Clemens, 1986; Edgar et al., 1995)). Reactions with diketenes produce reactive (potentially to a fault, thermally labile) acetoacetate ester polysaccharides. In the case of attachment of levulinoyl groups, this may lead to undesirable side products due to reduced hydroxyl reactivity as observed for polysaccharide levulinates (Zheng et al., 2015).

We first explored oxidation of the simpler HPC derivative, which possesses high DS (2.4) and MS(4.5) hydroxypropyl. The obtained DS(oxopropyl) values measured were in agreement with our prior work; DS(oxopropyl) is tunable by choosing or making a particular DS(HP), and/or by adjusting polysaccharide substrate/bleach stoichiometry (Chen et al., 2020; Nichols et al., 2020). We employed stoichiometry to explore reaction with fluorophores by targeting a range of DS(ketone) values, which were expected to lead to a range of DS(fluorophore) (Table 4.1 and Table S4.1). We began with higher DS(oxopropyl) HPC, due to the limited (and uncertain) DS of

oligo(hydroxypropyl) termini available for HPMC. It must be noted that while DS(HP) was measured as 0.32 for HPMC, it is uncertain spectroscopically whether some of the methyl groups are attached to the termini of the oligo(hydroxypropyl) chains rather than to the ring hydroxyls; depending on the order of addition of methyl chloride and propylene oxide during HPMC manufacture, this could be a significant issue. We hypothesized that a low target DS(fluorophore) range (ca. ~0.001-0.1) would be desired, in order to permit fluorescence detection but minimize the structural differences between the cellulose or CD ether, and its fluorescently substituted analog.

Table 4.1. Oxidation Conversion of HPC (HP DS 2.4/MS 4.5), HPMC (HP DS 0.17/MS 0.33), and HPβCD (HP DS 4.5) vs. Time and Stoichiometry

Sample	DS(ketone)[a]	NaOCl equiv	oxidation time (min)	% conversion[b]
HPC	0.14	5.07	120	5.8
HPC	0.52	8.44	120	20.9
HPC	0.88	8.24	180	34.0
HPC	1.20	8.55	210	54.8
HPMC	0.02	1.8	1440	13.0
HPMC	0.04	3.6	480	25.3
HPMC	0.06	8.16	120	33.1

Sample	DS(ketone)[a]	NaOCl equiv	oxidation time (min)	% conversion[b]
HPMC	0.16	9	240	99
HP-β-CD	0.14	1.1	510	3.1
HP-β-CD	1.00	1.4	300	22.2
HP-β-CD	2.2	2.9	120	48.0

[a] Measured by ^{1}H NMR spectroscopy.

[b] Conversion is calculated as the percentage of terminal secondary alcohols (of the 2-hydroxypropyl groups) that have been oxidized to ketones (**Figure S4.5-S4.7**).

See ESI S4.1-S4.4 for calculations of MS/DS for 2-hydroxypropyl methylcellulose starting materials.

The reaction progress and chemical structures of Ox-HPC, Ox-HPMC, and Ox-HPβCD were monitored and confirmed by the appearance, shift, and disappearance of ^{1}H and ^{13}C NMR resonances. Exemplary HPβCD and Ox- HPβCD ^{1}H and ^{13}C NMR spectra are shown in **Figs. 4.2** and **4.3**, respectively. Emergence of the downfield methyl group alpha to the new terminal ketone (denoted 'a') is evident at 2.07 ppm in DMSO-d_6, while the corresponding methylene protons alpha to the ketone shift into the cellulosic backbone region. The DS(oxopropyl) and oxidation conversion of 2-hydroxypropyl groups into 2-oxopropyl groups were determined as the ratio of the terminal ketone to the HP-methyl resonance

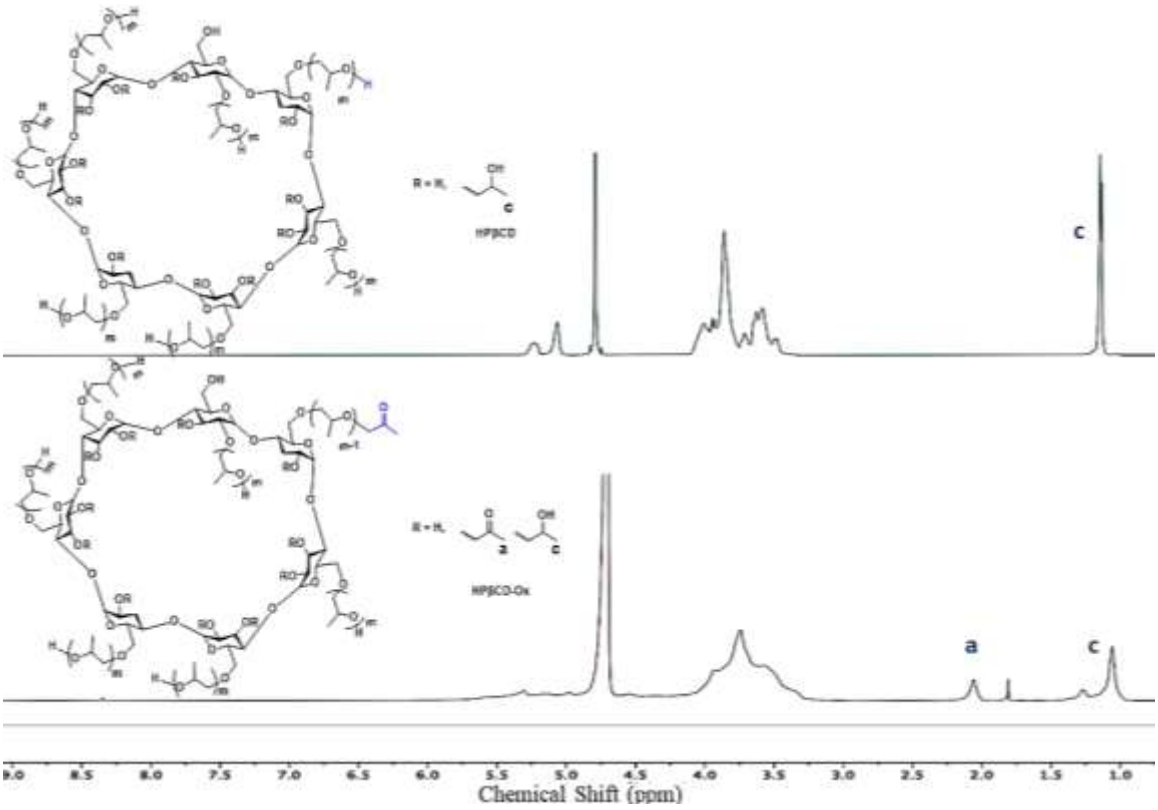

Figure 4.2 ^{1}H NMR of HPβCD and (top) Ox-HPβCD (bottom) in D_2O.

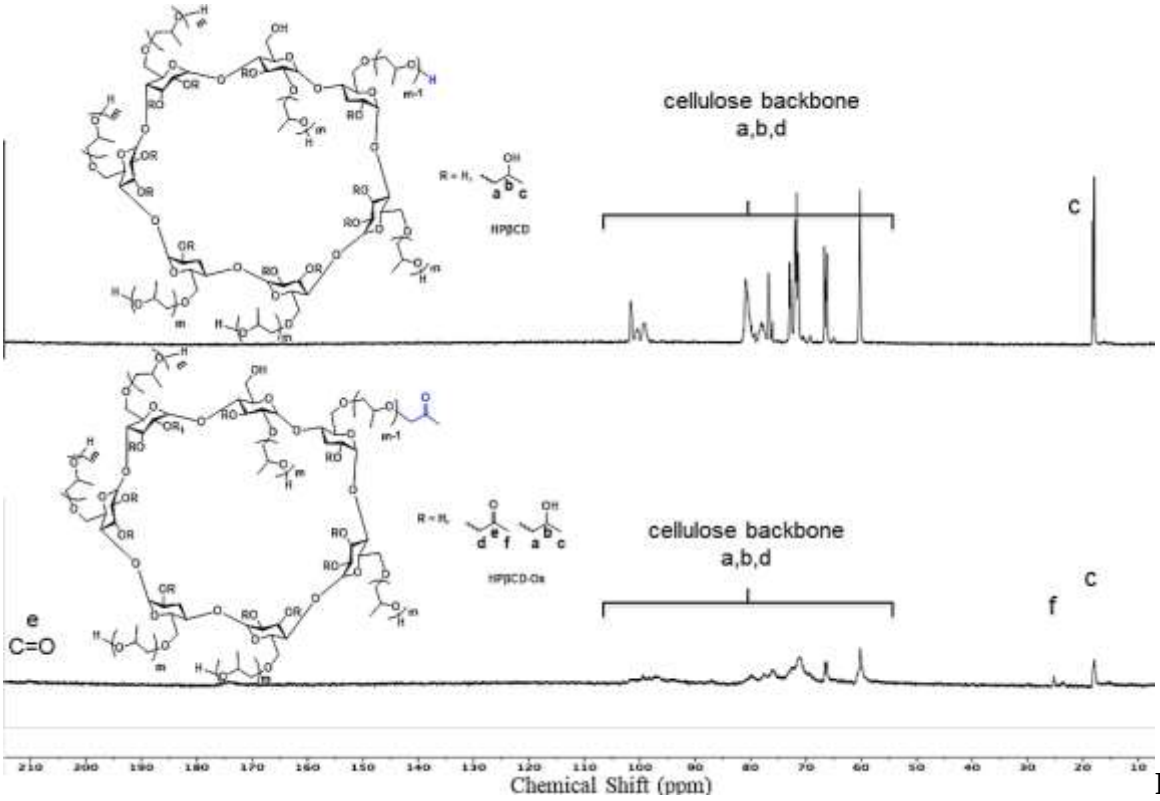

Figure 4.3 ^{13}C NMR spectra of HPβCD (top) and Ox-HPβCD (bottom) in DMSO-d_6.

3.2. Reductive amination

Synthesis of a Schiff-base becomes challenging when using a deactivated nucleophile such as the aryl amine from Nile Blue, then attempting to couple with a ketone-decorated macromolecule with its limited approach angles and slow diffusion. Such circumstances require specific measures to enhance reactivity. As Nile Blue is received from the manufacturer as an amine salt (we used Nile Blue perchlorate ($NBClO_4$)), prior activation of this poor nucleophile was necessary in order to generate the more nucleophilic free base (salt pK_A ca. 4, free base pK_A ca. 10) (Madsen et al., 2013). Thus, we explored *in situ* conversion to the free base using 1 equiv tertiary amine (TEA) in each of the direct or stepwise reductive-amination steps (Abdel-Magid & Mehrman, 2006). We also added 1 equivalent of acetic acid (AcOH) to hasten the sluggish reaction rates associated from using a ketone as a carbonyl source and to avoid enamine formation that can

occur in the absence of AcOH and with extended reaction periods (Abdel-Magid et al., 1996). These benefits do not come without caveats, as *N*-alkylation side-products are known to arise as reaction durations increase (Gribble et al., 1974), however it is unlikely for ketones as this pathway is thought to proceed via acetaldehyde formation. Conversion is clearly enhanced when applying these catalysts, with 28% conversion and DS(imine) = 0.13 when using TEA and AcOH, while in the absence of these reagents, only 10.3% conversion was observed for the indirect amination approach, affording DS (imine) = 0.1 for Ox-HPC-NB (Table S4.2), with slightly enhanced conversion for the one-pot strategy (Table 4.2, 12.6%, DS(amine) = 0.06). The acetoxy groups in $Na(OAc)_3BH$ contribute to its selective nature by imparting steric hindrance and electron-withdrawing properties (Gribble & Nutaitis, 1985) with tolerance to ketones, eliminating the formation of an intermediate imine (Carson et al., 1988). We investigated the effects of varying the $Na(OAc)_3BH$ and Nile Blue stoichiometry, solvent effects (DMF vs. DCE vs. MeOH), temperature (RT vs. 38 vs. 50°C), and reaction duration (24 vs. 48 and 72h) to optimize imine/amine conversion in stepwise and direct reductive amination (**Scheme 4.1: I and II) steps A, B**) for omega-ketone analogs Ox-HPC, Ox-HPMC, and Ox-HPBCD.

3.2.1. Stepwise imination and reduction of Ox-HPC and Ox-HPMC

The results for these reactions are summarized in Table S4.2. MeOH facilitates rapid formation of imines from primary amines, yielding a faster relative rate for ketones in MeOH vs. THF or DCE for small molecules (Abdel-Magid et al., 1996). For any Ox-HPC substrate, generally higher conversions to the Schiff-base were achieved for the two-step approach when performed in MeOH (vs. DCE or DMF). While Ox-HPMC was insufficiently soluble or gelled in MeOH, nearly full conversion was reached in DMF for DS(ketone) = 0.17 to DS(imine) = 0.16 at 50 °C in 3 days. Highest conversions to the amine product were observed in the two-step method with DMF as the

solvent, yielding 77% for Ox-HPC (ambient conditions and 48h). The highest conversion observed for MeOH, 48h and 2.9 equiv. $NaB(OAc)_3BH$) and elevated temperatures (50 °C) solely reached 43.4% conversion in MeOH. Unsurprisingly, isolation followed by reduction of the imine (two-step approach) generally gave lower conversion to amine versus the one-pot approach, as observed in previous works from our laboratory with Staudinger iminophosphorane ylide reduction (Zhang et al., 2017). Despite our efforts to maintain anhydrous conditions, including running reactions in the presence of molecular sieves, nearly complete hydrolysis of the isolated imine was observed for substrates with initially low DS imine, likely due to the hydrolytically labile imine bond, and the considerable hydrophilicity of the polymer, leading to the presence of adventitious water. Such low conversions were difficult to quantify by ^{1}H NMR spectroscopy, and were confirmed via elemental analysis. The less polar DCE solvent afforded low conversions even at longer reaction times and higher temperatures. Molar excesses of Nile Blue over 2.5 equiv/equiv ketone afforded at best minor conversion benefits, while forcing lengthier purification to remove the excess deeply pigmented Nile Blue amine, which may have contributed to greater opportunities to introduce water, and thus lower conversions to imine and amine. For this reason, we proceeded with the one-pot strategy with moderate molar excess of the amine reagent.

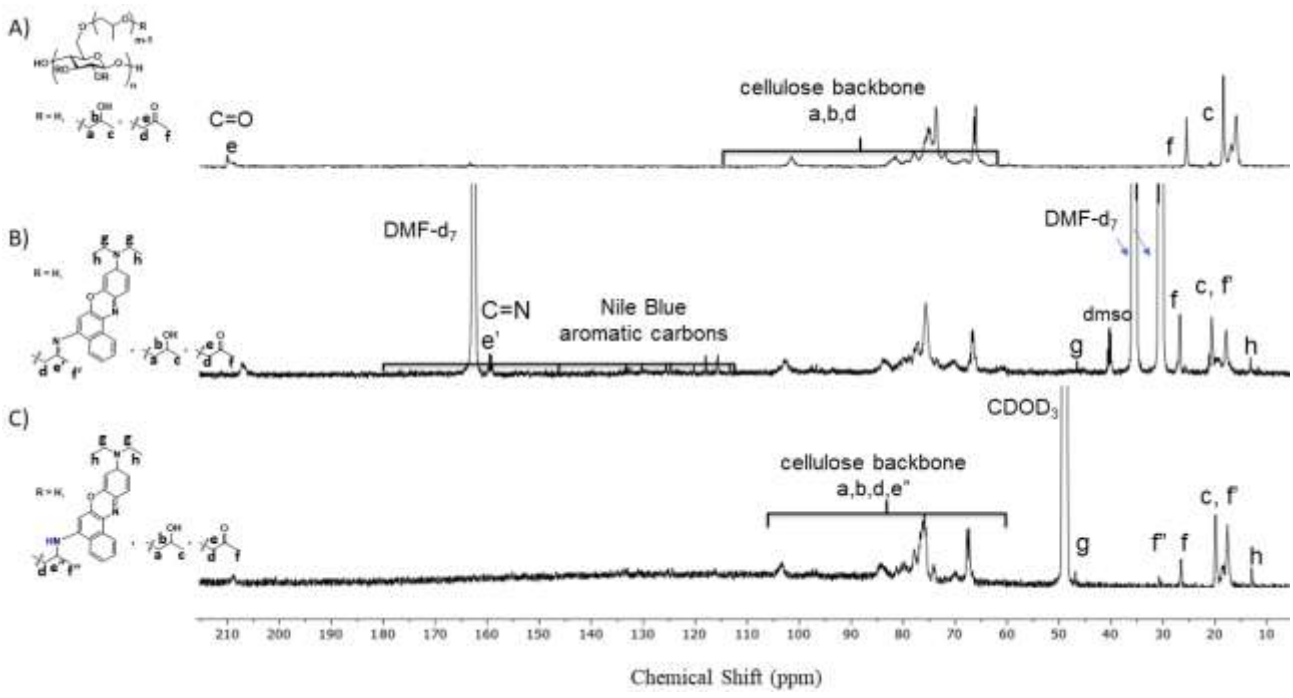

Figure 4.4. ^{13}C NMR spectra of A) Ox-HPC in D_2O, B) imine species Ox-HPC-Nile Blue in DMF-d_7, and C) reduced amine species Ox-HPC-NB-H CD_3OD.

Reaction progress was monitored by ^{1}H and ^{13}C NMR spectroscopy; an exemplary reaction with Ox-HPC is shown (**Fig. S4.8** and **Fig. 4.4**, respectively). Reduction in ketone-related resonances (CH_3 α to ketone at 2.07 ppm in ^{1}H spectrum; ketone carbonyl at 205 ppm in ^{13}C spectrum) and the clear emergence of the imine carbon, C=N at 160.1 ppm in the ^{13}C spectrum (**Fig. 4.4**) were strong indicators of conversion to Ox-HPC-Nile-Blue Schiff-base. Diagnostic Nile Blue's resonances for its corresponding aromatic protons (6.8-9.1 ppm; carbons 115-180 ppm); methyl unit on ethylamine (t, 1.28 ppm ^{1}H; 12 ppm ^{13}C) and methylene (3.8 ppm ^{1}H; 49 ppm ^{13}C) were also observed. The disappearance of the imine resonance in the ^{13}C and emergence of the methyl group beta to the amine assigned as f" confirmed the successful reduction of the imine.

3.2.2 One-pot reductive-amination of Ox-HPC, Ox-HPMC, and Ox-HPβCD

The one-pot strategy afforded greater yields and overall improved amine conversion vs. the stepwise method. In equivalent conditions, polar aprotic DMF outperformed DCE (46.8% vs. 17%, respectively) when using 1.4 eq $Na(OAc)_3BH$. With less reducing agent, DMF still outperformed MeOH (37.5% vs. 28.6% conversion, respectively) as the ideal solvent for enhanced imine reduction. Amine conversion improved in each solvent with longer reaction time for Ox-HPC despite providing greater potential for imine solvolysis.

Tracking cyclodextrins is of particular interest, including for determining bioavailability of these species that have lower Mw (in the 1-2K range) than cellulose ethers like HPC or HPMC (in the tens or hundreds of K range). Fluorescent labeling of HPβCD could also permit investigation of kinetics and thermodynamics of complexation. In addition, a primary use of cyclodextrins in drug delivery is for intravenous administration, for which HPβCD is a very important derivative (Buchanan et al., 2007); thus fluorescent labeling could also help track distribution of the cyclodextrin via the circulation (Váradi et al., 2019). Ox-HPβCD (2.20) was insoluble in DCE and MeOH, but one-pot reductive amination of this substrate were run in DMF at 50 °C for 2 days. One would expect the isolation of Ox-HPβCD-NB-H to be simpler than the higher Mw, more polydisperse cellulose derivatives. Dialysis (500-1000 and 1000 MWCO) of the solution demonstrated no reaction by the presence of the substrate in the retentate and Nile Blue in the dialysate. Alternatively, purification via precipitation of the solution with water or acetone only provided excess Nile Blue, as the desired product was absent from the filtrate. It is possible that the hydrophobic cavity from the cyclodextrin is strongly complexing to Nile Blue, thereby preventing the desired reaction with the polar oxopropyl endgroups.

Table 4.2. Conditions and conversions achieved by one-pot reductive-amination products of Ox-HPC, Ox-HPMC, and Ox-HPβCD.

Starting Ketone	$Na(OAc)_3BH$ (eq./mmol ketone)	Solvent	Temp. (°C)	Time (h)	DS (amine)/ conversion (%)
Ox-HPC(0.2)	2.0	DMF	37	72	0.06/41.4
Ox-HPC(0.5)	1.4	DMF	37	72	0.22/46.8
Ox-HPC(0.5)	1.4	DCE	37	72	0.08/17.0
Ox-HPC(0.8)	0.9	DMF	37	48	0.30/37.5
Ox-HPC(0.8)	0.9	MeOH	37	48	0.23/28.6
Ox-HPC(0.8)	0.9	MeOH	50	48	0.26/29.7
Ox-HPC(0.35)	0.9	MeOH	37	72	0.15/43.1
Ox-HPC(0.8) *‡	0.9	MeOH	37	72	0.06/12.6
Ox-HPMC(0.07)	2	DMF	37	48	0.06/82.9
		DCE	37	48	0.01/16.3
Ox-HPMC(0.17)	2	DMF	37	72	0.07/39.3
		DMF	50	72	0.16/91.9
		DCE	30	72	0.06/35.4
Ox-HPβCD(2.20)	2	DMF	50	48	not isolated

* = In the absence of acetic acid, ‡ = in the absence of TEA.

3.3 Fluorometry measurements

Although economical and commercially available, Nile Blue derivatives (Simmonds, A.; Miller, J. N.; Moody, C. J.; Swann, E.; Briggs, M. S. J.; Bruce, 1997) are reported to have

diminished fluorescence (Mank et al., 1995) after being covalently linked from the free amine (at C5), reducing the extinction coefficient by 20-fold (75000 to 4000) and quantum yield by 10-fold (27 to 2.5) (Karnes et al., 1995). Despite these caveats, we have observed retention of Nile Blue's solvatochromic character upon being appended to poly- and oligosaccharides. When Nile-Blue derivatives were placed in the polar solvents DMF and DMSO they had λ_{max} values around ca. 580-590 nm, the fluorescence intensity was suppressed by 7-8% (Table 4.3) for each solvent as the environment became less polar upon introduction of toluene was introduced to the solvents (**Fig. 4.5**).

A)

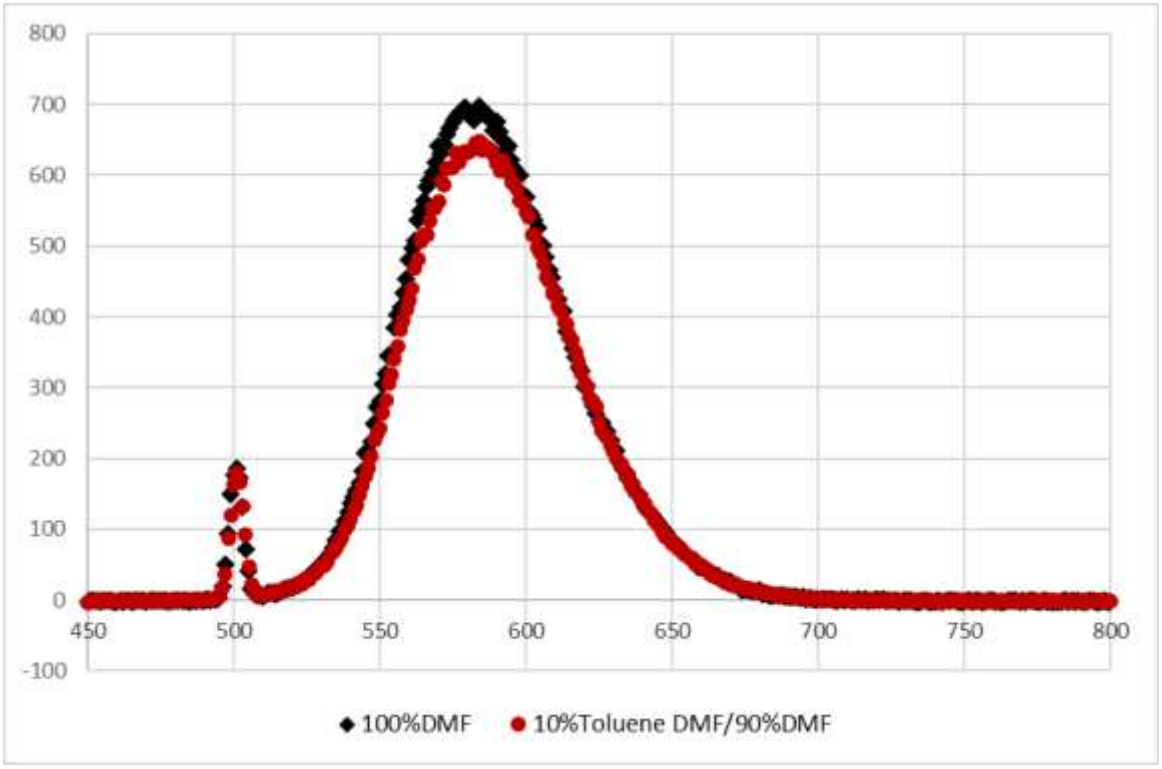

B) 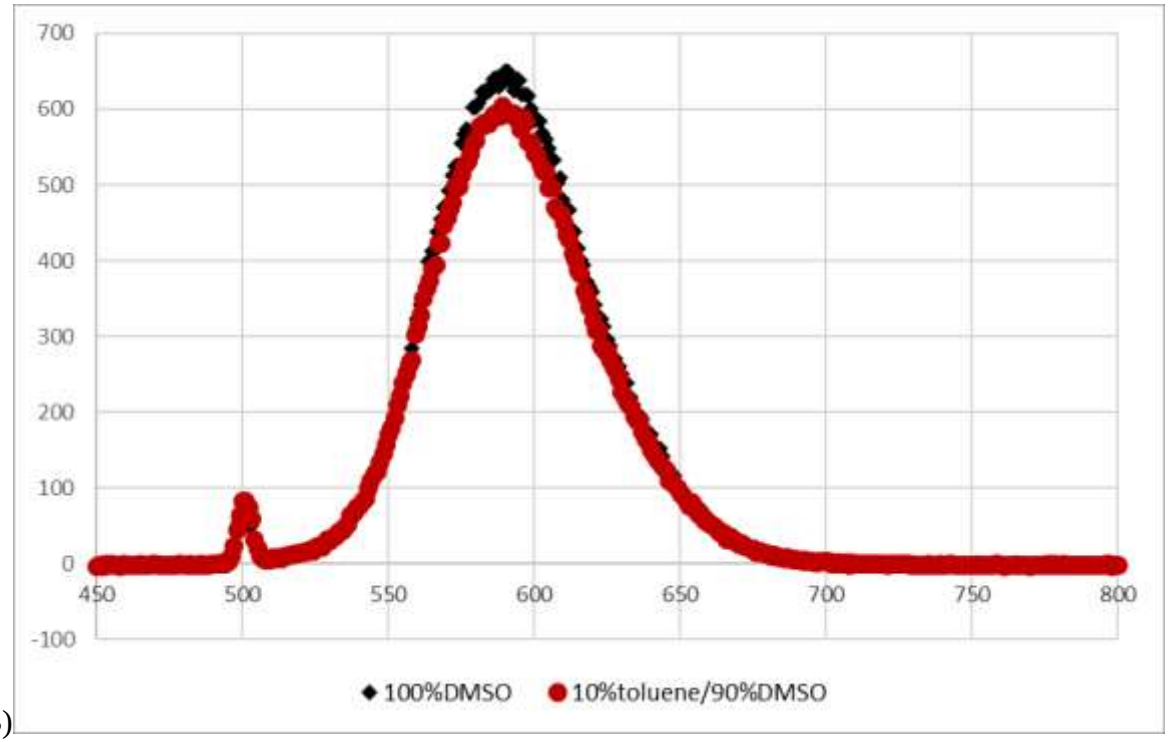

Figure 4.5. Fluorescence emission spectra of Ox-HPC-NB-H in A) 100% DMF (black), and 90%DMF/10%toluene (red), and B) 100% DMSO (black) and 90%DMF/10%toluene (red).

Table 4.3. Fluorescence emission spectrum summary (wavelength and intensity) for Ox-HPC-NB-H in pure DMF, DMSO and corresponding solvents with 10%toluene.

Solvent	nm, intensity
100% DMF	584, 697
10%toluene/90%DMF	580, 647
100% DMSO	591, 649
10%toluene/90%DMSO	589, 604

Conclusions

We have successfully developed a route to append amine-containing fluorophores to the family of ketone terminated oligo(hydroxypropyl) ethers of cellulose and β-CD using stepwise, or preferably, one-pot reductive amination. We were able to produce a series of selectively oxidized

HPC, HPMC, and HPβCD derivative. Tunable oxidation was accomplished by adjusting bleach stoichiometry, in agreement with the previous literature. We evaluated reductive amination kinetics and conversion and their responses to variation of key reaction conditions (temperature, reaction time, solvent choice) with one-pot and stepwise reductive amination in order to optimize results. We found that in the stepwise strategy, for either HPC or HPMC, MeOH provides the most efficient and rapid imine conversion in the first step, while DMF provides the highest conversion to the amine in the second step. One-pot reductive amination gave superior results, reducing the potential for adventitious water to hydrolyze the Schiff-base vs. stepwise conditions, and affording higher conversions (with DMF) independent of reaction conditions, polymer, or starting DS(ketone). Our hypothesis that Nile Blue environmental responsiveness would be preserved even after attachment to cellulosic or cyclodextrin moieties by reductive amination was supported by exhibiting solvatochromism, that is, changes in fluorescence emission spectrum in different solvents. Although a Stokes shift was not significant identified, quenching was observed with an increasingly hydrophobic environment. This work provides a successful proof of concept that showcases how to append fluoroprobes to polymers that contain hydroxypropyl or oligo(hydroxypropyl) groups and are of interest for biomedical or other applications, creating the potential to determine or explore the environments that surround the labeled materials. These new techniques enable us to monitor amine containing dyes and potentially unveil mechanisms that are key to drug delivery systems, to act as a theranostic sensor, or to use in other fields such as in environmental waste detection.

References

Abdel-Magid, A. F., Carson, K. G., Harris, B. D., Maryanoff, C. A., & Shah, R. D. (1996). Reductive amination of aldehydes and ketones with sodium triacetoxyborohydride. Studies

on direct and indirect reductive amination procedures. *Journal of Organic Chemistry*, *61*(11), 3849–3862. https://doi.org/10.1021/JO960057X/SUPPL_FILE/JO3849.PDF

Abdel-Magid, A. F., & Mehrman, S. J. (2006). A Review on the Use of Sodium Triacetoxyborohydride in the Reductive Amination of Ketones and Aldehydes. *Organic Process Research & Development*, *10*(5), 971–1031. https://doi.org/10.1021/op0601013

Amidon, G. L., Lennernas, H., Shah, V. P., Crison, J. R., Shah, V. P., & Amidon, G. L. (2014). G.L. Amidon, H. Lennernas, V.P. Shah, and J.R. Crison. A Theoretical Basis for a Biopharmaceutic Drug Classification: The Correlation of In Vitro Drug Product Dissolution and In Vivo Bioavailability, Pharm Res 12, 413–420, 1995—Backstory of BCS. *The AAPS Journal 2014 16:5*, *16*(5), 894–898. https://doi.org/10.1208/S12248-014-9620-9

Arca, H. C., Mosquera-Giraldo, L. I., Bi, V., Xu, D., Taylor, L. S., & Edgar, K. J. (2018). Pharmaceutical Applications of Cellulose Ethers and Cellulose Ether Esters. *Biomacromolecules*, *19*(7), 2351–2376. https://doi.org/10.1021/acs.biomac.8b00517

Auerbach, M., Pappadakis, J. A., Bahrain, H., Auerbach, S. A., Ballard, H., & Dahl, N. V. (2011). Safety and efficacy of rapidly administered (one hour) one gram of low molecular weight iron dextran (INFeD) for the treatment of iron deficient anemia. In *American Journal of Hematology* (Vol. 86, Issue 10, pp. 860–862). https://doi.org/10.1002/ajh.22153

Benet, L. Z. (2013). The Role of BCS (Biopharmaceutics Classification System) and BDDCS (Biopharmaceutics Drug Disposition Classification System) in Drug Development. *Journal of Pharmaceutical Sciences*, *102*(1), 34–42. https://doi.org/https://doi.org/10.1002/jps.23359

Buchanan, C. M., Buchanan, N. L., Edgar, K. J., Klein, S., Little, J. L., Ramsey, M. G., Ruble, K. M., Wacher, V. J., & Wempe, M. F. (2007). Pharmacokinetics of itraconazole after

intravenous and oral dosing of itraconazole-cyclodextrin formulations. *Journal of Pharmaceutical Sciences*, *96*(11), 3100–3116. https://doi.org/10.1002/JPS.20878

Carson, J. R., Almond, H. R., Brannan, M. D., Carmosin, R. J., Flaim, S. F., Gill, A., Gleason, M. M., Keely, S. L., & Ludovici, D. W. (1988). 2-Ethynylbenzenealkanamines. A new class of calcium entry blockers. *Journal of Medicinal Chemistry*, *31*(3), 630–636.

Chen, J., B Nichols, B. L., Norris, A. M., Frazier, C. E., & Edgar, K. J. (2020). *All-Polysaccharide, Self-Healing Injectable Hydrogels Based on Chitosan and Oxidized Hydroxypropyl Polysaccharides*. https://doi.org/10.1021/acs.biomac.0c01046

Chen, J., Edgar, K. J., & Frazier, C. E. (2021). Photo-curable, double-crosslinked, in situ-forming hydrogels based on oxidized hydroxypropyl cellulose. *Cellulose*, *28*(7), 3903–3915. https://doi.org/10.1007/S10570-021-03788-9/FIGURES/7

Clemens, R. J. (1986). Chemical Reviews Volume 86, Number 2 April 1986 Diketene. *Chemical Reviews*, *86*, 241–318. https://pubs.acs.org/sharingguidelines

Dong, Y., Mosquera-Giraldo, L. I., Taylor, L. S., & Edgar, K. J. (2016). Amphiphilic Cellulose Ethers Designed for Amorphous Solid Dispersion via Olefin Cross-Metathesis. *Biomacromolecules*, *17*(2), 454–465. https://doi.org/10.1021/acs.biomac.5b01336

Dong, Y., Mosquera-Giraldo, L. I., Troutman, J., Skogstad, B., Taylor, L. S., & Edgar, K. J. (2016). Amphiphilic hydroxyalkyl cellulose derivatives for amorphous solid dispersion prepared by olefin cross-metathesis. *Polymer Chemistry*, *7*(30), 4953–4963. https://doi.org/10.1039/C6PY00960C

Dong, Y., Novo, D. C., Mosquera-Giraldo, L. I., Taylor, L. S., & Edgar, K. J. (2019). Conjugation of bile esters to cellulose by olefin cross-metathesis: A strategy for accessing complex polysaccharide structures. *Carbohydrate Polymers*, *221*, 37–47.

https://doi.org/10.1016/J.CARBPOL.2019.05.061

Edgar, K., Arnold, K., Blount, W., Lawniczak, J., & Lowman, D. (1995). Synthesis and Properties of Cellulose Acetoacetates. *Macromolecules*, *28*(12), 4122–4128. https://doi.org/10.1021/ma00116a011

Evrard, B., Chiap, P., DeTullio, P., Ghalmi, F., Piel, G., Van Hees, T., Crommen, J., Losson, B., & Delattre, L. (2002). Oral bioavailability in sheep of albendazole from a suspension and from a solution containing hydroxypropyl-β-cyclodextrin. *Journal of Controlled Release*, *85*(1), 45–50. https://doi.org/https://doi.org/10.1016/S0168-3659(02)00270-5

Fahr, A., & Liu, X. (2007). Drug delivery strategies for poorly water-soluble drugs. *Expert Opinion on Drug Delivery*, *4*(4), 403–416.

Frömming, K.-H., & Szejtli, J. (1994). *Pharmacokinetics and Toxicology of Cyclodextrins BT - Cyclodextrins in Pharmacy* (K.-H. Frömming & J. Szejtli (eds.); pp. 33–44). Springer Netherlands. https://doi.org/10.1007/978-94-015-8277-3_3

Gribble, G. W., Lord, P. D., Skotnicki, J., Dietz, S. E., Eaton, J. T., & Johnson, J. (1974). Reactions of sodium borohydride in acidic media. I. Reduction of indoles and alkylation of aromatic amines with carboxylic acids. *Journal of the American Chemical Society*, *96*(25), 7812–7814.

Gribble, G. W., & Nutaitis, C. F. (1985). Organic Preparations and Procedures International SODIUM BOROHYDRIDE IN CARBOXYLIC ACID MEDIA. A REVIEW OF THE SYNTHETIC UTILITY OF ACYLOXYBOROHYDRIDES. *Organic Preparations and Procedures International*, *17*, 317–384. https://doi.org/10.1080/00304948509355522

Hosseinkhani, H., Aoyama, T., Ogawa, O., & Tabata, Y. (2002). Liver targeting of plasmid DNA by pullulan conjugation based on metal coordination. *Journal of Controlled Release*, *83*(2),

287–302. https://doi.org/https://doi.org/10.1016/S0168-3659(02)00201-8

Johnson, C. S., & Angeles, L. (n.d.). *Intravenous Iron.Dextran in the Treatment of Iron Deficient Anemia*.

Jose, J., & Burgess, K. (2006). Benzophenoxazine-based fluorescent dyes for labeling biomolecules. *Tetrahedron*, *62*(48), 11021–11037. https://doi.org/https://doi.org/10.1016/j.tet.2006.08.056

Joshi, V. M., & Devarajan, P. V. (2014). Receptor-mediated hepatocyte-targeted delivery of primaquine phosphate nanocarboplex using a carbohydrate ligand. *Drug Delivery and Translational Research*, *4*(4), 353–364. https://doi.org/10.1007/s13346-014-0200-4

Kaneo, Y., Tanaka, T., Nakano, T., & Yamaguchi, Y. (2001). Evidence for receptor-mediated hepatic uptake of pullulan in rats. *Journal of Controlled Release*, *70*(3), 365–373. https://doi.org/10.1016/S0168-3659(00)00368-0

Karnes, H. T., Rahavendran, S. V, & Gui, M. (1995). Long-wavelength derivatization reagents for use in diode laser-induced fluorescence detection. *Proc.SPIE*, *2388*, 21–31. https://doi.org/10.1117/12.208489

Lee, D. Y., Park, K., Kim, S. K., Park, R. W., Kwon, I. C., Kim, S. Y., & Byun, Y. (2008). Antimetastatic effect of an orally active heparin derivative on experimentally induced metastasis. *Clinical Cancer Research*, *14*(9), 2841–2849. https://doi.org/10.1158/1078-0432.CCR-07-0641

Lee, Y., Kim, S. K., Lee, D. Y., Lee, S., Kim, C.-Y., Shin, H.-C., Moon, H. T., & Byun, Y. (2006). Efficacy of orally active chemical conjugate of low molecular weight heparin and deoxycholic acid in rats, mice and monkeys. *Journal of Controlled Release*, *111*(3), 290–298. https://doi.org/https://doi.org/10.1016/j.jconrel.2005.12.011

Liu, H., Ilevbare, G. A., Cherniawski, B. P., Ritchie, E. T., Taylor, L. S., & Edgar, K. J. (2014). Synthesis and structure-property evaluation of cellulose ω-carboxyesters for amorphous solid dispersions. *Carbohydrate Polymers*, *100*, 116–125. https://doi.org/10.1016/j.carbpol.2012.11.049

Liu, H., Taylor, L. S., & Edgar, K. J. (2015). The role of polymers in oral bioavailability enhancement; a review. *Polymer*, *77*, 399–415. https://doi.org/10.1016/J.POLYMER.2015.09.026

Loftsson, T., & Brewster, M. E. (2011). *Pharmaceutical applications of cyclodextrins: effects on drug permeation through biological membranesj*. https://doi.org/10.1111/j.2042-7158.2011.01279.x

Madsen, J., Canton, I., J. Warren, N., Themistou, E., Blanazs, A., Ustbas, B., Tian, X., Pearson, R., Battaglia, G., L. Lewis, A., & P. Armes, S. (2013). Nile Blue-Based Nanosized pH Sensors for Simultaneous Far-Red and Near-Infrared Live Bioimaging. *Journal of the American Chemical Society*, *135*(39), 14863–14870. https://doi.org/10.1021/ja407380t

Mamula, P., Piccoli, D. A., Peck, S. N., Markowitz, J. E., & Baldassano, R. N. (2002). Total Dose Intravenous Infusion of Iron Dextran for Iron-Deficiency Anemia in Children With Inflammatory Bowel Disease. *Journal of Pediatric Gastroenterology and Nutrition*, *34*(3). https://journals.lww.com/jpgn/Fulltext/2002/03000/Total_Dose_Intravenous_Infusion_of_Iron_Dextran.11.aspx

Mank, A. J. G., van der Lean, H. T. C., Lingeman, H., Gooijer, C., Brinkman, U. A. T., & VeKhorst, N. H. (1995). Visible Diode Laser-Induced Fluorescence Detection in Liquid Chromatography after Precolumn Derivatization of Amines. *Analytical Chemistry*, *67*(10), 1742–1748. https://doi.org/10.1021/ac00106a015

Martinez, V., & Henary, M. (2016). & Photostable Organic Dyes Nile Red andNile Blue:A pplications and Syntheses of Structural Analogues. In *Chem. Eur.J* (Vol. 22). www.chemeurj.org

Mays, T., & Mays, T. (1976). Intravenous iron-dextran therapy in the treatment of anemia occurring in surgical, gynecologic and obstetric patients. *Surgery, Gynecology & Obstetrics*, *143*(3), 381–384. http://europepmc.org/abstract/MED/959957

Miller, J. M., Beig, A., Carr, R. A., Spence, J. K., & Dahan, A. (2012). A Win−Win Solution in Oral Delivery of Lipophilic Drugs: Supersaturation via Amorphous Solid Dispersions Increases Apparent Solubility without Sacrifice of Intestinal Membrane Permeability. *Mol. Pharmaceutics*, *9*. https://doi.org/10.1021/mp300104s

Mosquera-Giraldo, L. I., Borca, C. H., Meng, X., Edgar, K. J., Slipchenko, L. V, & Taylor, L. S. (2016). Mechanistic Design of Chemically Diverse Polymers with Applications in Oral Drug Delivery. *Biomacromolecules*, *17*(11), 3659–3671. https://doi.org/10.1021/acs.biomac.6b01156

Mosquera-Giraldo, L. I., H. Borca, C., S. Parker, A., Dong, Y., J. Edgar, K., P. Beaudoin, S., V. Slipchenko, L., & S. Taylor, L. (2018). Crystallization Inhibition Properties of Cellulose Esters and Ethers for a Group of Chemically Diverse Drugs: Experimental and Computational Insight. *Biomacromolecules*, *19*(12), 4593–4606. https://doi.org/10.1021/acs.biomac.8b01280

Nichols, B. L. B., Chen, J., Mischnick, P., & Edgar, K. J. (2020). Selective Oxidation of 2-Hydroxypropyl Ethers of Cellulose and Dextran: Simple and Efficient Introduction of Versatile Ketone Groups to Polysaccharides. *Biomacromolecules*, *21*(12), 4835–4849. https://doi.org/10.1021/ACS.BIOMAC.0C01045/SUPPL_FILE/BM0C01045_SI_001.PDF

Perrin, J. H., Field, F. P., Hansen, D. A., Mufson, R. A., & Torosian, G. (1978). beta-Cyclodextrin as an aid to peritoneal dialysis. Renal toxicity of beta-cyclodextrin in the rat. *Research Communications in Chemical Pathology and Pharmacology*, *19*(2), 373–376.

Pitha, J., Irie, T., Sklar, P. B., & Nye, J. S. (1988). Drug solubilizers to aid pharmacologists: Amorphous cyclodextrin derivatives. *Life Sciences*, *43*(6), 493–502. https://doi.org/https://doi.org/10.1016/0024-3205(88)90150-6

Pokharkar, V. B., Mandpe, L. P., Padamwar, M. N., Ambike, A. A., Mahadik, K. R., & Paradkar, A. (2006). Development, characterization and stabilization of amorphous form of a low Tg drug. *Powder Technology*, *167*(1), 20–25. https://doi.org/10.1016/J.POWTEC.2006.05.012

Saboo, S., Kestur, U. S., Flaherty, D. P., & Taylor, L. S. (2020). Congruent Release of Drug and Polymer from Amorphous Solid Dispersions: Insights into the Role of Drug-Polymer Hydrogen Bonding, Surface Crystallization, and Glass Transition. *Cite This: Mol. Pharmaceutics*, *17*, 1261–1275. https://doi.org/10.1021/acs.molpharmaceut.9b01272

Schellenberg, K. A. (1963). The Synthesis of Secondary and Tertiary Amines by Borohydride Reduction1. *The Journal of Organic Chemistry*, *28*(11), 3259–3261. https://doi.org/10.1021/jo01046a537

Simmonds, A.; Miller, J. N.; Moody, C. J.; Swann, E.; Briggs, M. S. J.; Bruce, I. E. (1997). *WO1997029154A1 - Benzophenoxazine dyes - Google Patents*. https://patents.google.com/patent/WO1997029154A1/en?oq=Simmonds%2C+A.;+Miller%2C+J.+N.;+Moody%2C+C.+J.;+Swann%2C+E.;+Briggs%2C+M.+S.+J.;+Bruce%2C+I.+E.+WO9729154%2C+1997.

Stevens, R. V, Chapman, K. T., & Weller, H. N. (1980). Convenient and inexpensive procedure for oxidation of secondary alcohols to ketones. *The Journal of Organic Chemistry*, *45*(10),

2030–2032.

Ting, J. M., Porter, W. W., Mecca, J. M., Bates, F. S., & Reineke, T. M. (2018). *Advances in Polymer Design for Enhancing Oral Drug Solubility and Delivery*. https://doi.org/10.1021/acs.bioconjchem.7b00646

Váradi, J., Hermenean, A., Gesztelyi, R., Jeney, V., Balogh, E., Majoros, L., Malanga, M., Fenyvesi, É., Szente, L., Bácskay, I., Vecsernyés, M., Fehér, P., Ujhelyi, Z., Vasvári, G., Árvai, I., Rusznyák, Á., Balta, C., Herman, H., & Fenyvesi, F. (2019). Pharmacokinetic properties of fluorescently labelled hydroxypropyl-beta-cyclodextrin. *Biomolecules*, *9*(10). https://doi.org/10.3390/biom9100509

Wilson, V. R., Lou, X., Osterling, D. J., Stolarik, D. F., Jenkins, G. J., Nichols, B. L. B., Dong, Y., Edgar, K. J., Zhang, G. G. Z., & Taylor, L. S. (2020). Amorphous solid dispersions of enzalutamide and novel polysaccharide derivatives: investigation of relationships between polymer structure and performance. *Scientific Reports*, *10*(1), 18535. https://doi.org/10.1038/s41598-020-75077-7

Zhang, R., Liu, S., & Edgar, K. J. (2017). Efficient synthesis of secondary amines by reductive amination of curdlan staudinger ylides. *Carbohydrate Polymers*, *171*, 1–8. https://doi.org/10.1016/j.carbpol.2017.04.093

Zheng, X., Xu, D., & Edgar, K. J. (2015). Cellulose levulinate: a protecting group for cellulose that can be selectively removed in the presence of other ester groups. *Cellulose*, *22*(1), 301–311. https://doi.org/10.1007/s10570-014-0508-8

Chapter 5. Capturing flavanol benefits using cellulose-based amorphous solid dispersions: Enhanced genistein and quercetin solution concentrations *in vitro*

Diana C. Novo [a, b], Emily G. Benson [e], Stella P. Petrova [a, b], Jeffrey E. Thompson [c], Laura I. Mosquera-Giraldo [d], Lynne S. Taylor [e], and Kevin J. Edgar* [a, c]

[a]*Department of Sustainable Biomaterials, Virginia Tech, Blacksburg, VA 24061, United States*

[b]*Department of Chemistry, Virginia Tech, Blacksburg, VA 24061, United States*

[c]*Macromolecules Innovation Institute, Virginia Tech, Blacksburg, VA 24061, United States*

[d]*Pharmaceutical Candidate Optimization, Bristol Myers Squibb, Route 206 and Province Line Road, Princeton, NJ 08540, United States*

[e]*Department of Industrial and Physical Pharmacy, College of Pharmacy, West Lafayette, Indiana 47907, United States*

Abstract

Flavonoids are natural, abundant radical scavengers that offer promise in enhancing human health, including in areas such as chemoprevention, anti-proliferation, and the treatment of diabetes. However, this class of compounds suffers from extensive phase II metabolism and poor aqueous solubility. These characteristics reduce therapeutic evaluation and effectiveness by limiting bioavailability. Crystallization inhibitors have been employed as excipients in amorphous solid dispersions (ASDs) to enable them to release the active compound and form metastable, supersaturated solutions of the bioactive. We hypothesized that solution concentration of the flavonoids genistein and quercetin could be improved using pH responsive cellulose-based derivatives as ASD matrices, creating the potential for enhanced bioavailability. In this study, we evaluated the effectiveness of three cellulose derivatives as flavonoid crystallization inhibitors; the ether 5-carboxypentyl hydroxypropyl cellulose (CP-HPC), the ester cellulose acetate glutarate (CAG), and the commercially available ether-ester hydroxypropyl methyl cellulose acetate succinate (HPMCAS). We studied the effects of varying drug-to-

polymer ratios on ASD performance, which was evaluated through *in vitro* dissolution studies for supersaturated solutions vs. a negative control, crystalline genistein or quercetin. An ASD comprising 90% CP-HPC and 10% flavonoid provided excellent crystallization inhibition, enhancing the aqueous solubility of each flavonoid, giving solution concentration increases of ca. 70-fold for genistein and ca. 8-fold for quercetin vs. the pure flavonoids. An auspicious polymer ASD matrix using CAG achieved 40-fold solution concentration enhancement for genistein at 10% drug loading and 25.7-fold at 25%, while enhancing quercetin solution concentration ca. 8-fold at either drug loading. We found that all three cellulose derivatives provided significant solubility enhancement for these flavonoids. The amorphous character of the polymer and ASD formulations was analyzed and characterized using XRD, FTIR, SEM, polarized light microscopy (PLM), and nanotracking analysis (NTA).

1. Introduction

Genistein is a naturally occurring phytoestrogen found in plants such as peanuts, soybeans, fava beans, and lupines (Sirtori et al., 2004) that has received attention due to medically beneficial properties that have been attributed to it by investigators (**Fig. 5.1**). Therapeutic properties described in the literature include heart disease reduction (Bian et al., 2004), bone-protection and composition improvement (Atteritano et al., 2014; M. Kim et al., 2018; Miao et al., 2012), and inhibiting hormone-related cancers (Messina et al., 1994) including (prostate (Peterson & Barnes, 1993), breast (Peterson & Barnes, 1991; Zhang et al., 1999), colon (Gruca et al., 2014), and pancreatic (Bi et al., 2018). This isoflavone displays thermodynamic and chemical stability (up to 70 °C, pH = 7, nearly 3 weeks) (Ungar et al., 2003). It possesses antioxidant activity *in vitro* by signaling anti-tumor pathways that are purported to retard cancer cell growth, induce apoptosis, prevent cancer metastasis, and retard aging (Si et al., 2010).

Similarly, quercetin is an interesting bioactive compound that is a naturally abundant (walnuts, apple, asparagus, broccoli (Russo et al., 2012)) flavonoid that is also reported to possess therapeutic properties due to its strong antioxidant (anticancer (Firdous et al., 2014; Murakami et al., 2008), antidiabetic (Dias et al., 2005), apoptosis-inducing (Wei et al., 1994), and obesity-reducing (Moon et al., 2013) activities, as well as its ability to protect the heart (Patel et al., 2018), liver (Lin et al., 2008), and brain (J. Kim et al., 2010)). These flavonoids are extensively metabolized by the liver and small intestine (Z. Yang et al., 2012). Their low oral bioavailability is further influenced by very low aqueous solubility (at 25 °C genistein:1.43 μg/mL (J.-G. Wu et al., 2010) and quercetin: 2.63-7.7 μg/mL (Lauro et al., 2005; Srinivas et al., 2010)). They are categorized as Class II compounds (poorly water soluble/highly permeable) in the Biopharmaceutical Classification System (Amidon et al., 1995).

Several delivery approaches have been explored to overcome the poor aqueous solubility of these interesting drug candidates. For genistein, recent approaches include complexation by cyclodextrins (Daruházi et al., 2008; Zafar et al., 2021; Zhao et al., 2011)) and amylose (Cohen et al., 2008), matrix retention via hydrocolloids such as kappa-carrageenans (Chen et al., 2013), nanoparticle systems comprised of mesoporous starch (Soleimanpour et al., 2020), carboxymethyl chitosan (Si et al., 2010), zein/alginate (Hu & McClements, 2015), zein/carboxymethyl chitosan (Xiao et al., 2020), Eudragit E100 (Tang et al., 2011), mannitol/ PLGA-TPGS (B. Wu et al., 2016)), or mixed micelles containing polymers (Cheng et al., 2020). To date, the only genistein solid dispersions (de Oliveira et al., 2013) include Bio 300, a proprietary blend of genistein prepared by hot melt extrusion (Serebrenik et al., 2023), freeze dried with Pluronic F127 (Suk et al., 2007), or spray dried with gelatin (Panizzon et al., 2014)). Contemporary attempts to improve quercetin solubility (Khursheed et al., 2020) include

nanoemulsification (Tran et al., 2014), nanoparticles (metallic (Ahmed et al., 2018; Mittal et al., 2014; Ugru et al., 2018), liposomes (Caddeo et al., 2017; Cruz dos Santos et al., 2019; Silva-Weiss et al., 2018), poly(lactic-co-glycolic acid) (PLGA) (Giannouli et al., 2018), chitosan-poly(ethylene) glycol-PLGA (Abd-Rabou & Ahmed, 2017), succinyl chitosan-alginate (Mukhopadhyay et al., 2018)), inclusion complexes (Diamantis et al., 2018; S. L. Yang et al., 2019), and ASDs (Gilley et al., 2017; Li, Konecke, Harich, et al., 2013). Amorphous solid dispersions (ASDs), shown to be highly valuable in oral drug delivery, are molecular dispersions of small molecules in polymer(s) that eliminate the energy barrier of crystal disruption, thereby facilitating drug dissolution and creating supersaturated solutions of the small molecules. These supersaturated solutions simultaneously enhance permeation through the gastrointestinal (GI) epithelium by increasing the concentration gradient across the membrane; thus, they address both key physical barriers to bioavailability. Strategic selection of a polymer matrix that is miscible with the hydrophobic, crystalline drug, is readily prepared, and that will enhance the drug candidate's aqueous solubility is a challenging task, due to the multiple criteria that must be met and our still imperfect knowledge of ASD polymer requirements (Ilevbare et al., 2013; H. Liu et al., 2015; Marks et al., 2014; Mosquera-Giraldo et al., 2016). The following criteria are favorable for ASD polymer selection: T_g sufficiently higher than the highest expected ambient temperature so that it will prevent drug migration in the solid ASD even at high humidity and even when the drug is a plasticizer for the polymer; amphiphilicity (to facilitate interaction with a hydrophobic drug and dissolution in the aqueous environment of the GI tract); and pH responsive carboxyl groups to promote triggered dissolution in the neutral milieu of the small intestine (these carboxyl groups can also drive strong polymer-drug interactions that protect against drug self-association in the solid phase and after dissolution (Pereira et al., 2013)). Derivatives of cellulose

are particularly attractive ASD candidates due to its natural abundance, benign nature, and the typically high T_g values of its derivatives. The Edgar and Taylor groups have found that cellulosic matrices are successful at enhancing stability and solubility of flavonoids at high concentrations, using carboxylated cellulose esters (carboxymethyl cellulose acetate butyrate (CMCAB), cellulose acetate adipate propionate (CAAdP), and HPMCAS) matrices containing ellagic acid (Li, Harich, Wegiel, Taylor, et al., 2013), naringenin (Li, Liu, Amin, Wegiel, et al., 2013), curcumin (Li, Konecke, Wegiel, et al., 2013), or quercetin (Li, Konecke, Harich, et al., 2013). Quercetin also performed well with ASD polymers cellulose ether (5-carboxypentyl hydroxypropyl cellulose, CP-HPC) and cellulose acetate suberate (DS(suberate) = 0.9 (CASub(0.9)); the latter polymer maintained solution concentration 12.7-fold higher than that from quercetin alone (Gilley et al., 2017). Additionally, ASD systems based on the synthetic polymer poly(vinylpyrrolidone) (PVP) mixed with soy-lecithin have been designed for oral delivery of quercetin, and have been found to provide 1.50-2.20-fold supersaturation (Shao et al., 2019). A quercetin/polysaccharide-based formulation employing chitosan has been discovered to reach 2.27-fold quercetin thermodynamic solubility at C_{max} (Han et al., 2021), and other quercetin formulations have not exceeded ca. 4.5-fold supersaturation, as was the case with hydroxypropyl methylcellulose (HPMC) and poloxamer 188 (F68) (Shi et al., 2020). While some commercially available polymers are also able to form ASDs with flavonoids, solubilize them, and release them, carboxylated cellulose derivatives are for some therapeutics advantages since they are pH-responsive, dissolving at the pH of the neutral intestinal environment. PVP, for example, which contains no carboxyl groups, undesirably releases flavonoids at pH 1.2, promoting crystallization. Other than some complex inclusion (Chen et al., 2013; Cohen et al., 2008; Daruházi et al., 2008; Zafar et al., 2021; Zhao et al., 2011) and nanoparticle (Soleimanpour

et al., 2020; Wu et al., 2016; Xiao et al., 2020) systems, only limited studies have employed cellulose derivatives to deliver genistein, and none using ASDs for oral administration.

We hypothesized that properly designed, amphiphilic cellulose-based ASD polymers could enhance genistein and quercetin aqueous solubility and promote its pH-responsive release. Herein we describe an investigation of the performance of CP-HPC (Dong et al., 2016) and cellulose acetate glutarate (CAG) ((Petrova et al., *manuscript in preparation*), both designed and synthesized as ASD polymers by the Edgar group, for prevention of quercetin and genistein crystallization and enhancing aqueous solubility under physiological conditions (simulated gastric and intestinal pH at 37 °C) as compared to controls, both negative (drug alone) and positive (HPMCAS, one of the leading commercial ASD polymers (Arca et al., 2018; Del Gaudio et al., 2017; Friesen et al., 2008; Pereira et al., 2013)) (**Fig. 5.1**).

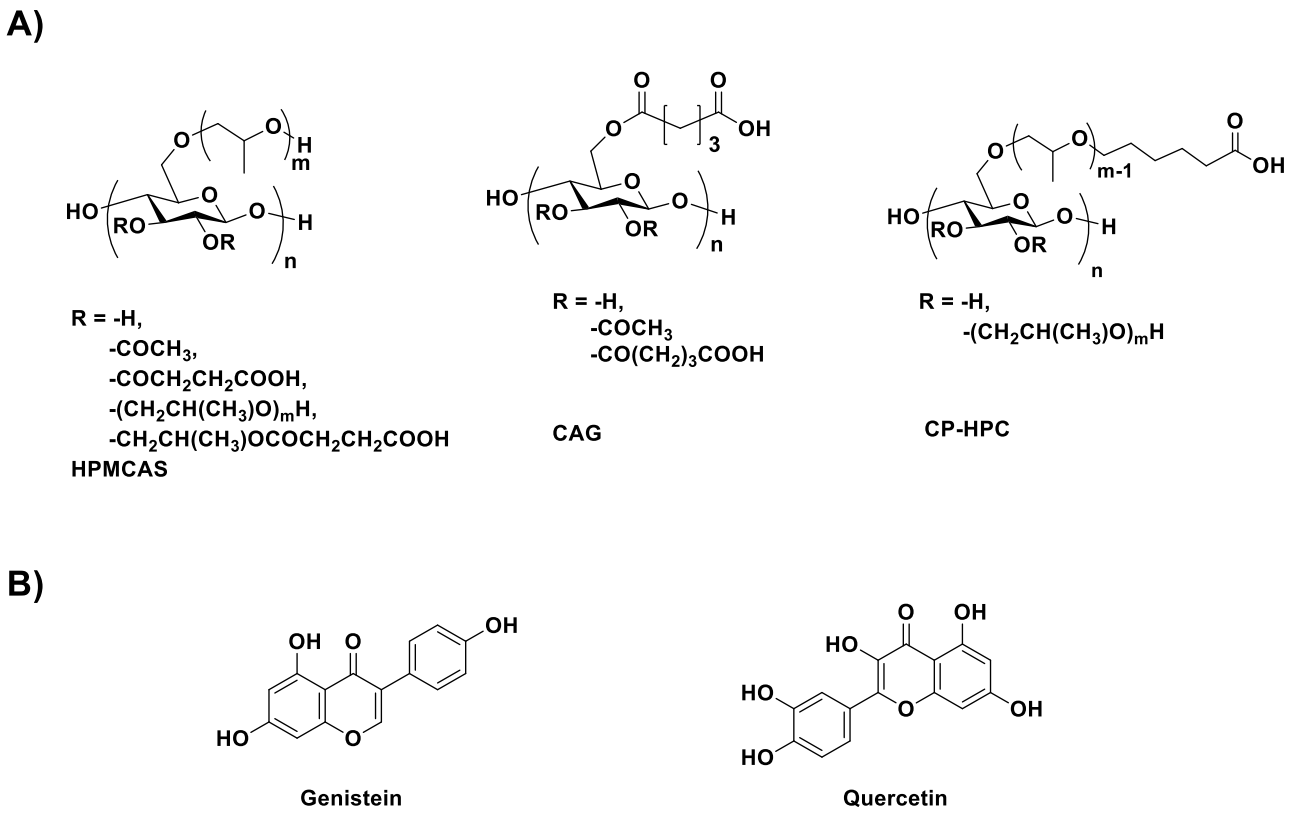

Figure 5.1. Structures of A) HPMCAS, CP-HPC, CAG; B) flavonoids genistein and quercetin. Cellulosic structures do not imply regioselectivity; particular positions of substitution in all schemes are only for convenience of depiction and clarity.

2. Experimental

2.1. Materials and methods

HPMCAS (AS-MF grade, wt. %: methoxyl 20-24%, hydroxypropyl 5-9%, acetyl 5-9%, succinoyl 14-18%; M_w = 18,000 (reported by manufacturer)) was from Shin-Etsu Chemical Co., Ltd. (Tokyo, Japan). Cellulose acetate (CA-320S, DS (acetate) = 1.82, DS(6-OH) = 0.50 (calculated via perpropionylated samples by ^{1}H NMR, adapted from (Gao & Edgar, 2019; S. Liu & Edgar, 2017) and originally described by (Liebert et al., 2005), M_n = 50,000 (via SEC)) was

from Eastman Chemical Company. Hydroxypropyl cellulose (HPC, M_w = 100 kg mol^{-1}, DP = 100, DS (HP) 2.2, MS(HP) 4.4) (Dong et al., 2016), sodium hydride (95%), anhydrous tetrahydrofuran (THF), 5-bromo-pent-1-ene, Hoveyda-Grubbs' 2nd generation catalyst, 3,5-di-*tert*-butylhydroxytoluene (BHT), *para*-toluenesulfonyl hydrazide (*p*TSH), and potassium bromide (KBr) were from Sigma-Aldrich (Saint Louis, MO, USA). *N*, *N*-Dimethylacetamide (DMAc), lithium chloride (LiCl), dichloromethane (DCM), methanol, ethanol, and dialysis tubing (MWCO 3.5k Da) were from Fisher Scientific (Fair Lawn, NJ, USA). Dimethylimidazole (DMI) was purchased from TCI Chemical (Montgomeryville, PA, USA). HPLC grade methanol (MeOH) and acetonitrile (ACN), reagent ethanol, sodium phosphate monobasic, monopotassium phosphate (KH_2PO_4), dichloromethane (DCM), isopropanol, *N*, *N*-dimethylformamide (DMF), dialysis tubing (MWCO 3.5 kDa), and sodium hydroxide (NaOH) were purchased from Fisher Scientific (Hampton, NH) and used as received. HCl (12.1 M) was obtained from Macron Chemicals by Avantor (Center Valley, PA). Water was purified by reverse osmosis and ion exchange using a Barnstead RO pure ST from Barnstead/Thermolyne (Ramsey, MN) purification system. Potassium phosphate dibasic (K_2HPO_4) was purchased from Acros Organics (Geel, Belgium). Ethyl vinyl ether was purchased from Fluka Analytical by Honeywell (Mexico City, Mexico).

^1H and ^{13}C NMR spectra were acquired on a Bruker Avance II spectrometer operating at 500 MHz. Polymer (ca. 10 mg for ^1H NMR and 50 mg for ^{13}C NMR) was dissolved in ca. 1 mL of deuterated chloroform or dimethyl sulfoxide ($CDCl_3$ or DMSO-d_6, respectively) and three drops of trifluoroacetic acid was added to shift the water peak downfield. Fourier transform-infrared (FT-IR) spectra were recorded in transmission mode with a Thermo Nicolet 8700 instrument (Madison, WI, USA) prepared by using the KBr pellet method (1mg ASD / 99 mg KBr) mixed by mortar and pestle.

2.2 Polymer synthesis

5-Carboxypentyl hydroxypropyl cellulose (CP-HPC-106) (MW 70,400 g/mol, carboxylic acid DS (COOH = 1.06)) was synthesized from HPC (DS, MS as listed in Materials section) as reported by Dong et al., 2016. CAG (MW 70,000 g/mol determined by DLS, DS(Ac) 1.6, DS(glutarate) 1.22 (both as measured by integration of ^{1}H NMR spectra (Petrova et al., *manuscript in preparation*))). Molecular weights were determined by size-exclusion chromatography (SEC) or dynamic light scattering (DLS), and DS by ^{1}H NMR spectroscopy, as described in the references (Dong et al., 2016; (Petrova et al., *manuscript in preparation*)). See SI for ^{1}H and ^{13}C NMR spectra (**Fig. S5.1-S5.2**). Polymer properties are summarized in Table S5.1.

2.3 Preparation of ASDs as amorphous films via rotary evaporation

ASD formulations of flavonoid:polymer at weight ratios 1:9 and 1:3 were prepared using HPMCAS-MF, CP-CHC, and CAG. Each polymer was separately dissolved in a suitable solvent (DCM:MeOH for HPMCAS-MF, THF for CP-HPC, pyridine for CAG) and were sonicated or allowed to stir (overnight for CAG). Genistein (or quercetin) was then sonicated in minimal solvent (MeOH) at RT for 10 min and added dropwise with stirring for 2-3h resulting in homogenous, single-phase solutions. The solvent was then rapidly removed by rotary evaporation (Cole Parmer, Vernon Hills, IL) over 10 min, and the residue was subsequently vacuum dried at 40 °C for 8-12 h to remove residual solvent.

2.4 Solid state characterization

Genistein, polymers, and ASD formulations were characterized by powder X-ray diffraction (PXRD), FTIR, and SEM. PXRD patterns were measured with a Bruker D8 Discover X-ray Diffractometer (Billerica, MA) with Lynxeye detector and KFL CU 2K X-ray source.

Analyses used a 1 mm slit window with scan range 10° to 50° 2θ. FTIR spectra were recorded between 4000 and 500 cm^{-1}, using a resolution of 4 cm^{-1} and 40 accumulations, on a Nicolet 8700 FT-IR Spectrometer (Thermo Fisher). Pellets were prepared from sample/KBr mixtures (1:100 weight ratio). We also investigated the morphology and particle size of each formulation by SEM.

2.5. Genistein crystalline and amorphous solubilities

Genistein crystalline and amorphous solubilities were measured via dissolution experiments. We evaluated polymer efficiency by creating and sustaining supersaturation under non-sink conditions, as supersaturation is reduced in sink conditions (Qiu et al., 2016). All measurements employed scintillation vials that were placed in water-circulating jacketed flasks in simulated physiological conditions at 37 °C and filled with 10 mL pH 6.8 phosphate buffered saline (PBS, 50 mM) to detect the extent of supersaturation.

2.5.1 Equilibrium solubility (Crystalline solubility)

An amount of genistein (20 mg) well in excess of its maximum thermodynamic solubility was added to each scintillation vial (2 mg/mL added) and stirred for 72h. The absorbance from the phosphate buffer solution was measured with a SI Photonics UV/vis spectrometer (Tucson, AZ, USA) fiber optically coupled with a dip probe of path length 10 mm. After 72h, the suspension was centrifuged for 30 min. at 37 °C (14, 800 G), and the supernatant was collected to evaluate drug concentration using a SI Photonics UV/vis spectrometer (Tucson, AZ, USA) with a fiber optically coupled with a dip probe of path length 10 mm.

2.5.2 Amorphous solubility: Fluorescence emission

Fluorescence spectroscopy was employed to evaluate whether phase separation originating from liquid-liquid phase separation occurred. A polarity sensitive probe was used to

evaluate the liquid-liquid phase separation concentration based on changes to the emission spectrum triggered by the dye partitioning into a new phase. Alternatively, no change in emission spectrum concurrent with the evolution of turbidity implies crystallization. 4-di-2-ASP fluorescent dye was selected as it has a characteristic emission spectrum at 600 nm which is known to shift upon partitioning into the hydrophobic nanodroplets formed upon LLPS. A stock solution of drug (1 mg/mL) was titrated into 10 mL phosphate buffer (pH 6.8) containing a fixed concentration of 4-di-2-ASP (1 mg/mL) and HPMCAS (1mg/mL) for a final 4-di-2-ASP concentration of 1-2 μg/mL, stirring at 300 RPM and 37 °C. The excitation wavelength used for 4-di-2-ASP was 488 nm, and the emission spectrum was collected in the range of 500-800 nm after each addition using a Shimadzu RF-5301PC spectrofluorometer (Kyoto, Japan).

2.6. ASD in vitro dissolution experiments

Small intestinal conditions (50 mM pH 6.8 phosphate buffer, 37^{o}C) were simulated in a dissolution experiment similar to the crystalline solubility experiment, under non-sink conditions to measure the extent of supersaturation. Each experiment was adjusted (based on drug loading) to contain a fixed amount of drug (targeting amorphous solubilities: 100 μg/mL genistein or 30 μg/mL quercetin in buffer). Temperature controlled jacketed flasks (50 mL, n = 3) were stirred at 300 rpm for the duration of the experiment. The experiment employed 10 mL pH 6.8 phosphate buffer. The absorbance spectrum (330 nm for genistein, 375 nm for quercetin) from the solution was measured using a UV dip probe spectrometer for 240 min.

2.7 Polarized Light Microscopy (PLM)

Polarized light microscopy (PLM) was performed with a Nikon LV100 Eclipse optical microscope and an AmScope MU503B digital camera. Samples were analyzed using polarized light with an analyzer set to 90° with respect to the polarizer and a λ (530 nm) tint plate. Sample

aliquots (250 μL) were collected at the completion of the ASD dissolution experiments (time = 240 min) as described in Section 2.5. Images were captured and processed using ImageJ software.

2.8 Nanoparticle Tracking Analysis (NTA)

Solution-state phase behavior was evaluated at the conclusion of ASD dissolution for the control, 1:9 genistein:HPMCAS as reported by (Jackson et al. 2016). One mL aliquots were withdrawn from the solution at the completion of the experiment (t = 240 min.) and analyzed using a NanoSight LM10 from Malvern Instruments (Westborough, MA) equipped with nanoparticle tracking analysis software. The LM10 was equipped with a 75 mW green (532 nm) laser and a temperature-controlled flow-through cell stage. Samples were analyzed at 25 °C for 30 s, and camera settings were held constant throughout all experiments (screen gain = 2.0, camera level = 7). The detection threshold upon analysis was also held constant (5) for all experiments along with camera gain (10.0).

3. Results and discussion

Maximizing drug concentration in the dosage form is a key obstacle in ASD development. High drug loadings (DL) can often lead to instability with regard to crystallization, either in the solid ASD or shortly after drug release into the lumen. While low DL may be acceptable or even convenient for high potency drugs, low potency drugs are at a disadvantage, since the overall dose size may exceed that which a person can comfortably swallow (or alternatively force the dose to be split into multiple pills or capsules, impairing patient compliance). Although the robust Bend Research map provided by (Friesen et al., 2008) categorizing low-solubility drugs into four groups serves as a guide for suggested DL in solid dispersions, we explored the effect of DL percentage on ASD performance in order to optimize

ASD dissolution and stability. The map plots the drug's T_m (melting temperature; T_m (genistein) = 301 °C and T_m (quercetin) = 326 °C)/T_g (glass transition temperature of amorphous drug) vs. the natural log of the drug partitioning coefficient, Log(P). Using the Bend Research map as a guide and using the positive control (1:9 genistein:HPMCAS) thermal behavior for the T_g (101.5 °C) and T_m (266 °C) values, the map suggests 10-35% suggested DL would yield optimal dissolution and stability for genistein ASDs. We evaluated 10% and 25% DL and tested these predictions.

HPMCAS is perhaps the most important commercial polymeric ASD crystallization inhibitor, while CP-HPC has shown ASD promise in several recent studies, leading to its exploration both *in vitro* and *in vivo* (Dong et al., 2016; Wilson et al., 2020). CAG was designed specifically as an ASD polymer that can be readily prepared using dietary or endogenous, inexpensive components, and simple and inexpensive processes. CAG has higher carboxylic acid DS than the other polymers in this study, which may prove advantageous by enhancing dissolution rate and/or polymer-drug specific interactions. Analytical techniques that are highly sensitive at identifying crystals (XRD, PLM and XRD) were chosen to evaluate whether flavonoid crystals were present in the polymeric dispersions (X. Liu et al., 2018; Ma & Williams, 2019).

3.1 Solid state characterization of solid dispersions

3.1.1 Powder X-ray diffraction (PXRD)

PXRD was performed to confirm the amorphous character of each solid dispersion by the presence of an amorphous halo and absence of crystalline peaks. Each genistein dispersion appeared to be amorphous by PXRD, presenting an amorphous halo (**Fig. 5.2b**) and no sharp

crystalline peaks as those observed in pure genistein (**Fig. 5.2a**). Quercetin alone and corresponding formulations displayed similar trends (**Figures S5.3A-S5.3B**).

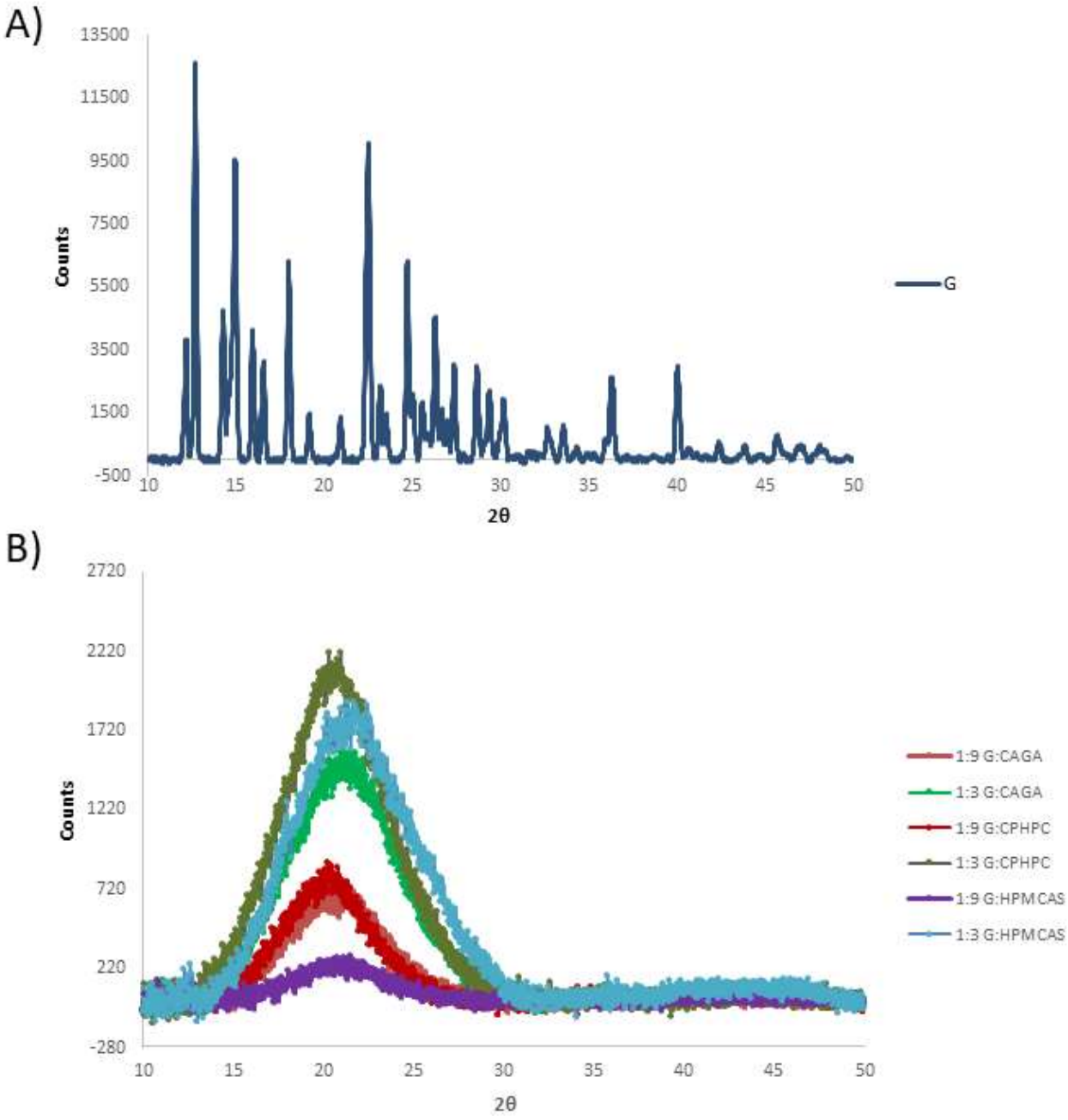

Figure 5.2. XRD spectra of A) crystalline genistein (abbreviated G in Figure) and B) Dispersions of G in polymers at various concentrations.

3.1.2 Molecular interactions by FTIR

Molecular interactions between polymer and drug in ASDs can cause shifts in IR absorbances of the groups involved. FTIR spectroscopy can be diagnostic of those functional group interactions that can reduce system energy and enhance ASD stability. These pairwise interactions often involve a hydrogen bond donor and acceptor, resulting in changes in spectral shape and peak intensity (Marks et al., 2014; Williams III et al., 2022). Genistein demonstrates a strong absorption at 3300-3500 cm^{-1}, indicative of the phenol hydroxyl group, whereas the same peak is broadened for each amorphous formulation, exemplified by the 10% and 25% genistein:CP-HPC dispersion (**Fig. 5.3**). The broadening of the hydroxyl absorption likely indicates hydrogen bonding between genistein hydroxyl and CP-HPC carboxyl groups, as expected in the presence of interactions between drug and excipient (Liu et al., 2018; Williams III et al., 2012). Similar changes are observed in the infrared spectra of genistein formulations with HPMCAS and CAG (**Figures S5.4-S5.5**), quercetin (alone) and corresponding formulations with the polymers studied herein are displayed in **Figures S5.6-S5.9**.

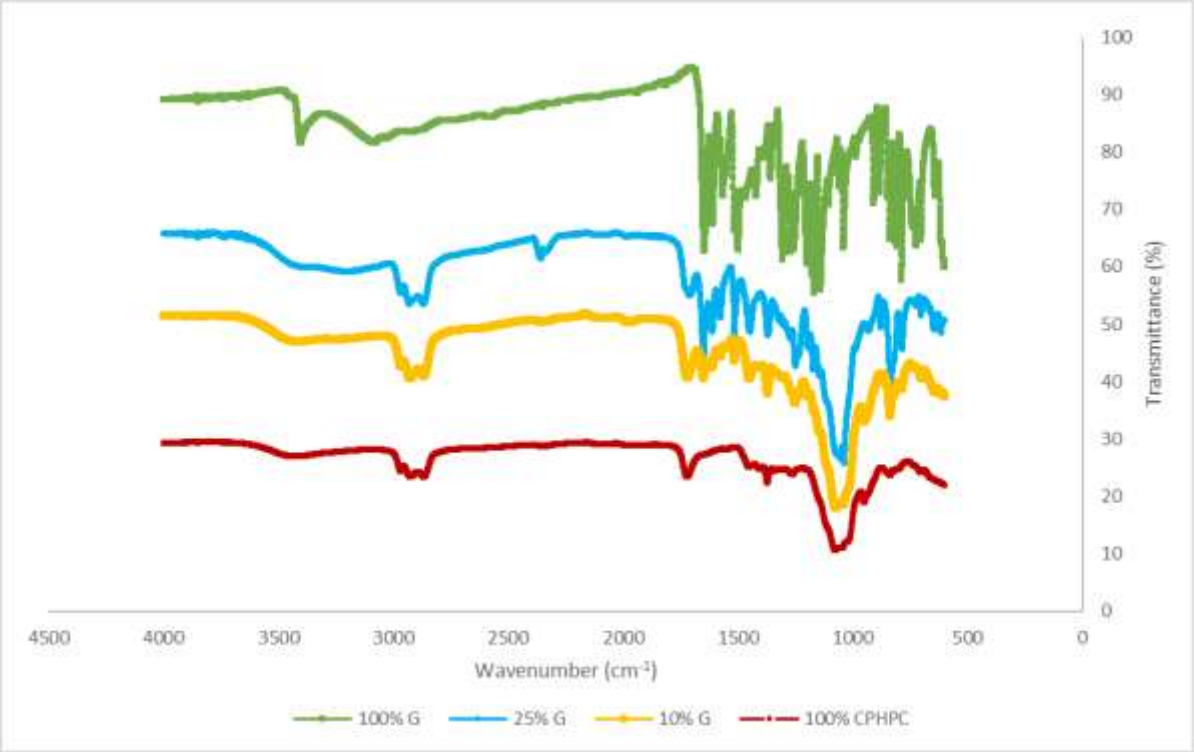

Figure 5.3 FTIR spectra in order from top to bottom: 100% G (drug alone, top), 25% G:CP-HPC, 10% G:CP-HPC, and 100% CP-HPC.

3.1.3 Scanning electron microscopy (SEM)

The morphology and surface properties of pure genistein, quercetin, CAG, CP-HPC, HPMCAS and their corresponding drug formulations were examined by SEM (**Fig. 5.4**). Rough textures indicative of crystalline material were observed for pure genistein and quercetin (**Fig. 5.4a** and **S5.8a**, respectively). Each ASD (**Fig. 5.4b-d**) and their corresponding pure polymer demonstrated a smooth surface that is consistent with the hypothesis that these materials are amorphous (**Fig. 5.4e-4j**).

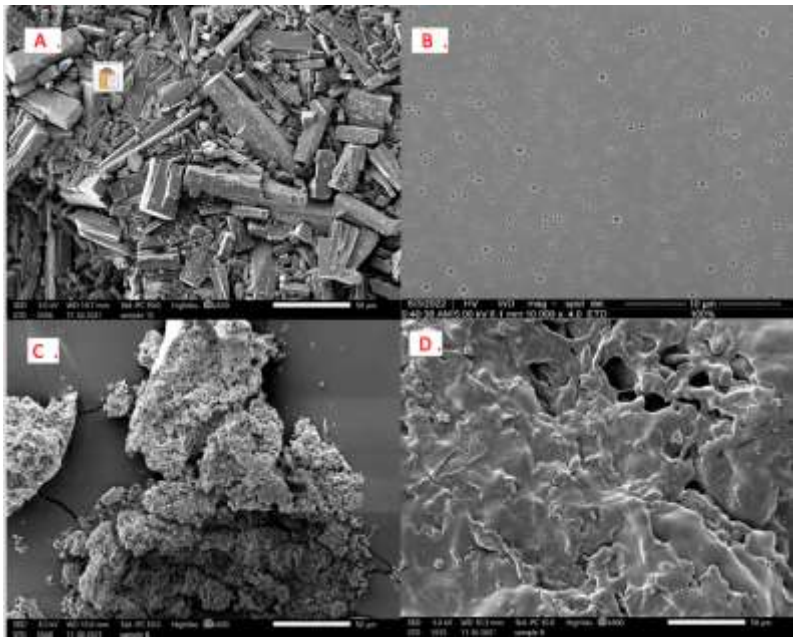
A
B
C
D

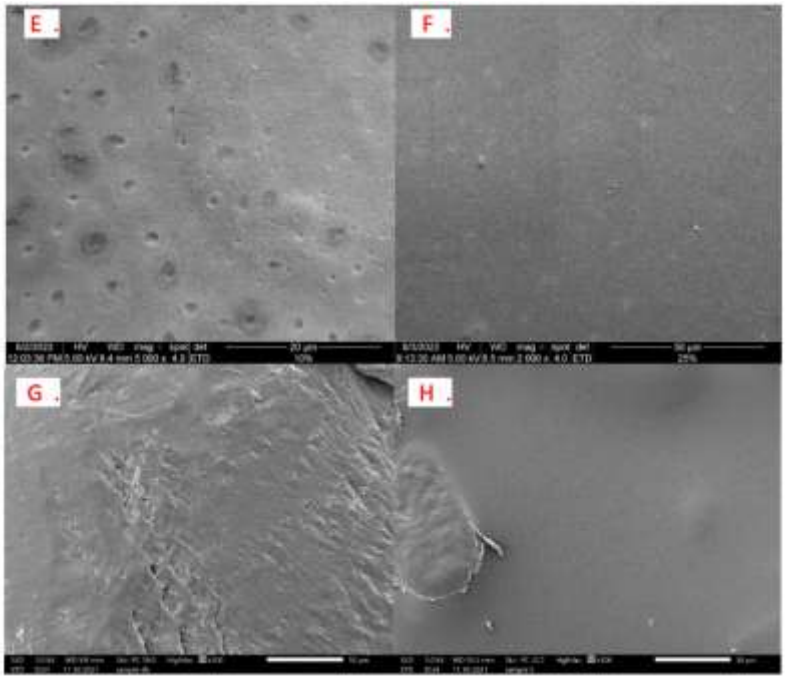
E
F
G
H

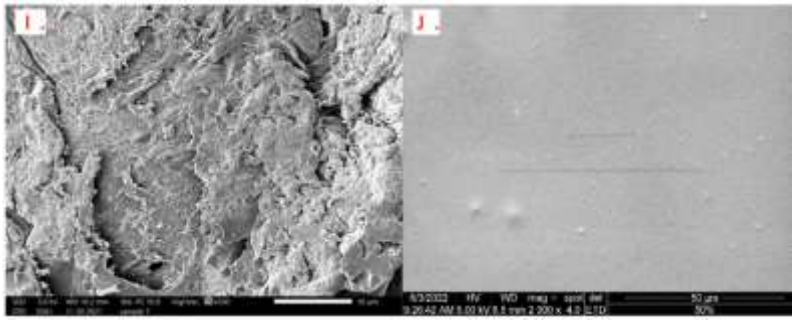
I
J

Figure 5.4. SEM of A) 100% crystalline genistein, 100% polymers B) HPMCAS, C) CAG, D) CP-HPC, ASD formulations D) HPMCAS, E) 10% DL CAG, F) 25% G:CAG, G) 10% G:CP-HPC, H) 25% G:CP-HPC, I) 10% G:HPMCAS, J) 25% G:HPMCAS.

3.2 Determination of crystalline and amorphous genistein solubilities

Genistein crystalline solubility was determined by exposing buffer to an excess of drug under small intestinal pH conditions (pH = 6.8 phosphate buffer). In contrast, the maximum achievable concentration of free drug in solution after intentional supersaturation is considered its amorphous solubility; this value can set the maximum possible solution concentration achievable in the presence of a polymer that is effective at stabilizing against crystallization. Amorphous solubility is determined experimentally by creating a supersaturated solution of drug, the concentration above which leads to phase separation and the emergence of a drug-rich phase (Fig. S10a, b). Fluorescent probes that are sensitive to changes in polarity can be used as sensors by partitioning into the disorderly, hydrophobic, drug-rich phase. Fluorescence emission is superior to UV extinction when determining phase separation for fast crystallizers, since unlike UV extinction, fluorescence allows one to discriminate between crystallization and liquid-liquid phase separation (Almeida E Sousa et al., 2015). We selected the cationic 4-di-2-ASP (λ, emission ≅600 nm) to determine the presence of liquid-liquid phase separation (Almeida E Sousa et al., 2015; Jackson et al., 2016; Purohit & Taylor, 2017), since it experiences a large fluorescence Stokes shift (ca. 30 nm and quench/dequenched quantum yield) when undergoing a shift in polarity in the local environment. The absence of a shift of the dye's emission spectrum with changes in turbidity or absorption spectrum should indicate that the probe has not partitioned into a different phase, and that crystallization has occurred. Herein, we observed a red shift in the maximum wavelength emission and diminished fluorescence intensity indicating

formation of a hydrophobic drug-rich phase upon liquid-liquid phase separation (Fig. S10). We employed a low concentration of HPMCAS (1 mg/mL) to facilitate measurement of the fast-crystallizing genistein, since it otherwise crystallizes essentially immediately upon addition to an aqueous environment. We compared the maximum concentrations from the aforementioned experiments, which then served to guide experimental design for the ASD dissolution experiments that followed. Genistein crystalline solubility was in agreement with the literature (1.43 µg/mL water solubility for free genistein at 25 °C) (J.-G. Wu et al., 2010)), with an equilibrium concentration of 5.11 ± 0.09 µg/mL pH 1.2 and 7.5 ± 0.5 µg/mL at pH 6.8. The relatively higher values obtained for genistein crystalline solubility vs. the reported aqueous solubility can be attributed to acquisition at a slightly higher temperature (literature T = 25 °C, this work T = 37 °C), and since genistein is partially ionized in pH 6.8 phosphate buffer since it possesses pKa = 6.5 - 7.25 (Kelly et al., 2015; Nan et al., 2014; Tsujimoto et al., 2009). We observed that genistein amorphous solubility (~100 µg/ml) under simulated intestinal conditions was 13.3-fold higher than its crystalline solubility (values are summarized in Table 5.1).

Table 5.1. Crystalline, amorphous, and reported aqueous solubility of genistein and quercetin.

Drug	Crystalline solubility (µg/mL)[a]	Amorphous solubility (µg/mL)[a]
Genistein	1.43[c], 7.51 ± 0.50[a]	99.0± 2.0[a]
Quercetin[b]	2.63[d], 1.03 ± 0.08[a]	31.23 ± 1.8[a]

[a] in simulated small intestinal conditions (pH 6.8 PBS buffer at 37 °C).

[b] Quercetin solubility as reported by Gilley et al., (2017)

[c] Reported by J.-G. Wu et al. (2010) in distilled water at 25 °C.

[d] Reported by Srinivas et al., (2010) in distilled water at 25 °C.

3.3 In vitro ASD dissolution studies

Solid dispersions containing 10 and 25 wt. % DL flavonoid were prepared using our synthetic polymers, CP-HPC and CAG. HPMCAS served as a positive ASD polymer control at equal DL due to its well-known strong performance as an ASD excipient (Curatolo et al., 2009; Friesen et al., 2008; Tanno et al., 2004). At the end of the ASD dissolution studies (240 min), polarized light microscopy (PLM) was used to evaluate the presence of amorphous and/or crystalline material. Crystalline morphology can be inferred by examining whether a sample presents birefringent particles under polarized light microscopy, whereas the absence of birefringence paired with dark particles infers amorphous material.

Dispersions with HPMCAS enhance solubility of genistein (reported for transdermal application only (Del Gaudio et al., 2017)) and quercetin (Gilley et al., 2017). In the current studies, formulations containing quercetin provided significant solubility enhancement (ca. 30 μg/mL) vs. drug alone. The polymers displayed similar degrees of solubility enhancement for each DL, indicating that even the higher loading investigated does not impair quercetin supersaturation. However, the dissolution profiles for a given polymer diverge with respect to the time at which quercetin solution concentration diminishes. This decrease occurred more rapidly in 25% DL while 10% DL appeared to exhibit more stable and sustained supersaturation.

The cellulose derivative CAG from our lab is an excellent crystallization inhibitor for a number of drugs (Petrova et al., *manuscript in preparation*); CAG has a much simpler structure than HPMCAS, useful for both synthesis and complete characterization. Maximum concentrations reached from quercetin loaded CAG were increased ~ 20-fold vs. drug alone despite incomplete release. Both quercetin/CAG ASDs evidenced some crystallization in

solution; solutions also contained undissolved polymer. Matrix crystallization from CAG formulations was more evident by PLM in 25% than the 10% DL (**Fig. 5.6a**).

The purpose-designed 5-carboxypentyl hydroxypropyl cellulose (CP-HPC) provided slightly better ASD performance than CAG, comparable to that of commercial HPMCAS-MF at each DL. Some crystals and amorphous material were present in 25% DL quercetin/CAG, while being absent in the 10% sample (**Fig. 5.6b**). Our synthetic cellulose-derivatives provided useful enhancements to quercetin concentrations, although HPMCAS ultimately provided the highest overall quercetin supersaturation.

Near complete dissolution with minimal crystallization was observed with HPMCAS at 10% DL. By the end of the experiment, the latter solution remained clear with minimal birefringence or crystallization as indicated by PLM (**Fig. 5.6c**). Crystallization may have occurred more rapidly at 25% DL HPMCAS, as evidenced by the quercetin solution concentration beginning to slope down (an indicator of crystallization) around 15 min. vs. at 30 min. with 10% DL.

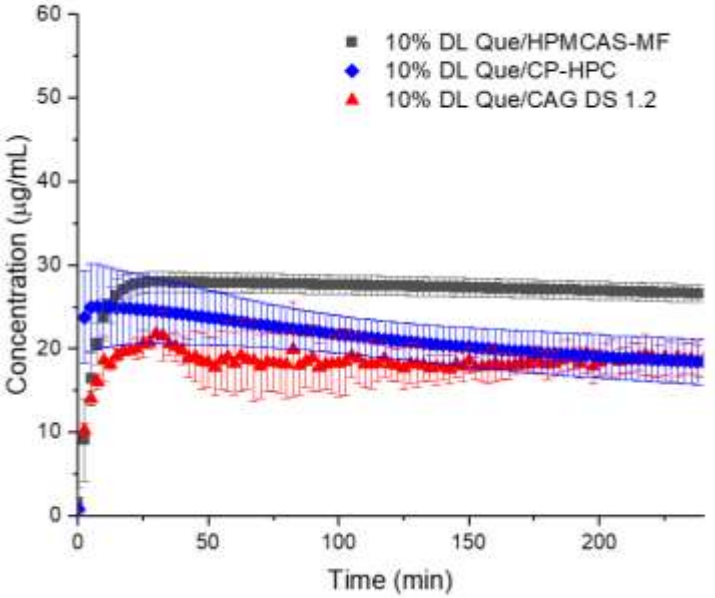

A)

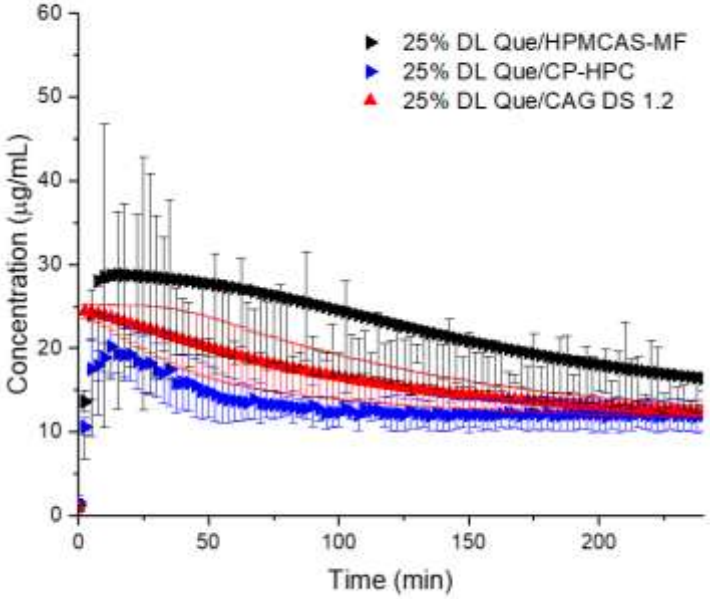

B)

Figure 5.5. Average ASD dissolution vs. time release profiles for quercetin (Que) for different polymers CP-HPC, CAG, and HPMCAS at A) 10% and B) 25% drug loading.

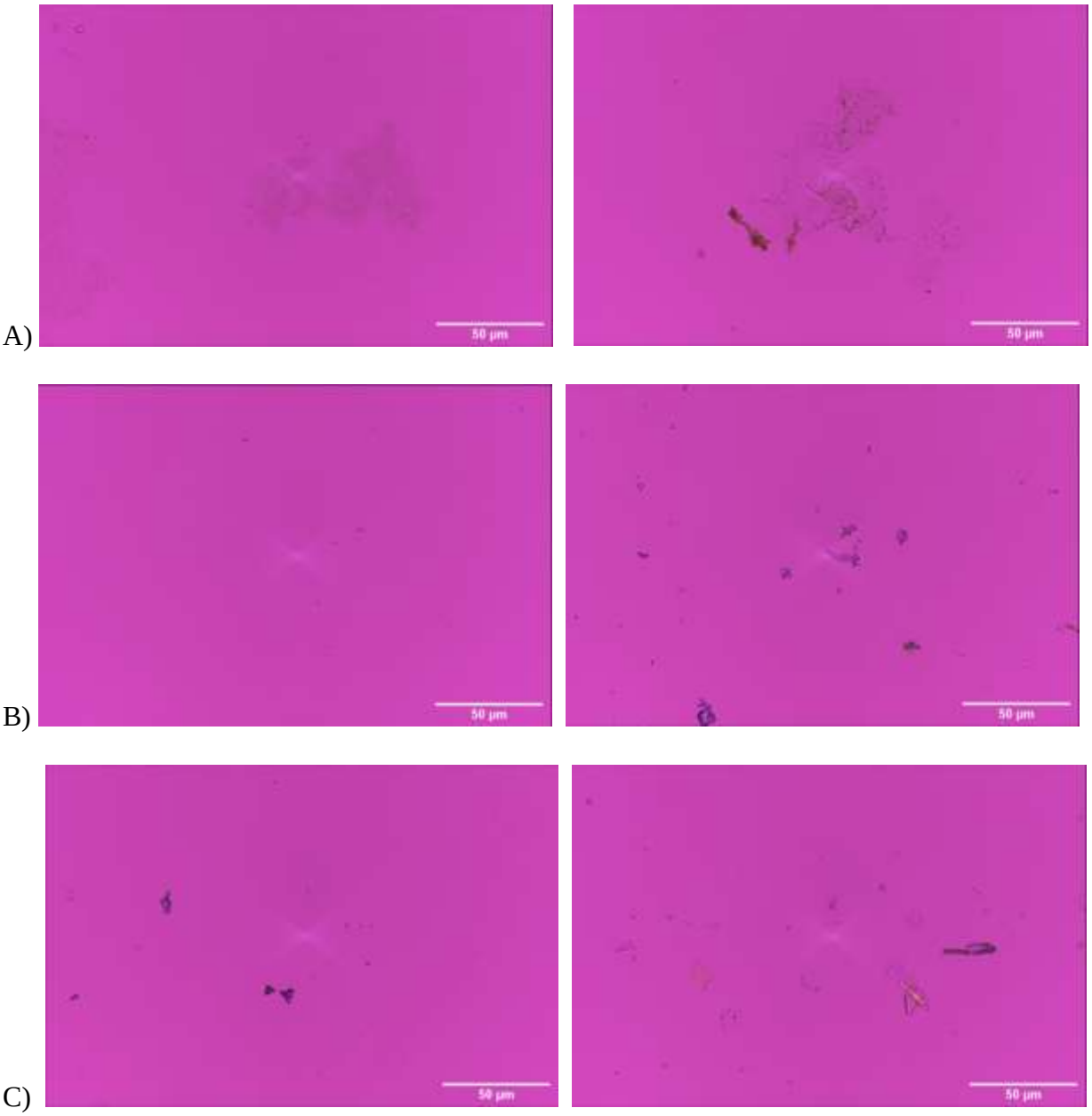

Figure 5.6. Polarized light microscopy (PLM) of quercetin ASD solutions at the end of dissolution study (t = 240 min.) at 10% (left) and 25% (right) DL. A) CAG (right), B) CP-HPC, and C) HPMCAS.

The novel genistein ASD formulations exhibited similar trends in release profiles with the degree of enhancement observed being CP-HPC > HPMCAS > CAG, and higher overall drug release for ASDs with lower DL (**Fig. 5.7**). Genistein ASD in CAG enhanced solubility

nearly 40-fold at 10% DL and 25.7-fold at 25% DL vs. drug only. As with quercetin:CAG ASDs, some undissolved polymer was evident. Some genistein crystallization was also observed at both loadings by 240 min (**Fig. 5.8a**); this of course might or might not be an issue *in vivo*, where drug permeation from solution would also be ongoing. CP-HPC provided ASD performance exceeding that of commercial HPMCAS-MF at 10% DL, and similar to that observed with HPMCAS at 25% DL. The greater variance in genistein solution concentrations observed from CP-HPC ASDs is suspected to originate from scattering which may occur due to the formation of a drug-rich phase (nanodroplets), crystallization, or undissolved ASD. From each genistein:CP-HPC ASD, drug solubility was significantly enhanced, achieving full amorphous solubility at 10% genistein loading, reaching levels approximately 70-fold (10% DL) and 46-fold (25% DL) higher than genistein thermodynamic solubility. Amorphous material (dark spots) were observed with evidence of some crystallization (birefringent spots) upon examination of genistein/CP-HPC solutions by PLM (**Fig. 5.8b**).

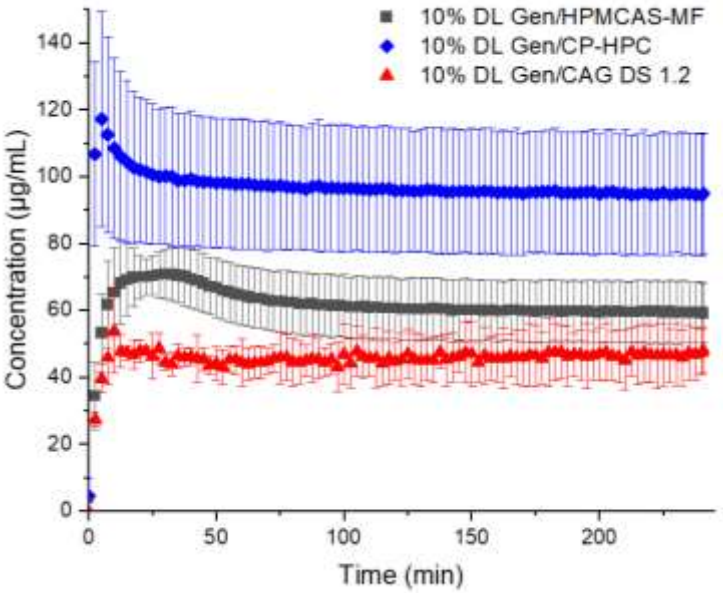
10% DL Gen/HPMCAS-MF
10% DL Gen/CP-HPC
10% DL Gen/CAG DS 1.2
Concentration (µg/mL)
Time (min)
0
20
40
60
80
100
120
140
0
50
100
150
200

A)

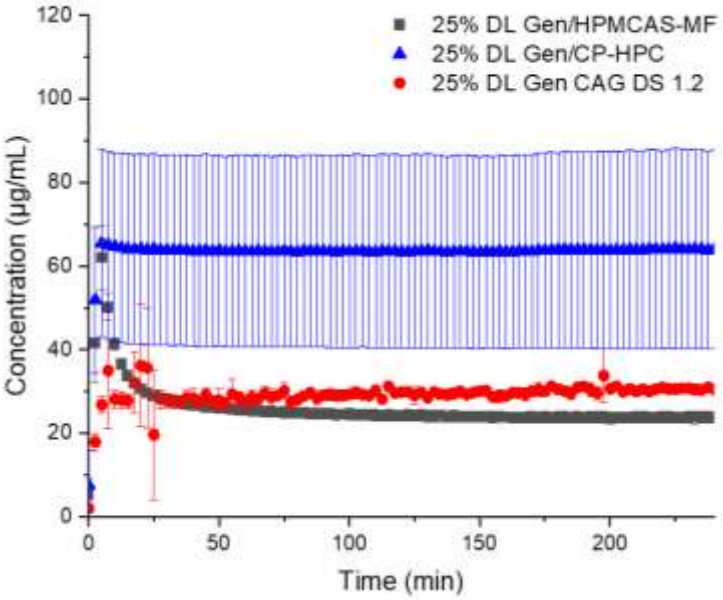
25% DL Gen/HPMCAS-MF
25% DL Gen/CP-HPC
25% DL Gen CAG DS 1.2
Concentration (µg/mL)
Time (min)
0
20
40
60
80
100
120
0
50
100
150
200

B)

Figure 5.7. Average ASD dissolution vs. time release profiles for genistein (Gen) for different polymers CP-HPC, CAG, and HPMCAS at A) 10% and B) 25% drug loading.

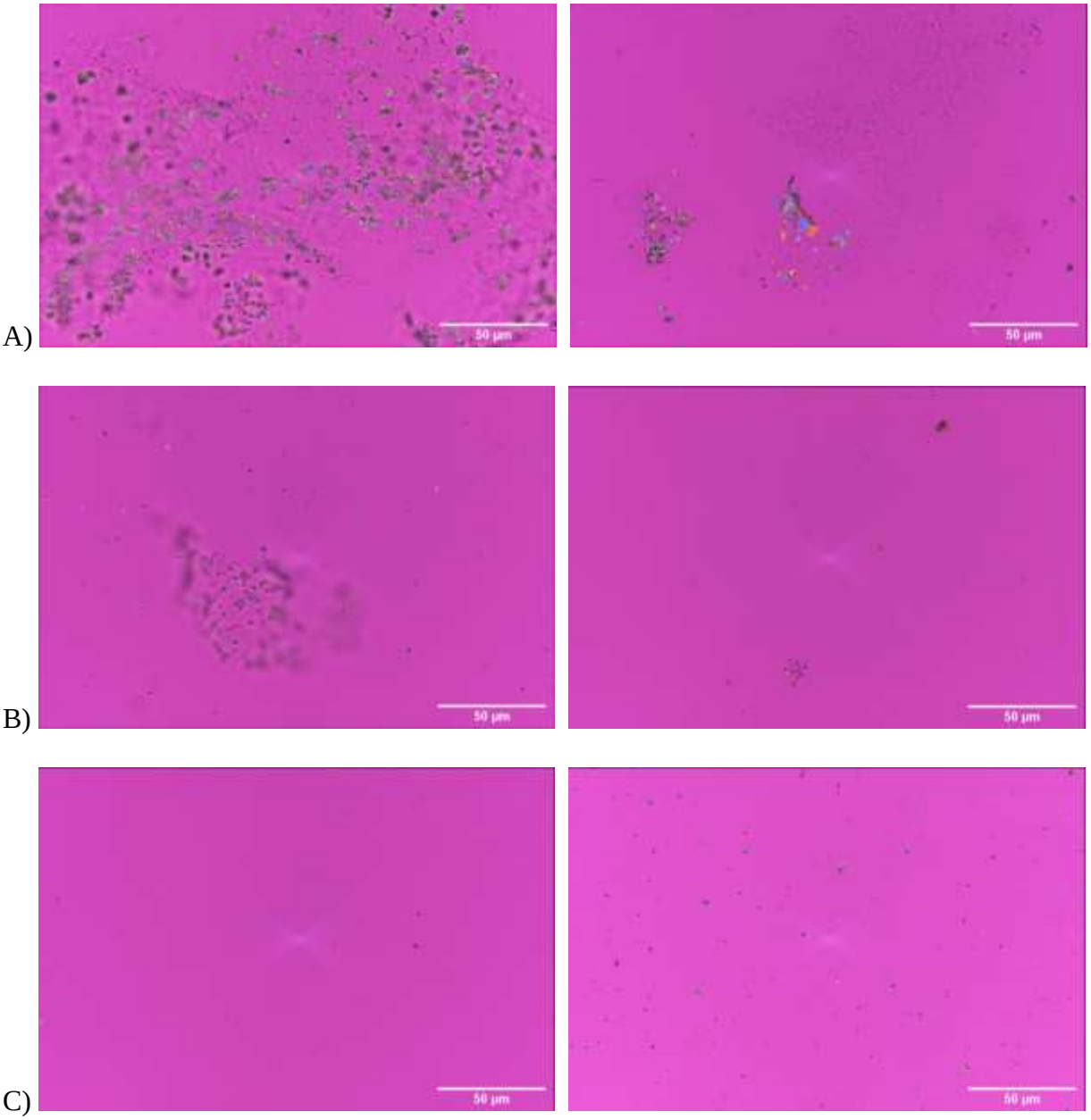

Figure 5.8. Polarized light microscopy (PLM) of genistein ASD solutions at the end of dissolution study (t = 240 min.) at 10% DL (left) and 25% (right) DL for A) CAG (right), B) CP-HPC and C) HPMCAS.

G:HPMCAS ASD also improved genistein aqueous solubility, sustaining a higher drug release for a longer duration with a maximum concentration achieved with 10% DL (70.1 ± 7.9 μg/mL) up to ~ 31.5 min. vs. the 25% DL (63.4 ± 9.9 μg/mL) which began to drop in concentration around 5 min. Turbidity was seen in the supersaturated solutions arising from each G:HPMCAS ASD, with crystallization observed at 25% DL (**Fig. 5.8c**). Nanoparticle tracking analysis (NTA) was employed for 10% G:HPMCAS as particles were too small to characterize via PLM. NTA analysis suggested the presence of crystals (flashing signal) since they are anisotropic and as a result, blink as the rotating particles scatter light, while amorphous nanoparticles (constant signal) do not blink as they are isotropic (**Fig. 5.9**).

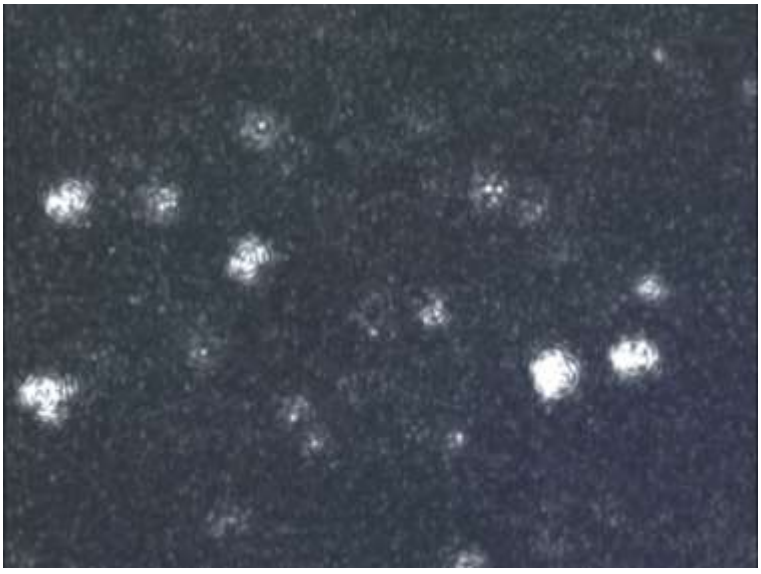

Figure 5.9. Nanoparticle tracking analysis of 10% G:HPMCAS solution after ASD dissolution (240 min).

Table 5.2. Maximum genistein (G) and quercetin (Q) concentrations from CP-HPC, CAG, and HPMCAS ASDs from *in vitro* dissolution experiments in simulated small intestinal conditions.

ASD formulation drug loading	Cmax (μg/mL) Genistein (G)	Cmax (μg/mL) Quercetin (Que)
10% drug:CP-HPC	**118 ± 33**	**25.1 ± 5.1**
25% drug:CP-HPC	**66 ± 23**	**24.5 ± 0.8**
10% drug:CAG	**55.7 ± 8.1**	**21.2 ± 1.6**
25% drug:CAG	**37 ± 14**	**20.2 ± 3.5**
10% drug:HPMCAS	**70.1 ± 7.9**	**28.0 ± 1.2**
25% drug:HPMCAS	**63.4 ± 9.9**	**28.8 ± 0.6**
Amorphous solubility	**99.0 ± 2.0**	**31.3 ± 1.8**
Crystalline solubility	**7.5 ± 0.5**	**1.0 ± 0.1**

The solubility parameter of a given compound or polymer is a useful indicator of its hydrophobic/hydrophilic character (Table 3). As used to evaluate the polymers used herein, solubility parameter provides perspective on the relative hydrophilicity of these cellulose derivatives in their un-ionized forms, where higher solubility parameter corresponds to more hydrophilic character. In this study, we observed that higher concentrations of the flavonoids were achieved in intestinal conditions when the Fedor's solubility parameter of the polymer was lower than that of the flavonoid (genistein solution concentrations CP-HPC>HPMCAS>CAG; quercetin solution concentrations HPMCAS>CP-HPC>CAG). Therefore, within this polymer group, polymers with moderate to increasing hydrophobic character (lower SP) gave higher flavonoid concentration from ASDs of equal drug loading. While CAG is slightly more hydrophilic than CP-HPC (SP 23.7 vs. 22.9 $MPa^{1/2}$, respectively), SP indicates only the polarity of the un-ionized form; CAG has higher carboxyl DS than the other two polymers so will be

more highly ionized at neutral pH. CAG may also be more miscible with genistein (39.1 $MPa^{1/2}$) as their SP are more closely matched. It is possible that CAG hydrophilicity may have restricted miscibility with the flavonoids, thus impairing solubility enhancement in contrast to HPMCAS (21.5 $MPa^{1/2}$) and CP-HPC. For quercetin, it appears that greater solution concentration enhancement is associated with the lowest polymer SP. In the scope of the polymers in this study, it may be that it is more important to impart greater hydrophobic character with quercetin whose SP is even higher (indicative of more hydrophilic character per Fedor SP), to achieve greater drug release concentration. This claim can be supported by HPMCAS drug release profiles achieving the highest quercetin concentrations paired with the polymer possessing the lowest SP (or more hydrophobic character) herein.

Table 3. Fedor's solubility parameters for genistein and polymers

Compound	Solubility parameter, δ ($MPa^{1/2}$)
Genistein	**39.1**
Quercetin	**45.0**
CAG	**23.7**
CP-HPC	**22.9** [a]
HPMCAS-MF	**21.5**

a. As reported by (Novo et al., 2022).

4. Conclusions

In this work, we created flavonoid-based ASDs with quercetin and genistein. We confirmed our hypothesis; each of these cellulosic polymers that were designed to be effective ASD polymers indeed effectively inhibited crystallization for both drug candidates. By exploring

different drug loadings, we were able to identify polymers that were effective inhibitors even at relatively high drug concentration, with results in good agreement with the Bend Research map (Friesen et al., 2008) for the suggested 10-35% drug loading for high performance. The ability to increase drug percentage in an ASD formulation is extremely valuable, permitting improvements such as reduction in pill size, and the ability to extend application of ASD formulation to lower potency active ingredients. For each flavonoid, we found more stable supersaturation with less crystallization at 10% DL. Quercetin ASDs had similar drug release at both DL, creating the potential for oral dosage forms with up to 25% DL. Exceptionally enhanced solubility was yielded for genistein at 10% DL of each polymer, achieving maximum possible supersaturation from ASDs with the effective ASD polymer 5-carboxypentyl hydroxypropyl cellulose (CP-HPC), reaching levels 70-fold that of genistein thermodynamic solubility. The promising new cellulose acetate glutarate (CAG) was able to achieve high levels of supersaturation for each flavonoid, with enhanced dissolution vs. drug alone up to 40-fold for genistein at 10% DL, and 8-fold enhancement for quercetin at 25% DL. Comparison of the solubility parameters of these polymers confirms that for genistein ASD, CP-HPC possesses an appropriate balance between hydrophilic and hydrophobic character with similar SP to HPMCAS (but achieving substantially higher genistein supersaturation/concentration values than at equal concentrations in HPMCAS ASDs). That balance may contribute to the fact that CP-HPC most strongly improved genistein solution concentration at 10% DL among this group of ASD polysaccharide derivatives.

The small-scale polymer screening strategy herein provided insight that should assist design of larger scale dissolution studies. Previous studies inferred that polymer screening using the rotary evaporation technique provides results in agreement with those from spray-drying to prepare ASDs, provided that amorphous character is achieved and confirmed by characterization

(Mosquera-Giraldo et al., 2021). ASD of genistein and quercetin employing our promising cellulosic polymers, including CAG, has been shown in this work to afford substantially high levels of supersaturation, which should permit future *in vivo* bioavailability studies, enable establishment of dose-response relationships, and create results which, if successful, could underpin human clinical trials of these promising flavonoids.

References

Abd-Rabou, A. A., & Ahmed, H. H. (2017). CS-PEG decorated PLGA nano-prototype for delivery of bioactive compounds: A novel approach for induction of apoptosis in HepG2 cell line. *Advances in Medical Sciences*, *62*(2), 357–367. https://doi.org/10.1016/j.advms.2017.01.003

Ahmed, B., Hashmi, A., Khan, M. S., & Musarrat, J. (2018). ROS mediated destruction of cell membrane, growth and biofilms of human bacterial pathogens by stable metallic AgNPs functionalized from bell pepper extract and quercetin. *Advanced Powder Technology*, *29*(7), 1601–1616. https://doi.org/10.1016/j.apt.2018.03.025

Almeida E Sousa, L., Reutzel-Edens, S. M., Stephenson, G. A., & Taylor, L. S. (2015). Assessment of the amorphous "solubility" of a group of diverse drugs using new experimental and theoretical approaches. *Molecular Pharmaceutics*, *12*(2), 484–495. https://doi.org/10.1021/mp500571m

Amidon, G. L., Lennernäs, H., Shah, V. P., & Crison, J. R. (1995). A Theoretical Basis for a Biopharmaceutic Drug Classification: The Correlation of in Vitro Drug Product Dissolution and in Vivo Bioavailability. *Pharmaceutical Research: An Official Journal of the American Association of Pharmaceutical Scientists*, *12*(3), 413–420.

https://doi.org/10.1023/A:1016212804288

Arca, H. C., Mosquera-Giraldo, L. I., Bi, V., Xu, D., Taylor, L. S., & Edgar, K. J. (2018). Pharmaceutical Applications of Cellulose Ethers and Cellulose Ether Esters. *Biomacromolecules*, *19*(7), 2351–2376. https://doi.org/10.1021/acs.biomac.8b00517

Atteritano, M., Mazzaferro, S., Bitto, A., Cannata, M. L., D'Anna, R., Squadrito, F., Macrì, I., Frisina, A., Frisina, N., & Bagnato, G. (2014). Genistein effects on quality of life and depression symptoms in osteopenic postmenopausal women: A 2-year randomized, double-blind, controlled study. *Osteoporosis International*, *25*(3), 1123–1129. https://doi.org/10.1007/s00198-013-2512-5

Bian, Q., Liu, J., Tian, J., & Hu, Z. (2004). Binding of genistein to human serum albumin demonstrated using tryptophan fluorescence quenching. *International Journal of Biological Macromolecules*, *34*(5), 275–279. https://doi.org/10.1016/j.ijbiomac.2004.09.005

Caddeo, C., Pons, R., Carbone, C., Fernàndez-Busquets, X., Cardia, M. C., Maccioni, A. M., Fadda, A. M., & Manconi, M. (2017). Physico-chemical characterization of succinyl chitosan-stabilized liposomes for the oral co-delivery of quercetin and resveratrol. *Carbohydrate Polymers*, *157*, 1853–1861. https://doi.org/10.1016/j.carbpol.2016.11.072

Chen, F., Peng, J., Lei, D., Liu, J., & Zhao, G. (2013). Optimization of genistein solubilization by κ-carrageenan hydrogel using response surface methodology. *Food Science and Human Wellness*, *2*(3–4), 124–131. https://doi.org/10.1016/j.fshw.2013.06.001

Cheng, Q., Qin, W., Yu, Y., Li, G., Wu, J., & Zhuo, L. (2020). Preparation and Characterization of PEG-PLA Genistein Micelles Using a Modified Emulsion-Evaporation Method. *Journal of Nanomaterials*, *2020*, 1–15. https://doi.org/10.1155/2020/3278098

Cohen, R., Orlova, Y., Kovalev, M., Ungar, Y., & Shimoni, E. (2008). Structural and functional

properties of amylose complexes with genistein. *Journal of Agricultural and Food Chemistry*, *56*(11), 4212–4218. https://doi.org/10.1021/jf800255c

Cruz dos Santos, S., Osti Silva, N., dos Santos Espinelli, J. B., Germani Marinho, M. A., Vieira Borges, Z., Bruzamarello Caon Branco, N., Faita, F. L., Meira Soares, B., Horn, A. P., Parize, A. L., & Rodrigues de Lima, V. (2019). Molecular interactions and physico-chemical characterization of quercetin-loaded magnetoliposomes. *Chemistry and Physics of Lipids*, *218*, 22–33. https://doi.org/10.1016/j.chemphyslip.2018.11.010

Curatolo, W., Nightingale, J. A., & Herbig, S. M. (2009). Utility of hydroxypropylmethylcellulose acetate succinate (HPMCAS) for initiation and maintenance of drug supersaturation in the GI milieu. *Pharmaceutical Research*, *26*(6), 1419–1431. https://doi.org/10.1007/s11095-009-9852-z

Daruházi, Á. E., Szente, L., Balogh, B., Mátyus, P., Béni, S., Takács, M., Gergely, A., Horváth, P., Szoke, É., & Lemberkovics, É. (2008). Utility of cyclodextrins in the formulation of genistein. Part 1. Preparation and physicochemical properties of genistein complexes with native cyclodextrins. *Journal of Pharmaceutical and Biomedical Analysis*, *48*(3), 636–640. https://doi.org/10.1016/j.jpba.2008.06.007

de Oliveira, S. R., Taveira, S. F., Marreto, R. N., Valadares, M. C., Diniz, D. G. A., & Lima, E. M. (2013). Preparation and characterization of solid oral dosage forms containing soy isoflavones. *Revista Brasileira de Farmacognosia*, *23*(1), 175–181. https://doi.org/10.1590/S0102-695X2013005000007

Del Gaudio, P., Russo, P., Rodriguez Dorado, R., Sansone, F., Mencherini, T., Gasparri, F., & Aquino, R. P. (2017). Submicrometric hypromellose acetate succinate particles as carrier for soy isoflavones extract with improved skin penetration performance. *Carbohydrate*

Polymers, *165*, 22–29. https://doi.org/10.1016/j.carbpol.2017.02.025

Diamantis, D. A., Ramesova, S., Chatzigiannis, C. M., Degano, I., Gerogianni, P. S., Karadima, K. E., Perikleous, S., Rekkas, D., Gerothanassis, I. P., Galaris, D., Mavromoustakos, T., Valsami, G., Sokolova, R., & Tzakos, A. G. (2018). Exploring the oxidation and iron binding profile of a cyclodextrin encapsulated quercetin complex unveiled a controlled complex dissociation through a chemical stimulus. *Biochimica et Biophysica Acta - General Subjects*, *1862*(9), 1913–1924. https://doi.org/10.1016/j.bbagen.2018.06.006

Dias, A. S., Porawski, M., Alonso, M., Marroni, N., Collado, P. S., & González-Gallego, J. (2005). Quercetin decreases oxidative stress, NF-κB activation, and iNOS overexpression in liver of streptozotocin-induced diabetic rats. *Journal of Nutrition*, *135*(10), 2299–2304. https://doi.org/10.1093/jn/135.10.2299

Dong, Y., Mosquera-Giraldo, L. I., Troutman, J., Skogstad, B., Taylor, L. S., & Edgar, K. J. (2016). Amphiphilic hydroxyalkyl cellulose derivatives for amorphous solid dispersion prepared by olefin cross-metathesis. *Polymer Chemistry*, *7*(30), 4953–4963. https://doi.org/10.1039/c6py00960c

Firdous, A. B., Sharmila, G., Balakrishnan, S., RajaSingh, P., Suganya, S., Srinivasan, N., & Arunakaran, J. (2014). Quercetin, a natural dietary flavonoid, acts as a chemopreventive agent against prostate cancer in an in vivo model by inhibiting the EGFR signaling pathway. *Food and Function*, *5*(10), 2632–2645. https://doi.org/10.1039/c4fo00255e

Friesen, D. T., Shanker, R., Crew, M., Smithey, D. T., Curatolo, W. J., & Nightingale, J. A. S. (2008). Hydroxypropyl methylcellulose acetate succinate-based spray-dried dispersions: An overview. *Molecular Pharmaceutics*, *5*(6), 1003–1019. https://doi.org/10.1021/mp8000793

Gao, C., & Edgar, K. J. (2019). Efficient Synthesis of Glycosaminoglycan Analogs.

Biomacromolecules, *20*(2), 608–617. https://doi.org/10.1021/acs.biomac.8b01150

Giannouli, M., Karagkiozaki, V., Pappa, F., Moutsios, I., Gravalidis, C., & Logothetidis, S. (2018). Fabrication of quercetin-loaded PLGA nanoparticles via electrohydrodynamic atomization for cardiovascular disease. *Materials Today: Proceedings*, *5*(8), 15998–16005. https://doi.org/10.1016/j.matpr.2018.05.044

Gilley, A. D., Arca, H. C., Nichols, B. L. B., Mosquera-Giraldo, L. I., Taylor, L. S., Edgar, K. J., & Neilson, A. P. (2017). Novel cellulose-based amorphous solid dispersions enhance quercetin solution concentrations in vitro. *Carbohydrate Polymers*, *157*, 86–93. https://doi.org/10.1016/j.carbpol.2016.09.067

Gruca, A., Krawczyk, Z., Szeja, W., Grynkiewicz, G., & Rusin, A. (2014). Synthetic genistein glycosides inhibiting EGFR phosphorylation enhance the effect of radiation in HCT 116 colon cancer cells. *Molecules*, *19*(11), 18558–18573. https://doi.org/10.3390/molecules191118558

Han, J., Tong, M., Li, S., Yu, X., Hu, Z., Zhang, Q., Xu, R., & Wang, J. (2021). Surfactant-free amorphous solid dispersion with high dissolution for bioavailability enhancement of hydrophobic drugs: a case of quercetin. *Drug Development and Industrial Pharmacy*, *47*(1), 153–162. https://doi.org/10.1080/03639045.2020.1862173

Hu, K., & McClements, D. J. (2015). Fabrication of biopolymer nanoparticles by antisolvent precipitation and electrostatic deposition: Zein-alginate core/shell nanoparticles. *Food Hydrocolloids*, *44*, 101–108. https://doi.org/10.1016/j.foodhyd.2014.09.015

Ilevbare, G. A., Liu, H., Edgar, K. J., & Taylor, L. S. (2013). Impact of polymers on crystal growth rate of structurally diverse compounds from aqueous solution. *Molecular Pharmaceutics*, *10*(6), 2381–2393. https://doi.org/10.1021/mp400029v

Jackson, M. J., Kestur, U. S., Hussain, M. A., & Taylor, L. S. (2016). Dissolution of Danazol Amorphous Solid Dispersions: Supersaturation and Phase Behavior as a Function of Drug Loading and Polymer Type. *Molecular Pharmaceutics*, *13*(1), 223–231. https://doi.org/10.1021/acs.molpharmaceut.5b00652

Kelly, M. M., Rearick, D. C., Overgaard, C. G., Schoenfuss, H. L., & Arnold, W. A. (2015). Sorption of isoflavones to river sediment and model sorbents and outcomes for larval fish exposed to contaminated sediment. *Journal of Hazardous Materials*, *282*, 26–33. https://doi.org/10.1016/j.jhazmat.2014.03.059

Khursheed, R., Singh, S. K., Wadhwa, S., Gulati, M., & Awasthi, A. (2020). Enhancing the potential preclinical and clinical benefits of quercetin through novel drug delivery systems. In *Drug Discovery Today* (Vol. 25, Issue 1, pp. 209–222). Elsevier Current Trends. https://doi.org/10.1016/j.drudis.2019.11.001

Kim, J., Lee, H. J., & Lee, K. W. (2010). Naturally occurring phytochemicals for the prevention of Alzheimer's disease. *Journal of Neurochemistry*, *112*(6), 1415–1430. https://doi.org/10.1111/j.1471-4159.2009.06562.x

Kim, M., Lim, J., Lee, J. H., Lee, K. M., Kim, S., Park, K. W., Nho, C. W., & Cho, Y. S. (2018). Understanding the functional role of genistein in the bone differentiation in mouse osteoblastic cell line MC3T3-E1 by RNA-seq analysis. *Scientific Reports*, *8*(1), 1–12. https://doi.org/10.1038/s41598-018-21601-9

Lauro, M. R., Maggi, L., Conte, U., De Simone, F., & Aquino, R. P. (2005). Rutin and quercetin gastro-resistant microparticles obtained by spray-drying technique. *Journal of Drug Delivery Science and Technology*, *15*(5), 363–369. https://doi.org/10.1016/s1773-2247(05)50066-2

Li, B., Harich, K., Wegiel, L., Taylor, L. S., & Edgar, K. J. (2013). Stability and solubility enhancement of ellagic acid in cellulose ester solid dispersions. *Carbohydrate Polymers*, *92*(2), 1443–1450. https://doi.org/10.1016/j.carbpol.2012.10.051

Li, B., Konecke, S., Harich, K., Wegiel, L., Taylor, L. S., & Edgar, K. J. (2013). Solid dispersion of quercetin in cellulose derivative matrices influences both solubility and stability. *Carbohydrate Polymers*, *92*(2), 2033–2040. https://doi.org/10.1016/j.carbpol.2012.11.073

Li, B., Konecke, S., Wegiel, L. A., Taylor, L. S., & Edgar, K. J. (2013). Both solubility and chemical stability of curcumin are enhanced by solid dispersion in cellulose derivative matrices. *Carbohydrate Polymers*, *98*(1), 1108–1116. https://doi.org/10.1016/j.carbpol.2013.07.017

Li, B., Liu, H., Amin, M., Wegiel, L. A., Taylor, L. S., & Edgar, K. J. (2013). Enhancement of naringenin solution concentration by solid dispersion in cellulose derivative matrices. *Cellulose*, *20*(4), 2137–2149. https://doi.org/10.1007/s10570-013-9970-y

Liebert, T., Hussain, M. A., & Heinze, T. (2005). Structure determination of cellulose esters via subsequent functionalization and NMR spectroscopy. *Macromolecular Symposia*, *223*(1), 79–92. https://doi.org/10.1002/masy.200550506

Lin, L. Y., Peng, C. C., Liang, Y. J., Yeh, W. T., Wang, H. E., Yu, T. H., & Peng, R. Y. (2008). Alpinia zerumbet potentially elevates high-density lipoprotein cholesterol level in hamsters. *Journal of Agricultural and Food Chemistry*, *56*(12), 4435–4443. https://doi.org/10.1021/jf800195d

Liu, H., Taylor, L. S., & Edgar, K. J. (2015). The role of polymers in oral bioavailability enhancement; A review. *Polymer*, *77*, 399–415. https://doi.org/10.1016/j.polymer.2015.09.026

Liu, S., & Edgar, K. J. (2017). Water-soluble co-polyelectrolytes by selective modification of cellulose esters. *Carbohydrate Polymers*, *162*, 1–9. https://doi.org/10.1016/j.carbpol.2017.01.008

Liu, X., Feng, X., Williams, R. O., & Zhang, F. (2018). Characterization of amorphous solid dispersions. In *Journal of Pharmaceutical Investigation* (Vol. 48, Issue 1, pp. 19–41). https://doi.org/10.1007/s40005-017-0361-5

Ma, X., & Williams, R. O. (2019). Characterization of amorphous solid dispersions: An update. In *Journal of Drug Delivery Science and Technology* (Vol. 50, pp. 113–124). https://doi.org/10.1016/j.jddst.2019.01.017

Marks, J. A., Wegiel, L. A., Taylor, L. S., & Edgar, K. J. (2014). Pairwise polymer blends for oral drug delivery. *Journal of Pharmaceutical Sciences*, *103*(9), 2871–2883. https://doi.org/10.1002/jps.23991

Messina, M. J., Persky, V., Setchell, K. D. R., & Barnes, S. (1994). Soy intake and cancer risk: A review of the in vitro and in vivo data. *Nutrition and Cancer*, *21*(2), 113–131. https://doi.org/10.1080/01635589409514310

Miao, Q., Li, J. G., Miao, S., Hu, N., Zhang, J., Zhang, S., Xie, Y. H., Wang, J. B., & Wang, S. W. (2012). The bone-protective effect of genistein in the animal model of bilateral ovariectomy: Roles of phytoestrogens and PTH/PTHR1 against post-menopausal osteoporosis. *International Journal of Molecular Sciences*, *13*(1), 56–70. https://doi.org/10.3390/ijms13010056

Mittal, A. K., Kumar, S., & Banerjee, U. C. (2014). Quercetin and gallic acid mediated synthesis of bimetallic (silver and selenium) nanoparticles and their antitumor and antimicrobial potential. *Journal of Colloid and Interface Science*, *431*, 194–199.

https://doi.org/10.1016/j.jcis.2014.06.030

Moon, J., Do, H. J., Kim, O. Y., & Shin, M. J. (2013). Antiobesity effects of quercetin-rich onion peel extract on the differentiation of 3T3-L1 preadipocytes and the adipogenesis in high fat-fed rats. *Food and Chemical Toxicology*, *58*, 347–354. https://doi.org/10.1016/j.fct.2013.05.006

Mosquera-Giraldo, L. I., Borca, C. H., Meng, X., Edgar, K. J., Slipchenko, L. V, & Taylor, L. S. (2016). Mechanistic Design of Chemically Diverse Polymers with Applications in Oral Drug Delivery. *Biomacromolecules*, *17*(11), 3659–3671. https://doi.org/10.1021/acs.biomac.6b01156

Mosquera-Giraldo, L. I., Donoso, M., Stefanski, K., Foster, K., Gesenberg, C., Abraham, P., Ren, Y., Rose, A., Freeden, C., & Ranasinghe, A. (2021). Solvent-Casted Films to Assist Polymer Selection for Amorphous Solid Dispersions During Preclinical Studies: In-vitro and In-vivo Exploration. *Pharmaceutical Research*, *38*(5), 901–914. https://doi.org/10.1007/s11095-021-03040-w

Mukhopadhyay, P., Maity, S., Mandal, S., Chakraborti, A. S., Prajapati, A. K., & Kundu, P. P. (2018). Preparation, characterization and in vivo evaluation of pH sensitive, safe quercetin-succinylated chitosan-alginate core-shell-corona nanoparticle for diabetes treatment. *Carbohydrate Polymers*, *182*, 42–51. https://doi.org/10.1016/j.carbpol.2017.10.098

Murakami, A., Ashida, H., & Terao, J. (2008). Multitargeted cancer prevention by quercetin. In *Cancer Letters* (Vol. 269, Issue 2, pp. 315–325). Elsevier. https://doi.org/10.1016/j.canlet.2008.03.046

Nan, G., Shi, J., Huang, Y., Sun, J., Lv, J., Yang, G., & Li, Y. (2014). Dissociation constants and solubilities of daidzein and genistein in different solvents. *Journal of Chemical and*

Engineering Data, *59*(4), 1304–1311. https://doi.org/10.1021/je4010905

Novo, D. C., Gao, C., Qi, Q., Mosquera-Giraldo, L. I., Spiering, G. A., Moore, R. B., Taylor, L. S., & Edgar, K. J. (2022). Designing synergistic crystallization inhibitors: Bile salt derivatives of cellulose with enhanced hydrophilicity. *Carbohydrate Polymers*, *292*, 119680. https://doi.org/10.1016/j.carbpol.2022.119680

Panizzon, G. P., Bueno, F. G., Ueda-Nakamura, T., Nakamura, C. V., & Filho, B. P. D. (2014). Preparation of spray-dried soy isoflavone-loaded gelatin microspheres for enhancement of dissolution: Formulation, characterization and in vitro evaluation. *Pharmaceutics*, *6*(4), 599–615. https://doi.org/10.3390/pharmaceutics6040599

Patel, R. V., Mistry, B. M., Shinde, S. K., Syed, R., Singh, V., & Shin, H. S. (2018). Therapeutic potential of quercetin as a cardiovascular agent. *European Journal of Medicinal Chemistry*, *155*, 889–904. https://doi.org/10.1016/J.EJMECH.2018.06.053

Pereira, J. M., Mejia-Ariza, R., Ilevbare, G. A., McGettigan, H. E., Sriranganathan, N., Taylor, L. S., Davis, R. M., & Edgar, K. J. (2013). Interplay of degradation, dissolution and stabilization of clarithromycin and its amorphous solid dispersions. *Molecular Pharmaceutics*, *10*(12), 4640–4653. https://doi.org/10.1021/mp400441d

Peterson, G., & Barnes, S. (1991). Genistein inhibition of the growth of human breast cancer cells: Independence from estrogen receptors and the multi-drug resistance gene. *Biochemical and Biophysical Research Communications*, *179*(1), 661–667. https://doi.org/10.1016/0006-291X(91)91423-A

Peterson, G., & Barnes, S. (1993). Genistein and biochanin A inhibit the growth of human prostate cancer cells but not epidermal growth factor receptor tyrosine autophosphorylation. *The Prostate*, *22*(4), 335–345. https://doi.org/10.1002/pros.2990220408

Petrova, S. P., Wu, H., Davidson, K., & Edgar, K. J. (2023). *Synthetic routes to direct esterification of cellulose based polymers using ring opening of cyclic anhydrides for asd application*. In Preparation.

Purohit, H. S., & Taylor, L. S. (2017). Phase Behavior of Ritonavir Amorphous Solid Dispersions during Hydration and Dissolution. *Pharmaceutical Research*, *34*(12), 2842–2861. https://doi.org/10.1007/s11095-017-2265-5

Qiu, Y., Chen, Y., Zhang, G. G. Z., Yu, L., & Mantri, R. V. (2016). Developing Solid Oral Dosage Forms: Pharmaceutical Theory and Practice: Second Edition. In *Developing Solid Oral Dosage Forms: Pharmaceutical Theory and Practice: Second Edition*. Academic press.

Russo, M., Spagnuolo, C., Tedesco, I., Bilotto, S., & Russo, G. L. (2012). The flavonoid quercetin in disease prevention and therapy: Facts and fancies. In *Biochemical Pharmacology* (Vol. 83, Issue 1, pp. 6–15). Elsevier. https://doi.org/10.1016/j.bcp.2011.08.010

Serebrenik, A. A., Verduyn, C. W., & Kaytor, M. D. (2023). Safety, Pharmacokinetics, and Biomarkers of an Amorphous Solid Dispersion of Genistein, a Radioprotectant, in Healthy Volunteers. *Clinical Pharmacology in Drug Development*, *12*(2), 190–201. https://doi.org/10.1002/cpdd.1188

Shao, Y., Yu, H., Yang, Y., Li, M., Hang, L., & Xu, X. (2019). A Solid Dispersion of Quercetin Shows Enhanced Nrf2 Activation and Protective Effects against Oxidative Injury in a Mouse Model of Dry Age-Related Macular Degeneration. *Oxidative Medicine and Cellular Longevity*, *2019*. https://doi.org/10.1155/2019/1479571

Shi, X., Fan, N., Zhang, G., Sun, J., He, Z., & Li, J. (2020). Quercetin amorphous solid

dispersions prepared by hot melt extrusion with enhanced solubility and intestinal absorption. *Pharmaceutical Development and Technology*, *25*(4), 472–481. https://doi.org/10.1080/10837450.2019.1709502

Si, H. Y., Li, D. P., Wang, T. M., Zhang, H. L., Ren, F. Y., Xu, Z. G., & Zhao, Y. Y. (2010). Improving the anti-tumor effect of genistein with a biocompatible superparamagnetic drug delivery system. *Journal of Nanoscience and Nanotechnology*, *10*(4), 2325–2331. https://doi.org/10.1166/jnn.2010.1913

Silva-Weiss, A., Quilaqueo, M., Venegas, O., Ahumada, M., Silva, W., Osorio, F., & Giménez, B. (2018). Design of dipalmitoyl lecithin liposomes loaded with quercetin and rutin and their release kinetics from carboxymethyl cellulose edible films. *Journal of Food Engineering*, *224*, 165–173. https://doi.org/10.1016/j.jfoodeng.2018.01.001

Sirtori, C. R., Lovati, M. R., Manzoni, C., Castiglioni, S., Duranti, M., Magni, C., Morandi, S., D'Agostina, A., & Arnoldi, A. (2004). Proteins of White Lupin Seed, a Naturally Isoflavone-Poor Legume, Reduce Cholesterolemia in Rats and Increase LDL Receptor Activity in HepG2 Cells. *Journal of Nutrition*, *134*(1), 18–23. https://doi.org/10.1093/jn/134.1.18

Soleimanpour, M., Tamaddon, A. M., Kadivar, M., Abolmaali, S. S., & Shekarchizadeh, H. (2020). Fabrication of nanostructured mesoporous starch encapsulating soy-derived phytoestrogen (genistein) by well-tuned solvent exchange method. *International Journal of Biological Macromolecules*, *159*, 1031–1047. https://doi.org/10.1016/j.ijbiomac.2020.05.124

Srinivas, K., King, J. W., Howard, L. R., & Monrad, J. K. (2010). Solubility and solution thermodynamic properties of quercetin and quercetin dihydrate in subcritical water. *Journal*

of Food Engineering, *100*(2), 208–218. https://doi.org/10.1016/j.jfoodeng.2010.04.001

Suk, H. K., Sun, Y. K., Kyoung, W. H., Myung, J. K., Jin, S. H., Tae, J. I., Yong, M. K., Young, M. P., Kyoung, H. K., Lee, S., Jung, Y. C., Lee, J., & Young, W. C. (2007). Pharmaceutical evaluation of genistein-loaded pluronic micelles for oral delivery. *Archives of Pharmacal Research*, *30*(9), 1138–1143. https://doi.org/10.1007/bf02980249

Tang, J., Xu, N., Ji, H., Liu, H., Wang, Z., & Wu, L. (2011). Eudragit nanoparticles containing genistein: formulation, development, and bioavailability assessment. *International Journal of Nanomedicine*, *6*, 2429–2435. https://doi.org/10.2147/IJN.S24185

Tanno, F., Nishiyama, Y., Kokubo, H., & Obara, S. (2004). Evaluation of Hypromellose Acetate Succinate (HPMCAS) as a Carrier in Solid Dispersions. *Drug Development and Industrial Pharmacy*, *30*(1), 9–17. https://doi.org/10.1081/DDC-120027506

Tran, T. H., Guo, Y., Song, D., Bruno, R. S., & Lu, X. (2014). Quercetin-containing self-nanoemulsifying drug delivery system for improving oral bioavailability. *Journal of Pharmaceutical Sciences*, *103*(3), 840–852. https://doi.org/10.1002/jps.23858

Tsujimoto, M., Horie, M., Honda, H., Takara, K., & Nishiguchi, K. (2009). The structure-activity correlation on the inhibitory effects of flavonoids on cytochrome P450 3A activity. *Biological and Pharmaceutical Bulletin*, *32*(4), 671–676. https://doi.org/10.1248/bpb.32.671

Ugru, M. M., Sheshadri, S., Jain, D., Madhyastha, H., Madhyastha, R., Maruyama, M., Navya, P. N., & Daima, H. K. (2018). Insight into the composition and surface corona reliant biological behaviour of quercetin engineered nanoparticles. *Colloids and Surfaces A: Physicochemical and Engineering Aspects*, *548*, 1–9. https://doi.org/10.1016/j.colsurfa.2018.03.055

Ungar, Y., Osundahunsi, O. F., & Shimoni, E. (2003). Thermal stability of genistein and daidzein and its effect on their antioxidant activity. *Journal of Agricultural and Food Chemistry*, *51*(15), 4394–4399. https://doi.org/10.1021/jf034021z

Wei, Y. Q., Zhao, X., Kariya, Y., Fukata, H., Teshigawara, K., & Uchida, A. (1994). Induction of Apoptosis by Quercetin: Involvement of Heat Shock Protein. *Cancer Research*, *54*(18), 4952–4957.

Williams III, R. O., Davis Jr., D. A., & Miller, D. A. (2022). Preface. In *Formulating Poorly Water Soluble Drugs* (Vol. 3, pp. VII–X). Springer.

Williams III, R. O., Watts, A. B., & Miller, D. A. (2012). *Formulating poorly water soluble drugs* (Vol. 3). Springer.

Wilson, V. R., Lou, X., Osterling, D. J., Stolarik, D. F., Jenkins, G. J., Nichols, B. L. B., Dong, Y., Edgar, K. J., Zhang, G. G. Z., & Taylor, L. S. (2020). Amorphous solid dispersions of enzalutamide and novel polysaccharide derivatives: investigation of relationships between polymer structure and performance. *Scientific Reports*, *10*(1), 18535. https://doi.org/10.1038/s41598-020-75077-7

Wu, B., Liang, Y., Tan, Y., Xie, C., Shen, J., Zhang, M., Liu, X., Yang, L., Zhang, F., Liu, L., Cai, S., Huai, D., Zheng, D., Zhang, R., Zhang, C., Chen, K., Tang, X., & Sui, X. (2016). Genistein-loaded nanoparticles of star-shaped diblock copolymer mannitol-core PLGA-TPGS for the treatment of liver cancer. *Materials Science and Engineering C*, *59*, 792–800. https://doi.org/10.1016/j.msec.2015.10.087

Wu, J.-G., Ge, J., Zhang, Y.-P., Yu, Y., & Zhang, X.-Y. (2010). Solubility of Genistein in Water, Methanol, Ethanol, Propan-2-ol, 1-Butanol, and Ethyl Acetate from (280 to 333) K. *Journal of Chemical & Engineering Data*, *55*(11), 5286–5288. https://doi.org/10.1021/je100261w

Xiao, Y., Ho, C. T., Chen, Y., Wang, Y., Wei, Z., Dong, M., & Huang, Q. (2020). Synthesis, Characterization, and Evaluation of Genistein-Loaded Zein/Carboxymethyl Chitosan Nanoparticles with Improved Water Dispersibility, Enhanced Antioxidant Activity, and Controlled Release Property. *Foods*, *9*(11). https://doi.org/10.3390/foods9111604

Yang, S. L., Zhao, L. J., Chi, S. M., Du, J. J., Ruan, Q., Xiao, P. L., & Zhao, Y. (2019). Inclusion complexes of flavonoids with propylenediamine modified β-cyclodextrin:Preparation, characterization and antioxidant. *Journal of Molecular Structure*, *1183*, 118–125. https://doi.org/10.1016/j.molstruc.2019.01.046

Yang, Z., Kulkarni, K., Zhu, W., & Hu, M. (2012). Bioavailability and Pharmacokinetics of Genistein: Mechanistic Studies on its ADME. *Anti-Cancer Agents in Medicinal Chemistry*, *12*(10), 1264–1280. https://doi.org/10.2174/187152012803833107

Zafar, A., Alruwaili, N. K., Imam, S. S., Alsaidan, O. A., Alkholifi, F. K., Alharbi, K. S., Mostafa, E. M., Alanazi, A. S., Gilani, S. J., Musa, A., Alshehri, S., Rawaf, A., & Alquraini, A. (2021). Formulation of genistein-hp β cyclodextrin-poloxamer 188 ternary inclusion complex: Solubility to cytotoxicity assessment. *Pharmaceutics*, *13*(12). https://doi.org/10.3390/pharmaceutics13121997

Zhang, Y., Song, T. T., Cunnick, J. E., Murphy, P. A., & Hendrich, S. (1999). Daidzein and genistein glucuronides in vitro are weakly estrogenic and activate human natural killer cells at nutritionally relevant concentrations. *Journal of Nutrition*, *129*(2), 399–405. https://doi.org/10.1093/jn/129.2.399

Zhao, C., Wang, Y., Su, Y., Zhang, H., Ding, L., Yan, X., Zhao, D., Shao, N., Ye, X., & Cheng, Y. (2011). Inclusion complexes of isoflavones with two commercially available dendrimers: Solubility, stability, structures, release behaviors, cytotoxicity, and anti-oxidant activities.

International Journal of Pharmaceutics, *421*(2), 301–309.

https://doi.org/10.1016/j.ijpharm.2011.09.044

Chapter 6: Summary and Future work

6.1 Summary

This thesis has described the design and preparation of efficient amorphous solid dispersion polymers and a pathway to smart, self-reporting fluorescently labeled oligo and polysaccharides for tracking purposes. We have successfully synthesized high performing crystallization inhibitors based on hydroxypropyl cellulose (HPC) by selectively modifying using complex bile acid derivatives, appended by olefin cross-metathesis (CM). These new polymers have considerable promise for amorphous solid dispersion.

In **Chapter 3,** we successfully demonstrate the marriage of two crystallization inhibitors via olefin-cross metathesis. We selectively favor cross-metathesis by the strategic design of the Type-I and Type II olefins, and by using Hoveyda-Grubbs' 2nd generation catalyst. We derivatized hydroxypropyl cellulose into a Type-I olefin via Williamson etherification with a pentenyl appendage. Then, we regioselectively and chemoselectively decorated bile salt analogs, thereby creating Type-II olefin derivatives. We were further able to probe structure-property relationships by controlling the degree of substitution of the Type-I olefin (pentenyl hydroxypropyl cellulose (CP-HPC), and the selection of bile acid as the Type-II olefin (lithocholic acid or deoxycholic acid) by employing protection-deprotection group chemistry or direct esterification. The enhanced hydrophilicity of these HPC derivatives (vs. alkyl cellulose derivatives decorated with bile salts, prepared by previous members of our group) has imparted improved solubility in aqueous media, as well as in a variety of polar organic solvents. This solubility enhancement of the polymer paired with the improved rates of olefin metathesis initiation when using polar solventetween solvent (EtOAc) (Sanford et al., 2001) facilitated sharp reduction in the reaction times previously reported for olefin CM of cellulose derivatives

and bile esters (3h vs. 20h). Our collaborators at Purdue explored structure-property relationships of these new polymers as ASD matrices by nucleation-induction time studies, using the fast-crystallizing, commercially available prostate-cancer drug, enzalutamide. The induction times of the new polymer were compared to negative (starting material, pent-5-enyl hydroxypropyl cellulose (PenHPC)) and positive (5-carboxypentyl HPC) controls, with matching DS Pen (0.6 and 1) to facilitate direct comparison (and in the case of the two carboxylic acid containing derivative types, DS(COOH) was matched at 0.6 and 1, respectively). We observed successful crystallization inhibition (longer *in vitro* crystallization times) for each novel ASD candidate vs. the drug alone. We found that methyl esters of bile salts appended to HPC at relatively low DS extended induction time 68-fold. Overall, we confirmed our starting hypothesis that we could achieve synergistic crystallization inhibition by creating bile salt-appended cellulose derivatives designed with enhanced hydrophilicity. Substantially improved ASD performance was demonstrated even with the highly challenging enzalutamide, an important current drug with severe bioavailability issues (low solubility, fast crystallizer), by employing these complex cellulose derivatives.

The ability to track oligosaccharides and polysaccharides in aqueous media is both physiologically and environmentally important. Fluorescent labeling, if successful, can provide the ability to obtain self-reporting and highly sensitive derivatives without the need for handling radioactive materials, with all the attendant complications. While ASDs are highly successful modern DDS, mechanistic understanding of ASD is seriously incomplete. We hypothesized that ASD mechanisms could be illuminated by environment-sensitive materials, which drew our interest to modifying oligo and polysaccharides for this purpose. In **Chapter 4,** we were able to tackle this challenge by selectively modifying glycans containing oligo(hydroxypropyl) groups;

hydroxypropyl cellulose, hydroxypropyl methylcellulose, and hydroxypropyl β-cyclodextrin, creating a simple, two-step process that afforded fluorophore appended materials. The materials were found to retain sensitivity to their environment as seen with the parent dye, Nile Blue by displaying solvatochromism. This sensitivity to polar / hydrophobic environment means that the new, fluorescent derivatives can potentially lend insight to ASD environment, as well as serving use in other environmental and biomedical applications.

Flavonoids are an interesting class of compounds that can act as anti-cancer drug candidates due to their radical scavenging properties. However, they suffer from poor aqueous solubility and extensive phase-II metabolism, effectively limiting bioavailability. In **Chapter 5**, we investigate cellulose derivatives designed and prepared by our group as ASD matrix polymers, 5-carboxypentyl hydroxypropyl cellulose (CP-HPC) and cellulose acetate glutarate (CAG), vs. the popular, repurposed, commercially available ASD polymer hydroxypropyl methyl cellulose acetate succinate (HPMCAS) as the positive control, with regard to their ability to inhibit crystallization of the challenging, important flavonoids, genistein and quercetin. The formulations were prepared using a small-scale process that enables efficient screening, and were evaluated and found to possess amorphous character using PXRD, SEM, polarized light microscopy, and nanotracking analysis. We targeted two practical flavonoid loadings (10% and 25%) in the polymer ASD formulations. Another important issue in ASD is developing the ability to formulate lower potency drugs that require higher loadings, which would be enabled by high-performance ASD polymers. We performed *in vitro* dissolution studies and found that each Edgar lab-designed cellulose derivative outperformed the drug alone. The highest solubility enhancement determined for genistein dispersions was achieved with CP-HPC at 10% drug loadings, and for quercetin, at 25% drug loading quercetin in HPMCAS. We also calculated

Fedor's solubility parameters of the polymer and flavonoids for further insight into the structure-property relationships. These parameters provide support for the concept that polymers with generally lower SP and greater hydrophobicity vs. flavonoid provide higher drug supersaturation *in vitro*. These studies clearly indicate the promise that these purpose-designed crystallization inhibitors have for enhancing bioavailability of flavonoids -- thereby potentially enabling more indicative and useful *in vivo* evaluations, potentially including clinical trials.

6.2 Future work

6.2.1 Probe bile salt D-ring carboxylic acid as olefin-metathesis handle

Olefin cross metathesis has served as an important tool to impart versatility to cellulose esters and ethers using small molecule Type II olefins including acrylates (Dong et al., 2016, 2019; Meng et al., 2014), acrylamides (Meng & Edgar, 2015), with the additional potential to react with thiols via thiol-Michael addition (Dong et al., 2017). In this work, we were able to overcome synthetic barriers (regioselectivity, chemoselectivity) and successfully append Type II olefins based on bile salts, that were more structurally complex than those used previously in our lab. We used the A-ring hydroxyl as the site for an olefin tether to probe whether degree of substitution of the initial pentenyl, bile acid type, and the state of the D-ring carboxylic acid (acid or ester form) were key to properties and performance, including crystallization inhibition. While we found that HPC derivatives with low DS(bile salt analog), where the bile salt carboxyl was present as a methyl ester, were more effective crystallization inhibitors than those with D-ring carboxylic acids, we would like to further elucidate structure-property relationships by determining which end of a bile salt (A-ring hydroxyl or D-ring carboxyl) is responsible for inhibiting crystallization. As proposed in Figure 6.6, we can use the D-ring carboxylic acid as the reactive site for appending a Type-II olefin. The synthetic strategy appending a Type-II olefin to

the bile acid D-ring carboxyl can involve either of two approaches: a) esterification of the D-ring carboxylic acid with a diol, then subsequent esterification of the free alcohol using acrylates (acryloyl chloride or acrylic anhydride), or b) direct esterification using 2-hydroxyethyl acrylate (Scheme 6.3). Appending the Type-II olefin to the D-ring carboxyl, if it led to successful inhibition, would also permit us to directly compare how the number and position of free bile salt hydroxyls affect performance by applying the D-ring carboxyl modification methodology to lithocholic, deoxycholic, cholic acid, and chenodeoxycholic acids (Fig. 6.5). Chemoselectivity would need to be explored, but would be expected to rely upon the wider approach angles of the D ring carboxyl, and on the higher nucleophilicity of the anionic form of the carboxylate. We can employ PenHPC (DS, Pen = 0.5 or 1) for this new approach, and directly compare performance to that of the A-ring acrylates. We can also continue to probe the hydrophilicity imparted by Type-I olefins from pentenylated cellulose ethers that possess branched hydroxyls (broader approach angles and reactivity), e.g., in-house synthesized hydroxyethyl cellulose via 2-chloroethanol (Scheme 6.4). The latter synthesis allows for tunable properties as one can control the DS(OH) and MS(OH) via the number of hydroxyethyl groups.

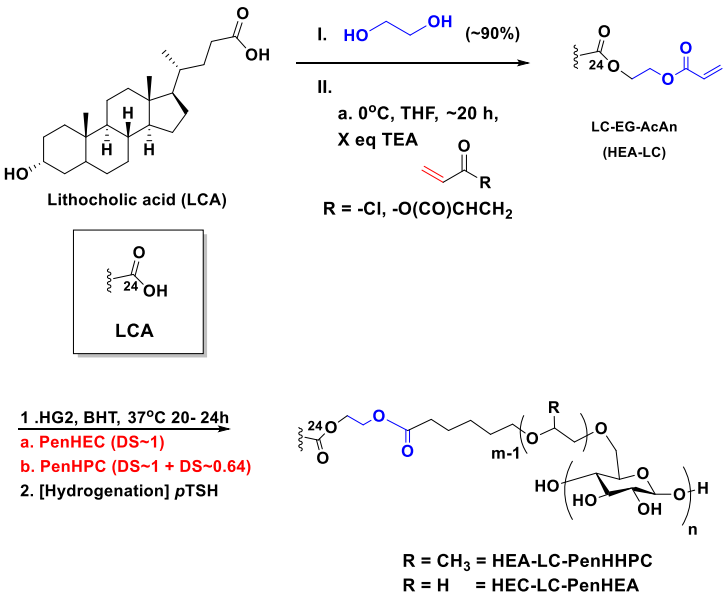

Scheme 6.3 3-Step synthetic strategy for synthesis of derivatives where Type II olefins are appended to the D-ring carboxylic acid of LCA

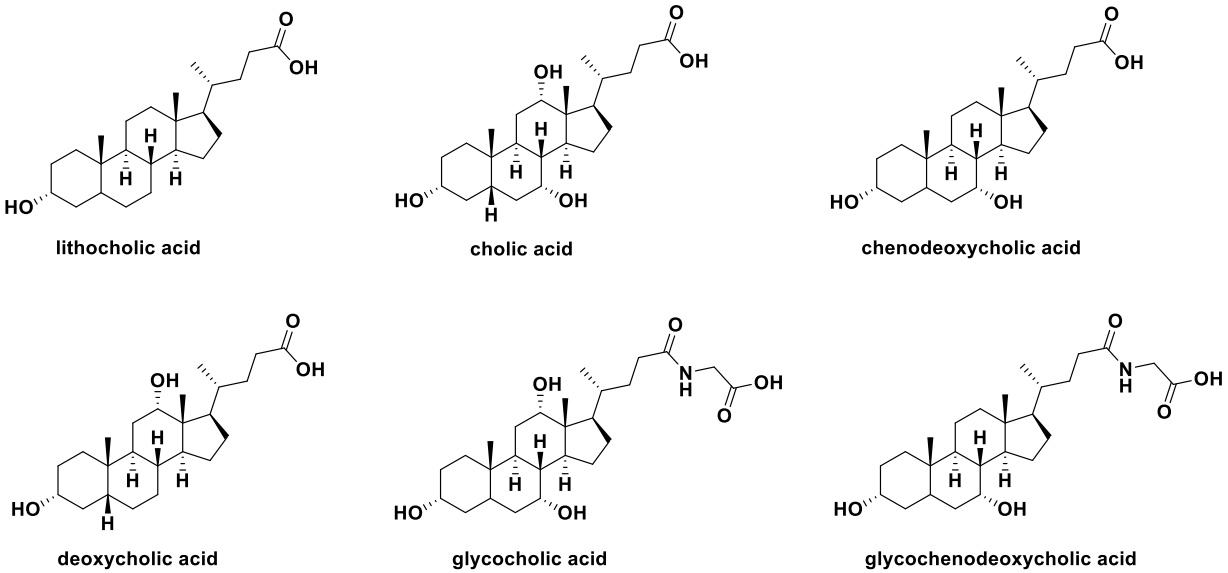

Figure 6.5 a) Bile salt analogs to probe D-ring-appended acrylates.

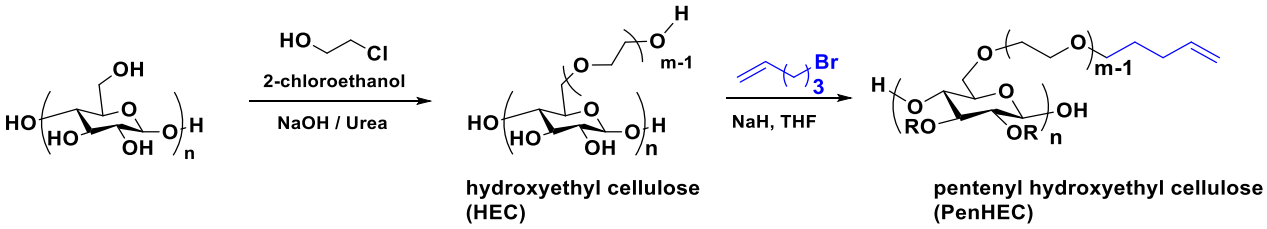

Scheme 6.4 Pen-HEC synthesis**.** Step 1 etherification of cellulose, Step 2 Williamson etherification of HEC.

6.2.2 Fluorescent labeling strategy using structurally complex polymers: Oxidation of HPMCAS and reductive-amination using other environment-sensitive dyes

Other than HPC, we were able to oxidize new polymer and oligomer backbones, HPMC and HPβCD. DS(HP) is relatively low in HPMC, restricting possible maximum DS(ketone). Commercial methods to manufacture HPMC are performed without isolation with methylation

via methyl chloride as the first step, which is the culprit for the limited number of hydroxypropyl units introduced via the subsequent of ring opening of propylene oxide (Greminger et al., 1974). This heterogeneous mixture also leads to partially methyl-capping the HP units, possessing a total MS, HP = 0.21-0.82 and HP DS, 0.08-0.27. The well-established, commercially important ASD polymer HPMCAS is extremely complex in structure. As its synthesis starts with HPMC, it embodies all the structural complexities and issues of that polymer, compounded by subsequent acetylation and succinylation. Three grades of HPMCAS are available (low (L), medium (M) and high (H), relative to acetyl content). The grade that is effective for ASD is MF (fine (F) for particle size) with MS(HP) = 0.21 and DS(HP) = 0.15. Although desirable to preserve structural integrity in mechanistic studies, the low DS(HP) of HPMCAS limits the possible DS (ketone) that can be obtained by bleach oxidation, and thus the DS(fluorophore) obtainable by subsequent reductive amination. This also poses analytical hurdles as the highest conversion would be difficult to disambiguate as the tell-tale ketone methyl would be buried with HPMCAS' acetate resonances in the proton NMR spectrum; quantification of the fluorophore could also be challenging. In **Scheme 6.5**, we suggest the rational design of in-house oxidized HPMCAS as shown in order to maximize DS (oxopropyl) units, and subsequent reductive-amination in order to monitor this high impact ASD. The following dyes shown in **Scheme 6.6** are of interest as well, as they would be more reactive than Nile Blue, permitting higher conversion and ease in analysis. Dansyl derivatives are beneficial as they are sensitive to solvent polarity (solvatochromic) with long emission maxima, while the ethylenediamine analog is advantageous due to more nucleophilic primary amine moiety that will promote high conversion for reductive-amination vs. prior Nile Blue derivatives. Fluorometric studies will follow to determine the fluorescent activity in different solvents, as well as *in vitro* and *in vivo* studies containing the

ASD to assess drug-polymer interactions. These materials can also be tailored for use as smart materials to monitor changes in the natural environment, and to detect pollutants such as heavy metal ions and dyes.

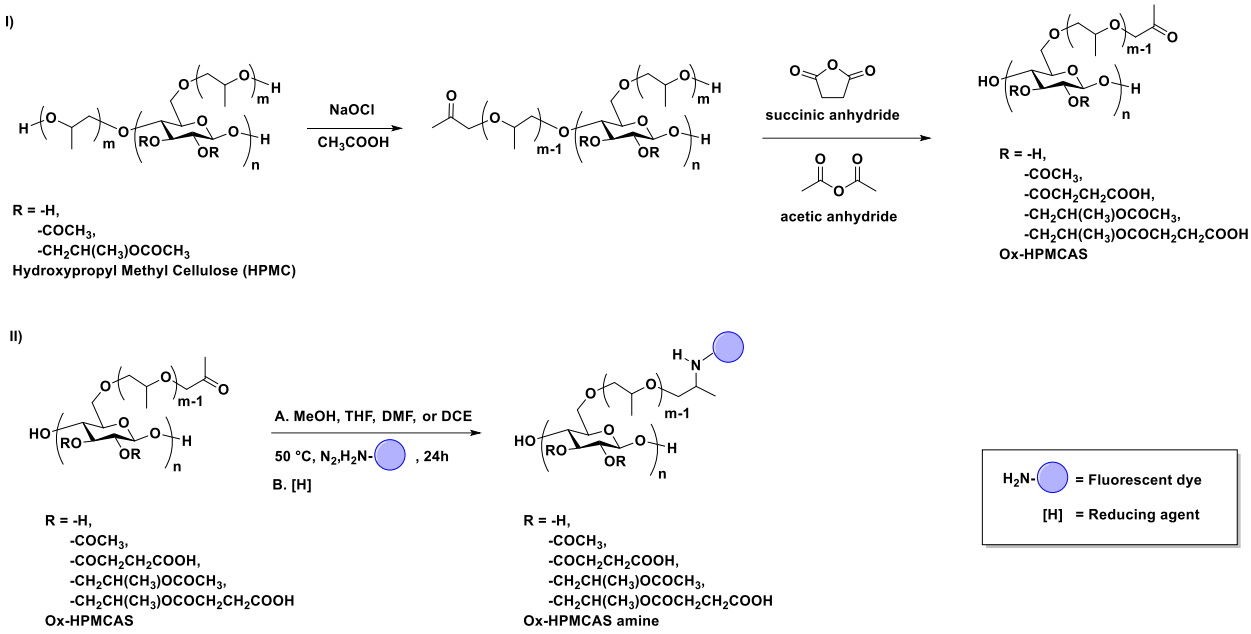

Scheme 6.5 Overall synthesis of I) in-house made Ox-HPMCAS, and II) Ox-HPMCAS amine.

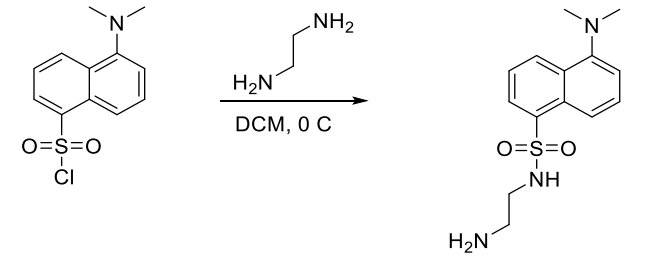

Scheme 6.6 Synthesis of dansyl ethylenediamine and structures of other fluorescent amine candidates.

References

Dong, Y., Mosquera-Giraldo, L. I., Taylor, L. S., & Edgar, K. J. (2017). Tandem modification of amphiphilic cellulose ethers for amorphous solid dispersion via olefin cross-metathesis and thiol-Michael addition. *Polymer Chemistry*, *8*(20), 3129–3139.

https://doi.org/10.1039/C7PY00228A

Dong, Y., Mosquera-Giraldo, L. I., Troutman, J., Skogstad, B., Taylor, L. S., & Edgar, K. J. (2016). Amphiphilic hydroxyalkyl cellulose derivatives for amorphous solid dispersion prepared by olefin cross-metathesis. *Polymer Chemistry*, *7*(30), 4953–4963. https://doi.org/10.1039/c6py00960c

Dong, Y., Novo, D. C., Mosquera-Giraldo, L. I., Taylor, L. S., & Edgar, K. J. (2019). Conjugation of bile esters to cellulose by olefin cross-metathesis: A strategy for accessing complex polysaccharide structures. *Carbohydrate Polymers*, *221*, 37–47. https://doi.org/10.1016/j.carbpol.2019.05.061

Greminger, G. K., Strange, C. P., Krumel, K. L., & Hudson, J. L. (1974). *Hydroxypropyl methylcellulose ethers and method of preparation*.

Meng, X., & Edgar, K. J. (2015). Synthesis of amide-functionalized cellulose esters by olefin cross-metathesis. *Carbohydrate Polymers*, *132*, 565–573. https://doi.org/https://doi.org/10.1016/j.carbpol.2015.06.052

Meng, X., Matson, J. B., & Edgar, K. J. (2014). Olefin cross-metathesis as a source of polysaccharide derivatives: Cellulose ω-carboxyalkanoates. *Biomacromolecules*, *15*(1), 177–187. https://doi.org/10.1021/bm401447v

Sanford, M. S., Love, J. A., & Grubbs, R. H. (2001). Mechanism and Activity of Ruthenium Olefin Metathesis Catalysts. *Journal of the American Chemical Society*, *123*(27), 6543–6554. https://doi.org/10.1021/ja010624k

Appendix: Supplementary Figures and Tables

Chapter 3. Designing synergistic crystallization inhibitors: bile salt derivatives of cellulose with enhanced hydrophilicity

FT-IR Spectra

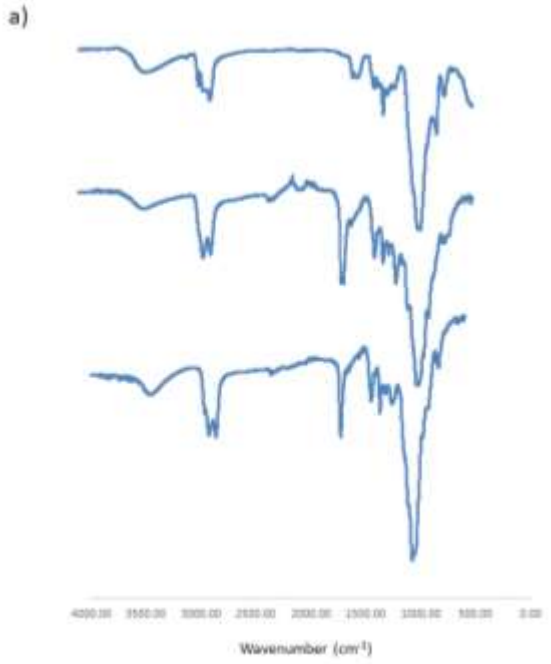

b)


4000.00 3500.00 3000.00 2500.00 2000.00 1500.00 1000.00 500.00 0.00
Wavenumber (cm-1)

c)

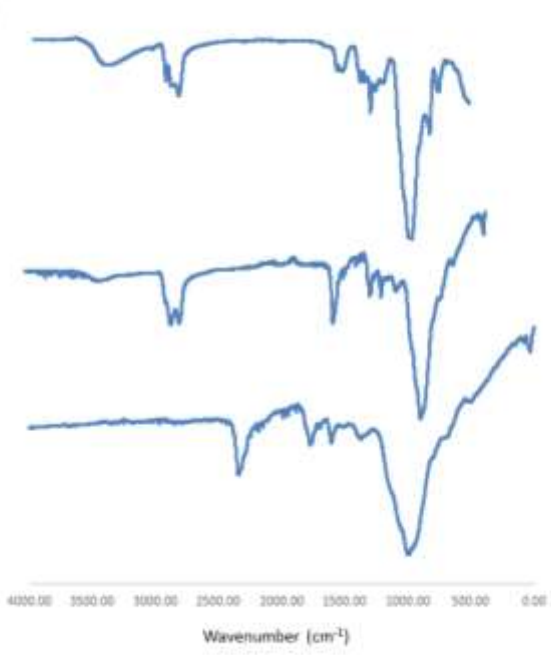
4000.00 3500.00 3000.00 2500.00 2000.00 1500.00 1000.00 500.00 0.00
Wavenumber (cm-1)

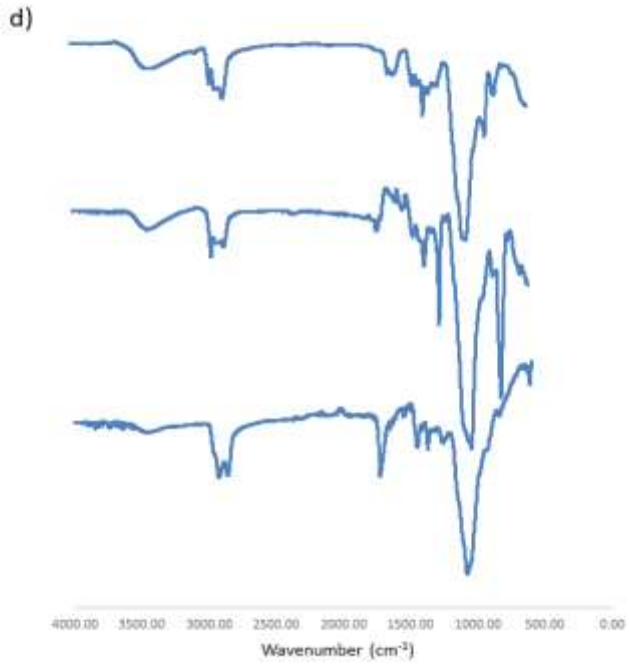

Figure S3.1. FT-IR spectra of starting material PenHPC (top), CM (center), and hydrogenated products (bottom) conjugated with (a) AcrMLC, (b) AcrMDC, (c) AcrLC, and (d) AcrDC.

Section S3.1 Synthetic Methods

S3.1.1 Synthesis of hydroxypropyl 1-pent-4-enyl cellulose (PenHPC DS 0.60 and 1.00)

PenHPC (DS = 0. 6 and 1) was prepared according to Dong et al., (2016). Briefly, HPC (5.00 g, 92.5 mmol OH) was dissolved by mechanically stirring overnight in anhydrous THF (50 mL) under N_2. The resulting light brown solution was gradually charged with NaH (95%, 1.42 g, 56.8 mmol, 3 equiv. / OH for DS 1; 1 g, 40 mmol, 2 equiv/OH for DS 0.60) under N_2, then 5-bromopent-1-ene (7.68 g, 2.7 equiv for DS 1; 1.42 g, 0.5 equiv for DS 0.60) was added. The solution was stirred 1 d at room temperature, then at 50 ^{o}C for 3 d. The solution was then cooled and quenched with isopropanol. The solution was added to 500 mL pH 7.4 buffer, then the resulting precipitate was isolated by vacuum filtration, and subsequent drying under vacuum at 40 ^{o}C.

PenHPC(1.00). Yield: 4.80 g, 90%. ^{1}H NMR (selected signals, $CDCl_3$) δ 1.12 (br s, $OCH_2C\underline{H}_3OH$), 1.64 (s, $OCH_2C\underline{H}_2CH_2CH=CH_2$), 2.10 (br, s, $OCH_2CH_2C\underline{H}_2CH=CH_2$), 2.80–4.55 (m, cellulose backbone, $OC\underline{H}_2CHCH_3OH$, $OC\underline{H}_2CH_2CH_2CH=CH_2$), 4.94-5.03 (dd, $OCH_2CH_2CH_2CH=C\underline{H}_2$), 5.74-5.86 (m, $OCH_2CH_2CH_2C\underline{H}=CH_2$). ^{13}C NMR (500 MHz, $CDCl_3$): 17.6 ($OCH_2CH\underline{C}H_3OH$), 29.4 ($OCH_2\underline{C}H_2CH_2CH=CH_2$), 30.2 ($OCH_2CH_2\underline{C}H_2CH=CH_2$), 66.4 (C6), 68.2 ($OCH_2\underline{C}HCH_3OH$), 73.4-77.4 (C2, C3, C6, $O\underline{C}H_2CHCH_3OH$), 83.6 (C4), 102.9 (C1), 114.5 ($OCH_2CH_2CH_2CH=\underline{C}H_2$), 138.4 ($OCH_2CH_2CH_2\underline{C}H=CH_2$). DS by ^{1}H NMR: DS (C5) 1.00.

S3.1.2. Syntheses of lithocholic acid (LCA) and deoxycholic acid (DCA) methyl esters

Methyl lithocholate (MLC). Yield: 2.50 g, 91%. ^{1}H NMR ($CDCl_3$, selected signals): 0.63 (s, CH_3), 0.89 (s, CH_3), 0.91 (s, CH_3), 3.62 (m, 1H, C3 $OC\underline{H}$), 3.66 (s, 3H, $COOC\underline{H}_3$). ^{13}C NMR δ 11.94, 18.17, 20.73, 23.33, 24.11, 26.37, 27.15, 28.10, 30.31, 30.90, 34.46, 35.24, 35.36, 35.72, 36.22,

40.09, 40.34, 42.02, 42.61, 51.39 (C=OO<u>C</u>H$_3$), 55.86, 56.39, 71.39 (C3 HO-<u>C</u>H), 174.66 (<u>C</u>=O-OCH$_3$).

Methyl deoxycholate (MDC). Yield: 1.99 g, 96%. ^{1}H NMR (CDCl$_3$, selected signals): 0.66 (s, CH$_3$), 0.89 (s, CH$_3$), 0.96 (d, CH$_3$), 3.63 (m, 1H, C12 HO-C<u>H</u>), 3.65 (s, 3H, COOC<u>H$_3$</u>), 3.96 (m, 1H, C3 HO-C<u>H</u>). ^{13}C NMR (CDCl$_3$) δ 12.66, 17.17, 23.12, 23.72, 26.14, 27.19, 27.56, 28.62, 30.28, 30.33, 30.89, 31.13, 33.49, 34.10, 35.32, 35.99, 36.34, 42.08, 46.43, 47.06, 48.07, 51.46 (C=OO<u>C</u>H$_3$), 71.46 (C3 HO-<u>C</u>H), 72.94 (C12 HO-<u>C</u>H), 174.75 (<u>C</u>=OOCH$_3$).

Methyl lithocholate acrylate (***AcrMLC).*** Yield: 1.32 g, 66%. ^{1}H NMR (CDCl$_3$, selected): 0.64 (s, CH$_3$), 0.90 (d, CH$_3$), 0.93 (s, CH$_3$), 3.66 (s, 3H, COOC<u>H$_3$</u>), 4.80 (m, 1H, C3 OC<u>H</u>), 5.79 (dd, COOCH=C<u>H$_2$</u>, *trans*), 6.10 (dd, COOC<u>H</u>=CH$_2$), 6.39 (dd, COOCH=C<u>H$_2$</u>, *cis*). ^{13}C NMR δ 12.09 (C19 and C21 -C<u>H$_3$</u>), 18.32, 20.89, 23.39, 24.23, 26.37, 26.67, 27.07, 28.23, 31.04, 32.27, 34.63, 35.08, 35.40, 35.83, 40.18, 40.47, 41.94, 42.77, 51.49 (C=OO<u>C</u>H$_3$), 56.03, 56.53, 74.55 (C3 CH$_2$=CHCOO<u>C</u>H), 129.15 (COOCH=<u>C</u>H$_2$), 130.20 (COO<u>C</u>H=CH$_2$), 165.74 (<u>C</u>OOCH=CH$_2$), 174.71 (<u>C</u>=OOCH$_3$).

Methyl deoxycholate acrylate (***AcrMDC).*** Yield: 255 mg, 45%. ^{1}H NMR (CDCl$_3$, selected): 0.68 (s, CH$_3$), 0.92 (s, CH$_3$), 0.97 (d, CH$_3$), 3.65 (s, 3H, COOC<u>H$_3$</u>), 3.98 (t, 1H, C12 HOC<u>H</u>), 4.80 (m, 1H, C3 CH$_2$=CHCOOC<u>H</u>), 5.78 (dd, COOCH=C<u>H$_2$</u>, *trans*), 6.08 (dd, COOC<u>H</u>=CH$_2$), 6.36 (dd, COOCH=C<u>H$_2$</u>, *cis*). ^{13}C NMR δ 12.81, 17.38, 23.19, 23.67, 26.08, 26.55, 27.02, 27.51, 28.81, 30.96, 31.10, 32.19, 33.71, 34.20, 34.94, 35.15, 36.04, 41.92, 46.54, 47.36, 48.33, 51.57 (C=OO<u>C</u>H$_3$), 73.13 (C3 CH$_2$=CHCOO<u>C</u>H), 74.49 (C12 HO-<u>C</u>H), 129.15 (COOCH=<u>C</u>H$_2$), 130.30 (COO<u>C</u>H=CH$_2$), 165.86 (<u>C</u>OOCH=CH$_2$), 174.76 (<u>C</u>=OOCH$_3$).

S3.1.3. General procedure for olefin CM of PenHPC (DS (Pen) =1.00)

AcrDC-PenHPC(1.00). Yield: 185 mg, 80%. ^{1}H NMR ($CDCl_3$, selected): δ = 0.69 (s, C$\underline{H}_3$), 0.93 (s, C$\underline{H}_3$), 0.98 (d, C$\underline{H}_3$), 1.00-2.42 (m, steroid ring protons, OCH$_2$C$\underline{H}_2$C$\underline{H}_2$CH=CHCOO-DCAc), 2.90-4.50 (m, cellulose backbone, OC$\underline{H}_2$CH$_2$CH$_2$CH=CHCOO-AcrDC, C12 HO-C$\underline{H}$), 4.80 (m, DCAc C3-C$\underline{H}$), 5.78 (OCH$_2$CH$_2$CH$_2$CH=C$\underline{H}$COO-AcrDC), 6.94 (OCH$_2$CH$_2$CH$_2$C$\underline{H}$=CHCOO-AcrDC). ^{13}C NMR (126 MHz, DMSO) δ 12.88, 17.78, 19.52, 20.74, 23.27, 23.93, 24.89, 25.69, 26.35, 26.58, 27.10, 27.62, 28.49, 28.96, 29.8, 31.31, 32.35, 33.25, 34.23, 34.98, 35.41, 35.98, 41.71, 46.46, 46.68, 47.85, 65.75, 71.48 - 79.10 (cellulose C2, C3, C5 and bile acid: C3 CH$_2$=CHCOOC$\underline{H}$, and C12 HO-C$\underline{H}$), 83.09 (cellulose C4), 102.14 (cellulose C1), 121.82 (OCH$_2$CH$_2$CH$_2$CH=C$\underline{H}$COO-AcrDC), 149.48 (OCH$_2$CH$_2$CH$_2$C$\underline{H}$=CHCOO-AcrDC), 165.57 (C$\underline{=}$OOAcrDC), 175.39 (C$\underline{=}$OOH).

AcrMLC-PenHPC(1.00). Yield: 215 mg, 85%. ^{1}H NMR ($CDCl_3$) δ 0.65 (s, C$\underline{H}_3$), 0.92 (s, C$\underline{H}_3$), 1.00-2.42 (m, steroid ring protons, OCH$_2$C$\underline{H}_2$C$\underline{H}_2$CH=CHCOO-MLCAc), 4.77 (m, MLCAc C3-C$\underline{H}$), 5.82 (OCH$_2$CH$_2$CH$_2$CH=C$\underline{H}$COO-MLCAc), 6.96 (OCH$_2$CH$_2$CH$_2$C$\underline{H}$=CHCOO-MLCAc). ^{13}C NMR (126 MHz, $CDCl_3$) δ 12.15, 15.83, 17.41, 18.39, 20.95, 23.47, 24.30, 26.45, 26.82, 27.16, 28.30, 28.64, 29.04, 31.12, 31.20, 32.44, 34.72, 35.18, 35.48, 35.91, 40.24, 40.52, 42.03, 42.85, 51.60 (C=OOC$\underline{H}_3$), 56.12, 56.58, 64.38, 65.82, 66.75, 68.40, 70.69-75.26 (cellulose C2, C3, C5, and bile ester C3 CH$_2$=CHCOOC$\underline{H}$), 83.08 (cellulose C4), 102.83 (cellulose C1), 122.08 (OCH$_2$CH$_2$CH$_2$CH=C$\underline{H}$COO-AcrMLC), 148.63 (OCH$_2$CH$_2$CH$_2$C$\underline{H}$=CHCOO-AcrMLC), 166.30 (C$\underline{=}$OOAcrMLC), 174.88 (C$\underline{=}$OOCH$_3$).

AcrMDC-PenHPC(1.00). Yield: 236 mg, 89%. ^{1}H NMR (selected, DMSO): δ = 0.68 (s, C$\underline{H}_3$), 0.92 (s, C$\underline{H}_3$), 0.96 (d, C$\underline{H}_3$), 1.00-2.42 (m, steroid ring protons, OCH$_2$C$\underline{H}_2$C$\underline{H}_2$CH=CHCOO-AcrMDC), 2.90-4.50 (m, cellulose backbone, OC$\underline{H}_2$CH$_2$CH$_2$CH=CHCOO-AcrMDC, 3.66 s C12 HO-C$\underline{H}$), 4.75 (m, AcrMDC C3-C$\underline{H}$), 5.77 (d, OCH$_2$CH$_2$CH$_2$CH=C$\underline{H}$COO-AcrMDC), 6.94 (m,

$OCH_2CH_2CH_2C\underline{H}$=CHCOO-AcrMDC). ^{13}C NMR (500 MHz) δ 12.40, 16.88, 17.31, 18.58, 20.27, 22.81, 23.47, 25.90, 26.15, 26.66, 27.16, 28.06, 28.47, 30.45, 30.69, 31.92, 33.76, 34.54, 34.94, 35.54, 35.80, 41.29, 46.00, 47.41, 51.17 (25C C=OO$\underline{C}H_3$), 56.04, 64.96, 65.26, 67.51, 71.00-76.74 (cellulose C2, C3, C5, and bile ester C3 CH_2=CHCOO$\underline{C}$H and C12 HO-$\underline{C}$H), 82.77 (cellulose C4), 101.62 (cellulose C1), 121.37 ($OCH_2CH_2CH_2CH=\underline{C}$HCOO-AcrMDC), 148.91 ($OCH_2CH_2CH_2\underline{C}$H=CHCOO-AcrMDC), 165.05 ($\underline{C}$=OOAcrMDC), 173.74 ($\underline{C}$=OOCH_3).

S3.1.4. General procedure for hydrogenation of PenHPC-Bile ester conjugates

We exemplify our general transfer hydrogenation methods: using AcrDC-PenHPC(1.00) (225 mg, 0.25 mmol C=C) and BHT (12 mg) were dissolved in DMF (12 mL) under N_2 at 37 °C. The solution was then treated with *p*TSH (305 mg, 1.69 mmol, 12 mol eq) pre-dissolved in 2 mL DMF, heated to reflux (135 °C), then stirred at reflux for 6 h. The solution was cooled to room temperature, then was dialyzed against methanol (3-5 days), then DI water (2 days). The product was collected from the retentate by lyophilization.

AcrLC-PenHHPC(1.00). Yield: 210 mg, 68%. ^{1}H NMR (selected, DMSO) δ 0.60 (s, C$\underline{H}_3$) 0.85 (s, C$\underline{H}_3$), 1.01-2.31 (m, steroid ring protons, $OCH_2C\underline{H}_2C\underline{H}_2C\underline{H}_2C\underline{H}_2$COO-AcrLC), 2.76-4.54 (m, cellulose backbone, O$\underline{C}H_2CH_2CH_2CH_2CH_2$COO-AcrLC), 4.59 (LCAcAn C3 -O$\underline{C}$H). ^{13}C NMR (500 MHz, $CDCl_3$) δ 11.86, 13.96, 17.33, 18.13, 19.10, 20.28, 22.12, 23.04, 23.82, 24.44, 25.25, 25.97, 26.32, 26.61, 27.71, 29.06, 29.34, 30.68, 30.73, 31.91, 33.87, 34.18, 34.54, 34.81, 35.31, 40.02, 41.22, 42.27, 55.60, 55.94, 64.97, 65.29, 68.08, 72.10- 78.36 (cellulose C2, C3, C5, and bile ester C3 $CH_2CH_2COO\underline{C}$H), 82.61 (cellulose C4), 101.68 (cellulose C1), 172.15 ($\underline{C}$=OOAcrLC), 174.81 ($\underline{C}$=OOCH_3).

AcrMLC-PenHHPC(1.00). Yield: 150 mg, 51%. ^{1}H NMR ($CDCl_3$): δ = 0.64 (s, C<u>H</u>$_3$), 0.90 (s, C<u>H</u>$_3$), 0.92 (d, C<u>H</u>$_3$), 1.00-2.45 (m, steroid ring protons, OCH$_2$C<u>H</u>$_2$C<u>H</u>$_2$C<u>H</u>$_2$C<u>H</u>$_2$COO-MLCAc), 2.84-4.53 (m, cellulose backbone, OC<u>H</u>$_2$CH$_2$CH$_2$CH$_2$CH$_2$COO-MLCAc, MLCAc COOC<u>H</u>$_3$, C12 HO-C<u>H</u>), 4.71 (m, MLCAc C3 C<u>H</u>). ^{13}C NMR: δ = 12.04, 14.13, 15.69, 17.52, 18.28, 20.83, 22.56, 23.35, 24.19, 24.92, 25.77, 26.33, 26.69, 27.03, 28.18, 29.83, 31.00, 32.29, 34.60, 35.05, 35.37, 35.79, 40.12, 40.39, 41.91, 42.73, 51.46 (25C C=OO<u>C</u>H$_3$), 56.01, 56.45, 65.72, 68.95 - 74.16 (cellulose C2, C3, C5, and bile ester C3 CH$_2$CH$_2$COO<u>C</u>H), 82.67 (cellulose C4), 102.39 (cellulose C1), 173.24 (<u>C</u>=OOMLCAc), 174.79 (<u>C</u>=OOCH$_3$).

AcrMDC-PenHHPC(1.00). Yield: 120 mg, 60 %. ^{1}H NMR (DMSO): δ = 0.68 (s, C<u>H</u>$_3$), 0.92 (s, C<u>H</u>$_3$), 0.96 (d, C<u>H</u>$_3$), 1.00-2.41 (m, steroid ring protons, OCH$_2$C<u>H</u>$_2$C<u>H</u>$_2$C<u>H</u>$_2$C<u>H</u>$_2$COO-MDCAc), 2.86-4.56 (m, cellulose backbone, OC<u>H</u>$_2$CH$_2$CH$_2$CH$_2$CH$_2$COO-MDCAc, MDCAc COOCH$_3$ 3.65 s, C12 HO-C<u>H</u> 3.98 s), 4.71 (m, MDCAc C3 C<u>H</u>). ^{13}C NMR: δ 12.40, 13.97, 16.88, 17.33, 19.04, 20.31, 22.81, 23.47, 24.44, 25.25, 25.90, 26.13, 26.65, 27.16, 28.53, 29.38, 30.46, 30.68, 31.87, 32.81, 33.76, 34.53, 34.94, 35.53, 40.43, 41.35, 46.01, 46.13, 47.41, 51.19 (C=OO<u>C</u>H$_3$), 74.56 - 78.72 (cellulose C2, C3, C5, and bile ester C3 CH$_2$CH$_2$COO<u>C</u>H and C12 HO-<u>C</u>H), 82.38 (cellulose C4), 101.50 (cellulose C1), 172.23 (<u>C</u>=OOMDCAc), 173.79 (<u>C</u>=OOCH$_3$).

^{13}C NMR spectra

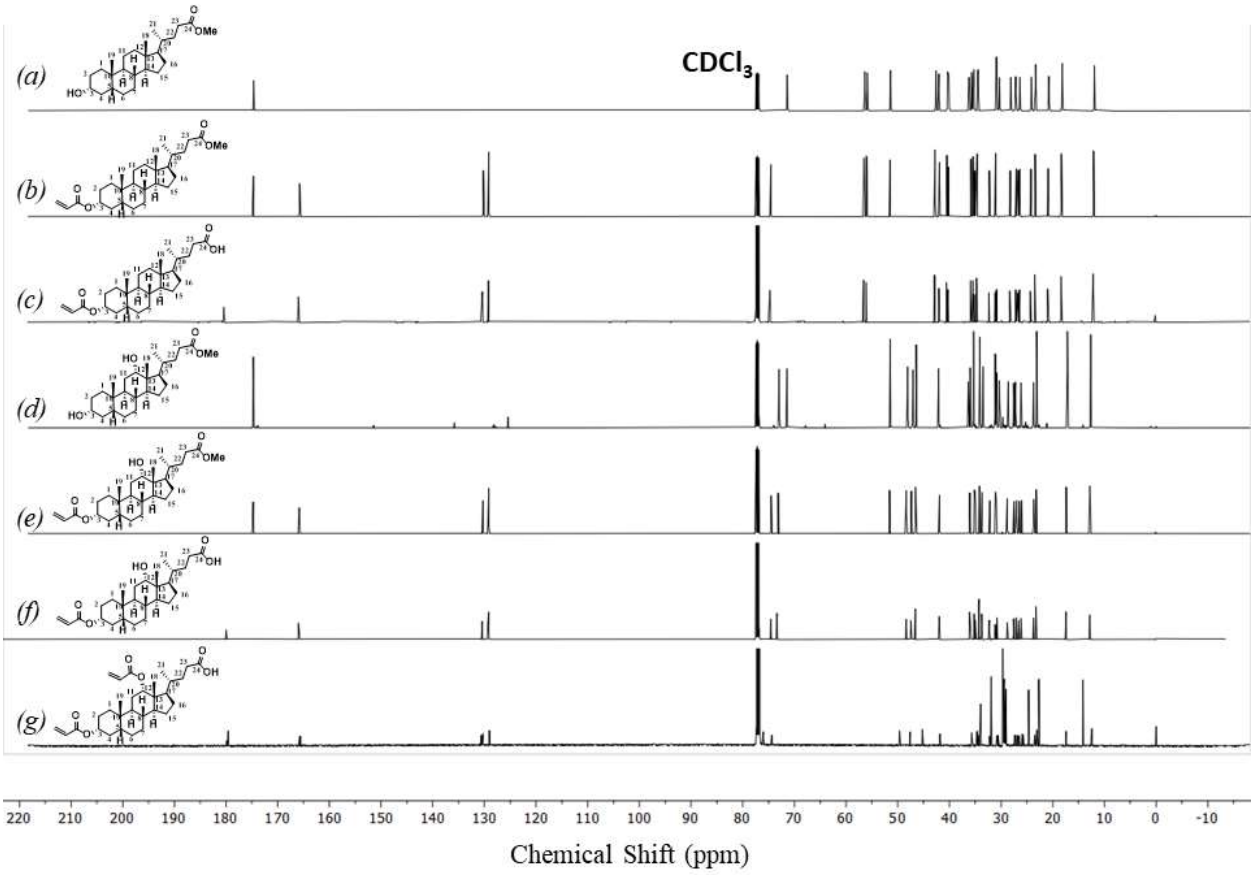

Figure S3.2. ^{13}C NMR spectra of (a) methyl lithocholic acid (MLC) (b) methyl lithocholate acrylate (Acr MLC), (c) lithocolate acrylate (AcrLC), (d) methyl deoxycholic acid (MDC), (e) methyl deoxycholate acrylate (AcrMDC), (f) deoxycholate 3-*O*-Ac monoacrylate (AcrDC) (g) deoxycholate diacrylate (AcrDC).

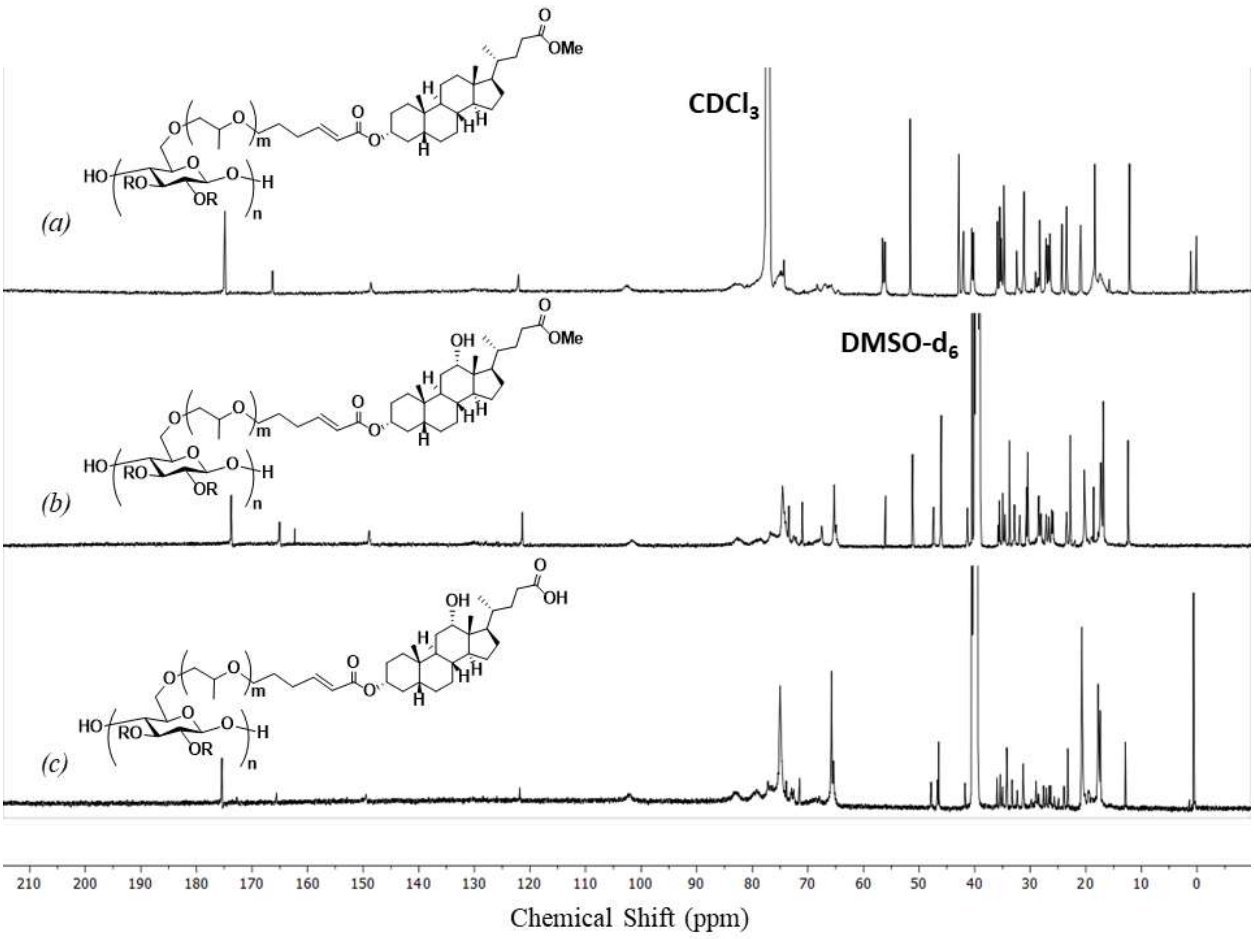

Figure S3.3. ^{13}C NMR spectra of CM conjugates of PenHPC and (a) 3-*O*-AcrMLC, (b) 3-*O*-AcrMDC, and (c) 3-*O*-AcrDC monoacrylate.

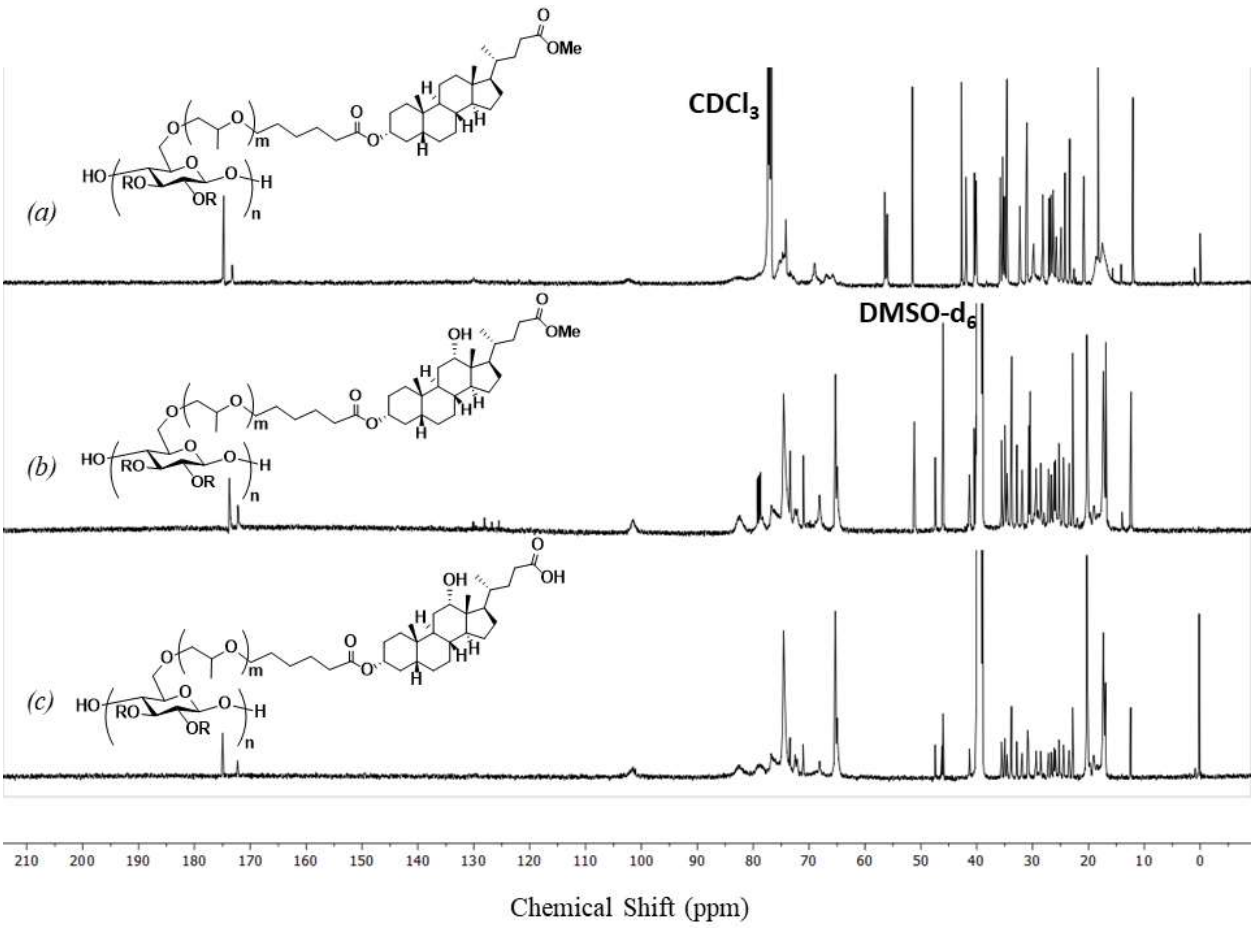

Figure S3.4. ^{13}C NMR spectra of hydrogenated PenHPC-cholates: (a) 3-*O*-PenHHPC-AcrMLC, (b) 3-*O*-PenHHPC-AcrMDC, and (c) 3-*O*-PenHHPC-AcrDC monoacrylate.

^{1}H NMR spectra

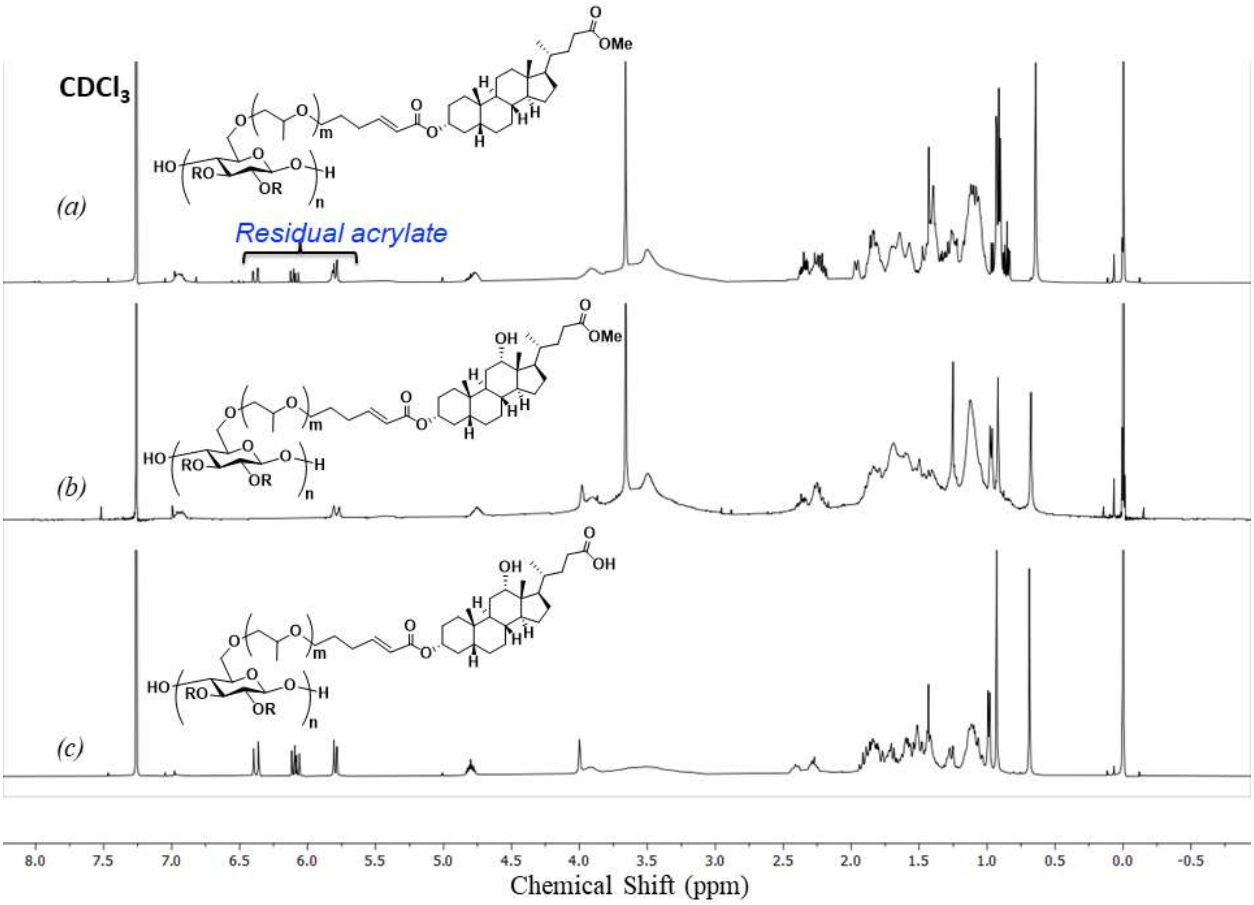

Figure S3.5. ^{1}H NMR spectra of CM conjugates of PenHPC from (a) 3-*O*-AcrMLC, (b) 3-*O*-AcrMDC, and (c) 3-*O*-AcrDC monoacrylate.

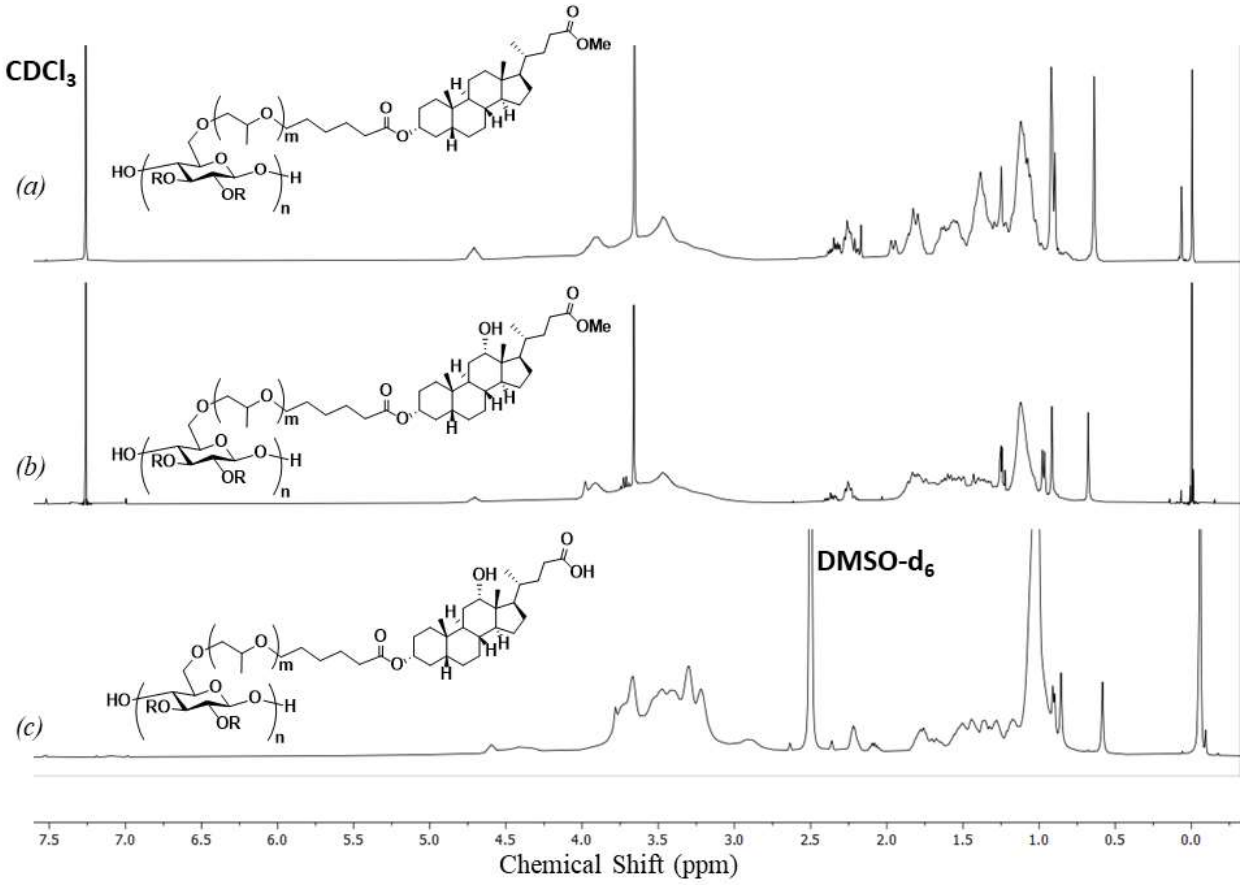

Figure S3.6. ^{1}H NMR spectra of hydrogenated PenHPC-cholates: (a) 3-*O*-PenHHPC-AcrMLC, (b) 3-*O*-PenHHPC-AcrMDC, and (c) 3-*O*-PenHHPC-AcrDC monoacrylate.

Sample degree of substitution calculation: preparation of PenHPC

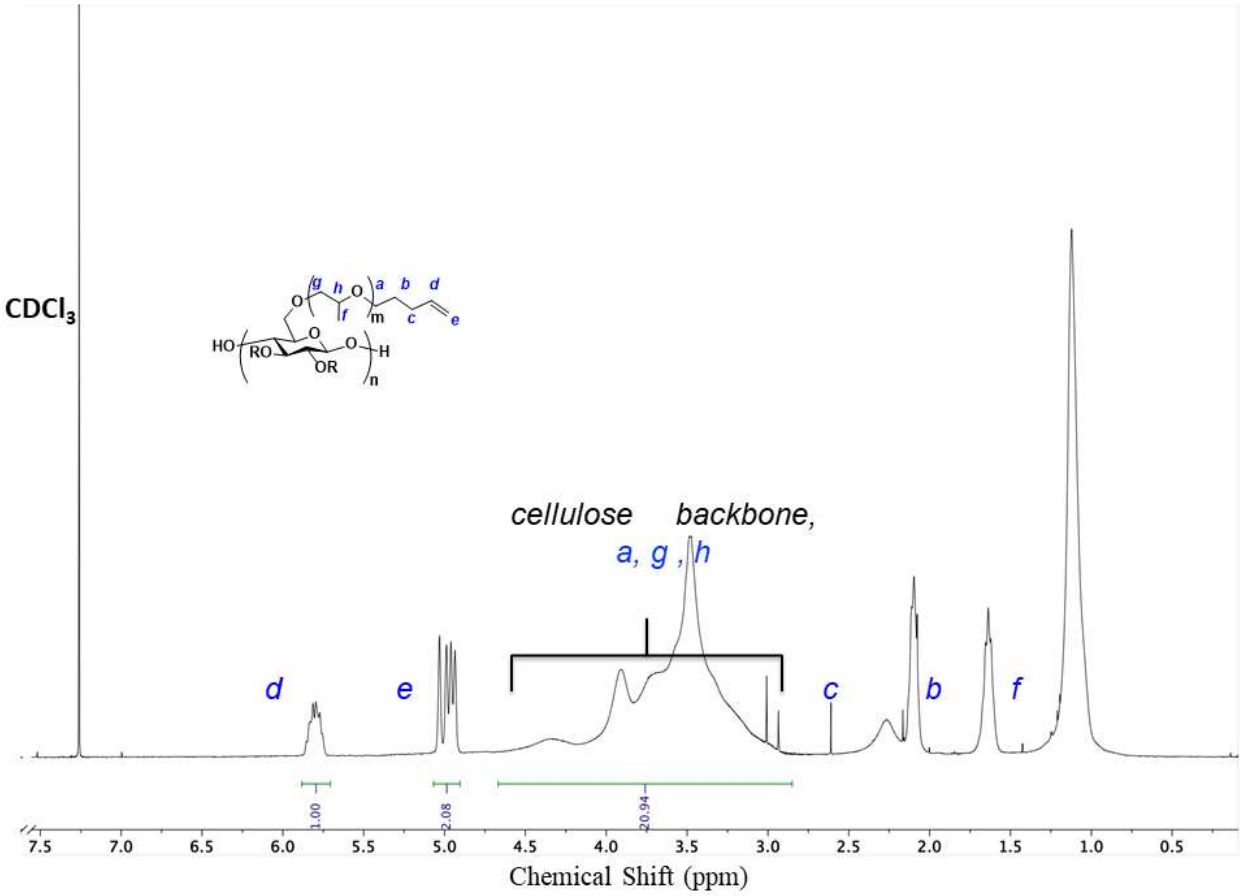

Figure S3.7. ^{1}H NMR spectrum of PenHPC prepared by one-pot synthesis with DS (C=C) = 1.00

The MS(HP) has been previously determined by a method described by Dong, Mosquera-Giraldo, Taylor, & Edgar, 2016, and is set to MS(HP, -$OCHCH_2CH_3$) = 4.4, while the DS (C=C) of the terminal proton (labeled 'e' in Figure S7) is set to x,

$$\frac{number\ of\ terminal\ olefin\ protons}{number\ of\ cellulosic\ backbone\ protons} = \frac{x_e}{7 + 2x_a + 3(4.4)} = \frac{1}{20.94}$$

Thus: x = DS (C=C) = 1.06

Sample degree of substitution calculation: CM product PenHPC-AcrMDC

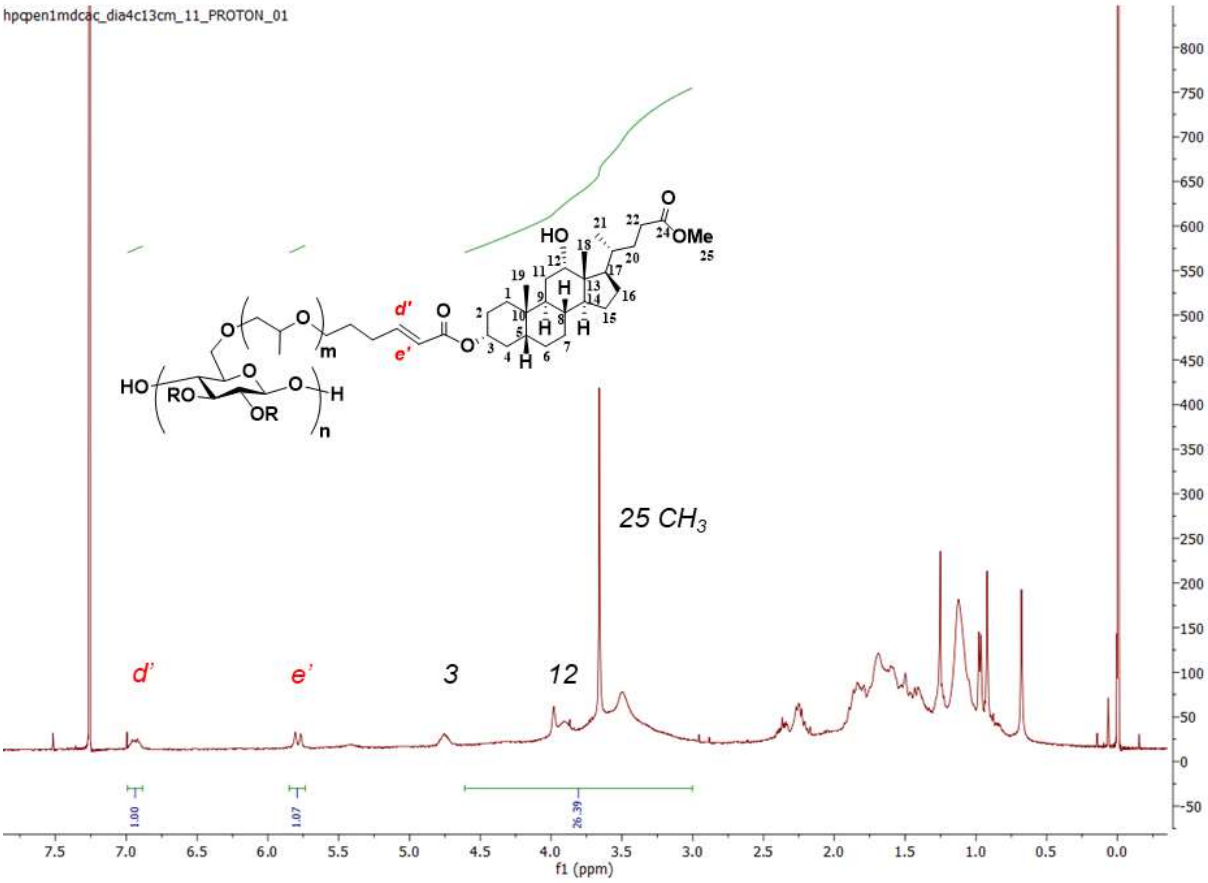

Figure S3.8. ^{1}H NMR spectrum of 3-*O*-PenHPC-AcrMDC. The DS (AcrMDC) is determined with the integration of the internal olefin **d'** as such:

$$\frac{integration\ value\ of\ terminal\ olefin, d'}{integration, cellulosic\ region} = \frac{x_{d'}}{7 + (3 * 4.4) + (1) + 4x} = \frac{1}{26.39}$$

Thus, DS(AcrMDC) = 0.98

MDSC Thermograms

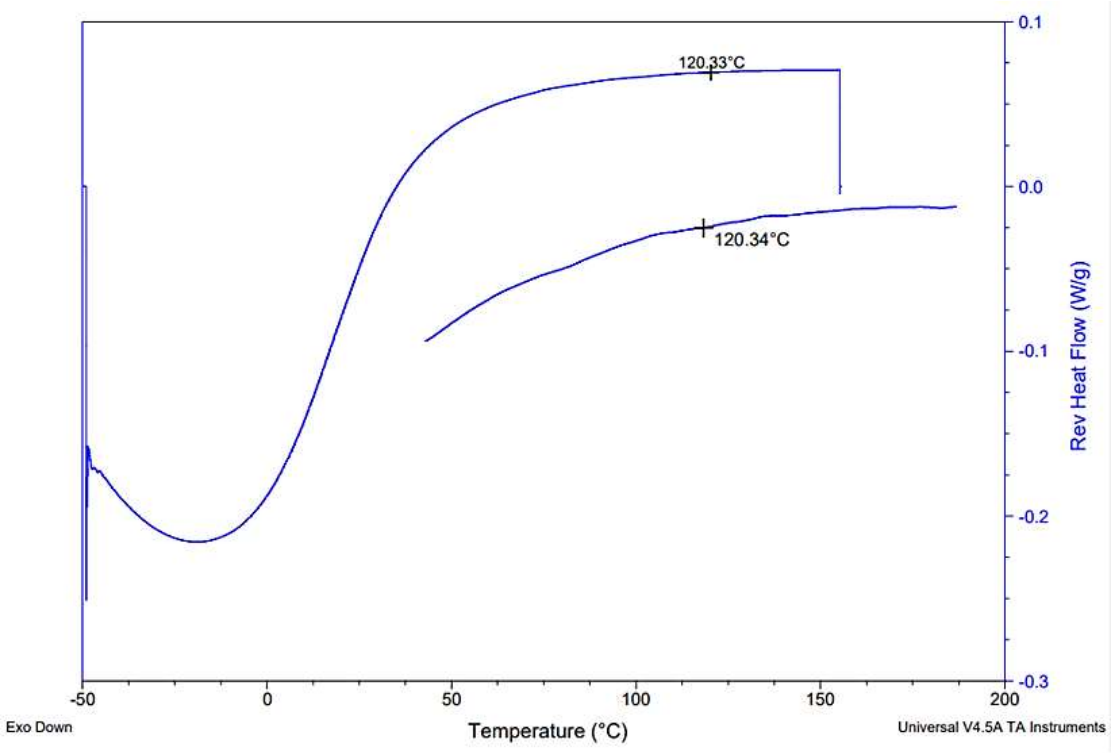

Figure S3.9. MDSC thermogram of 3-*O*-AcrMLC-PenHHPC (0.64)

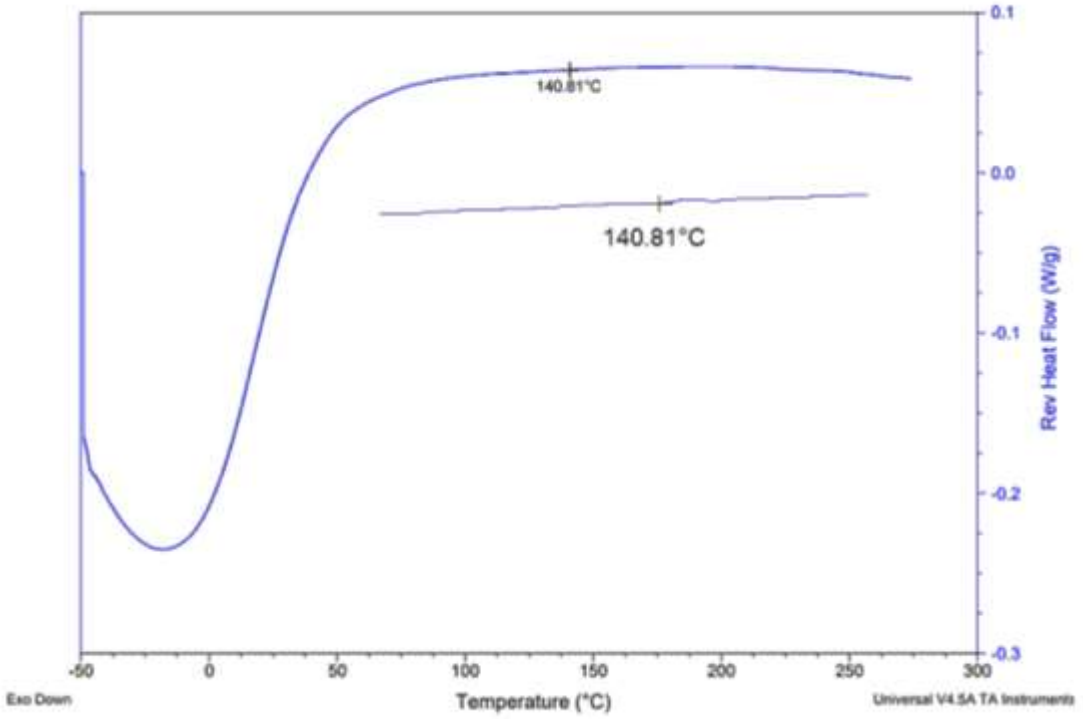

Figure S3.10. MDSC thermogram of 3-*O*-AcrMDC-PenHHPC (0.64)

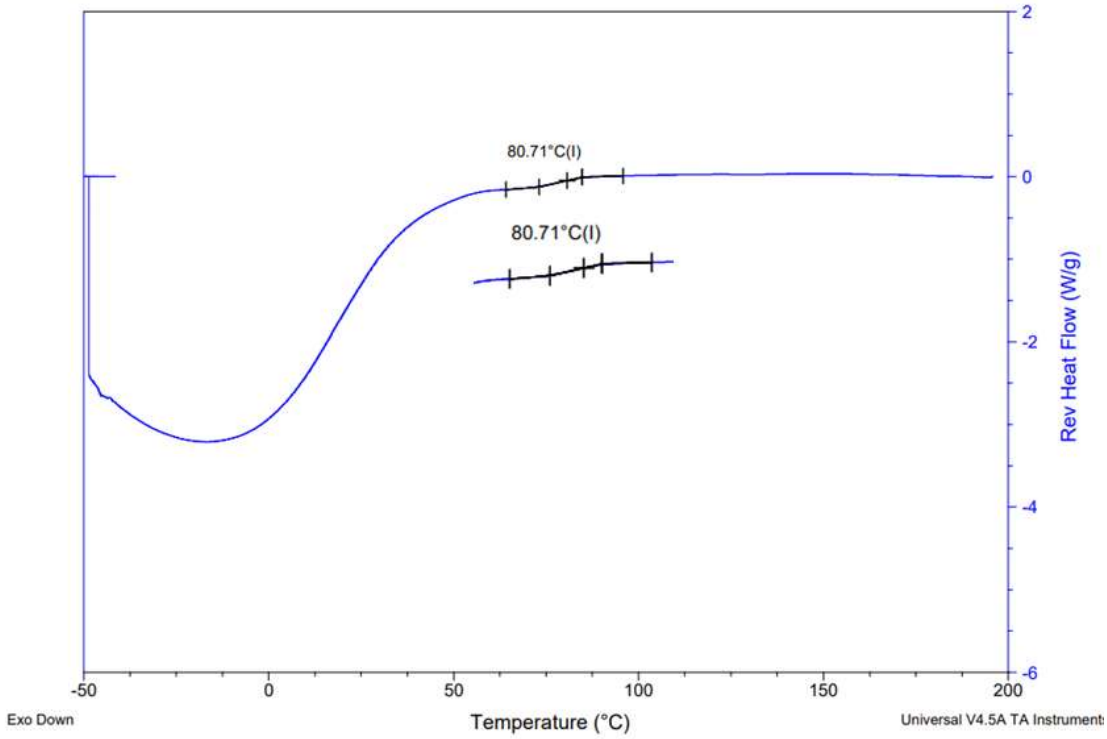

Figure S3.11. MDSC thermogram of 3-*O*-AcrLC-PenHHPC (0.64)

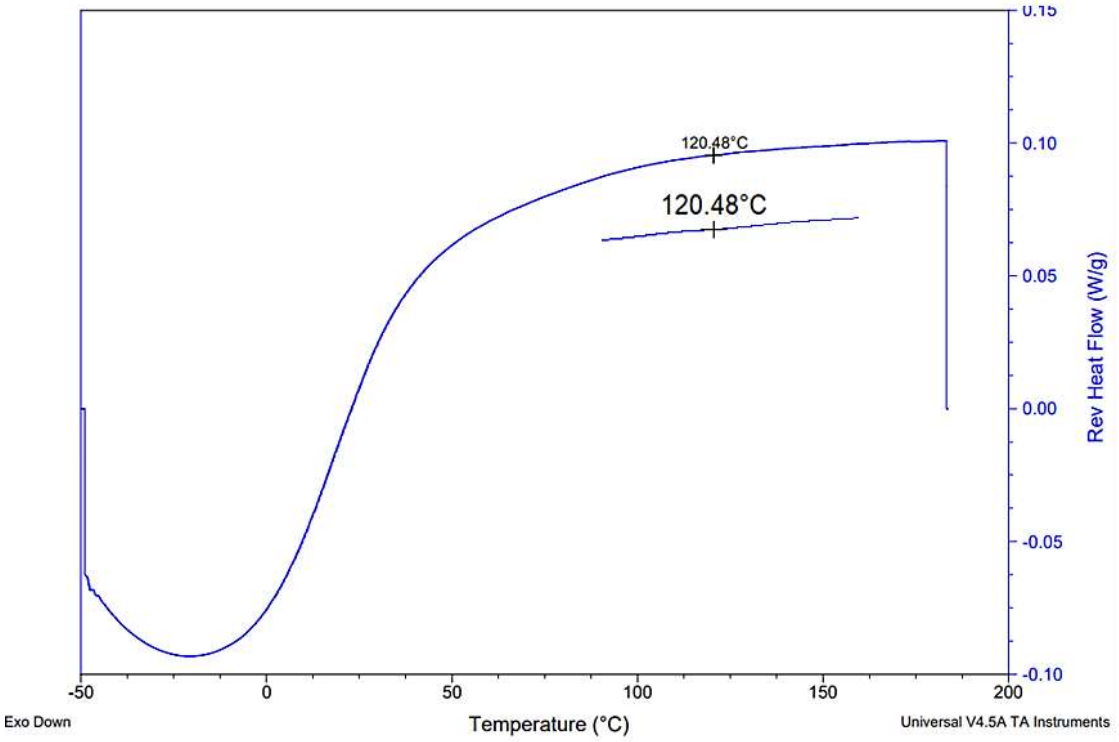

Figure S3.12. MDSC thermogram of 3-*O*-AcrDC-PenHHPC (0.64)

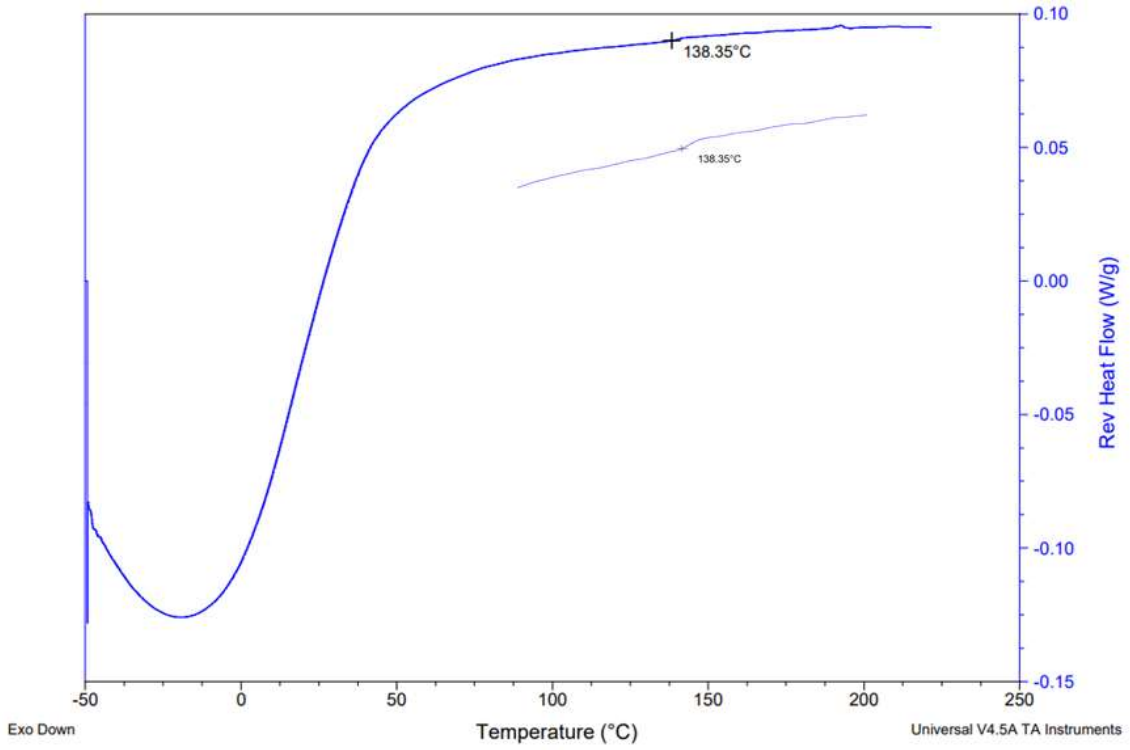

Figure S3.13. MDSC thermogram of 3-*O*-AcrMLC-PenHHPC (1.00)

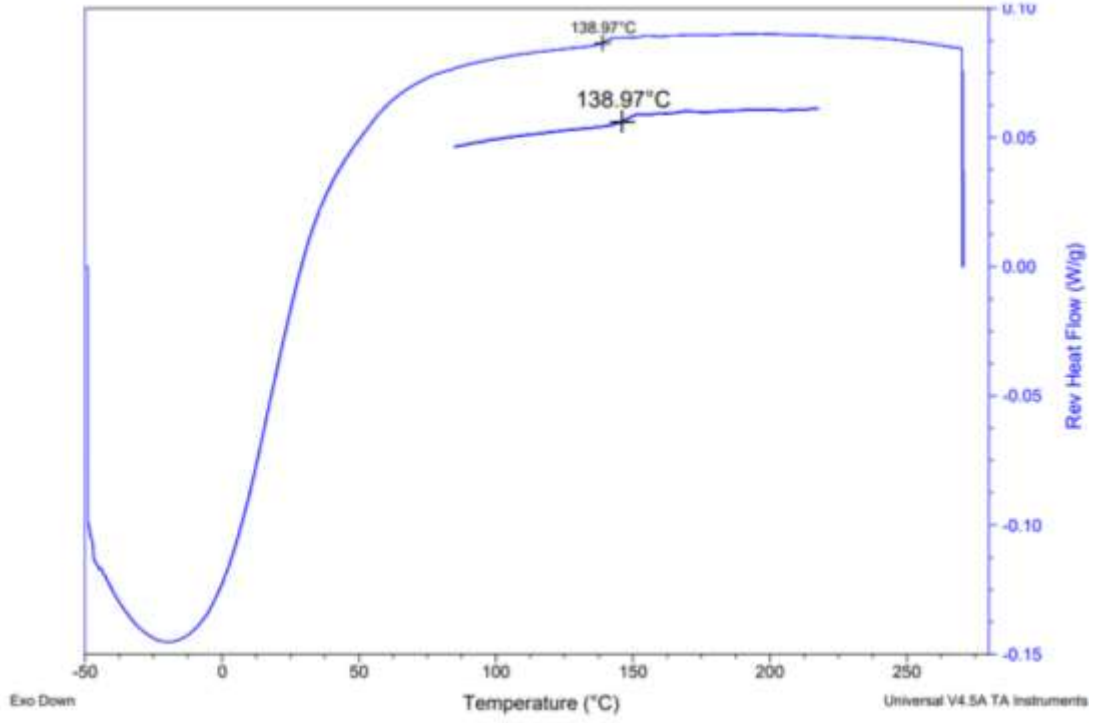

Figure S3.14. MDSC thermogram of 3-*O*-AcrMDC-PenHHPC (1.00)

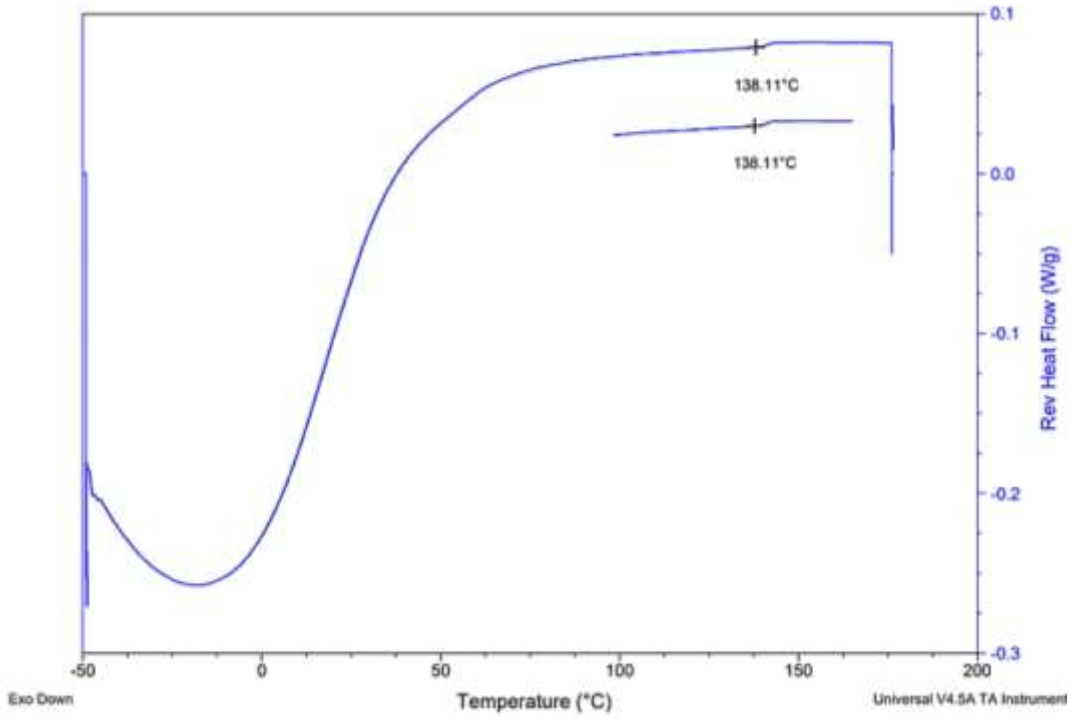

Figure S3.15. MDSC thermogram of 3-*O*-AcrLC-PenHHPC (1.00)

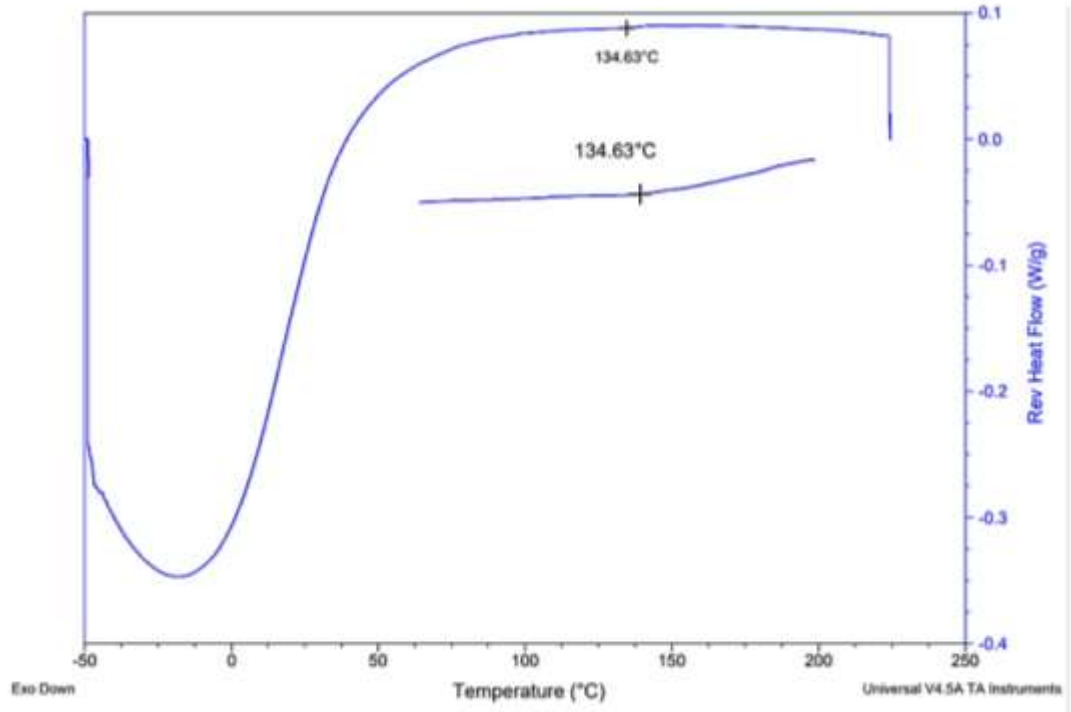

Figure S3.16. MDSC thermogram of 3-*O*-AcrDC-PenHHPC (1.00)

Table S3.1: Properties of hydrogenated HPC-bile acid ester (3-*O*-PenHHPC) products.

DS $_{\text{bile acid/ester}}$	Sample	Mn (Da)	Mw (Da)	PDI	T_g (° C)
0.64	AcrMLC	21920	53710	2.45	120.34
	AcrMDC	27480	31060	1.130	140.81
	AcrLC	*n/a*	*n/a*	*n/a*	80.71
	AcrDC	28890	47340	1.639	120.48
1.00	AcrMLC	13410	30693	2.072	138.35
	AcrMDC	*n/a*	*n/a*	*n/a*	139.97
	AcrLC	18480	24780	1.341	138.11
	AcrDC	*n/a*	*n/a*	*n/a*	134.63

* Samples listed as 'n/a' were not sufficiently soluble in any available SEC solvent system.

Table S3.2: Name, abbreviation, structure, and degree of substitution (DS)* of polymers described in this study.

Name	Abbreviation	Structure
Hydroxypropyl cellulose	HPC‡	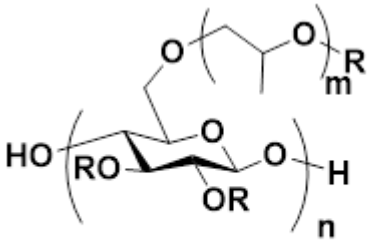 R = -H, or -$(CH_2CH(CH_3)O)_mH$
1-pent-4-enyl hydroxypropyl cellulose	PenHPC (DS)	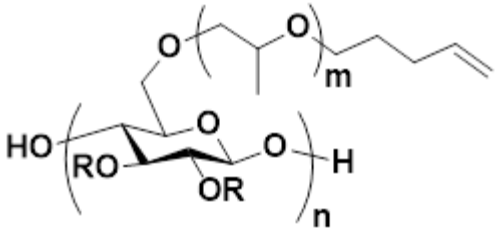 R = -H, or -$(CH_2CH(CH_3)O)_mH$

1-pent-4-enyl 3-acryloyl methyl lithocholate hydroxypropyl cellulose	3-*O*-AcrMLC PenHPC (DS)	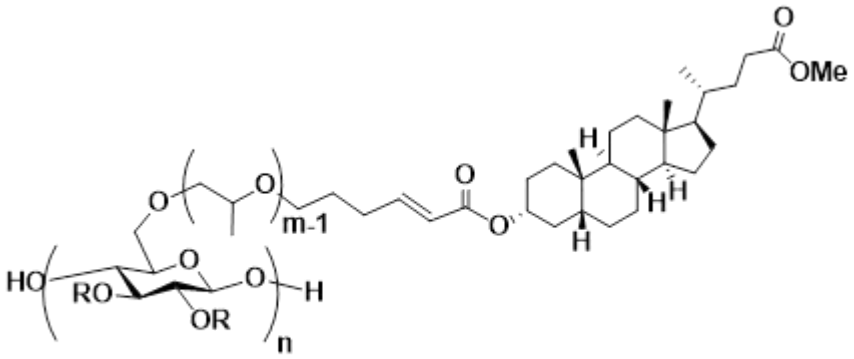 R = -H, or -$(CH_2CH(CH_3)O)_mH$
1-pent-4-enyl 3-acryloyl methyl deoxycholate hydroxypropyl cellulose	3-*O*-AcrMDC -PenHPC- (DS)	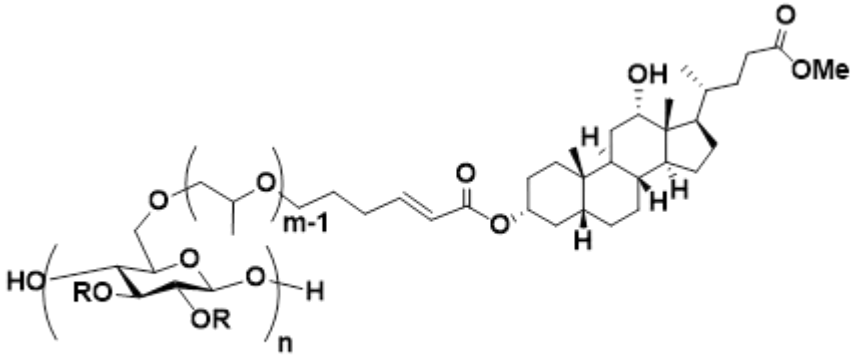 R = -H, or -$(CH_2CH(CH_3)O)_mH$
1-pent-4-enyl 3-acryloyl lithocholate hydroxypropyl cellulose	3-*O*-AcrLC-PenHPC (DS)	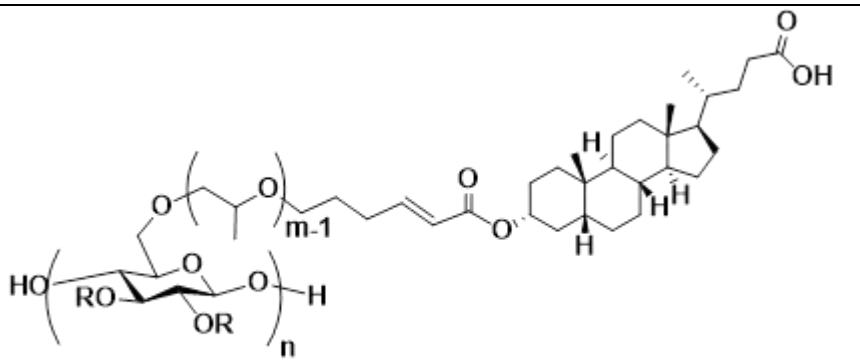 R = -H, or -$(CH_2CH(CH_3)O)_mH$

1-pent-4-enyl 3-acryloyl deoxycholate hydroxypropyl cellulose	3-*O*-AcrDC-PenHPC (DS)	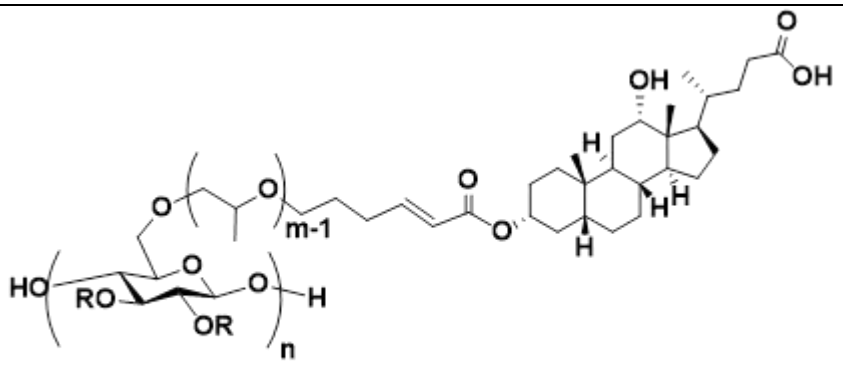 R = -H, or -$(CH_2CH(CH_3)O)_mH$
Pent-1-yl 3-methyl lithocholate hydroxypropyl cellulose	3-*O*-AcrMLC PenHHPC (DS)	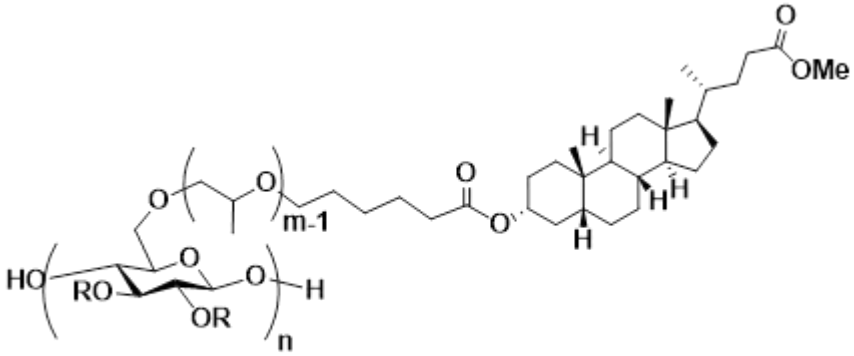 R = -H, or -$(CH_2CH(CH_3)O)_mH$
Pent-1-yl 3-methyl deoxyocholate hydroxypropyl cellulose	3-*O*-AcrMDC-PenHHPC (DS)	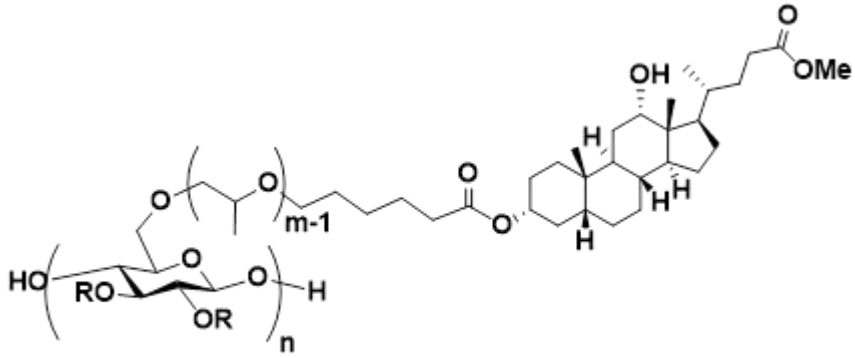 R = -H, or -$(CH_2CH(CH_3)O)_mH$

Pent-1-yl 3-lithocholic acid hydroxypropyl cellulose	3-*O*-AcrLC-PenHHPC (DS)	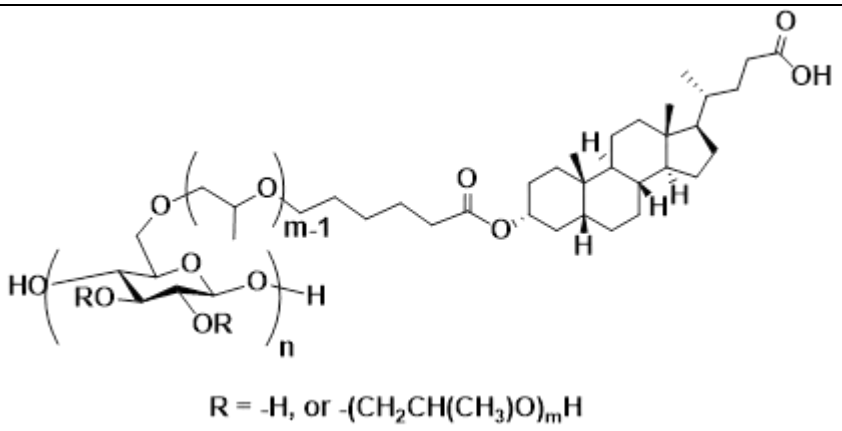
Pent-1-yl 3-deoxycholic acid hydroxypropyl cellulose	3-*O*-AcrDC-PenHHPC (DS)	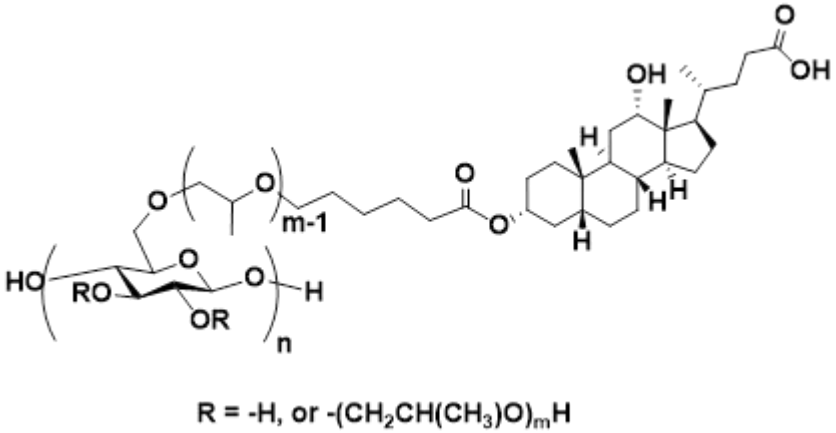
5-carboxypent-1-yl hydroxypropyl cellulose	HPC-Pen-AA-H (DS)	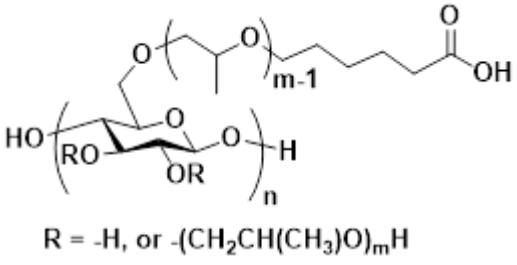
ethyl 1-pent-4-enyl cellulose	EC2.30C5	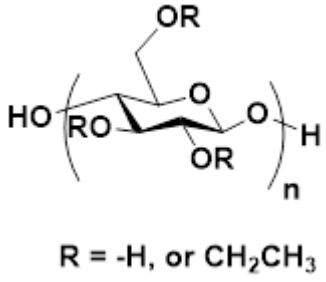

ethyl pent-1-yl cellulose cholesterol acrylate	EC2.30C5-ChAc-H	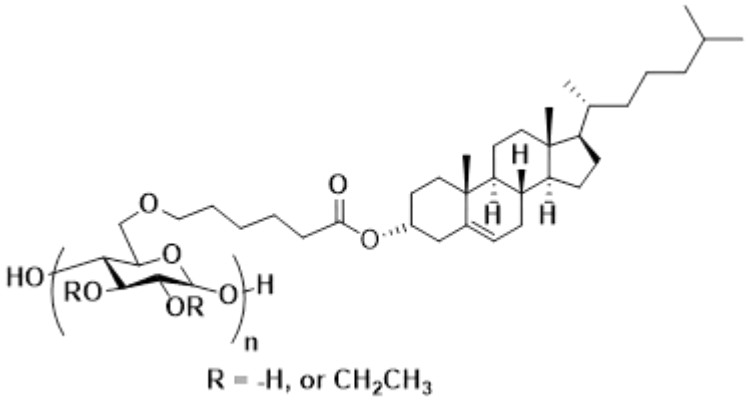
ethyl pent-1-yl cellulose 3-methyl lithocholate	EC2.30C5-MLCAc-H	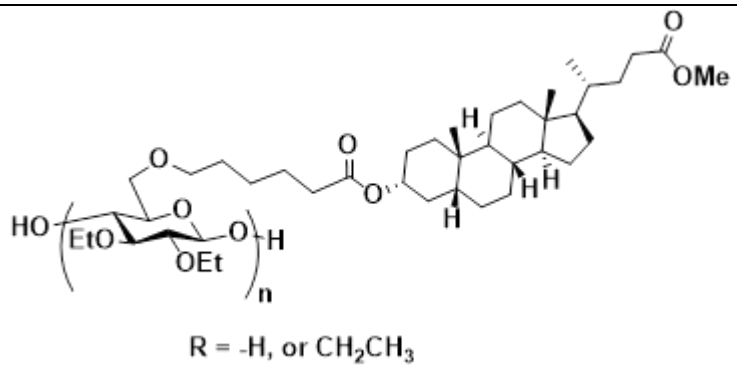
ethyl 5-carboxypent-1-yl cellulose 3-methyl deoxycholate	EC2.30C5-MDCAc-H	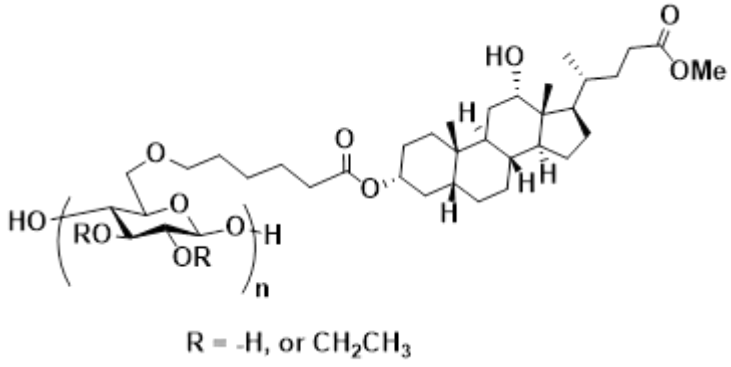

‡ DS (HP) = 2.2, MS = 4.4 for hydroxypropyl starting material, as described in (Dong, Mosquera-Giraldo, Troutman, et al., 2016)
* DS (pent-4-enyl, and bile ester/acid) = 0.64 or 1.00 for PenHPC derivatives, and 0.69 for EC2.30C5 derivatives (Dong et al., 2019).

Table S3.3: Fedor's solubility parameters for starting materials and cellulose ether derivatives

Polymer	Group 1	Group 2	Group 3	DS (Group 1)	DS (Group 2)	DS (Group 3)	SP ($MPa^{1/2}$)
HPC-Pen106-AA-H	$(CH_2CH(CH_3)O)_mH$	$(CH_2CH(CH_3)O)_mCH_2CH_2CH_2CH_2CH_2COOH$	OH	1.2	1.0	0.8	22.9
HPC-Pen064-AA-H	$(CH_2CH(CH_3)O)_mH$	$(CH_2CH(CH_3)O)_mCH_2CH_2CH_2CH_2CH_2COOH$	OH	1.56	0.64	0.8	23.4

PenHPC-(1.00)	$(CH_2CH(CH_3)O)_mH$	$(CH_2CH(CH_3)O)_mCH_2CH_2CH_2CH=CH_2$	OH	1.2	1.0	0.8	21.8
PenHPC-(0.64)	$(CH_2CH(CH_3)O)_mH$	$(CH_2CH(CH_3)O)_mCH_2CH_2CH_2CH=CH_2$	OH	1.56	0.64	0.8	22.8
AcrLC-PenHHPC (1.00)	$(CH_2CH(CH_3)O)_mH$	$(CH_2CH(CH_3)O)_mCH_2CH_2CH_2CH_2CH_2COO$-bilesalt	OH	1.2	1.0	0.8	21.5
AcrLC-PenHHPC (0.64)	$(CH_2CH(CH_3)O)_mH$	$(CH_2CH(CH_3)O)_mCH_2CH_2CH_2CH_2CH_2COO$-bilesalt	OH	1.56	0.64	0.8	22.2
AcrMLC-PenHHPC (1.00)	$(CH_2CH(CH_3)O)_mH$	$(CH_2CH(CH_3)O)_mCH_2CH_2CH_2CH_2CH_2COO$-bilesalt	OH	1.2	1.0	0.8	21.0
AcrMLC-PenHHPC (0.64)	$(CH_2CH(CH_3)O)_mH$	$(CH_2CH(CH_3)O)_mCH_2CH_2CH_2CH_2CH_2COO$-bilesalt	OH	1.56	0.64	0.8	21.8
AcrDC-PenHHPC (1.00)	$(CH_2CH(CH_3)O)_mH$	$(CH_2CH(CH_3)O)_mCH_2CH_2CH_2CH_2CH_2COO$-bilesalt	OH	1.2	1.0	0.8	22.4
AcrDC-PenHHPC (0.64)	$(CH_2CH(CH_3)O)_mH$	$(CH_2CH(CH_3)O)_mCH_2CH_2CH_2CH_2CH_2COO$-bilesalt	OH	1.56	0.64	0.8	23.2
AcrMDC-PenHHPC (1.00)	$(CH_2CH(CH_3)O)_mH$	$(CH_2CH(CH_3)O)_mCH_2CH_2CH_2CH_2CH_2COO$-bilesalt	OH	1.2	1.0	0.8	21.9
AcrMDC-PenHHPC (0.64)	$(CH_2CH(CH_3)O)_mH$	$(CH_2CH(CH_3)O)_mCH_2CH_2CH_2CH_2CH_2COO$-bilesalt	OH	1.56	0.64	0.8	22.5
EC2.30C5	CH_2CH_3	$CH_2CH_2CH_2CH=CH_2$	OH	2.3	0.69	0.01	18.2
EC2.30C5-ChAc-H	CH_2CH_3	$CH_2CH_2CH_2CH_2CH_2COO$-cholesterol	OH	2.3	0.69	0.01	18.0
EC2.30C5-MLCAc-H	CH_2CH_3	$CH_2CH_2CH_2CH_2CH_2COO$-bilesalt	OH	2.3	0.69	0.01	18.7
EC2.30C5-MDCAc-H	CH_2CH_3	$CH_2CH_2CH_2CH_2CH_2COO$-bilesalt	OH	2.3	0.69	0.01	19.9

Enzalutamide = 24.2 $MPa^{1/2}$

Figure S3.17. Bile salt derivative solubility parameter impact on crystallization inhibition

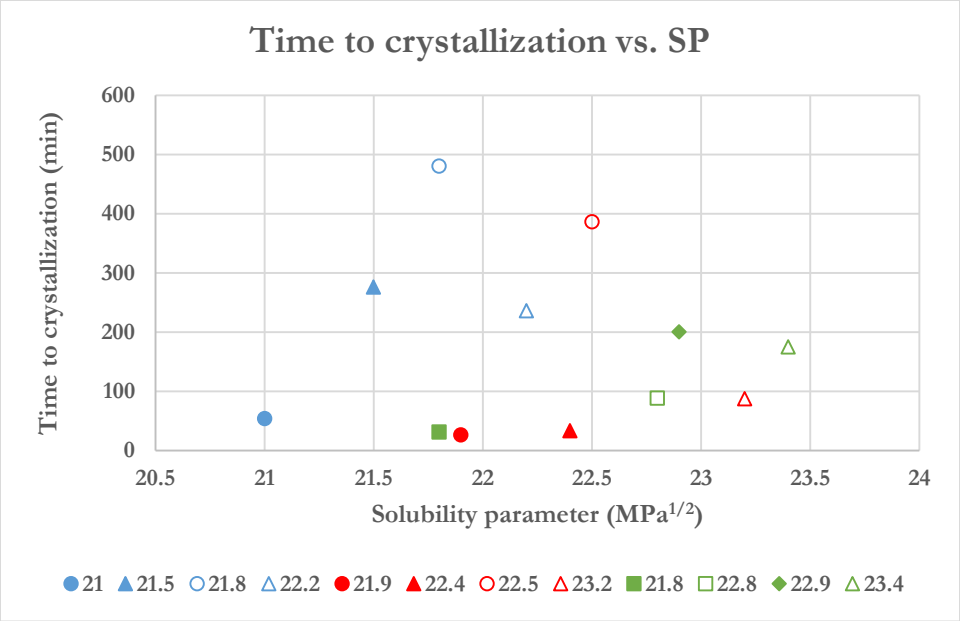

Key:

Blue = lithocholic acid deriv., red = deoxycholic acid deriv., green = control

Circle = methyl ester, triangle = acid

Solid = DS 1.00, Open = DS 0.64

Controls: Solid and open same as above, square denotes no bile salt appendage, diamond denotes bile salt appendage

Chapter 4. Tracking polysaccharides: Synthesis of environment-sensitive, polysaccharide-based fluorophores via reductive-amination

HSQC ^{13}C – ^{1}H NMR

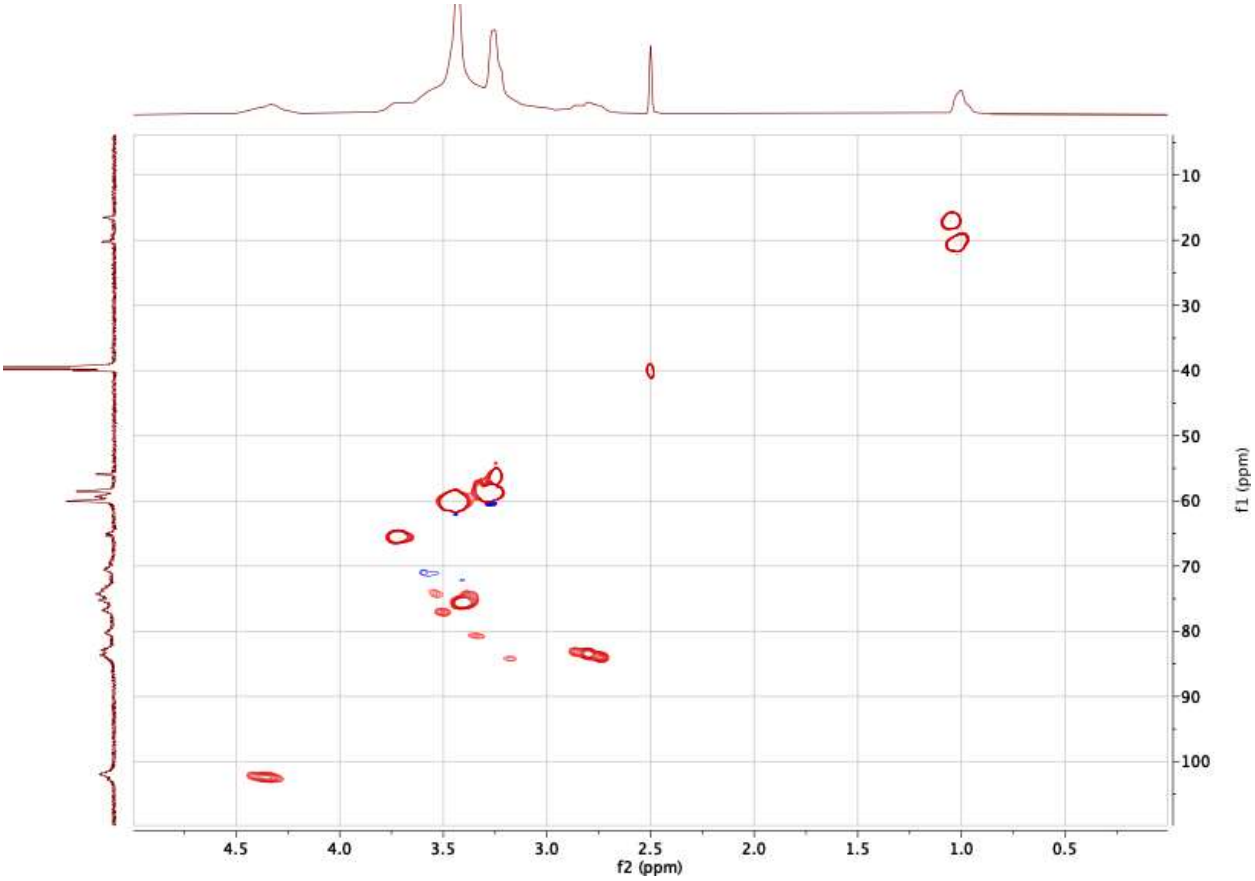

Fig. S4.1. HSQC ^{13}C – ^{1}H NMR spectrum of HPMC in DMSO-d_6 demonstrates the correlation of anomeric proton (4.35 ppm) and C1 carbon (102.1 ppm).

Determination of DS and MS of HP and DS OMe and free hydroxyl groups for HPMC 603.
Hydroxypropyl (HP) group molar substitution (MS) of hydroxypropylmethyl cellulose (HPMC) was determined by ^{1}H NMR spectroscopy in DMSO-d_6. We relate the integration of the carbon 1 (C1) to that of the HP methyls, which will provide MS.

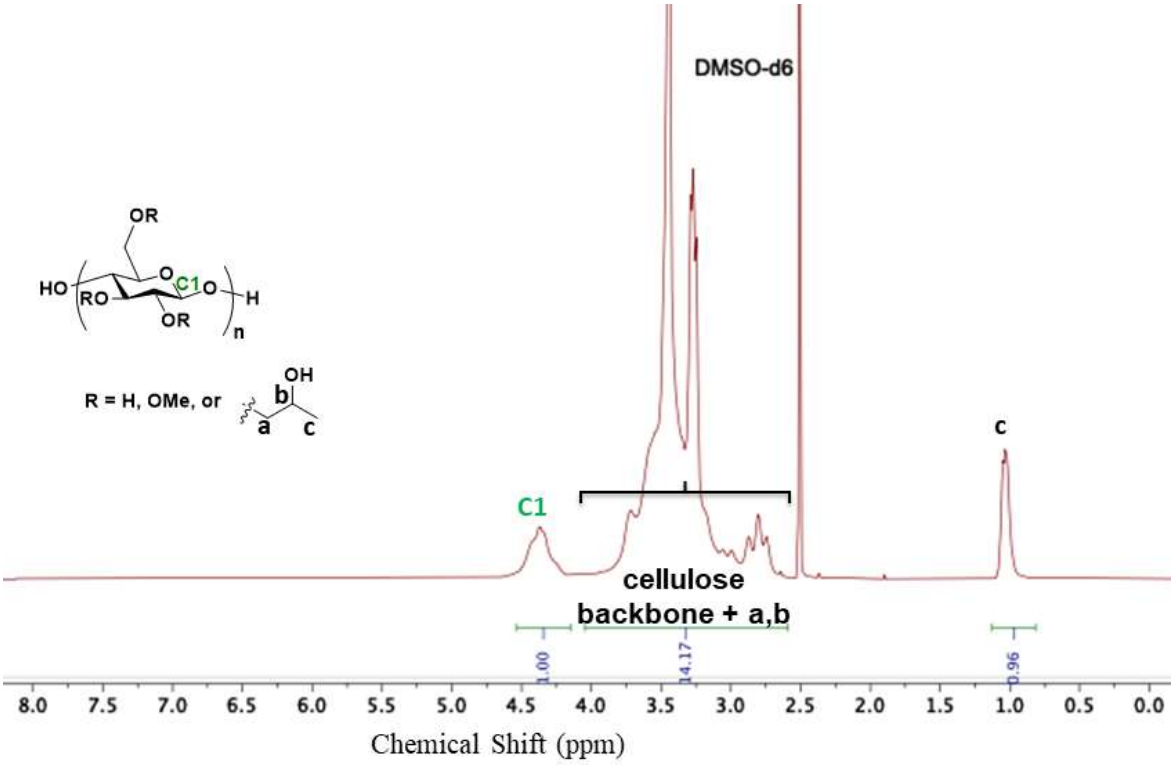

Fig. S4.2. **^{1}H NMR of hydroxypropyl methylcellulose (HPMC)**

1. Calculation for MS_{HP}:

$$MS_{HP} = \frac{3H_{\ HP,methyl}}{1H_{\alpha}} = \frac{I_{HP,methyl}}{I_{\alpha}} = 0.32$$

2. Calculation for DS_{OMe}:

$$I_{backbone\ -\ anomeric} = I_{6h,\ cellulosic} + I_{OMe}\left(\frac{1}{3H,\ methyl}\right) + I_{HP}\left(\frac{3\ HP\ methine+methylene}{3HP\ methyl}\right)$$

$$I_{OMe} = I_{backbone\text{-}anomeric} - I_{HP}\left(\frac{3\ HP\ methine+methylene}{3HP\ methyl}\right) = 14.17 - 6 - 0.95 = 7.16$$

$$DS_{OMe} = 7.16\,\frac{1}{3H,OMe} = 2.39$$

3. DS of free -OH on HPMC603

DS_{OH} = 3- DS_{OMe} = 0.61

^{1}H NMR of HPMC-Acetate

The DS was determined by peracetylation of HPMC using acetic anhydride, thereby shifting the

methyl resonances of the terminal HP units downfield. The ratio of the teminal HP: internal HP is used to calculate the DS from the calculated MS (determined in the previous step).

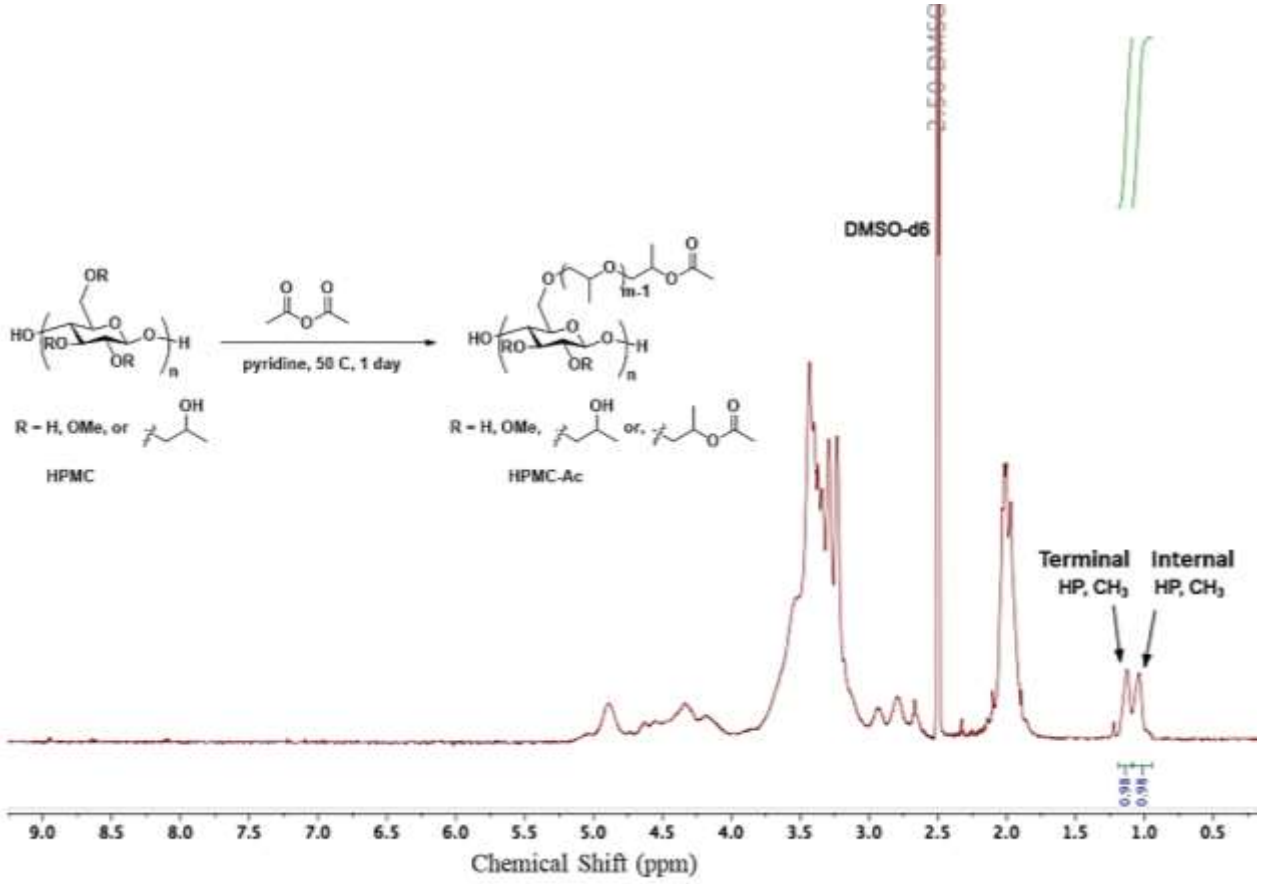

Fig S4.3. ^{1}NMR spectrum of HPMC-acetate DMSO-d_6.

Calculation for DS_{HP}

$$\mathbf{DS_{HP}} = \frac{I_{HP,\ internal+terminal\ methyl}}{I_{HP,\ terminal\ methyl}} * \mathrm{MS} = \frac{I_{HP,\ terminal\ methyl}}{I_{HP,\ terminal\ methyl} + I_{HP,\ internal\ methyl}}$$

$$\mathbf{DS_{HP}} = \frac{1}{2}\mathrm{MS} = 0.16$$

Determination of DS (ketone) for Ox-HPMC

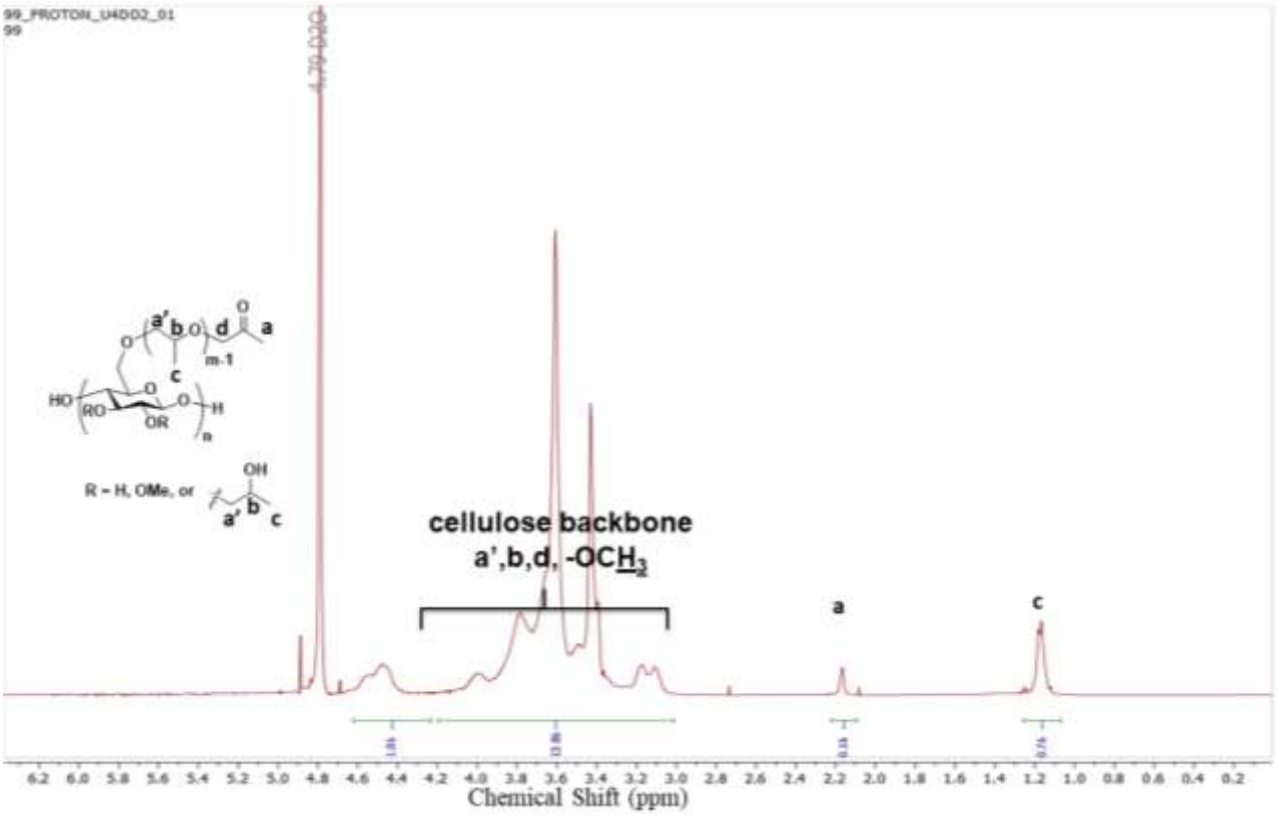

Fig. S4.4. ^{1}H NMR spectrum of Ox-HPMC in D_2O.

Calculation of $I_{backbone}$ - $I_{HP,CH+CH2}$

$$\mathbf{I_{backbone}} = I_{AGU,\,7H} + I_{HP,CH+CH2} + I_{OMe,3H} = 14.86 - \left(\frac{2(0.16)}{3} + 0.76\right) = 13.99$$

$$\textbf{Calculation of MS (HP)} = \frac{10}{3}\,\frac{\boldsymbol{I_a + I_c}}{I_{AGU,7H} + I_{OMe,3H}} = 0.22$$

$$\textbf{DS(oxopropyl/AGU)} = DS_{HP} * \frac{6}{3}\,\frac{\boldsymbol{I_a}}{\boldsymbol{I_a + I_c}} = 0.17 * \frac{2(0.01)}{0.01+0.05} = 0.06$$

$$\textbf{Percent terminal HP group conversion \%} = 100 * \frac{6}{3}\,\frac{\boldsymbol{I_a}}{\boldsymbol{I_a + I_c}} = 100 * \frac{2(0.01)}{0.01+0.05} = 33\%$$

Determination of DS (ketone) for Ox-HPC

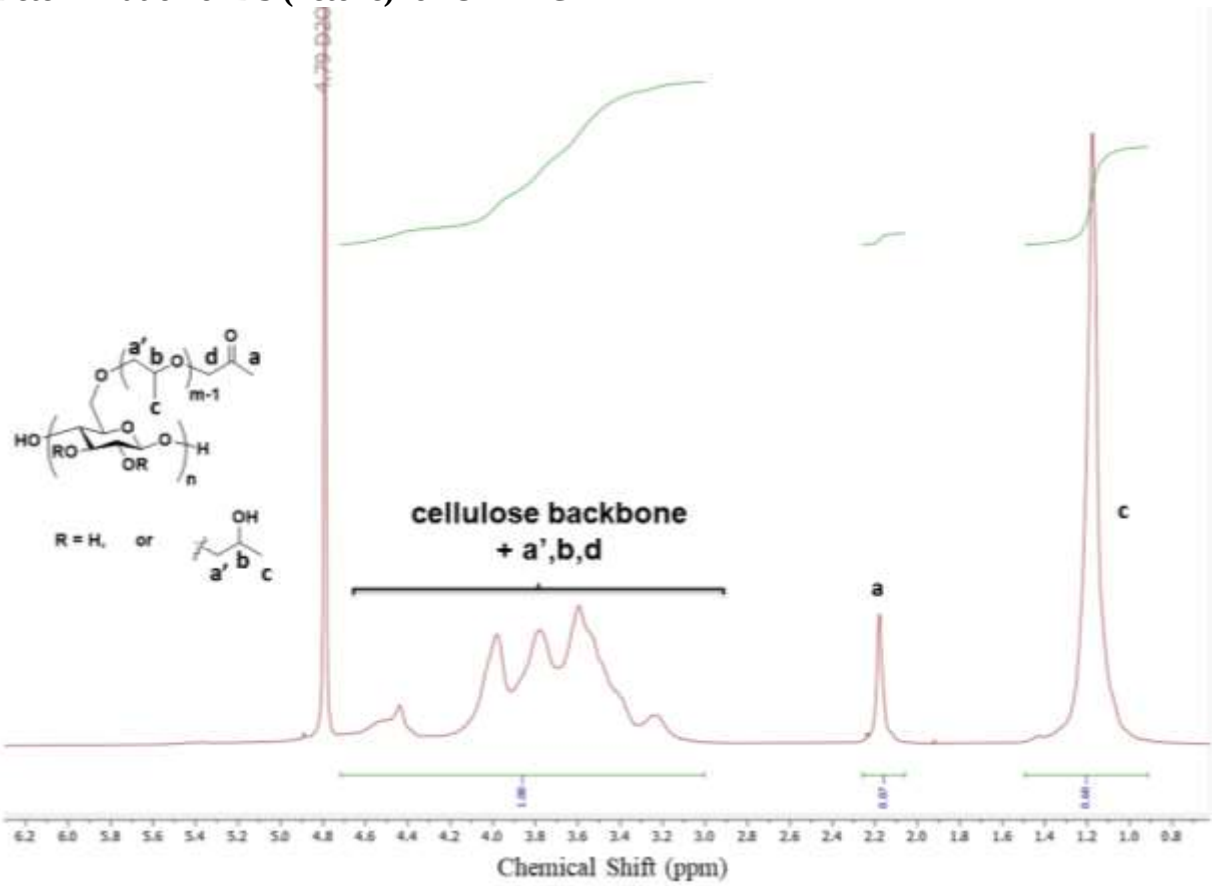

Fig. S4.5. ^{1}H NMR spectrum of Ox-HPC in D_2O.

Calculation of $I_{AGU,\,7H}$ = $I_{backbone}$ = $1 - \left(\frac{2(0.07)}{3} + 0.60\right)$ = 0.35

Calculation of MS (HP) = $\frac{7}{3}\frac{I_a + I_c}{I_{AGU,7H}}$ = 4.42

DS(oxopropyl/AGU) = $DS_{HP} * \frac{6}{3}\frac{Ia}{I_a + I_c} = 2.5 * \frac{2(0.07)}{0.07+0.60}$ = 0.52

Percent terminal HP group conversion % = $100 * \frac{6}{3}\frac{I_a}{I_a + I_c} = 100 * \frac{2(0.07)}{0.07+0.60}$ = 20.89%

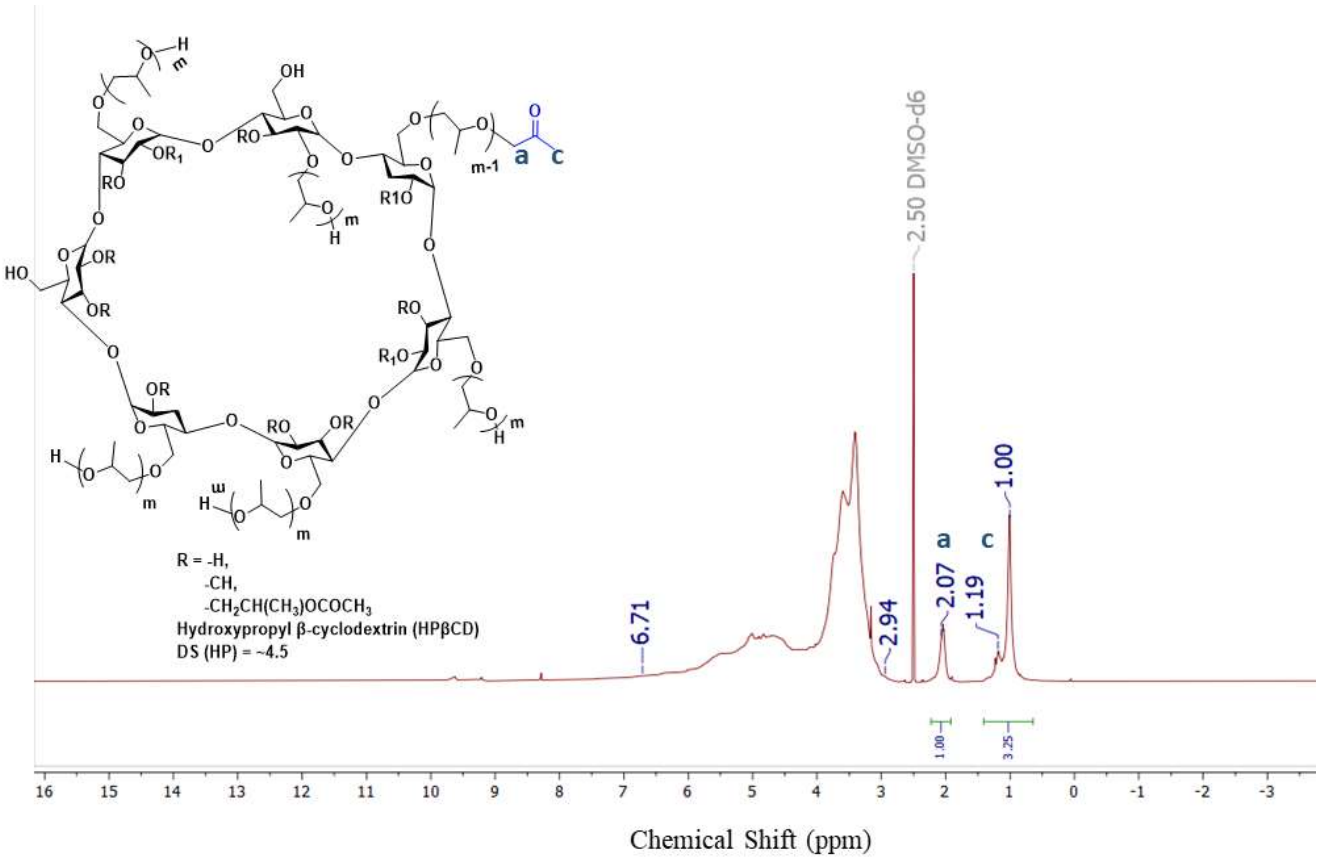

Fig. S4.6. ^{1}H NMR spectrum of Ox-HP-β-CD in D_2O.

Calculation of $I_{AGU,\,7H}$ = $I_{backbone}$ $= 1 - \left(\frac{2(0.07)}{3} + 0.60 \right) = 0.35$

Calculation of MS (HP) $= \frac{7}{3} \frac{I_a + I_c}{I_{AGU,7H}} = 4.42$

DS(oxopropyl/AGU) $= DS_{HP} * \frac{6}{3} \frac{Ia}{I_a + I_c} = 4.5 * \frac{2(1)}{1+3.25} = 2.2$

Percent terminal HP group conversion % $= 100 * \frac{6}{3} \frac{I_a}{I_a + I_c} = 100 * \frac{2(1)}{1+3.25} = 47.05\%$

Determination of DS (NB) imine for Ox-HPC-NB

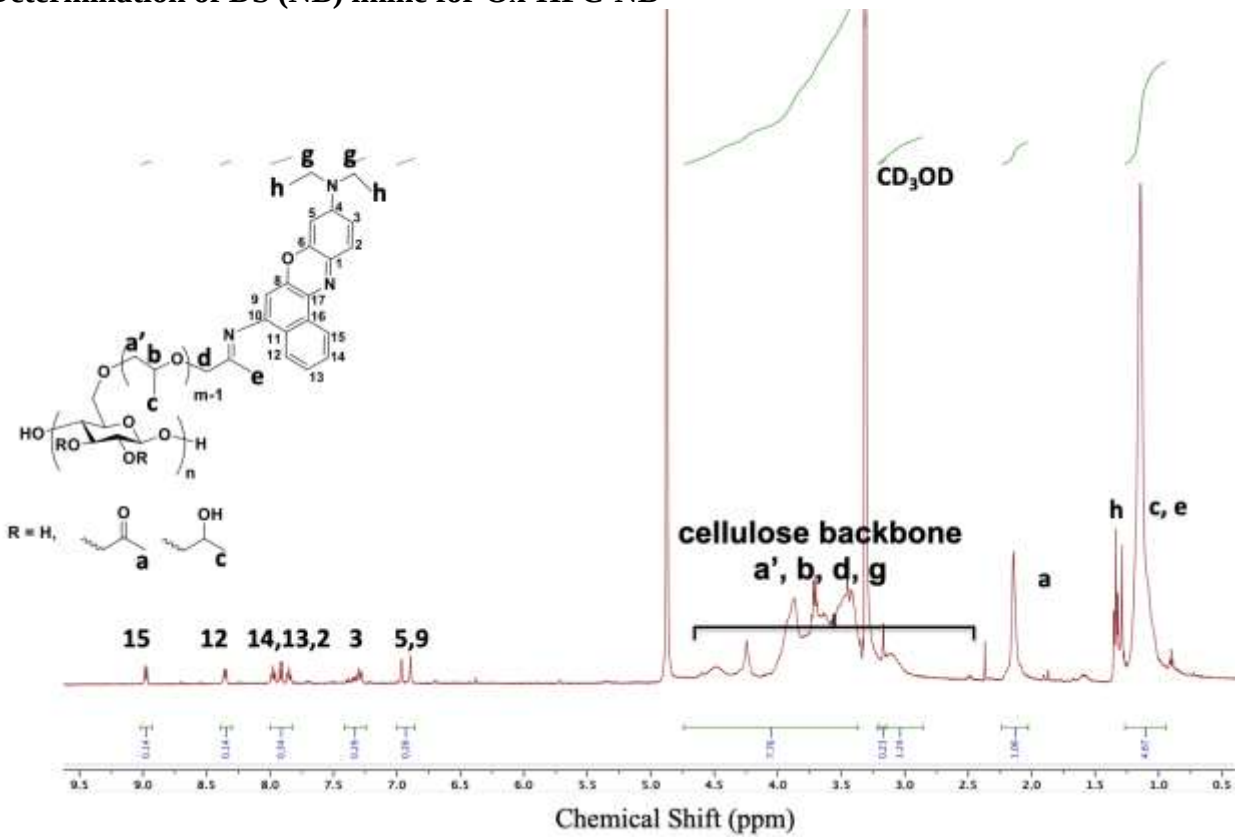

Fig. S4.7. ^{1}H NMR spectrum and calculations for Ox-HPC-NB-H in CD_3OD**.**

Calculation of $I_{AGU,\ 7H}$ = $I_{backbone}$ = $1 - \left(\frac{2(1)}{3} + 4.67\right)$ **= 3.42**

MS (HP) = $\frac{7 * I_{HP,CH3} + I_a}{3 * I_{AGU,\ 7H}}$ = $\frac{7(1+4.67)}{3*(3.42)}$ **= 3.87**

DS (oxopropyl/AGU) = $\frac{2\ I_a}{I_a + I_c}$ *** DS (HP)** = 2.5* $\frac{2(1.00)}{1+4.65}$ **= 0.88**

DS (imine) = $\frac{16\ I_{aromatic}}{8\ I_{AGU+a',b,d,e,g}} = \frac{16\ (0.14+0.14+0.34+0.29+0.26)}{8(7.76+1)}$ **= 0.34**

Percent conversion (%) = $\frac{DS(imine)}{DS(oxopropyl)}$***100** = $\frac{0.34}{0.88}$ ***100 = 38.66%**

Determination of DS (NB) amine for Ox-HPC-NB-H.

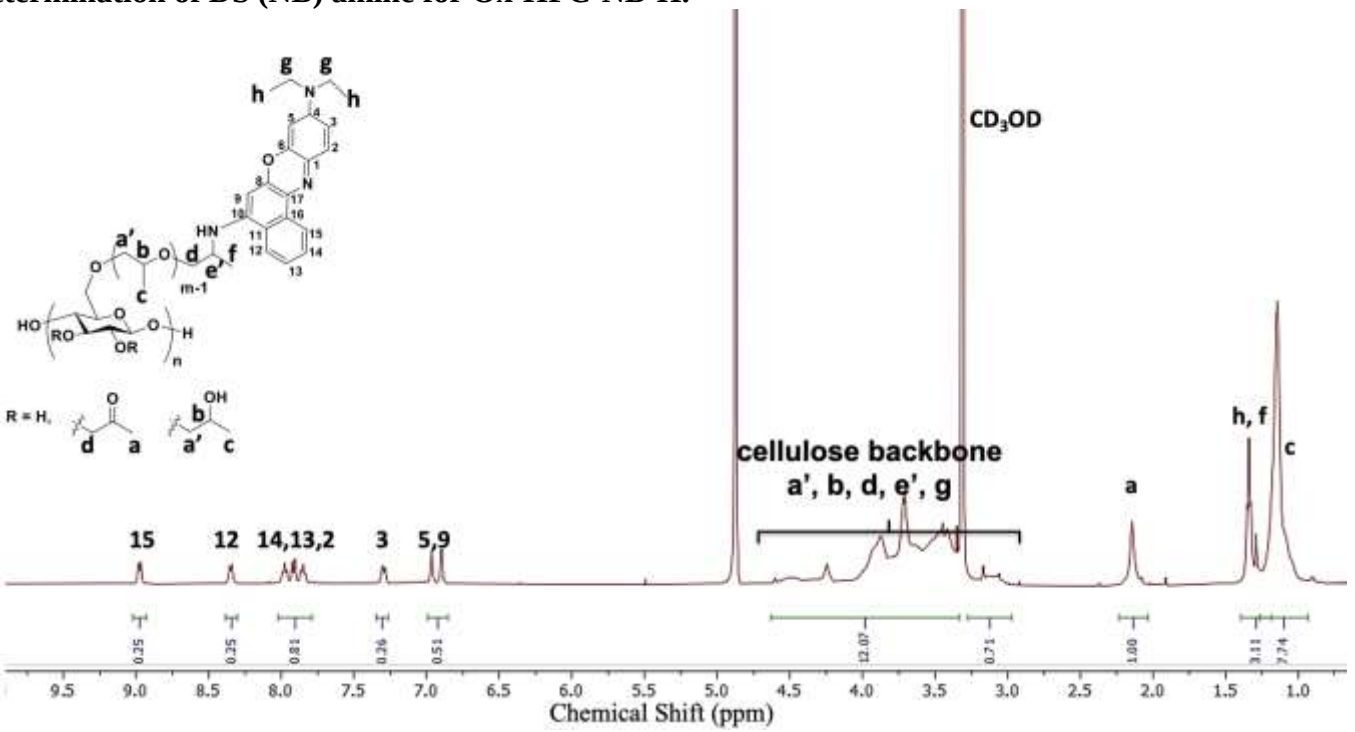

Fig. S4.8. ^{1}H NMR spectrum and calculations for Ox-HPC-NB-H in CD_3OD.

Calculation of $I_{AGU,\ 7H}$ = $I_{backbone}$ $= 12.78 - \left(\frac{2(1)}{3} + 7.74\right)$ **= 4.37**

MS (HP) $= \frac{7 * I_{HP,CH3} + I_a}{3 * I_{AGU,\ 7H}} = \frac{7(7.74 + 1)}{3 * 12.77}$ **= 4.67**

DS (oxopropyl/AGU) $= \frac{2\ I_a}{I_a + I_c}$ *** DS (HP)** $= 2.5 * \frac{2(1.00)}{1 + 7.74}$ **= 0.572**

DS (amine) $= \frac{16\ I_{aromatic}}{8\ I_{AGU+a',b,d,e',g}} = \frac{16\ (0.25+0.25+0.81+0.26+0.51)}{8(12.07)}$ **= 0.37**

Percent conversion (%) $= \frac{DS(amine)}{DS(oxopropyl)} * 100 = \frac{0.37}{0.80} * 100$ **= 46.25%**

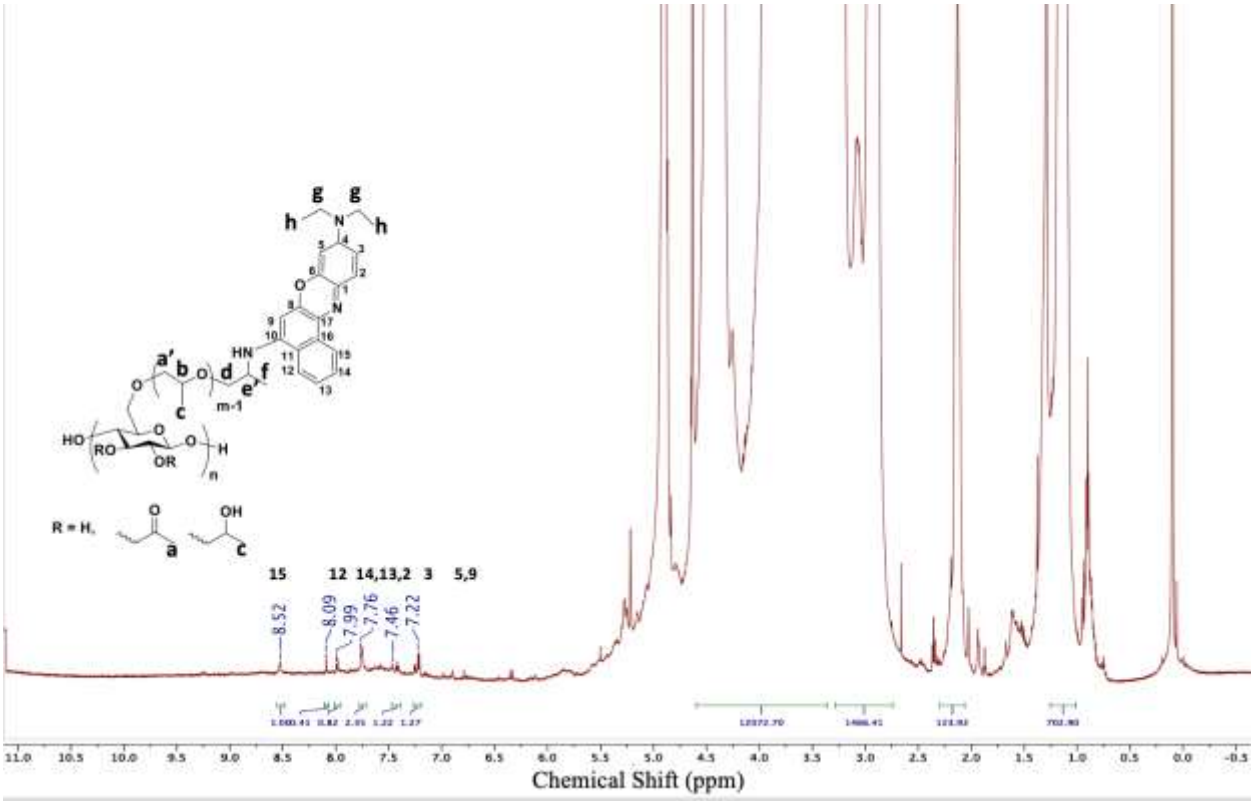

Fig. S4.9. ^{1}H NMR spectrum and calculations for Ox-HPMC-NB-H in CD_3OD**.**

Calculation of $I_{backbone}$ - $I_{HP,CH+CH2}$

$I_{backbone}$ = $I_{AGU,\ 7H}$ + $I_{HP,CH+CH2}$ + $I_{OMe,3H}$ +$I_{Nile\ Blue\ 2CH2}$ = $12072.70 - \left(\frac{2(123.92)}{3} + 702.9\right)$ = 11287.2

MS (HP) = $\frac{7 * I_{HP,CH3} + I_a}{3 * I_{AGU,\ 7H}} = \frac{14(677.62 + 113.29)}{3 * 11287.2}$ = **0.16**

DS (oxopropyl/AGU) = $\frac{2\ I_a}{I_a + I_c}$ * **DS (HP)** = 0.16* $\frac{2(1.00)}{123.92 + 702.9}$ = **0.0024**

DS (amine) = $\frac{19\ I_{aromatic}}{I_{AGU,7H+a',b,d,e,g+OMe}} = \frac{19(1.00)}{(12072.7+1466.41)}$ = **0.001**

Percent conversion (%) = $\frac{DS(amine)}{DS(oxopropyl)}$ *100 = $\frac{0.001}{0.0024}$ *100 = **41.3%**

^{13}C NMR

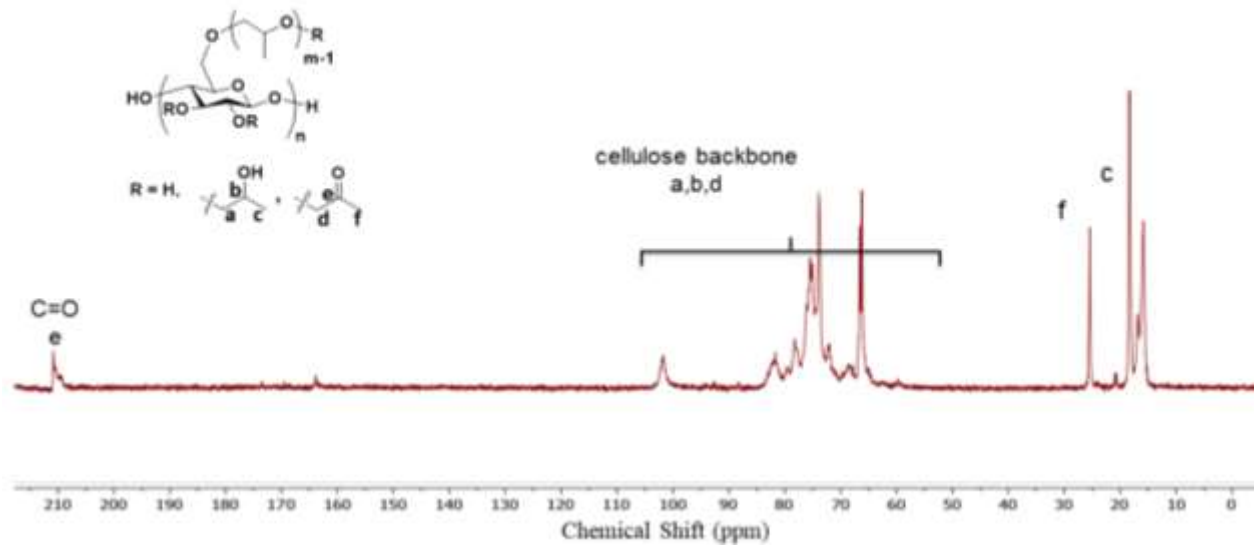

Figure S4.10. ^{13}C NMR spectrum of Ox-HPC in D_2O

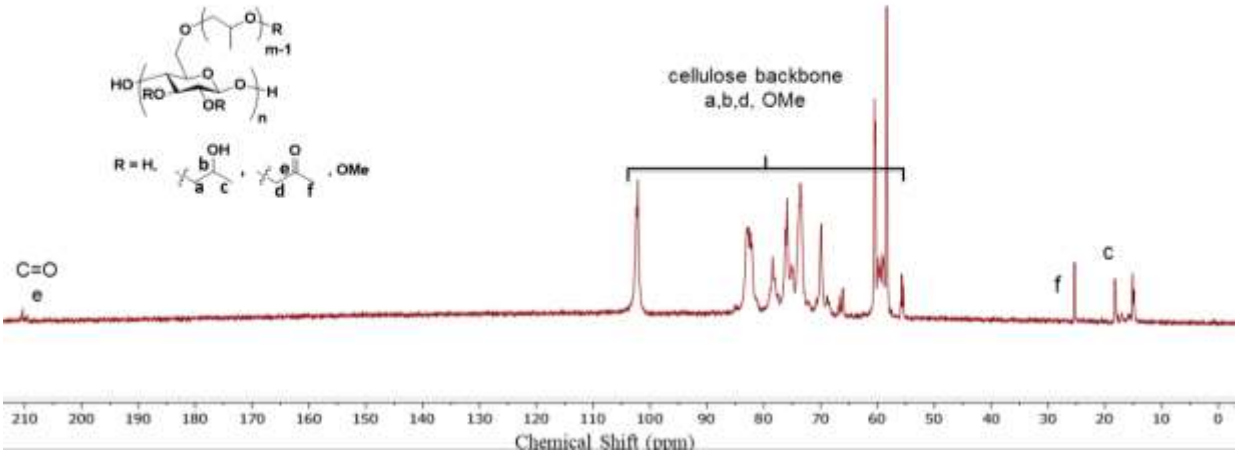

Figure S4.11. ^{13}C NMR spectrum of Ox-HPMC in D_2O

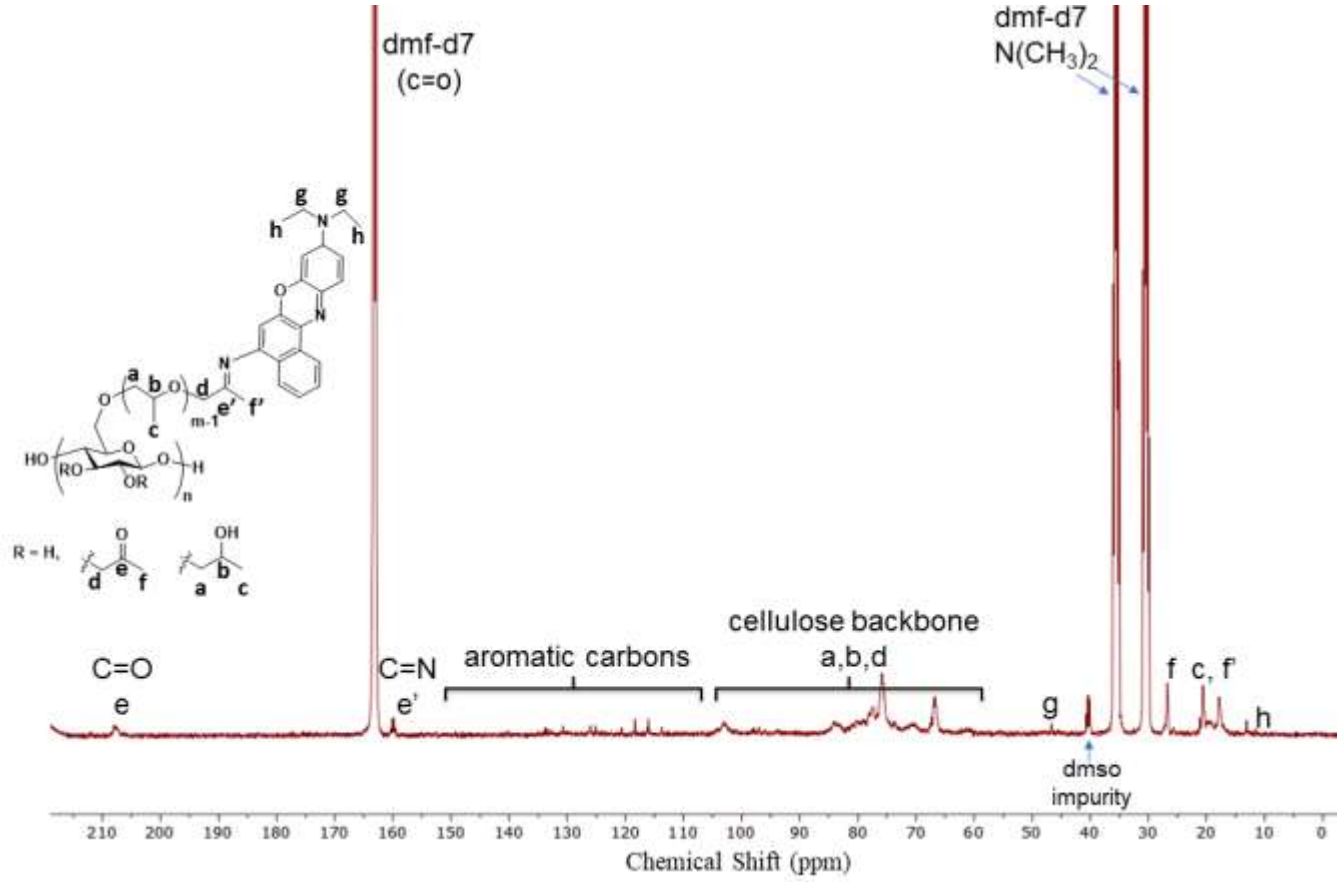

Figure S4.12. ^{13}C NMR spectrum of Ox-HPC-NB in DMF-d_7.

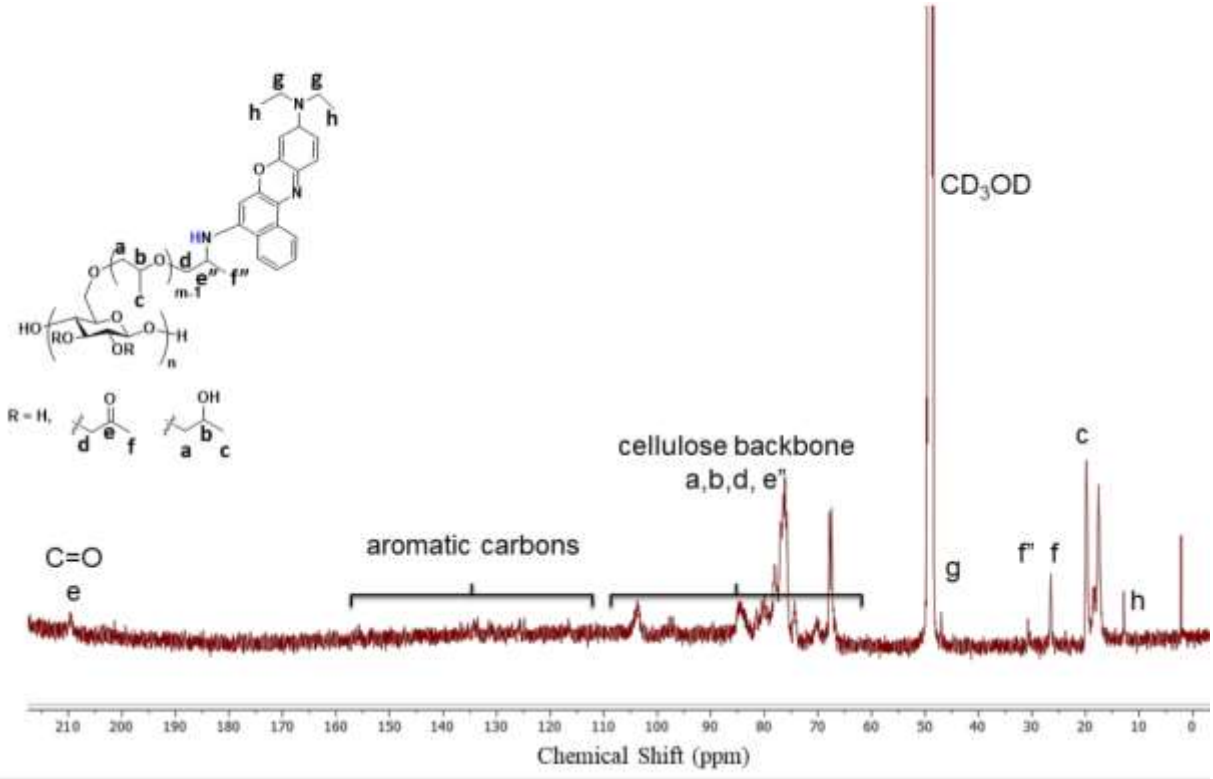

Figure S4.13. ^{13}C NMR spectrum of Ox-HPC-NB-H in CD_3OD.

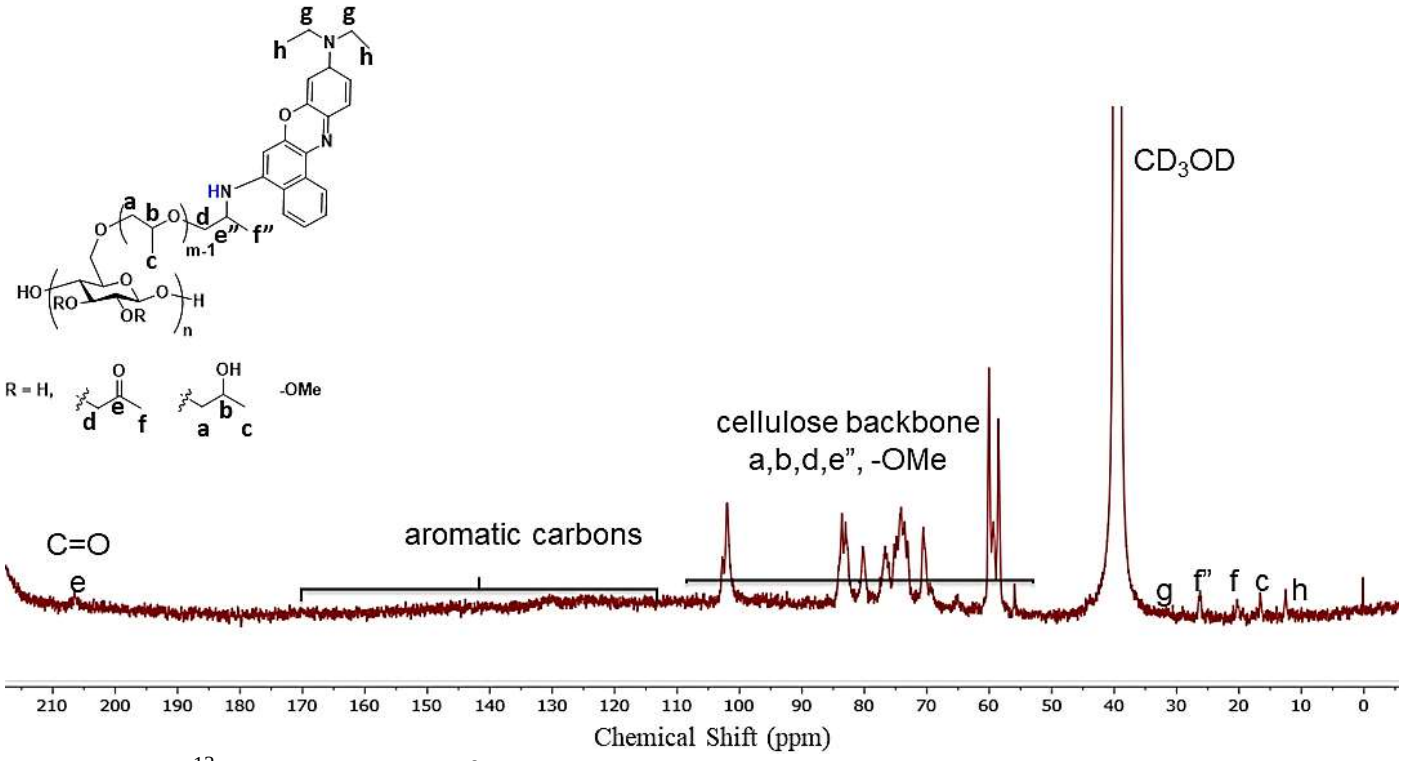

Figure S4.14. ^{13}C NMR spectrum of Ox-HPMC-NB-H in CD_3OD.

Table S4.1. Oxidation Conversion of HPC (HP DS 2.5/MS 5.0), HPMC (HP DS 0.17/MS 0.33), and HPβCD (HP DS 4.5) vs. Time and Stoichiometry

Sample	DS(ketone)[a]	% conversion[b]	NaOCl equiv	oxidation time (min)
HPC	0.14	5.8	5.07	120
HPC	0.52	20.9	8.44	120
HPC	0.88	34	8.24	180
HPC	1.20	54.8	8.55	210
HPMC	0	0	1.8	60
HPMC	0.02	10.7	1.8	240
HPMC	0.02	13.0	1.8	480
HPMC	0.02	13.0	1.8	1440
HPMC	0.04	21.3	3.6	30
HPMC	0.05	27.9	3.6	60
HPMC	0.05	30.5	3.6	240
HPMC	0.04	25.3	3.6	480
HPMC	0.07	42	3.6	1440

Sample	DS(ketone)[a]	% conversion[b]	NaOCl equiv	oxidation time (min)
HPMC	0.06	33	6.75	120
HPMC	0.06	33	8.16	120
HPMC	0.07	41	15.9	120
HPMC	0.16	99	20	120
HPMC	0.16	99	9	240
HP-β-CD	0.14	3.1	1.1	510
HP-β-CD	1.00	22.2	1.44	300
HP-β-CD	2.2	48	2.9	120

Table S4.2. Conditions and conversions achieved by two-step imination and reduction of Ox-HPC and Ox-HPMC. Note that temperatures are for the Schiff-base formation step.

Starting Ketone	Nile Blue (eq./mmol ketone))	$Na(OAc)_3BH$ (eq./mmol ketone)	Solvent	Temp. (°C)	Time (h)	DS (imine) /conversion (%)	DS (amine) /conversion (%)
Ox-HPC(0.8)	2	10	MeOH	RT	24	0.07/12.2	0.01/2.0
Ox-HPC(0.8)	5.5	2.9	MeOH	50	24	0.10/12.5	0.04/4.0
Ox-HPC(0.5)	2.5	2.9	MeOH	50	48	0.30/37.5	0.13/43.3
Ox-HPC(0.8)	4.5	2.9	DMF	RT	48	0.13/27.9	0.10/76.9
Ox-HPC(0.5)	10	2.9	DMF	RT	48	0.21/26.2	0.13/61.9
Ox-HPC(0.5)	10	2.9	DMF	50	48	0.11/22.0	0.05/45.5
Ox-HPC(0.5)	10	2.9	DCE	RT	48	0.06/12.0	--
Ox-HPC(0.5)	10	2.9	DCE	50	48	0.10/12.5	--
Ox-	1.2	1.2	DMF	50	72	0.16/94	--
HPMC(0.17)	1.2	1.2	DCE	50	72	0.07/42.3	--

Table S4.3: Properties of Ox-HPC and Ox-HPMC amine products.

Sample	Mn (Da)	Mw (Da)	PDI
Ox-HPC-014	30,490	60,630	1.988
Ox-HPC-047	28,790	68,500	2.379
Ox-HPC-088	28,570	77,020	2.724
Ox-HPMC-006	4,802	6,696	1.394
Ox-HPC-014-NBCl-H (DMF)	30,360	35,700	1.176
Ox-HPC-047- NBCl-H (DMF)	38,230	40,050	1.048
Ox-HPC-088- NBCl-H (DMF)	n/a	n/a	n/a
OX-HPMC-006-NBCl-H (DMF)**	2,463	n/a	n/a

* Samples listed as 'n/a' were insufficiently insoluble in all GPC solvent systems.
** Based on end group analysis by ^{1}H NMR spectroscopy

^{1}H NMR

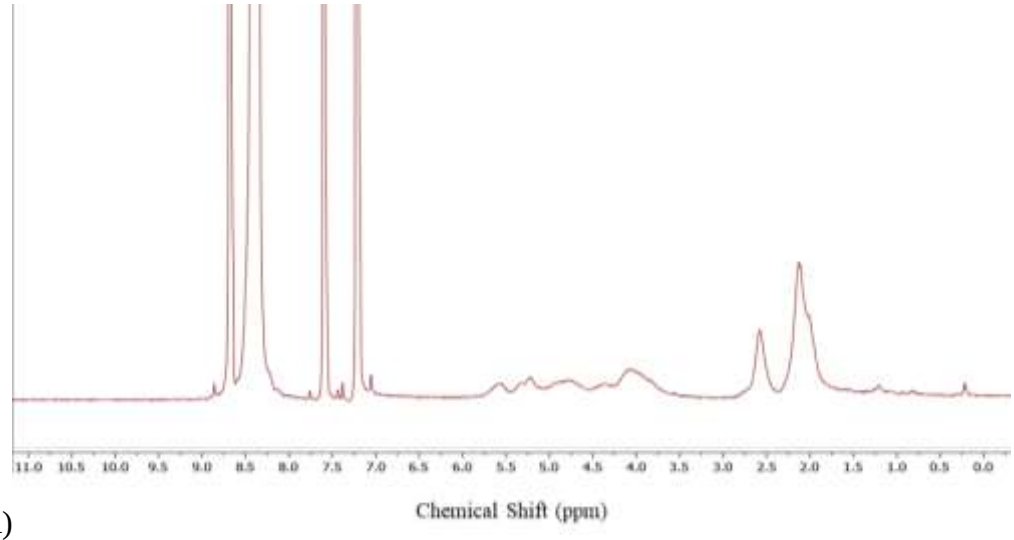

A)

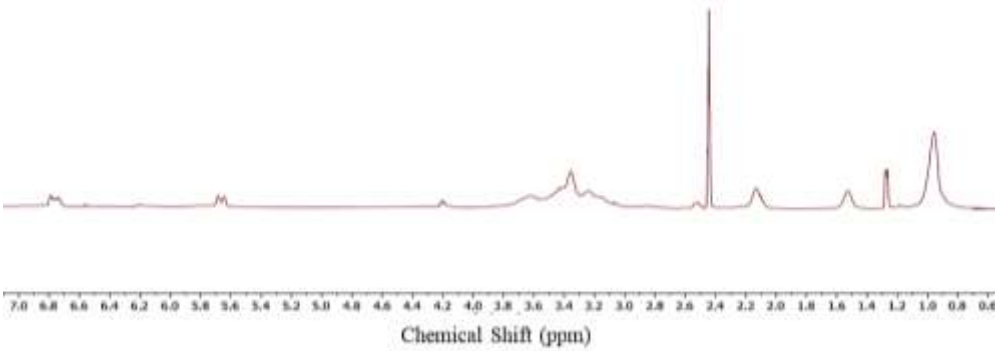

B)

Fig. S5.1. ^{1}H NMR spectra of a) CP-HPC in DMSO-d_6 and b) CAG in pyridine-d5.

^{13}C NMR

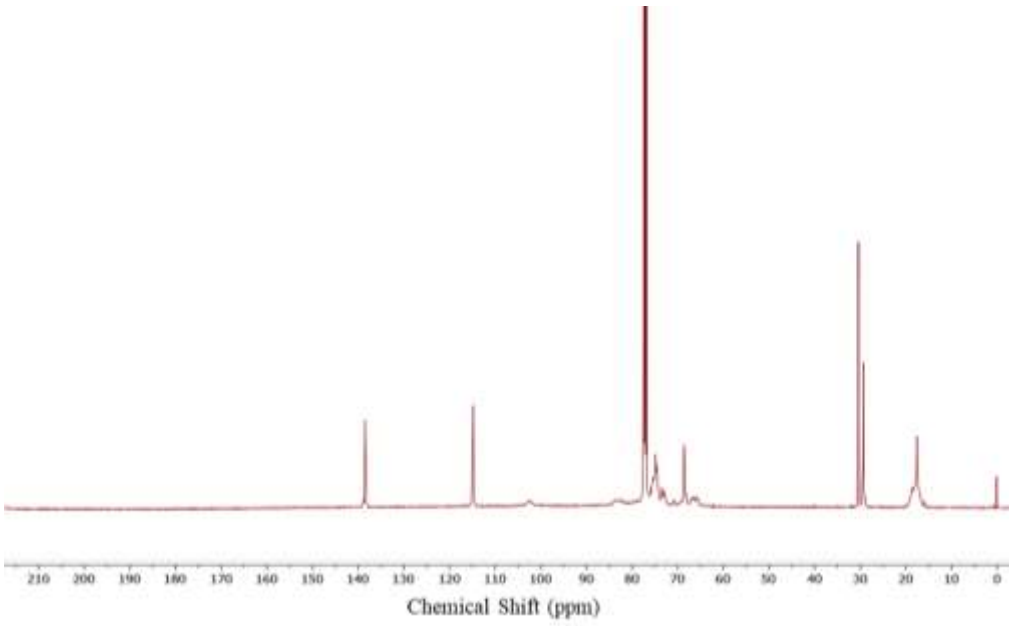

A)

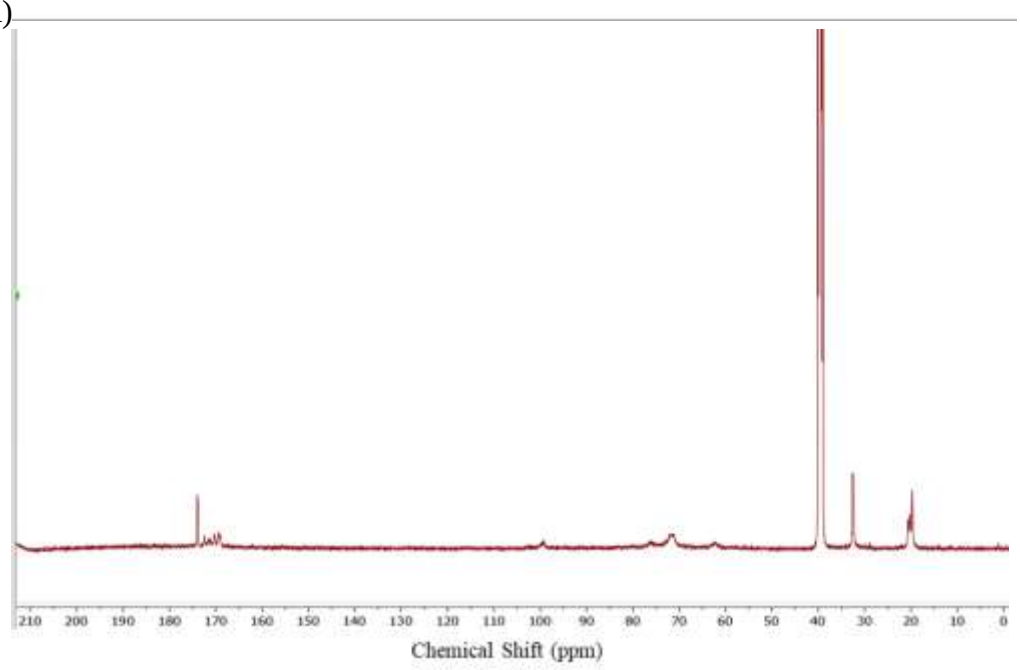

B)

Fig. S5.2. ^{13}C NMR spectra of a) CP-HPC and b) CAG in DMSO-d6.

Powder X-ray Diffraction (PXRD)

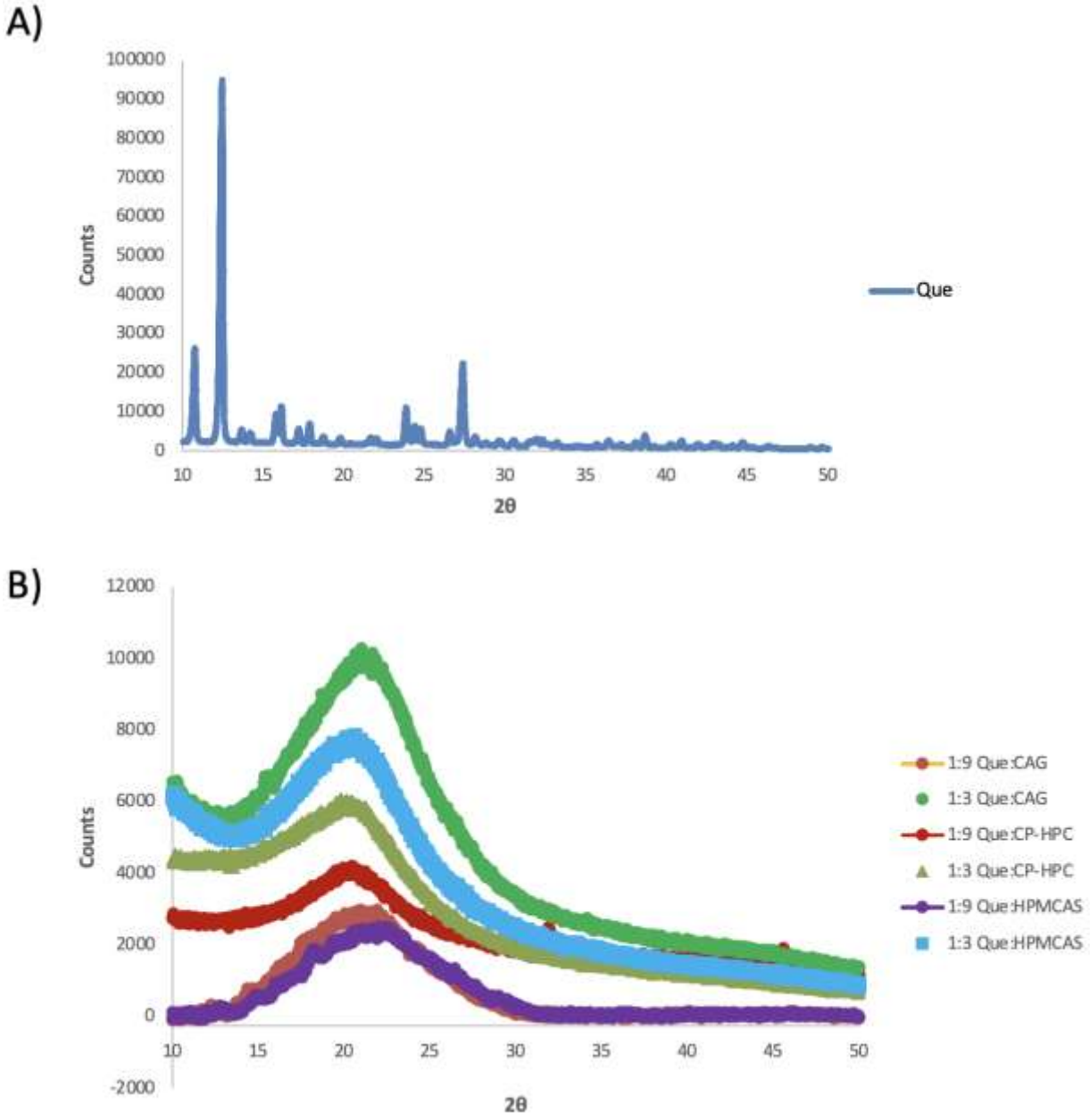

Fig. S5.3. XRD spectra of (A) crystalline quercetin (abbreviated Que in Figure) and (B) Dispersions of Que in polymers at various concentrations.

FTIR Spectra

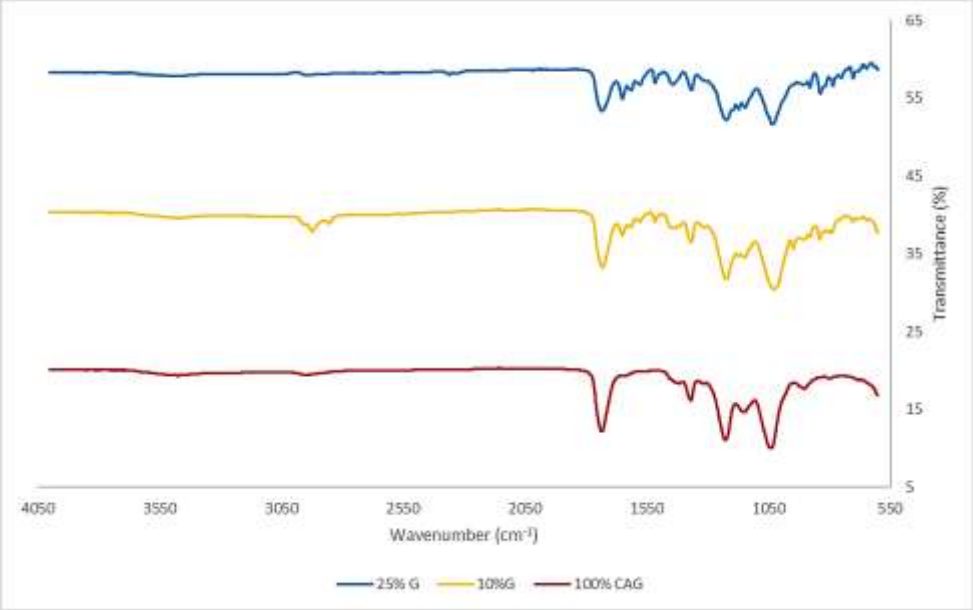

Fig. S5.4. FTIR spectra in order from top to bottom: 25% G:CAG formulation, 10% G:CAG, and 100% CAG.

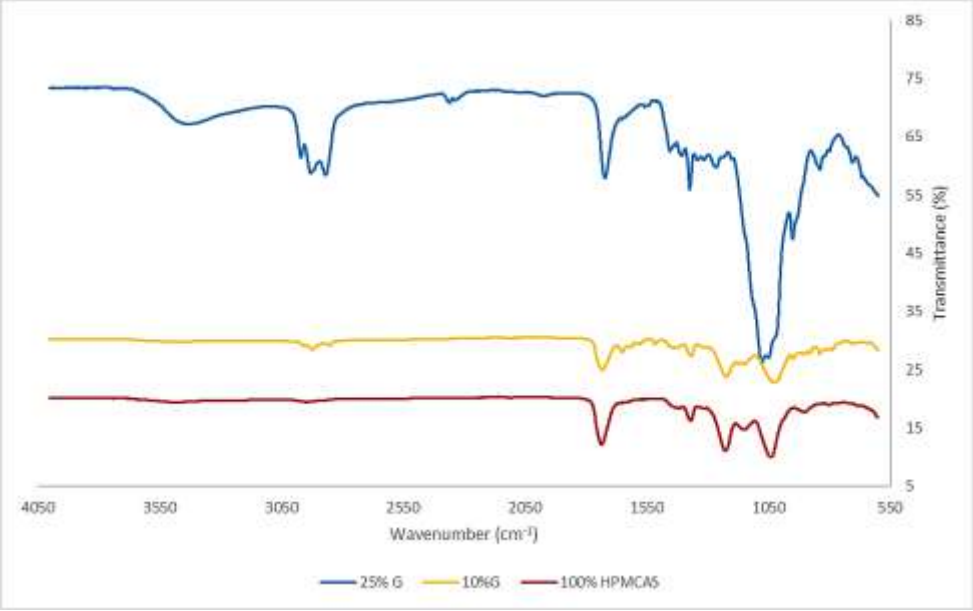

Fig. S5.5. FTIR spectra in order from top to bottom: 25% G:HPMCAS formulation, 10% G:HPMCAS, and 100% HPMCAS.

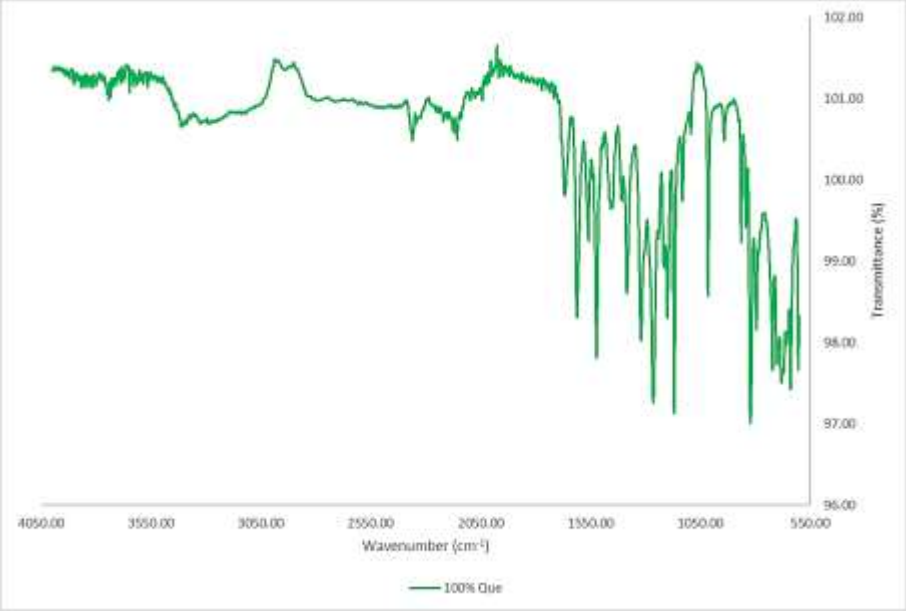

Fig. S5.6. FTIR spectrum of 100% quercetin (Que).

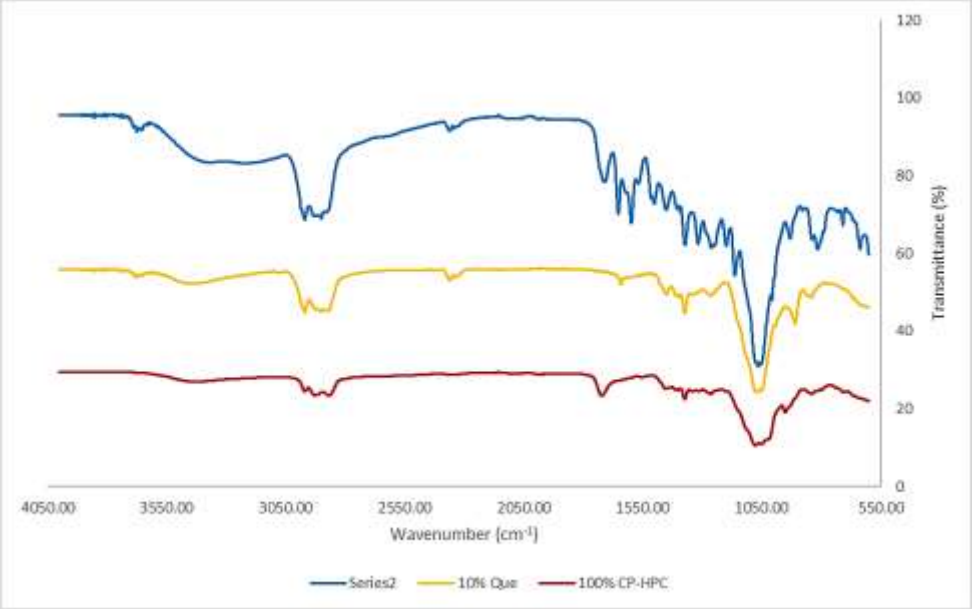

Fig. S5.7. FTIR spectra in order from top to bottom: 25% Que:CP-HPC formulation, 10% Que:CP-HPC, and 100% CP-HPC.

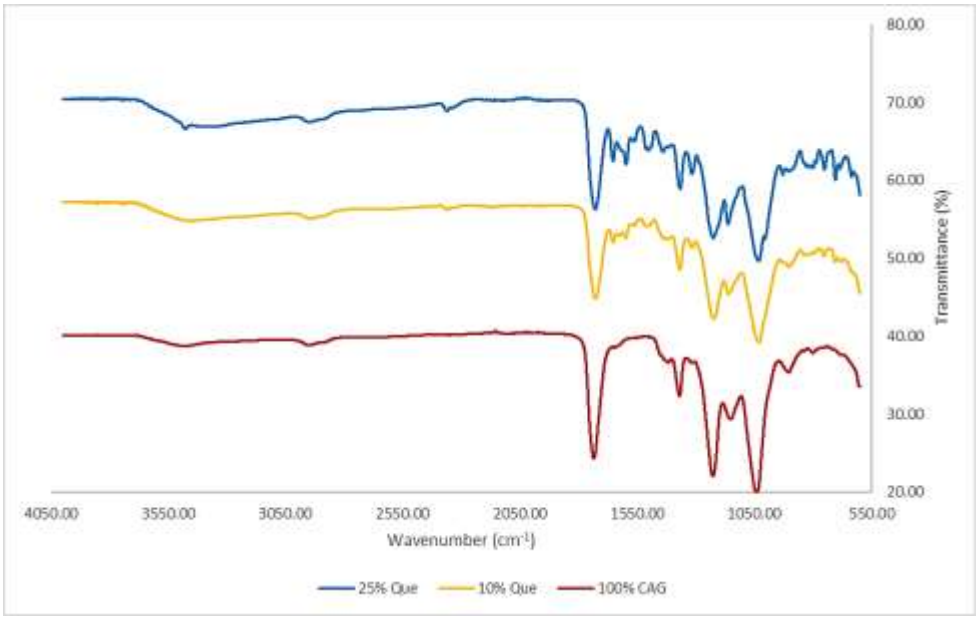

Fig. S5.8. FTIR spectra in order from top to bottom: 25% Que:CAG formulation, 10% Que:CAG, and 100% CAG.

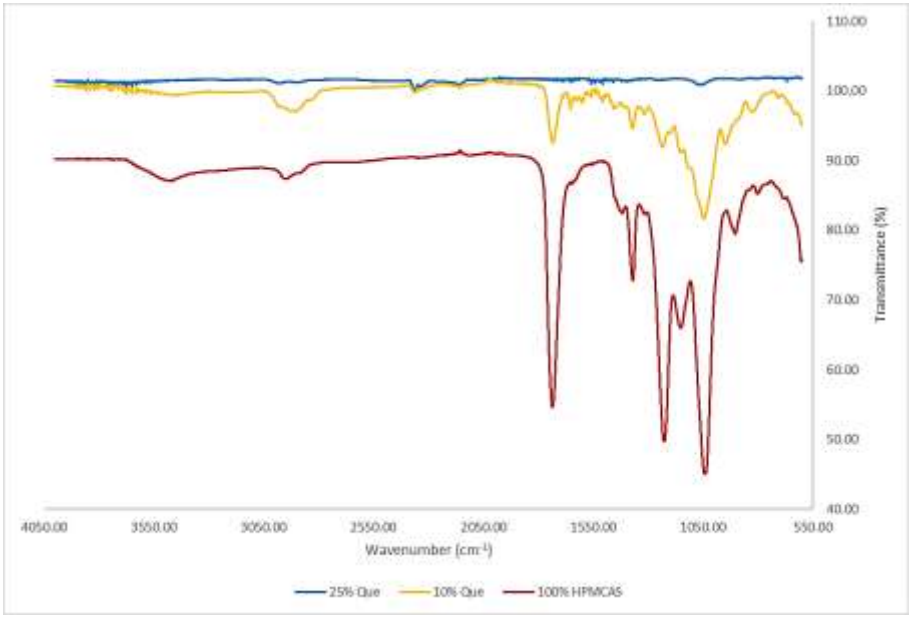

Fig. S5.9. FTIR spectra in order from top to bottom: 25% Que:HPMCAS formulation, 10% Que:HPMCAS, and 100% HPMCAS.

Amorphous solubility fluorescence spectrum

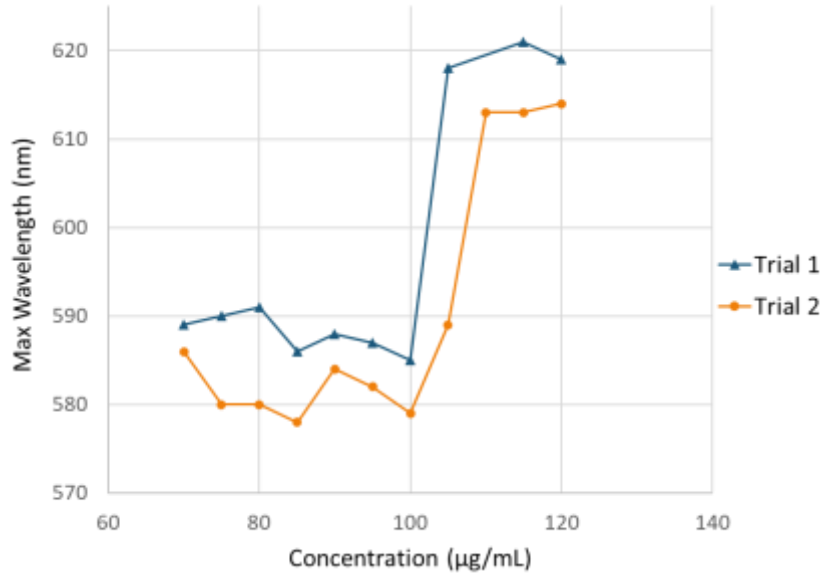

A)

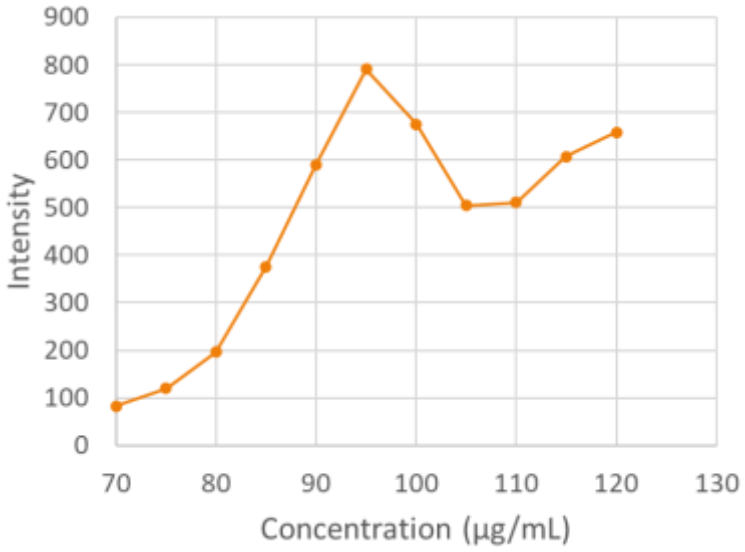

B)

Fig. S5.10. Fluorescence data obtained for genistein using dye, 4-di-2-ASP: Average solution concentration of genistein in pH 6.8 phosphate buffered saline (n = 4). Note: error bars plotted, but too small to be visible. A) maximum wavelength vs. solution concentration, and B) Intensity vs. solution concentration.

Table S5.1: Summary of polymer properties.

Properties	**HPMCAS-MF[1]**	**CP-HPC[2]**	**CAG**
T_g (°C)	120	94	159
DS (COOH)	~0.230	1.00	1.22
DS other	Me+HP* = 2.17 Ac = 0.31-0.51 Suc = 0.12-0.33	HP* = 2.2 (MS=4.4) OH = 2.2	Ac = 1.60 OH = 0.50

Mw (g/mol)	18,000	70,400	70,000
Mn (g/mol)	12,600	69,000	--
Solubility Parameter δ ($MPa^{1/2}$)	22.4	22.9	23.7
Water Solubility (mg/mL)	23.4	43.5	20
DP	70.0	129	--

Abbreviations: methoxy (Me), hydroxypropyl (HP), acetate (Ac), succinate (Suc), suberate (Sub).
*molar substitution (MS) used for hydroxypropyl due to chain extension ability
[A] Properties defined: T_g (glass transition temperature), DS (degree of substitution), Mw (molecular weight), Mn (average molecular weight), DP (degree of polymerization).
[B]Relative to polystyrene standards
[1]As reported by manufacturer, Shin-Etsu Chemical Co.
[2] As reported by Dong et al., (2016).

[3] As reported by Novo et al., (2022).

[4] (Petrova et al., unpublished data)

'- -' unmeasured.